

Sustainable Chemical Synthesis using Singlet Oxygen

Samuel Jacob Miller, MChem, AMRSC

Thesis submitted to the University of Nottingham for the degree of Doctor of Philosophy in Chemistry

August 2017

For years there have been no fish in the lake.
People hurrying through the park avoid it
like the plague. Birds steer clear
and the sedge of course has withered.
Trees lean away from it,
and at night it reflects, not the moon,
but the blackness of its own depths.
There are no fish in the lake.
But there is life there. There is life…

Underwater pigs glide between reefs of coral debris.
They love it here. They breed and multiply
in sties hollowed out of the mud
and lined with mattresses and bedsprings.
They live on dead fish and rotting things,
drowned pets, plastic and assorted excreta.
Rusty cans they like the best.
Holding them in webbed trotters
their teeth tear easily through the tin,
and poking in a snout, they noisily suck out
the putrid matter within.

There are no fish in the lake.
But there is life there. There is life…

For on certain evenings after dark
shoals of pigs surface
and look out at those houses near the park.
Where, in bathrooms,
children feed stale bread to plastic ducks,
and in attics,
toy yachts have long since run aground.

Where, in living rooms,
anglers dangle their lines on patterned carpets,
and bemoan the fate of the ones that got away.

Down on the lake, piggy eyes glisten.
They have acquired a taste for flesh.
They are licking their lips. Listen…

Roger McGough

Abstract

This Thesis describes the use of photochemically generated singlet oxygen as an efficient, low waste oxidant for Greener chemical processing.

Chapter 1 provides background on Green Chemistry and Process Chemistry. Strategies for improving the efficiency of multi-step chemical syntheses are discussed, including the use of continuous flow chemistry. Literature examples are given which highlight the process benefits of the examined strategies. A detailed review of singlet oxygen chemistry is also provided, focusing on the mechanism and synthetic utility of reactions of singlet oxygen with organic substrates. This Chapter also sets down the general aims for the work included in this Thesis.

The first synthetic Chapter 2 centres on attempts to improve a pre-existing process for the synthesis of an important antimalarial compound artemisinin – one of the few examples of an industrial-scale application of singlet oxygen. Unusual aqueous solvent systems are assessed as a way to reduce the quantity of hazardous waste produced, and continuous flow chemistry is applied in an attempt to improve material throughput, all in an attempt to lower the cost and environmental impact of artemisinin production. Chapter 3 describes the development of direct monitoring techniques combining flow photochemistry and nuclear magnetic resonance spectroscopy with a view to studying the mechanism of the artemisinin synthesis.

Chapter 4 presents work towards the use of singlet oxygen in a concise, divergent synthesis of a novel family of natural products, the Glaciapyrrols. Several members of this family show therapeutic potential as anti-cancer agents. Singlet oxygen is assessed as an efficient way to install these compounds' many oxygen-containing functional groups in a step economic manner.

Finally, Chapter 5 provides experimental detail for the methods and equipment used in this Thesis, and Chapter 6 considers the extent to which the Thesis aims have been fulfilled, placing the work herein within the wider context of Green Chemistry and Process Chemistry research.

Acknowledgements

The completion of this PhD would not have been possible without the help, guidance and support of a great many people. I have tried to include them all below, but if you find yourself forgotten, please assume you are just as appreciated as the people listed below.

Firstly, I would like to thank my supervisors Professor Mike George and Professor Sir Martyn Poliakoff, whose advice I have benefited from many times over the last four years. Sometimes they even agreed on what that advice should be! This has been a fantastic opportunity and I hope I have been worth your while.

I would also like to thank the Society of Chemical Industries for a generous Scholarship.

Many thanks to my colleagues who have helped me get through this, particularly Dr Zac Amara, who not only trained me in the lab but taught me to hold my own in (frequently heated) scientific discourse. It was good to be able to argue all day and still grab a friendly pint after work. To Dr Zahra Abada, thankyou for your friendship and hard work, and for making 48-hour NMR experiments less of a chore. To Dr Huw Williams, it was a pleasure to work with someone so eager to pass on knowledge and excited to try new and ambitious projects. To Dr Jess Bellamy, Dr Stéphanie Foltran, Dr Raph Horvath, Dr Darren Lee, Inès, Rowena, and all group members past and present. To Erica, for the mutual opportunity to vent when needed.

To all my friends for emotional support and escapism, who are almost definitely too many to list:

My oldest and best – Rich H, Charlie, Naomi – who have been with me through the whole thing. To the grand collective of the makers of bad decisions – Dr Bill, Dr

Jere, Dr Paul, Kirsty, Tom D, Becky A, Rob C, Dylan, Eamon, Rich G, Moon and all the rest – keep doing your thing, you're all great and I'll miss you.

To the chemists and denizens of the Johnson Arms – Dr Tom S, Dr Chris W, Dr Zoe D, Dr Johnny M, Dr Coby C, Chris B, Andreas, Steve and Sam, to name a few. You've made this whole ordeal so much better.

Finally, thankyou to my family who have been very supportive and understanding.

Declaration

I declare that the work presented in this Thesis is a record of my own work for the period of September 2013 to August 2017. Where any work has been carried out in collaboration with other researchers, credit has been given. This Thesis has not been accepted in partial or complete fulfilment of any other degree or personal qualification.

Samuel Jacob Miller, 11 August 2017

Table of Abbreviations.

$^1O_2$	Singlet oxygen in the $^1\Delta_g$ excited state
2-MeTHF	2-methyltetrahydrofuran
$^3O_2$	Ground state triplet oxygen
4-DMAP	4-(*N,N'*-dimethylamino)pyridine
AA	Artemisinic acid
ACT	Artemisinin-based combination therapy
Amb-15	Amberlyst-15 ion exchange reagent
API	Active pharmaceutical ingredient
ATR	Attenuated total reflectance
Bn	Benzyl
Boc	*tert*butyloxycarbamate
BPR	Back pressure regulator
bpy	2,2'-bipyridyl
COSY	(NMR) Correlation spectroscopy
DCA	9,10-dicycanoanthracene
DCC	*N,N'*-dicyclohexylcarbodiimide
DCM	dichloromethane, methylene dichloride
DDQ	2,3-dichloro-5,6-dicyano-1,4-benzoquinone
DHAA	Dihydroartemisinic acid
DMF	*N,N*-dimethylformamide
E factor	Sheldon's environmental factor
Et	Ethyl
FEP	Fluorinated ethylene propylene
FID	Free induction decay

GC	Gas chromatography
HFIP	hexafluoroisopropanol, 1,1,1,3,3,3-hexafluoro-2-propanol
HIV	Human immunodeficiency virus
HMBC	(NMR) Heteronuclear multi-bond cohesion spectroscopy
HOMO	Highest occupied molecular orbital
HPLC	High performance liquid chromatography
HRMS	High resolution mass spectroscopy
HSQC	(NMR) Heteronuclear single quantum coherence spectroscopy
HWE	Horner-Wadsworth-Emmons reaction
IC_{50}	Half maximal inhibitory concentration
IR	Infrared (light)
KIE	Kinetic isotope effect
LC-MS	Liquid chromatography-mass spectrometry
LDA	Lithium diisopropylamide
LED	Light emitting diode
MALDI-TOF	Matrix assisted laser desorption/ionisation time of flight mass spectrometry
MB	Methylene blue
NMO	*N*-methylmorpholine-*N*-oxide
NMP	*N*-methylpyrrolidine
NMR	Nuclear magnetic resonance spectroscopy
PAT	Process analytical technology
PCC	Pyridinium chlorochromate
PFR	Plug flow reactor
PMI	Process mass intensity
py	Pyridine

pyr	Pyrrolidine
RB	Rose Bengal
TBS	*tert*butyldimethylsilyl
TFA	Trifluoroacetic acid
THF	Tetrahydrofuran
TMP-Li	Lithium 2,2,6,6-tetramethylpiperidide
TMS	(Protecting group) trimethylsilyl; (NMR standard) tetramethylsilane
TPP	*meso*-tetraphenylporphyrin
UV	Ultraviolet (light)
vic	*vicinal*
WHO	World Health Organisation

Table of Contents.

Abstract ii

Acknowledgements iv

Declaration vi

Table of Abbreviations vii

Table of Contents x

Chapter 1: Introduction and Theoretical Background 1

Section 1.1: Green and Sustainable Chemical Production 2

Section 1.1.1: Green Chemistry – Principles and Motivations. 2

Section 1.1.2: Sustainable Synthesis. 4

Section 1.1.3: Sustainable Chemical Processes. 8

Section 1.1.4: Continuous Flow Chemistry. 14

Section 1.2: Singlet Oxygen Chemistry. 22

Section 1.2.1: Fundamentals of Photochemistry. 22

Section 1.2.2: Structure and Properties of Singlet Oxygen. 28

Section 1.2.3: Generation of Singlet Oxygen 30

Section 1.2.4: Reactions of Singlet Oxygen. 36

Section 1.2.5: Applications of Singlet Oxygen in Organic Synthesis. 49

Section 1.2.6: Technologies for Synthetic Photochemistry 57

Section 1.3: Summary of Thesis Aims and Content. 64

Chapter 2: Improving the Synthesis of the Antimalarial Natural Product Artemisinin. 67

Section 2.1: Introduction and Project Aims. 68

Section 2.2: Background. 70

Section 2.2.1: Sources and Syntheses of Artemisinin. 70

Section 2.2.2: Mechanism and Selectivity in the Synthesis of Artemisinin. . 82

Section 2.3: The Synthesis of Artemisinin in Aqueous Solvent Mixtures..... 89

Section 2.3.1: The Role of Water in the Artemisinin Synthesis..... 89

Section 2.3.2: Studies on the Schenck Reaction of DHAA in Aqueous Solvents. 90

Section 2.3.3: Process Development in Aqueous Mixtures. 97

Section 2.3.4: Continuous Flow Reactions..... 105

Section 2.3.5: Comparison of New and Existing Processes. 112

Section 2.5: Chapter Summary. 114

Section 2.6: Future Directions..... 117

Chapter 3: NMR Reaction Monitoring of the Synthesis of Artemisinin..... 119

Section 3.1: Introduction and Project Aims. 120

Section 3.2: Background. 121

Section 3.2.1: Process Analytics and Reaction Monitoring for Green Chemistry..... 121

Section 3.2.2: Nuclear Magnetic Resonance Spectroscopy..... 124

Section 3.2.3: Reaction Monitoring using NMR in Continuous Flow. 129

Section 3.3: NMR Monitoring of the Synthesis of Artemisinin. 134

Section 3.3.1: Preliminary Studies Assessing Yield Loss. 134

Section 3.3.2: Static Monitoring of the Artemisinin Synthesis by NMR. 137

Section 3.3.3: Continuous Monitoring of the Artemisinin Synthesis by NMR. 140

Section 3.4: Chapter Summary. 148
Section 3.5: Future Directions. 151
Chapter 4: Studies Towards the Synthesis of the Glaciapyrrol Family of Natural Products. 153
Section 4.1: Introduction and Project Aims. 154
Section 4.2: Background. 156
Section 4.2.1: The Glaciapyrrol Family of Natural Products. 156
Section 4.2.2: Synthetic Strategy. 160
Section 4.3: Synthesis of the Common Pyrrolosesquiterpene Precursor. 163
Section 4.3.1: Exploration of Aldehyde-Pyrrole Couplings. 163
Section 4.3.2: Exploration of Carboxylic Acid-Pyrrole Couplings. 166
Section 4.3.3: Formation of Weinreb Amides from Carboxylic Acids using DCC. 168
Section 4.3.4: Screening of Organometallic Couplings to Weinreb Amides. 170
Section 4.3.5: Synthesis of the Pyrrolosesquiterpene Precursor. 172
Section 4.3.6: Direct Pinnick-type Amidation of Farnesal. 175
Section 4.3.7: Scale-up and Telescoping of Reaction Steps. 179
Section 4.4: Synthesis of Glaciapyrrol Moieties Using Singlet Oxygen 181
Section 4.4.1: Model Studies on the Photo-Oxygenation of Citral. 181
Section 4.4.2: Photo-oxygenation of Precursors to the Glaciapyrrols 185
Section 4.5: Chapter Summary. 187
Section 4.6: Future Directions. 188
Chapter 5: Experimental Methods and Data 191
Section 5.1: General Experimental Information. 192

Section 5.2: Experimental Methods and Data for Chapter 2. 193

Section 5.2.1: General Procedure for Batch Photo-oxygenation: 193

Section 5.2.2: Studies on the Selectivity of the Schenk reaction of DHAA.. 194

Section 5.2.3: Studies on the One-pot Batch Synthesis of Artemisinin in Aqueous Solvent Mixtures. 198

Section 5.2.4: Studies on the Continuous Flow Production of Artemisinin in Aqueous Solvent Mixtures. 201

Section 5.3: Experimental Methods and Data for Chapter 3. 208

Section 5.4: Experimental Methods and Data for Chapter 4 213

Chapter 6: Overall Conclusions 229

References. 235

Chapter 1: Introduction and Theoretical Background

Section 1.1: Green and Sustainable Chemical Production.

Section 1.1.1: Green Chemistry – Principles and Motivations.

The advent of the synthetic chemical industries in the second half of the last century brought great benefits to those of us fortunate enough to receive them, *i.e.* cheaper materials, longer lasting food, treatments for disease.[1] Without large-scale chemical production it would not have been possible for society to grow or advance the way it has. However, the rapid growth of this sector with a focus on results and productivity was accompanied by a correspondingly large amount of pollution, waste and industrial accidents.[2] In many cases the negative effects of chemical production were in locations which receive disproportionately few of the benefits. The legacy of decades of such activity is a huge, negative environmental impact which continues to this day. Whilst individuals within both academic and industrial chemistry have acknowledged this impact for as long as the industry has existed, it was not until the early 1990s that a coordinated movement emerged to address this. This movement has grown into an active and productive field of research and is referred to as **Green Chemistry**.[3]

Green chemistry at its core is the philosophy that chemical processes, particularly those performed on an industrial scale, should be designed with an emphasis on their safety to the operator and impact on the environment.[4-6] This requirement that chemistry be environmentally benign means that it is not sufficient to only consider the reaction being performed, but to extend the analysis backwards to the sources, refinement and transport of raw materials, and forwards to the treatment of waste and to the ultimate fate of the product generated. Through this **life-cycle assessment** all industries are linked, extending the scope of Green Chemistry far beyond chemistry itself.[7-10]

The **risk** associated with a particular action can be separated into two parts – the severity of the **hazards** involved, *i.e.* how bad an incident could occur, and the likelihood of **exposure** to that hazard, *i.e.* how much control the operator has over the action:[4]

$$Risk = f(Hazard \times Exposure)$$

Clearly then the lowest risk operations are those for which the associated hazards are small, and the degree of control is large. This means that both chemical and engineering factors must all be optimised for risk to be minimised.

Green Chemistry as a concept was popularised with the publishing of Anastas and Warner's '12 Principles of Green Chemistry'.[3, 5] The 12 principles are a set of guidelines for chemists to aid in the design of safer, less hazardous chemical products and processes.[4] They highlight the factors which contribute most to a process' environmental impact and suggest ways that this impact can be reduced. The twelve principles cover the reduction of both hazard and waste, the former through the selection of less dangerous reagents and materials as well as safer and more controlled conditions, and the latter through a) decreasing the need for auxiliary materials (solvents, separating agents, drying agents etc.), b) using catalysts or otherwise recyclable materials in place of stoichiometric reagents and c) designing an efficient synthetic route. Later, Anastas and Zimmerman published the additional '12 Principles of Green Engineering', a more application-focused set of directives.[11] They focus on the holistic aspects of designing a multi-step chemical process, promoting efficient reactor design, integration of material and energy flows and the preservation or accumulation of molecular complexity during a synthesis.

Section 1.1.2: Sustainable Synthesis.

Consideration of the efficiency of a chemical synthesis is as old as the field of organic synthesis itself – a striking example being this excerpt from a paper by James B. Hendrickson from 1975 in which he describes the ideal synthesis:[12]

> *The ideal synthesis creates a complex skeleton from […] available small molecules […] in a sequence only of successive construction reactions involving no intermediary refunctionalizations, and leading directly to the structure of the target […]. If available, such a synthesis would be the most economical, and it would contain only construction reactions.*

In light of the Green Chemistry and Engineering Principles outlined above it is now quite simple to plan a synthesis that is inherently benign. The application of Green Chemistry to the planning of a synthetic route is summarised well in the three 'economies of synthesis':[13]

Atom Economy[14-15] – the mass added to the substrate in each step should be as large a proportion of the mass of reagents used as possible. This promotes addition reactions and rearrangements over substitutions and eliminations, and calls for the minimal use of protective groups and chiral auxiliaries. Atom Economy can be quantised simply by expressing the molecular weight of the product as a percentage of the sum of the reagent molecular weights:

$$Atom\ Economy\ (\%) = \frac{M_r(Product)}{\sum M_r(Reagents)} \times 100$$

Whilst this is a good metric by which to compare reactions in the context of designing of a synthetic route, it is not suitable for the comparison of completed

synthetic processes, since it does not take into account the product yield or any auxiliary materials used (solvents, purification materials, catalysts). Further discussion of metrics which can be used to assess and compare synthetic processes in terms of their environmental impact can be found in Section 1.1.3. below.

Step Economy[16-17] – the number of steps in a synthesis should be minimised as each step requires solvent, temperature control, reagents and purification, all of which consume energy and produce waste. Again, this means protective groups should be avoided, and also promotes the execution of multiple reactions in one pot without intermediate purifications or changes of conditions. Since the majority of waste by mass from a reaction tends to come from the solvent or from downstream operations like purifications, much improvement can be made by optimising the Step Economy of a reaction.

Redox Economy[18-19] – a substrate should not be oxidised just to be reduced again in a later step, or *vice versa*. Rather, oxidation state should change in a consistent way throughout a synthesis, or ideally, the starting materials should be in the same oxidation state as the products. This includes functional group interconversions that involve a change in oxidation state, e.g. ester reduction to alcohols or nitration/reduction protocols for installing aromatic amines. A major reason for this is the often poor chemoselectivity of oxidation or reduction reactions, and the poor atom economy of the reagents involved.[13] In addition, removal of such avoidable redox steps will naturally result in a more step efficient synthetic route.

To quantify the step and redox economy of a route, Gaich and Baran have published a metric that they call Percent Ideality.[20] Returning to Hendrickson's ideal synthesis, they define a necessary step in a reaction scheme as:

a) One that forms a skeletal bond, that is, a C—C or C—X bond that is retained in the product. These are **construction reactions**.
b) Redox reactions that establish the functionality of the product – **strategic redox reactions.**

They then calculate the Percent Ideality as the proportion of steps in a given route that fall into one of these two groups:

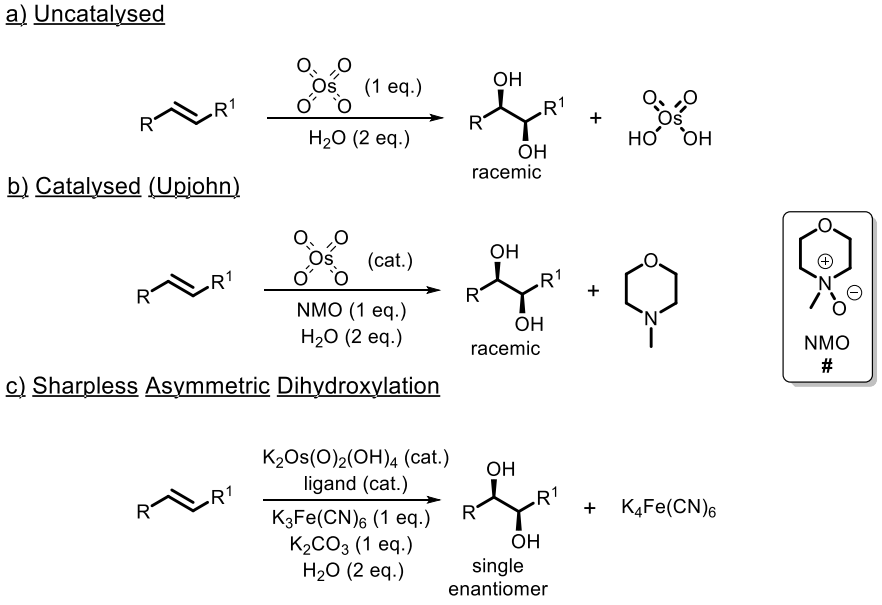
$$Ideality\ (\%) = \frac{no.construction\ reactions + no.of\ strategic\ redox\ reactions}{total\ number\ of\ steps} \times 100$$

Other steps that do not fit into these two necessary categories are referred to as '**concession steps**', and include nonessential redox steps, functional group interconversions and protecting group manipulations. The term 'concession step' acknowledges that sometimes these reactions are unavoidable.

These criteria for an efficient synthetic route – high atom, step and redox economy, and a high percentage ideality, are designed to minimise the waste produced by a chemical process, and if followed should lead to something closely resembling Hendrickson's ideal synthesis. For an efficient synthesis to also be sustainable, the materials used should be chosen in accordance with the principles described in Section 1.1.1. Ideally every component of a reaction should be non-toxic and derived from renewable feedstocks.[21] This is most important when it comes to the reaction solvent, which is usually the main component of a reaction by mass.[22] Many companies now provide their researchers with solvent selection guides, with solvents ranked in terms of sustainability and toxicity.[23-25]

In general, there is a correlation between the reactivity of a reagent and its associated hazard. This means that to perform difficult, high energy chemistry it is often necessary to use hazardous materials. Storage and use of these materials

in large quantities can present a risk to the operator and to the environment.[26] To minimise this risk, it is better to have the most reactive component of a reaction present either in catalytic amounts, or to generate a reactive species *in situ* from more benign precursors. A historical example of the former is the oxidation of alkenes to *cis*-vicinal diols with osmium tetraoxide.[27-29] Originally, the highly toxic and tightly controlled osmium species was used in stoichiometric amounts (Scheme 1a), though methods were quickly developed to regenerate the active osmium species using more benign oxidants e.g. hydrogen peroxide (the Milas oxidation)[27] or *N*-methylmorpholine-*N*-oxide (NMO, Upjohn dihydroxylation, Scheme 1b).[28] The Sharpless asymmetric dihydroxylation uses catalytic osmium with chiral amine ligands to provide single enantiomers of *cis*-*vic*-diols (Scheme 1c).[29]



Scheme 1: The evolution of osmium(IV)-mediated dihydroxylations from a) stoichiometric quantities of osmium tetraoxide through b) Upjohn's catalytic method to c) Sharpless' asymmetric variant. Requirements for safety and efficiency have driven the development of new, Greener chemistry.

The use of highly reactive reagents and catalysts can be avoided altogether by directly activating the substrate itself using thermal, electrochemical[30-31] or photochemical activation.[32-33] These so-called 'reagentless' methods reduce the

amount of toxic or hazardous reagents required for a chemical transformation.[34] Additionally, many electrochemical and photochemical reactions are umpolung,[35] leading to products that cannot be easily reached through standard chemical activation. Photochemistry in particular has seen widespread growth in recent decades and has been applied to the synthesis of many complex structures.[33]

The work presented in this Thesis centres on the use of photochemistry to activate dioxygen gas, an abundant and renewable resource, for the low waste, benign oxygenation of organic compounds. Section 1.2. provides detailed theoretical and literature background on this technique.

Section 1.1.3: Sustainable Chemical Processes.

When a chemical synthesis is to be implemented on an industrial scale, sustainability considerations can be different to those for planning a route, described in the previous Section.[11, 36] The field of research into the commercialisation and scaling up of chemical reactions is known as **Process Chemistry**. A Process Chemist is concerned with the efficiency of the entire operation, including purifications, storage and control of reagents and disposal of waste. This requires the optimisation of both chemical and engineering aspects of the process (Figure 1).[37-38]

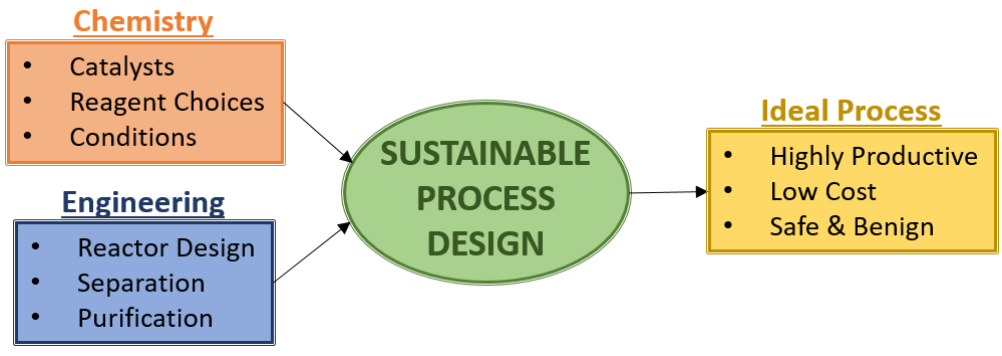


Figure 1: Stylised flow diagram showing the combination of engineering and chemical design factors in the development of a sustainable chemical process.

As well as environmental factors, a Process Chemist must consider the economic viability of a proposed route, for which the main drives are **productivity** and **cost** (although the kind of low-waste, low-risk synthesis described in the previous Section could be expected to save money on waste disposal and control measures).[39-40] Efficiency in a process sense describes the method that can make the most product in the shortest time, from the cheapest materials, under the mildest conditions. Sustainability in industry can be defined as the ability for a process to be continued indefinitely without re-investment, which requires renewable feedstocks, well-designed, low maintenance reactors and above all, low-risk chemistry. Clearly, there is a lot of overlap between the Process Chemistry definition of sustainability and the principles of Green Chemistry from Section 1.1.1.[39]

It is essential to the comparison of different processes in terms of efficiency, cost-effectiveness and environmental impact that these things be quantifiable.[40-42] Efficiency and economics are both easily quantified, but the many aspects contributing to a process' environmental impact can be difficult to compare in a meaningful way. Nevertheless, several metrics exist that aid in the comparison of different processes based on waste production or environmental hazard.[43]

The **mass efficiency** is similar to the atom economy presented in the previous Section, with the slight modification that it uses the actual mass of reagents used for a reaction.[44] This measure of atom economy includes the mass of catalysts, as well as excess reagents added for the sake of rate increase or equilibrium control:

$$Mass\ Efficiency\ (\%) = \frac{Mass\ of\ product\ produced}{Total\ mass\ of\ reagents\ used} \times 100$$

However, it neglects to account for any other materials used in the reaction, and so is unsuitable as a metric for comparing processes as a whole. Several metrics exist which do take this into account, of which two are most important – the Environmental Factor (E factor)[45] and the Process Mass Intensity (PMI).[46] Both include the mass of auxiliary materials used in a process, though differ in that E factor is defined as the mass of waste produced divided by the mass of desired product, whilst PMI is the total mass of material consumed divided by the same:

$$E\ Factor = \frac{Mass\ of\ waste\ produced}{Mass\ of\ product\ produced}$$

$$PMI = \frac{Mass\ of\ material\ consumed}{Mass\ of\ product\ produced}$$

Smaller values for either metric denote a Greener process. Table 1 shows a breakdown of the major chemical industries by sector, with the fine chemicals and pharmaceutical industries producing the most waste per unit product.[47] This correlates directly with the complexity of the targets and of the processes used to make them, as well as the purity requirements of the products.[48]

Industry Sector	Product Tonnage per Year	E Factor (kg waste/kg product)
Petrochemicals	10^6-10^8	< 0.1
Bulk Chemicals	10^4-10^6	< 1 – 5
Fine Chemicals	10^2-10^4	5 – 50+
Pharmaceuticals	10-10^3	25 – 100+

Table 1: Sheldon's E factor ranges typical of chemical processed by industry sector. A lower E factor denotes a less wasteful process.

In many cases the E-factor is simply (PMI – 1), which is a negligible difference considering the large values these numbers often take. Which of the two is preferred is simply a matter of convention.[42] Since water is considered benign, it is

'invisible' with regards to these calculations and is not included in the calculations of waste or input mass.[49] E-Factor can be further modified to account for the hazards associated with a particular waste stream by assigning an environmental quotient Q to each material, where Q = 1 for NaCl and usually 100-1000 for transition metal salts.[50-51]

$$Environment\ Quotient\ Factor\ = \frac{\sum(m_i Q_i)}{m_p}$$

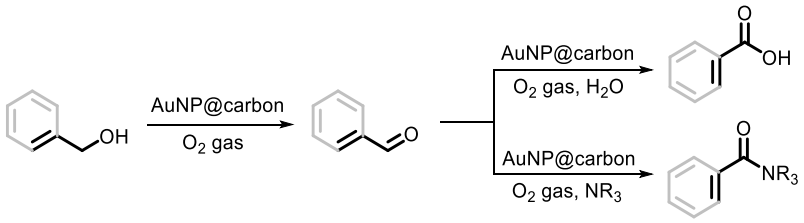
Where m_i is the mass of a particular waste material that is produced, Q_i the corresponding environmental quotient, and m_p the mass of product made. The values for Q_i should take into account the risk as calculated in Section 1.1.1, *i.e.* including the likelihood of exposure to a particular hazard.

Efficiency in a chemical process can be achieved by minimising the number of **unit operations** involved.[52] A unit operation in chemical engineering is defined as any individual manipulation of a system, chemical or physical. These can be separated in to three classes – combination, reaction and separation (Figure 2). A single chemical step on a reaction scheme will be comprised of multiple unit operations, and the number will vary, dependent on the complexity of the reaction (*i.e.* number of reagents, number of changes in temperature), the sensitivity of the reaction (*i.e.* requirements for anhydrous or anaerobic conditions) as well as the difficulty of purification of the products. Efficient processes therefore favour reactions that can be performed close to ambient conditions (room temperature, standard pressure) and under an air atmosphere.

Combination	Reaction	Separation
• Solvation	• Heating	• Crystallisation
• Compression	• Cooling	• Filtration
• Pumping	• Illumination	• Chromatography
• Mixing	• Pressure Control	• Distillation

Figure 2: The three classes of unit processes in chemical engineering and examples of each. A chemical reaction will involve several such processes from reagents to pure product.

The number of unit operations in a process can be greatly reduced by performing several steps without intermittent purification of the intermediates, or switching of solvents. Several related methods are often used to streamline a batch process, including cascade,[53-54] telescoped,[55] multicomponent[56] or one-pot reactions.[57] **Tandem** reactions are cases where a single reagent or catalyst can be used to initiate several chemical transformations, such as the oxidation of allylic and benzylic alcohols to acids and amides using carbon supported gold nanoparticles reported by Kobayashi *et al.*:[58]

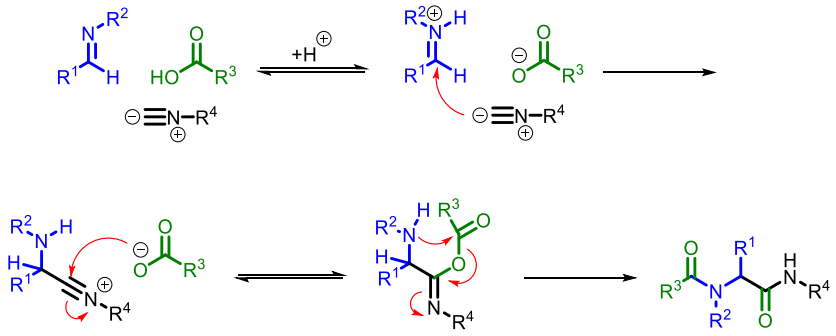


Scheme 2: Kobayashi *et al*'s tandem oxidation of allylic or benzylic alcohols to acids or amides, catalysed by gold nanoparticles.

A subset of this strategy is the use of a single activation event to form several chemical bonds by initiating reaction cascades.[54]

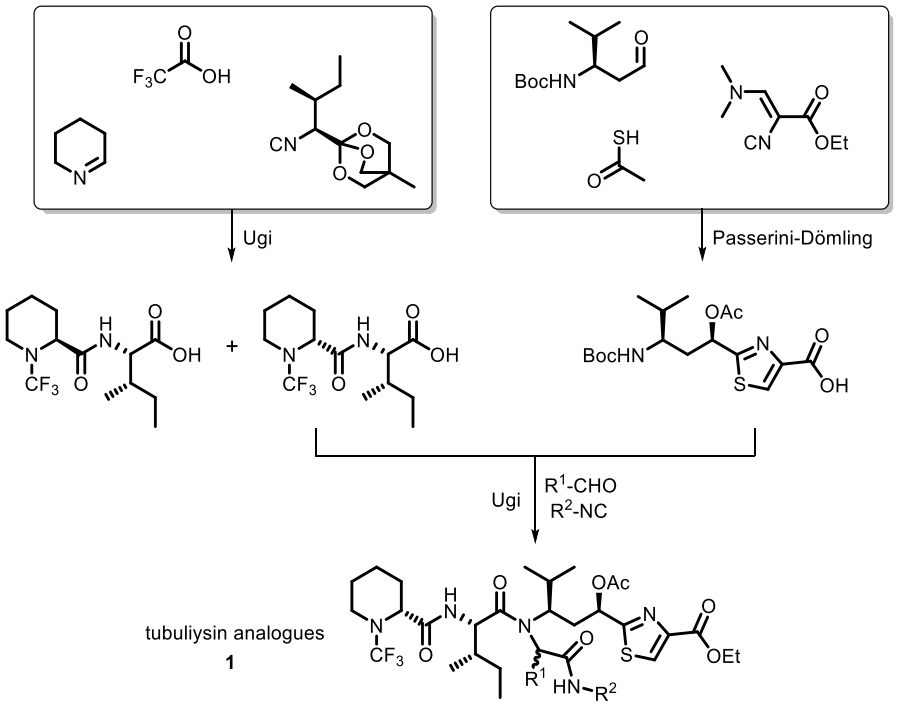
Multicomponent and **one-pot** reactions involve several distinct chemical steps performed at once using different reagents, with everything present in the reaction vessel from the start. This requires good chemoselectivity to avoid the formation of unwanted products. A classic example of a one-pot/multicomponent reaction is the Ugi reaction, in which an imine, a carboxylic acid and an isocyanide react

spontaneously to give high yields of α-aminoacyl amides by the mechanism shown in Scheme 3.[59]



Scheme 3: The 3-component Ugi reaction, chemoselectively providing α-aminoacyl amides in a single vessel.

The synthesis of tubulysin analogues **1** by Wessjohann *et al.* using several multi-component reactions in a convergent fashion, including two Ugi reactions and the related Passerini-Dömling reaction of thioesters, demonstrates the impressively rapid accumulation of molecular complexity possible using such methods (Scheme 4).[60]



Scheme 4: Wessjohann's highly efficient synthesis of tubulycin analogues (1) using convergent multicomponent reactions to quickly form molecular complexity.

The benefits of using multicomponent or one-pot reactions are demonstrated twice in this Thesis. Chapters 2 and 3 discuss the one-pot, three step synthesis of an important antimalarial product and in Chapter 4, a multicomponent oxidation of an aldehyde to an amide is used to streamline a chemical synthesis.

If the high chemoselectivity needed for one-pot chemistry is not possible, the waste generated by a process can be reduced by **telescoping**. In a telescoped synthesis, several reactions are performed sequentially in the same solvent, either without any purification at all, or with simple purification operations like filtration and liquid-liquid extraction which are neither material- nor time-intensive. Telescoping can greatly reduce the material and time costs of a process. Anderson and colleagues at Dow Chemicals projected a 50% reduction in cost for a 1 kg scale process using such a strategy.[55]

Section 1.1.4: Continuous Flow Chemistry.

The use of multi-step **continuous flow chemistry** is increasingly favoured by the chemical industries, particularly in the synthesis of active pharmaceutical ingredients (APIs).[61-63] Flow synthesis promotes the design of efficient processes with few unit operations, and can be thought of as telescoping taken to its extreme.[64] Unlike traditional batch methods where the entire reaction mixture is held in a stirred vessel for the full duration of the reaction, continuous methods use pumps to flow the reagents through a tubular reactor, with products eluting on the other side. This can impart a range of process benefits, described below.[65-66]

The simplest flow reactor is a tube through which the reagents are pushed or pulled using a pump or syringe. The reagents are combined at the inlet and if necessary the tube is heated to initiate a reaction. This type of system is called a **plug flow reactor** (PFR) and progress of the reaction within the tube can be

modelled kinetically using the **plug flow approximation**.[67] In the plug flow approximation, the reaction is modelled as a series of infinitely thin lateral cross sections, or plugs, moving in the direction of flow. Within the plug there is perfect radial mixing with no accompanying axial (forwards or backwards) mixing between plugs. The validity of the plug flow model requires that the reaction be at a steady state, with no accumulation of product within the reactor, that the rate of material flow through the reactor is stable and constant, and that the temperature does not change over time. Each plug, as it moves through the PFR, is treated as a batch reactor exhibiting standard reaction kinetics.

In a standard batch reactor, the rate of a reaction v_A in terms of a reagent A is defined as:

$$\nu_A = \frac{d[A]}{dt} = \frac{1}{V}\frac{dN_A}{dt}$$

where [A] is the concentration of A in the reaction mixture and N_A is the absolute amount of A present. In a standard batch reactor, such as a stirred round-bottomed flask, the amount of A at a time t can be given by

$$N_{A(t)} = N_{A(0)} + \int_0^t \frac{dN_A}{dt} dt$$

The composition of the reaction mixture at any point in time is constant in space, and at a fixed point in space, the composition of the reaction changes over time. Therefore, a reaction performed in a stirred flask or tank can be thought of as progressing in the **time domain**.

Under the plug flow approximation, the 'plug' of reaction mixture moves through the PFR at a volumetric flow rate, F. The reaction time is equal to the time which the plug has spent inside the reactor, the residence time, τ. The rate of reaction is given by:

$$\nu_A = \frac{d[A]}{d\tau} = \frac{1}{V}\frac{dN_A}{d\tau}$$

τ is dependent on the volumetric flow rate, F, and the volume of reactor through which the plug has passed, V:

$$\tau = \frac{V}{F}$$

$$\therefore \qquad d\tau = \frac{dV}{F}$$

at constant flow rate. Substituting this into the rate equation above gives:

$$\nu_A = \frac{1}{\tau}\frac{dN_A}{dV}$$

$$\therefore \qquad N_{A(V)} = N_{A(0)} + \int_0^V \frac{dN_A}{dV}$$

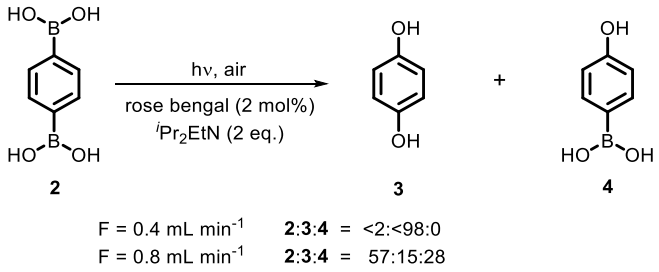
For a uniform PFR with a constant cross-sectional area:

$$N_{A(x)} = N_{A(0)} + \int_0^x \frac{dN_A}{dx}$$

So unlike a batch reaction, the composition of the reaction mixture at a particular time will vary axially in space, whereas the composition of the reaction mixture at

a particular point in space is constant over time. Reactions in PFRs can be thought of as proceeding in a **spatial domain**.

This leads to a major benefit of performing a reaction in flow – the end point of the reaction can be very precisely controlled by changing the residence time τ, either by altering the flow rate or the volume of the reactor. This can provide control over selectivity in cases where over-reaction is possible. An example of this can be seen in the flow photochemical synthesis of phenols from boronic acids reported by Penders *et al.*[68] When *para*-phenyldiboronic acid **2** was used as substrate, hydroquinone **3** was the exclusive product at low flow rates, whereas at higher flow rates the desymmetrised *para*-hydroxyphenylboronic acid **4** was received with a 64% selectivity, although at the cost of greatly reduced conversion (Scheme 5).



Scheme 5: The continuous flow synthesis of phenols from arylboronic acids. Desymmetrisation of *para*-penyldiboronic acid was achieved selectively by varying the flow rate.

Compared to a batch reaction, reactive intermediates generated in flow have short lifetimes and minimal contact with the starting materials. Reactive products are similarly removed quickly from the reactor and are exposed to the reaction conditions to a much lesser extent than in batch. This allows good control over the selectivity of such reactions by suppressing side-product formation. High selectivities ensure clean product streams, and reduce the need for purifications downstream, leading to more efficient processes.

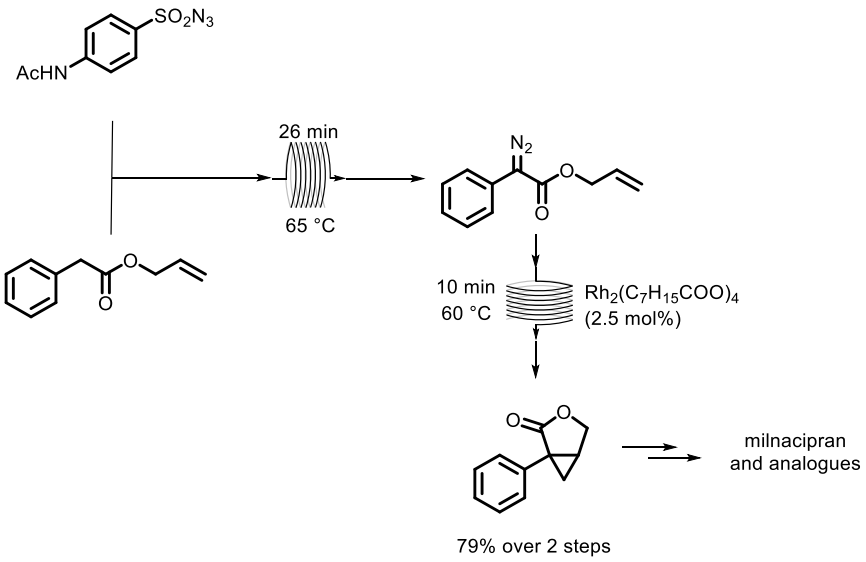
Whilst a PFR can be as simple as a coil of tubing, a major strength of flow chemistry is that heterogenous reactions can be performed easily by filling the flow

reactor with a solid reagent or catalyst.[69] Again, this leads to cleaner product streams, reducing the difficulty of purification of the product. There is also a considerable rate increase observed in reactions performed in this way – the stoichiometric ratio of catalyst to substrate can be very high inside the reactor, whilst the absolute amount of catalyst required compared to product formed can be very high. This means that high rates can be achieved without the cost of using large amounts of an expensive catalyst. This situation is only possible with the combination of continuous flow and a solid-phase catalyst.

Flow reactors typically have smaller volumes than their batch counterparts, and the surface-area-to-volume ratio is usually high. This can give good mixing, efficient mass transport and fine temperature control, all of which increase the efficiency of a process.[70] Additionally, these factors allow good control over hazardous chemistry, lowering the chance of exposure and so minimising the risk associated with an operation.[66, 71]

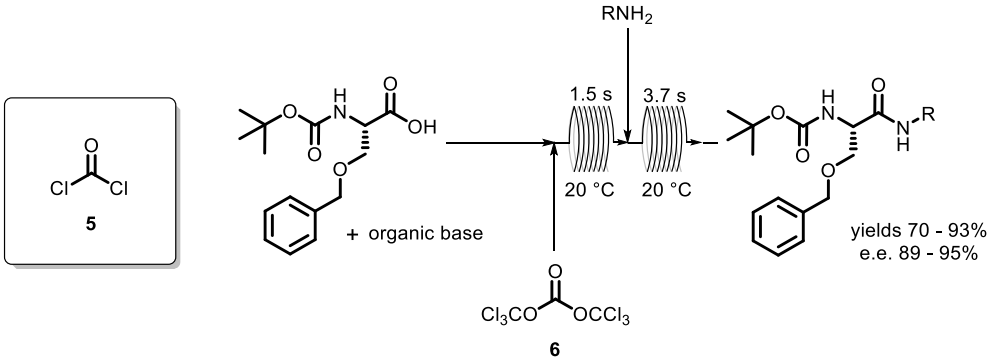
For example, the use of explosive diazo compounds in a batch synthesis would not be considered on an industrial scale, despite the wealth of chemistry that can be performed.[72] On the other hand, several groups[73-76] have reported their safe and controlled use in continuous flow, including recent work by Wirth *et al.* towards a large-scale synthesis of the serotonin-norepinephrine reuptake inhibitor milnacipran (Scheme 6).[77] In flow, the lifetime of the active diazo species is short, and the amount present at any one time is low, making it much safer to perform than a corresponding batch process. Continuous flow reactors can also allow the use of highly toxic reagents which would be undesirable on a batch scale, particularly toxic gasses. By generating such reagents *in situ* within the closed system of a flow reactor, the risk of exposure can be practically eliminated.[71] For example, phosgene **5** is useful for chlorination reactions, e.g. in the activation of

carboxylic acids for amide couplings, a frequently performed transformation in the pharmaceutical industry. Its use is strictly controlled and its storage in large quantities is prohibited.



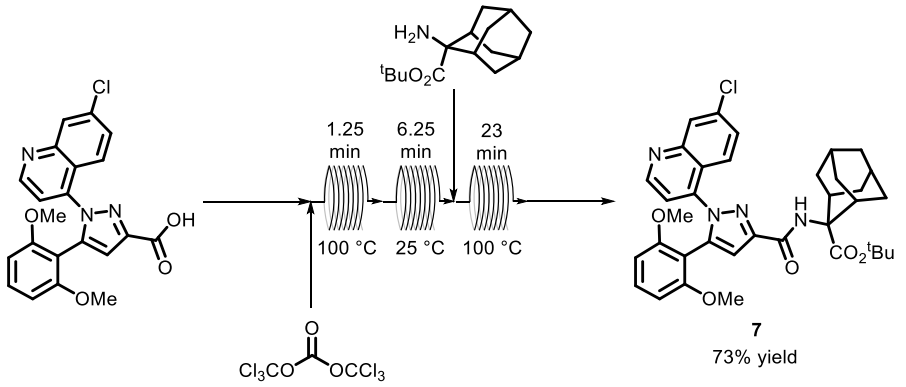
Scheme 6: Wirth *et al.*'s synthesis of milnacipran in continuous flow, *via* diazonation, carbene generation and insertion into the alkene bond. Diazo chemistry is hazardous to perform in batch but can be safely performed in flow.

Fuse *et al.* generated phosgene from degradation of the much less toxic triphosgene **6**, then used it directly for amide couplings.[78] An additional benefit of using flow chemistry for this reaction was that the short lifetime of the acyl chloride intermediates prevented epimerisation, which can be a problem in batch syntheses using similar techniques.



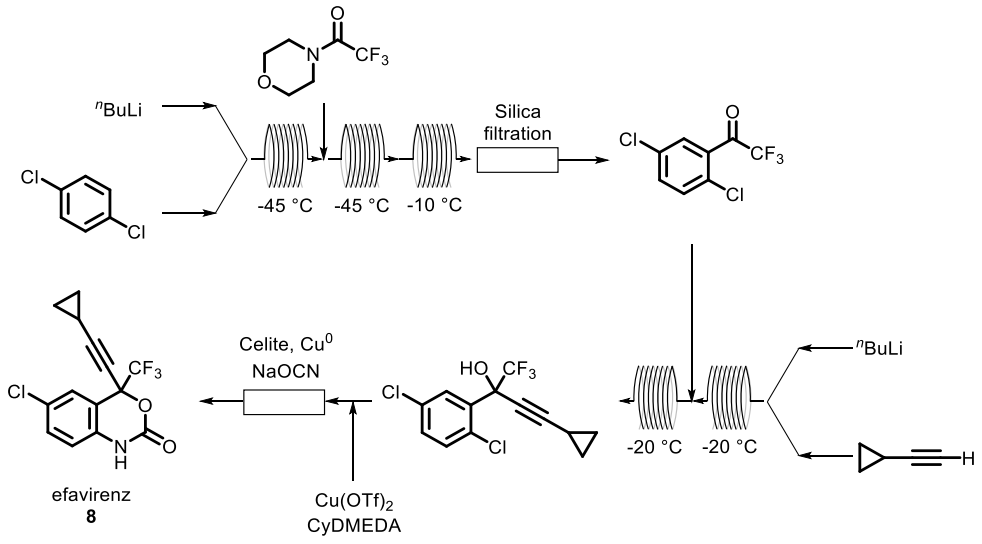
Scheme 7: *In situ* phosgene generation from triphosgene in flow, developed by Fuse *et al.* The toxic gas phosgene is only present inside the reactor and in small amounts.

Their chemistry was successfully applied by the Ley group to the synthesis of neurotensin inhibitor meclinertant **7** (Scheme 8).[79]



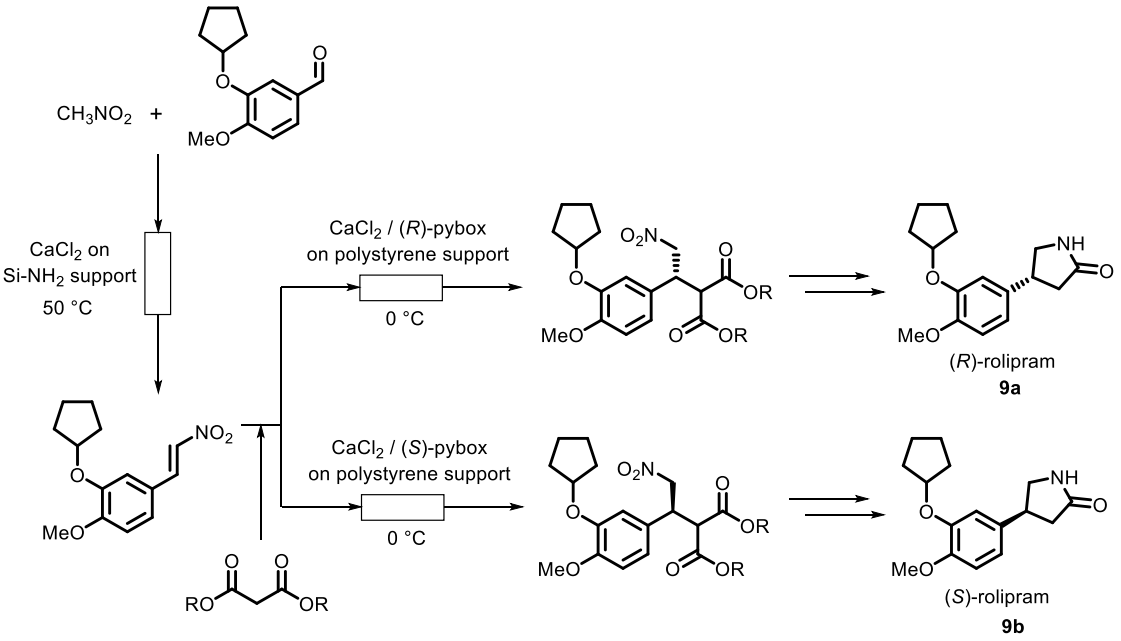
Scheme 8: The Lay group's synthesis of meclinertant (7) using *in situ* phosgene generation.

Continuous flow chemistry is being applied to the synthesis of ever more complicated APIs. Seeberger *et al.* have reported a concise synthesis of the drug efavirenz **8**, used in the treatment of HIV (Scheme 9). Using continuous flow chemistry, they could form the product in fewer steps than the batch processes currently applied by pharmaceutical companies Merck[80] and Lonza[81] (three as opposed to four or five, respectively) in a 45% overall yield, with a total residence time of only two hours. Their synthesis was telescoped through with only simple in-line purifications.



Scheme 9: Seeberger *et al.*'s flow synthesis of antiviral compound efavirenz.

Kobayashi *et al.* have recently demonstrated the use of a polystyrene supported calcium-pybox catalyst to perform an asymmetric Michael addition in their flow synthesis of the anti-inflammatory drug *(R)*-Rolipram **9a** (Scheme 10). The opposite *(S)*-enantiomer **9b** could be formed by using the enantiomeric pybox ligand.[82]



Scheme 10: The enantioselective flow synthesis of *(R)*- and *(S)*-rolipram reported by Kobayashi and coworkers.

Whilst chiral catalysis in flow had been previously reported,[83-85] this is the first instance of an asymmetric step being applied in a multistep flow synthesis.[61]

Work by Jamison *et al.* has extended flow processing beyond the synthesis of APIs to the production of completed, formulated pharmaceuticals. They have developed a reconfigurable, compact flow device which can produce any of four pharmaceutical products directly in forms that can be administered to a patient.[86-87]

The strategies presented above, particularly the use of continuous flow chemistry, demonstrate how fine chemical and pharmaceutical production can be made more efficient, safer and less wasteful by adhering to the Principles of Green Chemistry.

A sustainable chemical process is not only better for the environment but is often cheaper to perform and more productive, increasing profits for the manufacturers and lowering the costs to the consumers. In this Thesis, the use of photochemically generated singlet state dioxygen is used as an oxidant in the development of sustainable chemical processes. The following Section provides background on this technique.

Section 1.2: Singlet Oxygen Chemistry.

As discussed in Section 1.1.2, photochemical activation of otherwise inert reagents represents a powerful strategy for cleaner and more economical chemical processes.[88] The work presented in this thesis focuses on one specific aspect of photochemistry – the use of photochemically generated singlet excited state dioxygen (singlet oxygen, $^1O_2$) as a reagent for the clean and low-waste oxygenation of organic substrates. The following sections provide context on the theory, action and application of singlet oxygen and further describe how it can be used as a tool for Green Chemistry.

Section 1.2.1: Fundamentals of Photochemistry.

Light, whilst classically considered wave-like, exhibits particle-like properties in that it transmits energy in discrete 'packets' called **photons**, with photon energy strictly defined by the frequency of the light in question according to the equation:

$$E_{photon} = h\nu$$

Where E_{photon} is the photon energy, ν is the frequency of light and h is Planck's constant, 6.63×10^{-34} m^2 kg s^{-1}. This is related to the quantum theory of matter, which states that electronic, vibrational and rotational energy states of an atom or

molecule are also fixed, or **quantised**. Absorption of a photon of light can cause a transition between these states only when the photon energy corresponds precisely to the difference in energy between them. Light of frequency not corresponding to one of these transitions cannot be absorbed. Thus, every electronic, vibrational or rotational transition that a molecule can undergo has a particular frequency of light associated with it. The lowest energy state, in which a molecule usually exists, is known as the **ground state**. States of higher energy are called **excited states** and can be accessed through absorption of a photon. The properties of molecules in excited states is often very different from their ground states, particularly in the case of electronic transitions, which can open up a wide range of chemical reactivity. Additionally, due to the instantaneous nature of absorption, electronic excited states are often generated in a vibrational excited state (a vibronic transition, the **Franck-Condon principle**) increasing their reactivity.

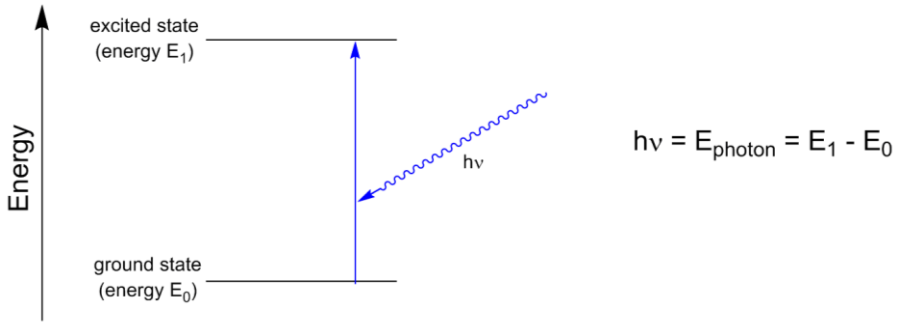


Figure 3: Absorption of a photon can cause a transition from one electronic energy state to another, if and only if the photon energy is equal to the difference in energy between the two states.

Interactions of light with matter which result in a chemical change are grouped together under the term **photochemistry**. This usually involves light in the visible or ultraviolet (UV) regions of the electromagnetic spectrum, which correlates to electronic transitions in molecules. There is a wide range of chemical changes that can be induced, dependent on the molecules involved and the light being absorbed. Figure 4 shows the possible deactivation pathways of an electronic excited state.

As indicated on the diagram, some of these pathways are reversible, leading to no chemical change, and some are irreversible and can be harnessed for photochemistry.

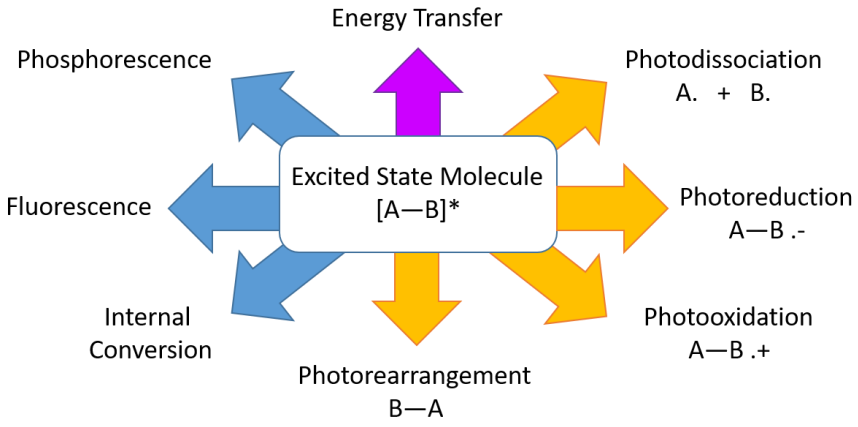


Figure 4: The possible fates of an electronic excited state. The pathways in blue result in no net chemical change, whereas those in orange can be used to perform photochemistry. Energy transfer (purple) is a special case.

Of the eight pathways depicted, the three shown in orange are irreversible and productive, leading to photochemical reactions:

In the simplest case, the excited state molecule forms a new bond directly to another substrate (**photoaddition**) or to itself (**photorearrangement**). Otherwise, the extra energy from the absorbed photon (**excitation energy**) may exceed the dissociation energy of a chemical bond, leading to fragmentation of the molecule in **photodissociation**. These routes usually occur with shorter wavelength, higher energy absorptions *i.e.* UV photochemistry. The two species formed are generally neutral radical species, and can go on to form rearranged products or participate in free radical chain reactions. Excited state molecules could also form **association** complexes either with another of the same molecule, or with another species present, followed by bond formation to give a product. These excited state complexes are often referred to by the contraction **exciplex.**

An excited state may be more able than the ground state to accept an electron from an appropriate electron donor, leading to **photoreduction**, or donate one to an appropriate acceptor, leading to **photooxidation**. Both of these electron transfer processes lead to the formation of radical ions, species with both a permanent ionic charge and an unpaired electron. These are very reactive, and rarely generated in ground state chemistry. So-called **photoredox** chemistry has found widespread use, and many comprehensive reviews have been published. Where multiple productive deactivation pathways are possible, multiple products can form, and so the selectivity of the photochemical reaction is lowered.

Of the three reversible, non-productive pathways, shown in blue, both **phosphorescence** and **fluorescence** involve the emission of a photon to return the excited molecule to its ground state. Fluorescence is a direct emission, with the photon emitted being close in energy to the absorbed photon. This is often a fast process. Phosphorescence is a slower emission involving intermediate electronic states reached through changes in electron spin, something that is explained in more detail in Section 1.2.3. **Internal conversion** is non-radiative, occurring when the excitation energy of the excited state molecule is converted to vibrational energy, which can be distributed to other molecules upon collision as heat. These three non-productive deactivation pathways occur in competition with the productive pathways describe above and can reduce the efficiency or of a photochemical reaction.

Energy transfer, shown in purple, is a special case, since it is both reversible and productive. No change occurs overall in the absorbing molecule but the excitation energy is transferred to another molecule, leaving the latter in a reactive excited state. As such, this can still lead to photochemical reactions since the newly excited molecule can undergo any of the aforementioned irreversible photochemical

changes. A very common example of this – and one important to this Thesis – is photosensitisation, where an absorbing molecule is used to harvest photons and transfer that energy to a reagent molecule. The use of photosensitisation to generate excited singlet state dioxygen is discussed in detail for much of the rest of this Chapter.

The efficiency of a given photochemical process with respect to the amount of light absorbed is referred to as the **quantum yield**, Φ, and is calculated in a similar way to chemical yield:

$$\Phi = \frac{molecules\ of\ product\ or\ excited\ state\ formed}{photons\ absorbed}$$

A quantum yield close to zero represents a poorly efficient reaction, whilst a quantum yield close to 1 usually means a reaction is very efficient. Values for Φ greater than 1 are possible for photoinitiated free radical chain reactions where a single absorption event can lead to the formation of several product molecules (see below). In the absence of any such reactions, the sum of the quantum yields for all processes shown in Figure 4 should equal 1.

The absorbance, or strength of a particular absorption is related to a property of the transition called the **molar extinction coefficient**, ε, as well as the concentration c and absorbing path length l. The relationship is described by the Beer-Lambert Law:

$$A = log_{10}\left(\frac{N_1}{N_0}\right) = \varepsilon cl$$

Where A is absorbance, N_1 is the number of molecules in the excited state and N_0 is the number of molecules in the ground state. The higher the value of ε, the

greater the proportion of molecules are promoted to the excited state when the sample is irradiated.

Often in organic photochemistry, the reactants or reagents do not absorb visible light, does so with a low extinction coefficient, or non-productive pathways dominate it's excited state reactivity. Because of this, strongly absorbing **dye** compounds are added that absorb light with a much greater extinction coefficient. These species are often only present in very small substoichiometric amounts. A dye can be chosen for its absorption wavelength as well as the available deactivation pathways of the excited state, providing vectors for control of the selectivity of a photochemical reaction.

If a dye reacts through photodissociation to give neutral radical species, it is called a **photoinitiator**. The dye is usually consumed in these reactions, but the radicals generated can initiate free-radical chain reactions, leading to quantum yields much greater than 1. This means that substoichiometric amounts of photoinitiator can be added and the reaction can still be very atom efficient.

If a dye reacts through electron transfer (photoreduction or photooxidation) it is a **photocatalyst**. Photoredox chemistry can be made catalytic with the addition of a sacrificial reductant or oxidant to the reaction mixture, allowing the ground state dye to be regenerated. Often very small amounts of **photocatalyst** are required to achieve good yields.

A dye that reacts preferentially by energy transfer is called a **photosensitiser**. Photosensitisers are regenerated directly without additional reagents, and again are only required in very small catalytic amounts. The mechanism of photosensitisation is discussed in Section 1.2.3. in the context of the specific case relevant to this Thesis – photosensitised generation of singlet excited state dioxygen.

In summary, for a photochemical reaction to be useful synthetically, the following conditions must be filled:

1. One or more of the components of the reaction should have an accessible electronic excited state, accessible through absorption of a visible or ultraviolet photon.
2. The extinction coefficient of this transition should be large to allow efficient light absorption and good energy efficiency.
3. The excited state generated should react selectively *via* one productive photochemical pathway, with as small a contribution from non-productive pathways as possible, giving a high quantum yield.

In addition to these conditions specific to photochemistry, the usual factors affecting the efficiency and selectivity of ground state chemical reactions also apply, meaning that achieving high yields in photochemical processes is the result of interplay of many parameters.

Section 1.2.2: Structure and Properties of Singlet Oxygen.

Molecular dioxygen, somewhat unusually for a diatomic molecule, exists in its ground state with a triplet electronic configuration, referred to in this text as triplet oxygen, $^3O_2$. The two degenerate highest occupied molecular orbitals (HOMOs) of $^3O_2$ each contain one of two unpaired electrons whose spins are oriented parallel to each other, providing a net electron spin and paramagnetic moment.[89-90] Since most organic substrates exist in a singlet ground state, reaction between these compounds and ground state O_2 would involve a change of total electron spin along the reaction co-ordinate and so violate the **spin selection rule**. Many potential oxidation reactions using $^3O_2$ which would be strongly favourable

considering only thermodynamics are precluded by the need for spin or electron transfer processes to occur before any bonds can be formed. This may help to prevent lab fires, but also limits the use of $^3O_2$ as an atom economic oxygen source for synthesis.[91]

Fortunately, other electronic states of dioxygen exist which can react spontaneously with organic molecules.[89-90, 92-93] O_2 has two low energy singlet excited states, in which all electron spins are coupled. The three electronic configurations of O_2 are shown with the term symbols describing them in Figure 5.

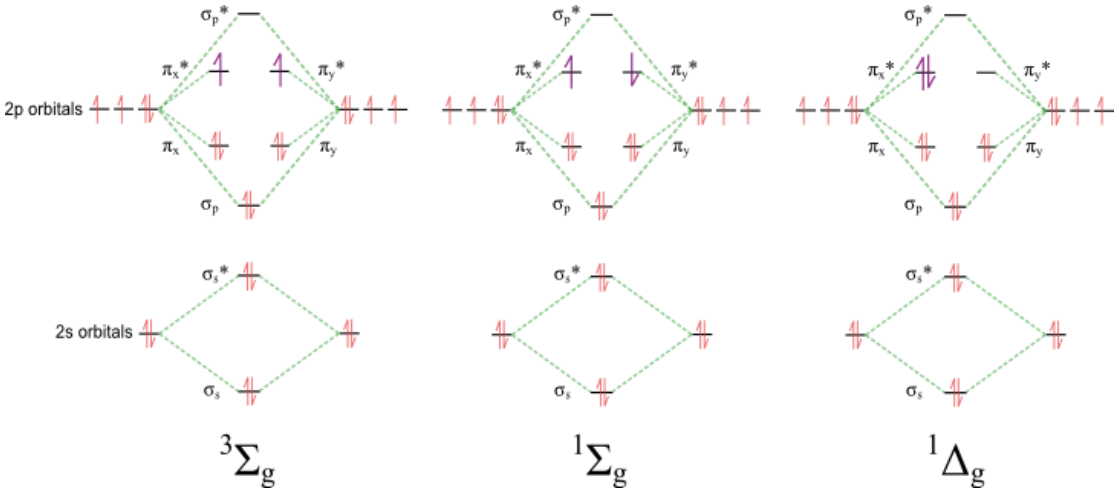


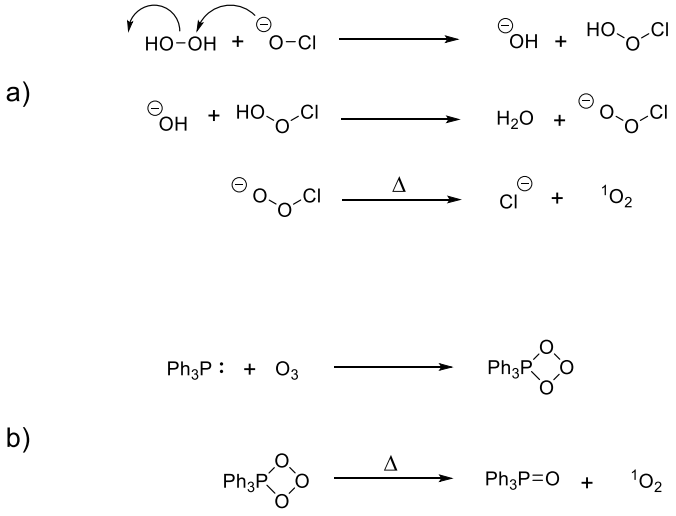
Figure 5: The triplet ground state (left) and two singlet excited states of dioxygen. The lower energy and longer lived $^1\Delta_g$ state (right) is the active species in singlet oxygen chemistry.

The higher energy $^1\Sigma_g$ state, like $^3O_2$ ($^3\Sigma_g$), has two partially filled HOMOs, although unlike $^3O_2$ the spins of these electrons are oriented antiparallel leading to a net spin of zero. This state is short-lived, with lifetimes in the order of 10^{-9} seconds since it can relax through spin-allowed radiative emission to the lower energy $^1\Delta_g$ state. The $^1\Delta_g$ configuration of O_2 has both highest-energy electrons paired in just one of the two frontier orbitals, with the second orbital completely empty. This gives the $^1\Delta_g$ state the property of being **ambiphilic**, *i.e.* simultaneously a strong nucleophile and a very potent electrophile. The $^1\Delta_g$ state in isolation has no spin-allowed relaxation processes and so a correspondingly long lifetime, in the

order of 10^{-4} seconds in the gas phase.[94] This makes it the more synthetically relevant singlet configuration of dioxygen, and is the configuration referred to in this text as singlet oxygen, $^1O_2$. In solution, the lifetime of $^1O_2$ varies greatly, dependent on the presence of species able to participate in non-radiative vibrational or energy transfer relaxation processes.[95-97] The factors affecting the lifetime and rate of reaction of $^1O_2$ are discussed further in Section 1.2.3.

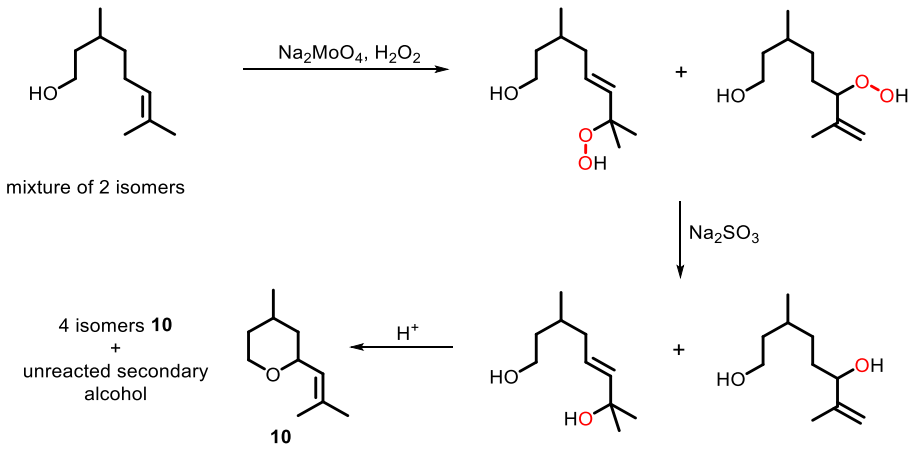
Section 1.2.3: Generation of Singlet Oxygen.

Singlet oxygen can be generated through both chemical and photochemical means. The chemical methods, some of which are shown in Scheme 11, all rely on the thermal degradation of an unstable precursor or intermediate, for which generation of $^3O_2$ would involve a spin-forbidden process. Scheme 11a shows the reaction of hydrogen peroxide with a hypochlorite salt.[98] Nucleophilic attack of the hypochlorite anion on hydrogen peroxide is thought to generate an unstable chloroperoxide anion, which would exist in a singlet ground state. Thermal decomposition gives the chloride anion, with a closed-shell singlet electron configuration, and a molecule of O_2.[99]



Scheme 11: Two thermal methods for generating $^1O_2$ – a) oxidation of hypochlorite with hydrogen peroxide and b) ozonolysis of triphenylphosphine.

Since a singlet molecule cannot react to form a singlet species and a triplet species without a change in spin multiplicity, the O_2 molecule is generated in a singlet excited state. Similarly, Scheme 11b shows the ozonolysis of phosphines, initially giving a singlet phosphine ozonide, which again degrades thermally, giving a phosphine oxide and $^1O_2$.[100-101] Neither method shown in Scheme 11 is ideal from a Green Chemistry perspective – the reaction shown in 11a involves storing large amounts of peroxide and hypochlorite, both reactive oxidants, and the reaction shown in 11b gives a full molar equivalent of phosphine oxide waste per molecule of $^1O_2$ generated, which would result in a superstoichiometric amount of waste produced compared to the desired product. This is contrary to the principle of atom economy outlined discussed throughout Section 1.1. Singlet oxygen can also be generated by disproportionation of hydrogen peroxide to $^1O_2$ and two molecules of water using catalytic amounts of molybdenum(IV) oxide.[102-104] This has been successfully applied on an industrial scale to the synthesis of the valuable scent compound rose oxide **10**, shown in Scheme 12.[105]



Scheme 12: Large scale production of valuable scent compound rose oxide (10) using molybdate-catalysed disproportionation of hydrogen peroxide.

Whilst preferable to the methods described above, catalyst loadings are often high and the molybdate catalyst can induce side reactions, including rearrangement of the peroxide reaction products.[106]

A much better method of $^1O_2$ generation from a Green Chemistry perspective uses photochemistry. Singlet oxygen can be formed *via* direct radiative excitation of $^3O_2$ to the $^1\Sigma_g$ state. However, reactions involving a change of electron spin are forbidden by the **spin selection rule**. The spin forbidden nature of this excitation leads to a very poor extinction coefficient and makes this an inefficient option in terms of rate and energy consumption. Alternatively, $^1O_2$ can be accessed indirectly *via* photosensitisation, as shown in Figure 6.[90, 93, 107-110]

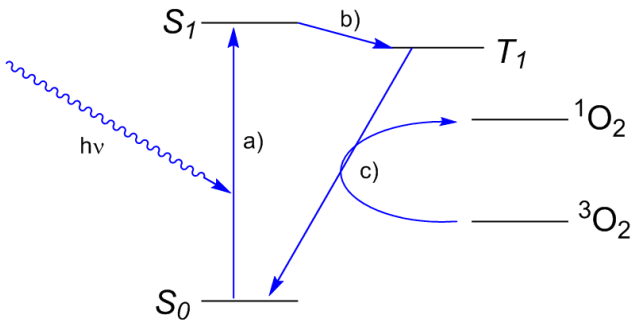
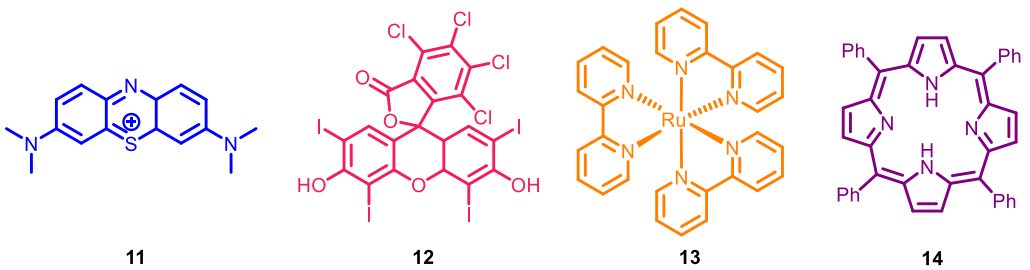


Figure 6: Photochemical generation of singlet oxygen by photosensitisation - a) a photon is absorbed, taking the dye to the singlet excited state S_1 b) intersystem crossing occurs to give the triplet excited state T_1 which c) transfers its excitation energy though collision to a ground state dioxygen molecule, generating $^1O_2$ and returning the dye to its ground state S_0.

Figure 6 shows the energy levels of a generic photosensitiser, each representing an electronic configuration. Under low-irradiation, standard temperature conditions the dye will exist almost exclusively in its ground state, S_0. When exposed to light of the correct wavelength excitation can occur to the singlet excited state S_1. Some of the time, this will be followed by **inter-system crossing** to the triplet excited state T_1. This triplet state is then able to react with $^3O_2$ *via* an energy transfer to generate $^1O_2$, with the photosensitiser simultaneously relaxing back to the ground state S_0. The photosensitiser acts as a catalyst and so photochemical generation of

$^1O_2$ is usually a low-waste procedure. The high rate of absorption by the ground state and rapid quenching of T_1 by $^3O_2$ mean most photosensitisers have very high turnover numbers and so are needed in very small amounts. The limiting factor for turnover and so for the rate of $^1O_2$ generation is the efficiency of the intersystem crossing from S_1 to T_1.[109-110]

Intersystem crossing is the direct transition from a singlet to triplet electronic configuration (or *vice versa*) occurring without intermediates. By its nature this transition is spin forbidden, and therefore slow. Transition from S_1 to T_1 should be impossible were it not for the fact that the spin and orbital angular momenta of these states are coupled. The mixing of spin and orbital magnetic moments mean that rather than a pure singlet to triplet transition, the molecule undergoes a not-quite-singlet to not-quite-triplet transition, which does not violate the spin selection rule.[109] Compared to direct excitation of ground state $^3O_2$, which is almost entirely impeded by its spin-forbidden nature,[111] many photosensitisers show strong intersystem crossing and give good quantum yields for the T_1 state, due to strong spin-orbit coupling. Figure 7 shows several commonly used photosensitisers – methylene blue (MB, **11**), rose bengal (RB, **12**), ruthenium(II) tris(2,2'-bipyridyl) chloride (Ru(bpy)$_3$, **13**) and *meso*-tetraphenylporphyrin (TPP, **14**):



11 **12** **13** **14**

Figure 7: Several common photosensitisers. All show strong spin-orbit coupling leading to efficient triplet state population.

The strength of the spin-orbit coupling in a photosensitiser can be affected by several factors.[93] Firstly, where the triplet state is close in energy to the singlet

excited state, the rate of intersystem crossing is enhanced. This corresponds to a similarity in structure between the two states. Dyes with extended π-systems, particularly those containing nitrogen atoms which have π-nonbonding orbitals, tend to have a small singlet-triplet energy gap and there is considerable overlap between the vibrational modes of the two electronic states. This means that little or no energy is lost during internal conversion and the spin-orbit coupling is strong. Another important factor is the presence of heavy atoms, of spin-orbit coupling increases with nuclear charge. Three of the photosensitisers in Figure 7 contain heavy atoms – sulfur in methylene blue, iodine in rose Bengal and the ruthenium metal centre of $[Ru(bpy)_3]^{2+}$. The final example TPP has no heavy atoms but a small enough n → π* transition to allow for an efficient triplet state quantum yield.

Deactivation, or **quenching** of singlet oxygen is the collective term given to any process which competes with reactive pathways by returning $^1O_2$ to its ground state. The long radiative lifetime of $^1O_2$ in isolation (see Section 1.2.2) means that the actual lifetime of singlet oxygen is determined by interactions with other molecules.[89] In solution, solvent molecules greatly outnumber other species present and so contribute most strongly to quenching. The lifetime of $^1O_2$ shows a correspondingly large solvent dependence, varying from microseconds in water to milliseconds in chlorinated solvents, as shown in Table 2.[96, 112-113] Solvent-mediated quenching takes two forms – radiative and non-radiative. The rate of radiative quenching depends on the extent to which the solvent can perturb the spin forbidden $^1O_2 \rightarrow {}^3O_2$ transition. This has been reported by several groups as being dependent on the bulk polarizability of the solvent. Several interpretations of this have been put forward, most of which assume the formation of transient solvent/$^1O_2$ exciplexes on collision.[96] These exciplexes have different transitions to isolated $^1O_2$ and so provide a pathway to relaxation.

Solvent	Singlet oxygen lifetime (μs)
gas phase	> 1 hour
carbon tetrachloride	59000
hexafluorobenzene	21000
chloroform-*d*	7000
acetone-d_6	992
benzene-d_6	681
chloroform	229
dichloromethane	99
acetonitrile	77
deuterium oxide	68
acetone	51
ethyl acetate	45
benzene	30
toluene	29
methanol	10
water	3

Table 2: The lifetimes of $^1O_2$ in a range of solvents. Chlorinated and deuterated solvents give the longest lifetimes but are undesirable from a Green Chemistry perspective.

Non-radiative solvent-mediated quenching is much more significant in determining the lifetime of $^1O_2$ in solution. This involves the transfer of electronic excitation energy into vibrational modes of the solvent.[97] The dependence of bond vibration energy on bond strength explains many of the trends seen in Table 2, particularly that deuterated[114] and halogenated[112] solvents give the longest $^1O_2$ lifetimes, and that the number of C-H and O-H bonds with high energy vibrations correlates negatively with $^1O_2$ lifetime.[96-97]

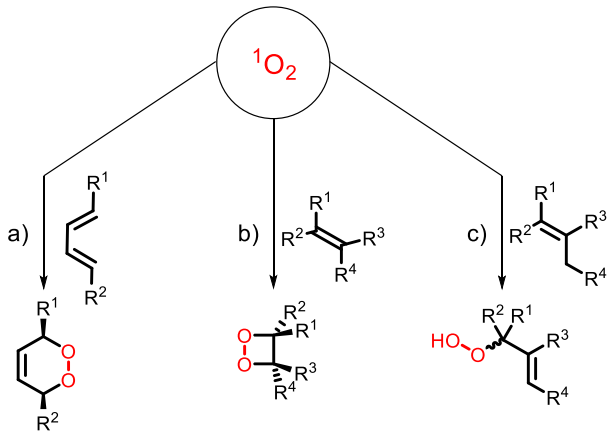
Other molecules present in solution can have a significant effect on the lifetime of $^1O_2$, particularly amines, which are reported as potent inhibitors of $^1O_2$ chemistry.[115-118] Molecules in excited triplet states can quench $^1O_2$ by energy transfer in the reverse process to its formation. This means that for photosensitised

generation of $^1O_2$, higher concentrations of sensitiser can sometimes inhibit the reaction rather than promote it. Species with low energy triplet excited states can quench $^1O_2$ by energy transfer, for example β-carotene.[89, 119] All of these processes will reduce the rate and quantum yield of a photo-oxygenation and should be avoided.

Finally, even in the gas phase, $^1O_2$ lifetime is limited by the ability of two $^1O_2$ molecules to self-quench through spin-allowed electron exchange. This is accompanied by the emission of light at 633.4 nm.[96]

Section 1.2.4: Reactions of Singlet Oxygen.

Singlet oxygen primarily reacts as an electrophile in addition reactions to electron rich C=C π-bonds.[120-122] The three most synthetically useful reactions of $^1O_2$ are shown in Scheme 13. They are a) endoperoxide formation with a diene, b) dioxetane formation with an alkene and c) reaction with alkenes to give allylic hydroperoxides.



Scheme 13: The three most synthetically useful reactions of $^1O_2$ – a) [4+2] reaction with dienes b) [2+2] reaction with alkenes and c) allylic 'ene' reaction with alkenes.

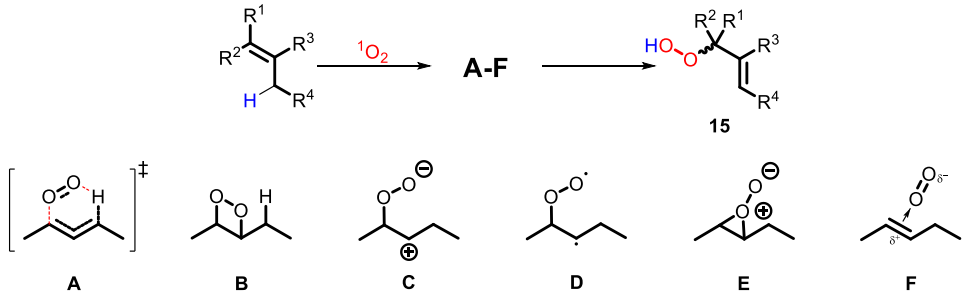
These are historically referred to as the [4+2], [2+2] and Schenck 'ene' reaction respectively, although as discussed later in this Section there is considerable

evidence that none of these reactions proceeds *via* the concerted mechanism that these labels might suggest. All three of these reactions have 100% atom economy, which is a major benefit from a Green Chemistry perspective, particularly considering the low atom economy and high risk associated with many oxidation reagents (see Section 1.1.2). The reaction of $^1O_2$ most relevant to the work presented in this thesis is the Schenck 'ene' reaction (Scheme 13c). Below is a detailed discussion of the mechanism of this reaction and the implications of this mechanism on its selectivity.

Additionally, $^1O_2$ reacts readily with lone-pair bearing heteroatoms, including sulfur,[123] phosphorus[101] and nitrogen.[115] The synthetic applicability of these reactions is low, though they must be considered as potential routes for side product formation in reactions of $^1O_2$.

Mechanism of the Schenck reaction.

In general terms, the Schenck reaction is the 1,3 reaction of olefins with $^1O_2$ to form allylic hydroperoxides such as **15** (Scheme 14). The reaction is deceptively complex, with many stereochemical and mechanistic intricacies.[92, 120, 122, 124-125]

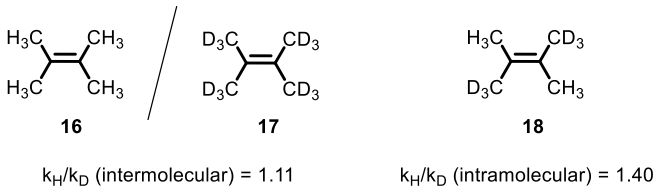


Scheme 14: The Schenck reaction of alkenes with $^1O_2$, and the six proposed intermediates A-F through which the reaction might proceed.

As well as the concerted pericyclic mechanism (Scheme 14, **A**) of the archetypical Alder ene reaction,[49] stepwise mechanisms have been proposed passing through a variety of intermediates (Scheme 14, **B**-**F**).[126] Extensive computational studies

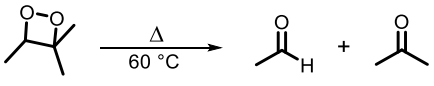
have been undertaken and have provided support for all of these pathways depending on the method used, reflecting the difficulty of modelling excited state molecules such as $^1O_2$. Therefore, conclusions must mainly be drawn based on experimental evidence.

If the Schenck reaction were to proceed through a pure pericyclic transition state **A** like a true ene reaction, all the bond formation and breaking occurs in a concerted fashion, including the breaking of the C—H bond.[127-128] It was proposed by Stephenson and co-workers that if this were the case, the intermolecular kinetic isotope effect (KIE) between **16** and **17** would be identical to the intramolecular KIE measured for **18**.[129] They showed this not to be the case, and so argued in favour of separate rate-determining and product-determining steps, as for intermediates **B**-**F** (Scheme 15).



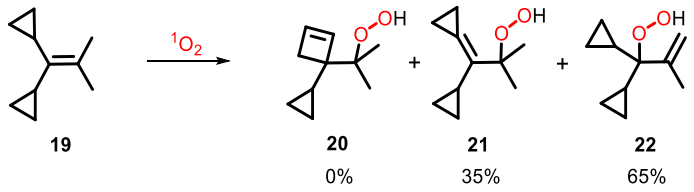
Scheme 15: Kinetic isotope effect (KIE) experiments performed by Stephenson *et al.* showing different inter- and intramolecular KIEs, supporting a multistep reaction mechanism for the Schenck reaction.

The dioxetane species such as intermediate **B** are the end products of the [2+2] reaction of $^1O_2$ with alkenes (Scheme 13b). It was therefore proposed that they might form in the same reaction with all alkenes, and subsequently rearrange to give hydroperoxides.[122] However, thermal decomposition of dioxetanes (Scheme 16) gives carbonyl species rather than hydroperoxides, ruling out dioxetanes as intermediates.[130]



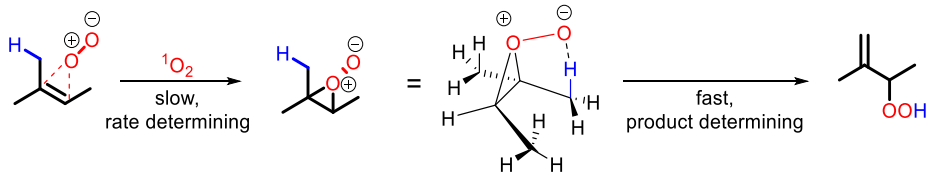
Scheme 16: Thermal decomposition of dioxetanes gives carbonyl compounds rather than allylic hydroperoxides, ruling these out as intermediates for the Schenck reaction.

The Schenck reaction is observed to be suprafacial, with $^1O_2$ addition and H abstraction occurring on the same face of the alkene.[129, 131] This argues against intermediates with free rotation such as **C** or **D**. Furthermore, Markovnikov regioselectivity, which would be expected for these kinds of intermediates, is not usually observed.[132] Some further evidence against the formation of diradical species like **D** can be drawn from the experiments performed by Frimer *et al.* on vinylcyclopropanes such as **19** (Scheme 17). If the oxidation were to proceed through a diradical mechanism then a significant amount of ring expansion product **20** would be expected compared to allylic hydroperoxides **21** or **22**. No **20** was observed in Frimer's experiment, discounting the radical route.[133]



Scheme 17: Schenck reaction of vinylcyclopropane 19, showing no formation of cyclobutene 20 and discounting the diradical intermediate D.

Any sensible mechanism for this reaction must explain both its suprafacial nature, and the kinetic isotope effect data suggesting that hydrogen abstraction occurs on a secondary step. It is now supposed that the reaction proceeds in two steps through an intermediate such as **E** or **F**, with a concerted rate determining first step and a fast second step involving formation of the hydroperoxide O-H bond.[131]



Scheme 18: The most commonly accepted perepoxide mechanism for the Schenck reaction, showing different rate and product determining steps as well as suprafacial stereospecificity.

The two cases **E** and **F** are very similar, differing only in that **E** is a perepoxide species with full C-O bond formation and formal charges on the oxygen atoms, whereas **F** is an exciplex for which the extent of bond formation is lower. The structural implications for the stereo and regioselectivity are the same in both cases, and it is possible that the true intermediate has a structure somewhere in between the two.[134-135] For the sake of ease of representation, the following discussion on selectivity in the Schenck reaction will assume intermediate **E** as the correct structure. A generalised mechanism of this reaction is given in Scheme 18.

Selectivity in the Schenck reaction.

The selectivity of the Schenck reaction is complex but predictable, and the factors affecting it are well known. Because the singlet oxygen molecule itself is small and devoid of any stereochemical features, any selectivity observed in its reactions comes solely from direction by stereochemical features of the substrate. Four stereochemical features of the olefin substrate control the outcome of the Schenck reaction and are shown in Figure 8.[125, 136]

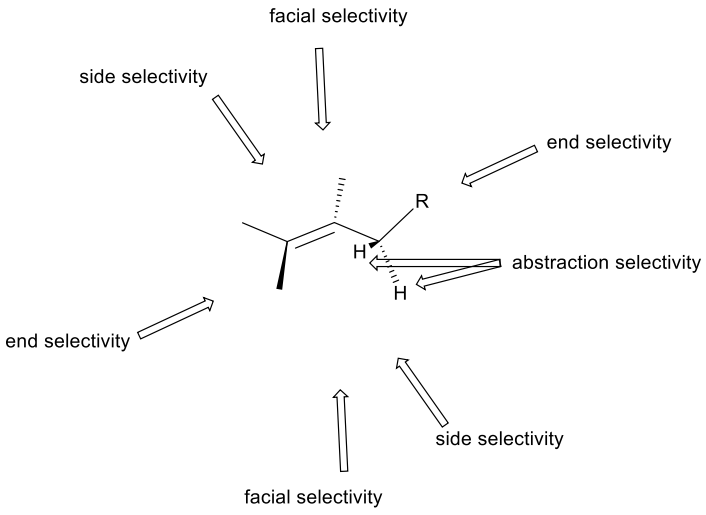


Figure 8: The stereochemical features of the olefin substrate which control the outcome of the Schenck reaction.

a) **End selectivity** – a preference for the end of the substrate's C=C double bond to which the C—O bond forms in the product.

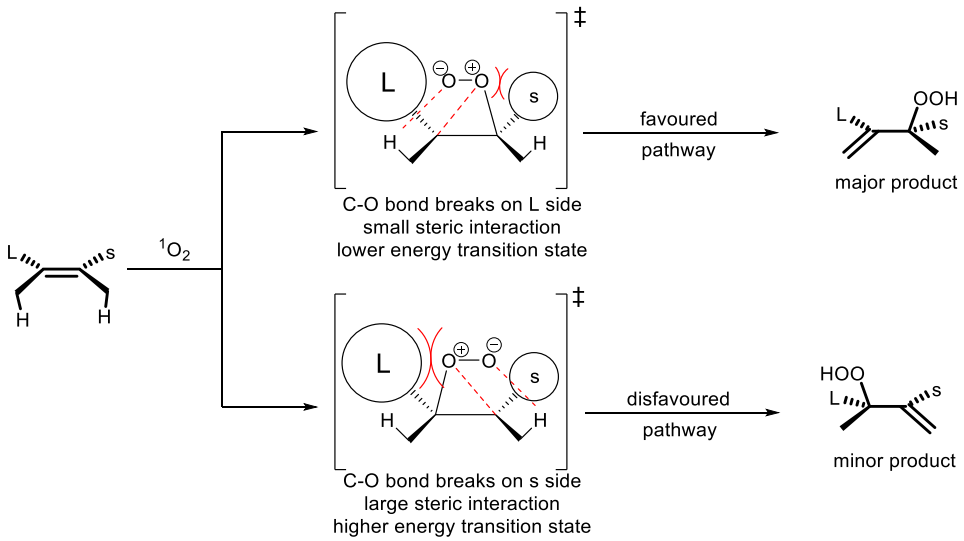
b) **Side selectivity** – the side of the double bond from which a hydrogen is abstracted.

c) **Facial selectivity** – whether $^1O_2$ approaches the substrate preferentially from the top or bottom face.

d) **Abstraction selectivity** – preference for the removal of one of a pair of diastereotopic hydrogens.

The first two features determine the regiochemistry of the product, whilst the last two determine the stereochemistry.

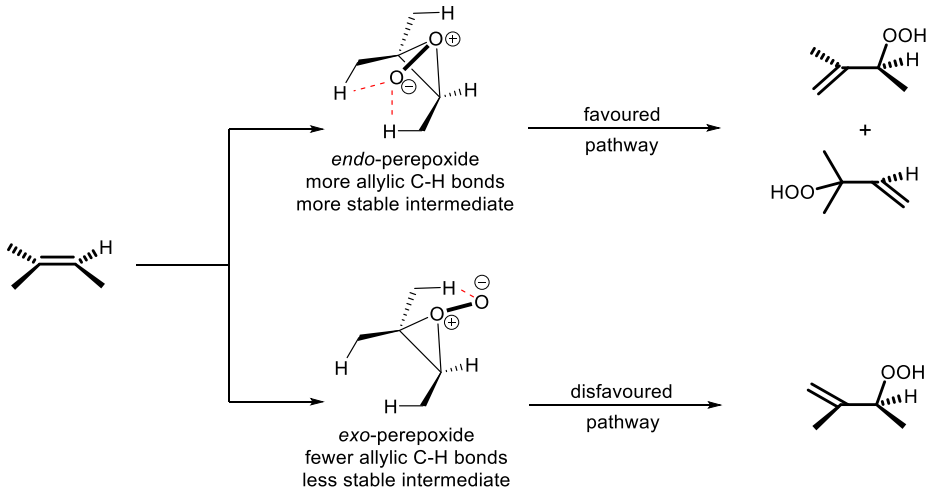
End selectivity – The end selectivity is mainly governed by steric interactions with the allylic substituents. As the perepoxide intermediate rearranges to the allylic hydroperoxide product, there is a lengthening of the C—O bond on the side where hydrogen abstraction takes place.



Scheme 19: End selectivity in the Schenck reaction resulting from the geminal ('large group non-bonding') effect.

The transition state with the lowest energy is that with the lengthened C—O bond on the same side as the largest allylic group, thus hydrogen abstraction takes place preferentially from that side.[137-138] This is commonly referred to as the **geminal effect**, or the 'large group non-bonding' effect. It is important to note that it is not the end with the most substituents that is favoured, but the end with the largest substituent.

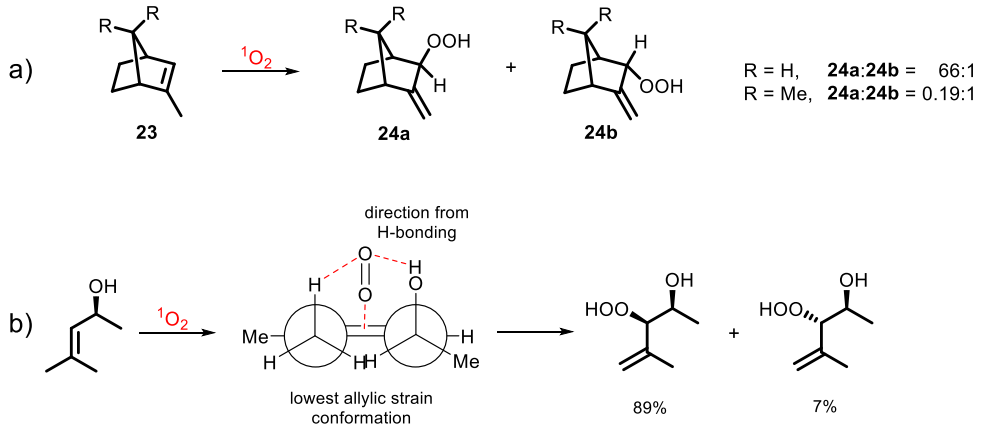
Side selectivity – Schenck reactions on highly substituted olefins show a strong selectivity for abstraction from the more substituted side of the double bond.[124, 139] This is known as the ***cis*-effect** and was originally observed separately by Foote and Conia in studies on enol ethers.[140-141] Various groups have proposed explanations for the *cis*-effect, using both experimental and theoretical evidence.[142-143] All of these explanations predict favourable interactions between the perepoxide tail oxygen and the allylic C—H bonds. The *endo* perepoxide has more of these interactions than the *exo* and so is the more stable intermediate, and so the *endo* pathway accounts for a greater proportion of products formed.



Scheme 20: The *cis*-effect – perepoxide intermediates with more allylic C—H bonds are more stable, leading to a preference for alkene formation on the more substituted side.

Facial selectivity – diastereoselectivity can be achieved in the Schenck reaction where there is a preference for $^1O_2$ to approach one face of the alkene over the

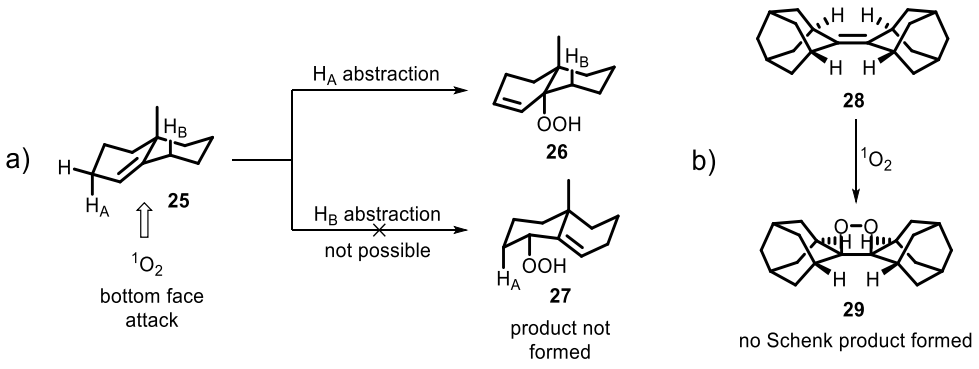
other. This requires chiral features in the substrate.[136] Direction can be due to steric factors, with one face of the alkene blocked by another group, as in the photo-oxygenation of norbornene derivatives **23** shown in Scheme 21a.[144] Here, singlet oxygen adds preferentially to the less hindered face, which can be switched by changing the bridgehead substituent. Facial selectivity has also been observed in substrates with a chiral face bearing a hydrogen bond donating group; the Lewis basic negative end of $^1O_2$ can act as an H-bond acceptor.[145-146] In this case the direction is attractive, and $^1O_2$ adds to the face closest to the donor group (Scheme 21b). Hydrogen bonding can also impart side selectivity and to a lesser extent, end selectivity. The synthesis of the antimalarial natural product artemisinin, discussed in detail in Chapter 2, involves a highly face-selective Schenck reaction.



Scheme 21: Examples of facial selectivity in the Schenck reactions of a) norbornene derivatives, directed by steric interactions and b) allylic alcohols, directed by hydrogen bonding.

Abstraction selectivity – competition in the rates of abstraction of different allylic hydrogens can also provide diastereoselectivity in the Schenck reaction. The formation of the product π-bond requires that the allylic C—H of the substrate can adopt a conformation that is perpendicular to the plane of the alkene, or *syn*-periplanar to the C—O bonds of the perepoxide intermediate. In cyclic substrates with rigid conformation, this requirement can have a strong effect on the

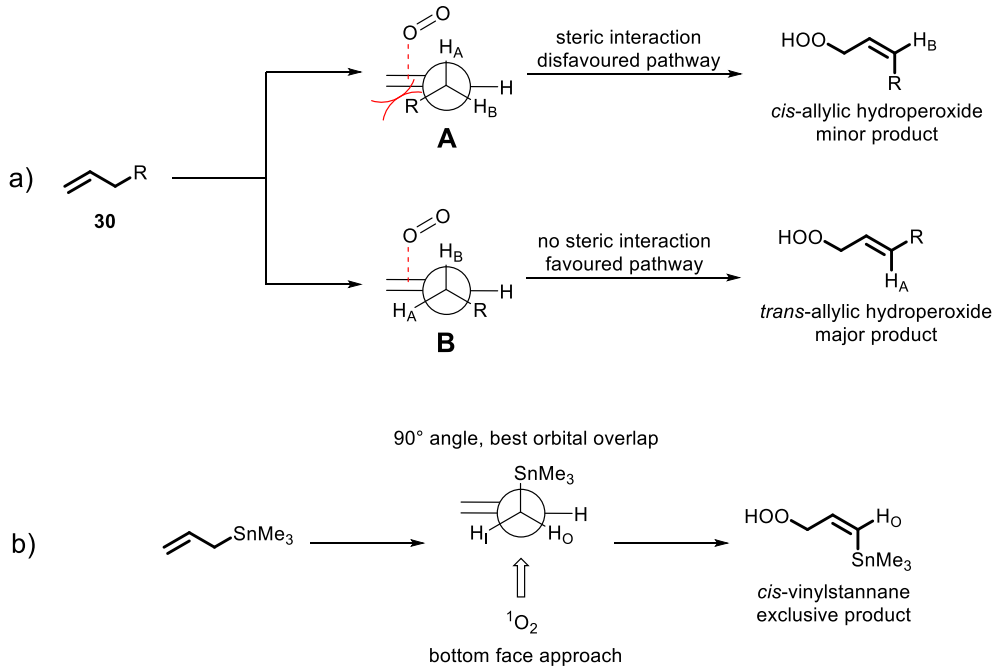
regioselectivity, or even prevent the Schenck reaction from occurring at all. The photo-oxygenation of substrate **25** (Scheme 22) which showed a preference for $^1O_2$ approach to the bottom face, gave only product **26** and none of the regioisomer **27**, due to the inability of hydrogen H_B to adopt the required conformation. In the photo-oxygenation of *bis*-adamantenyl alkene **28**, none of the allylic hydrogens can adopt the correct conformation and the [2+2] mode of reactivity is observed instead, giving dioxetane **29**.[147] In acyclic substrates, a strong preference is observed for the formation of trans-alkenes. This is again due to the conformational requirement for H-abstraction, in combination with steric factors. On a substrate such as **30** (Scheme 23a), there are two enantiotopic hydrogens in the allylic position. This provides two possible geometries for the transition state, **A** and **B**. In **A**, leading to the *cis*-alkene, there is a considerable steric interaction between the R group and the rest of the molecule. No such interaction exists in **B**, making this the favoured conformation. Abstraction of H_B leads to the observed *trans*-selectivity.[148]



Scheme 22: Examples of abstraction selectivity in cyclic substrates – a) providing regioselectivity in the photo-oxygenation of decalane 25 and b) preventing the photo-oxygenation of *bis*-adamantenyl alkene 28.

Work presented in Chapter 4 on the photo-oxygenation of acyclic terpenes takes advantage of this effect, giving exclusively *trans*-allylic hydroperoxides. An exception to this rule is the photo-oxygenation of allylic systems bearing a group that can stabilise a ß-positive charge, e.g. allyl silanes or allyl stannanes. In these

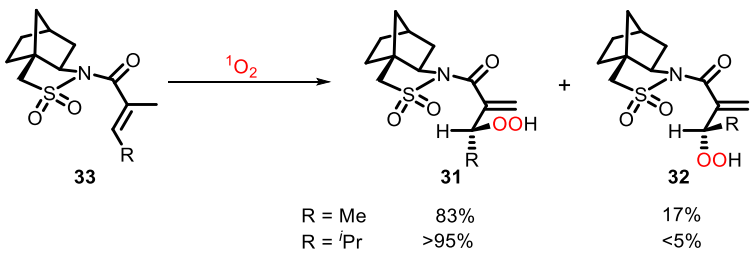
systems, the most favourable orientation of the allylic substituent is perpendicular to the alkene, and abstraction is from the 'inside' hydrogen H_I, stereospecifically giving *cis*-alkenes.[136]



Scheme 23: Abstraction selectivity in acyclic substrates – a) leading to *trans*-selectivity in most instances and b) the *cis*-specificity of photo-oxygenations of vinyl stannanes or silanes.

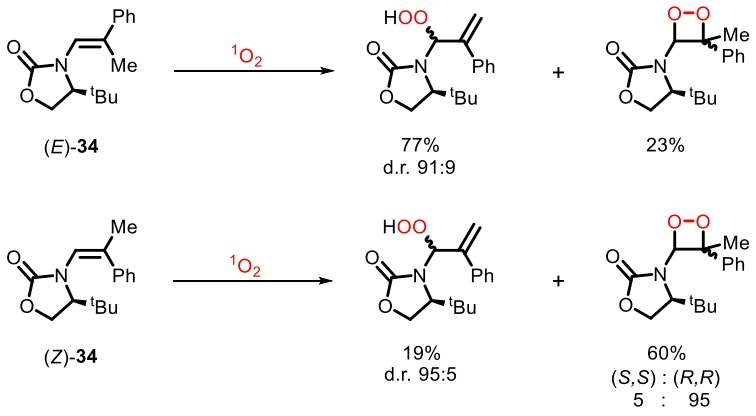
Diastereoselective Schenck reactions using auxiliaries

Although the regiochemistry and diastereoselectivity of the Schenck reaction can be easily influenced, very few successful stereoselective examples of this reaction on achiral substrates have been reported. Most work involves the use of chiral auxiliaries, where a chiral group is attached to a substrate prior to photo-oxygenation, then removed afterwards.



Scheme 24: Saha-Möller *et al.*'s stereoselective photo-oxygenation of 33 using Oppolzer's auxiliary.

Saha-Möller and co-workers received an impressive 95:5 diastereomeric ratio of allylic hydroperoxides **31** to **32** from the photo-oxygenation of **33**, bearing Oppolzer's camphorsultam auxiliary (Scheme 24).[149] This equates to an enantiomeric excess of 90% upon removal of the auxiliary. Adam *et al.* have extensively studied the photo-oxygenation of enecarbamates such as **34** and again received diastereomeric ratios of up to 95:5, though the yield was lowered by competition with the [2+2] mode of reactivity.[150] The competition arises from the directing effect of the nitrogen lone pair, so the Schenck product is favoured for the (*E*)-enecarbamate with the methyl and carbamate groups on the same side (Scheme 25).[151]



Scheme 25: Adam's work on the photo-oxygenation of enecarbamates, showing high diastereomeric ratios for the Schenck products, as well as mode selectivity dependant on the substrate geometry.

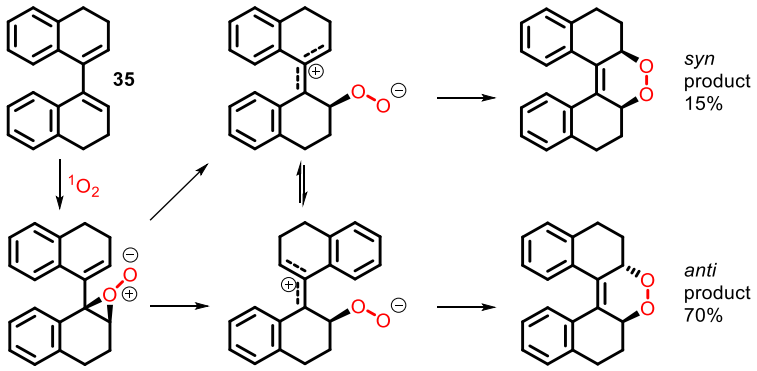
Whilst the diastereoselectivities achieved by these methods are impressive, the inclusion of these extra concession steps (see Section 1.1.2) reduces the efficiency of a synthesis, and creates unnecessary waste, so is less desirable from a Green Chemistry perspective.

Several asymmetric reactions of singlet oxygen have been performed by performing the reaction in a chiral environment, or by generating $^1O_2$ at a chiral surface.[152-154] Superstoichiometric quantities of chiral materials are required for good enantioselectivity, but they require no extra chemical steps and reuse of the chiral

element is easier than for auxiliary-based strategies. A truly catalytic asymmetric Schenck reaction has still not been achieved.

Mechanism and Selectivity in other Reactions of Singlet Oxygen.

The [4+2] reaction of dienes occurs *via* the same initial perepoxide formation as described for the Schenck reaction above.[155] The perepoxides formed would be resonance stabilised by the conjugated alkene, rearranging to give the 2,3-dehydro-1,4-endoperoxides (hereafter 'endoperoxides') observed. This mechanism explains the observation of Delogu *et al.* that whilst this reaction is usually suprafacial, giving *syn*-endoperoxides, in strained substrates such as bisdialine **35** mainly the *anti*-endoperoxide is observed (Scheme 26). A truly pericyclic (concerted) [4+2] reaction would always be suprafacial.[156]



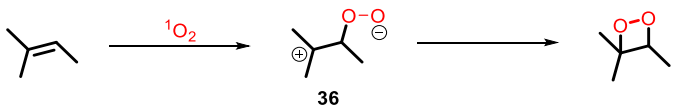
Scheme 26: Photo-oxygenation of bisdialine 35 giving the *anti*-endoperoxide in preference to the *syn*, suggesting that the [4+2] reaction of $^1O_2$ with dienes is not concerted.

Facial selectivity, just as in the Schenck reaction, can be caused by steric hindrance of one face,[157] or by preferential approach of $^1O_2$ to faces bearing hydrogen bond donating groups, which is reduced when in co-ordinating solvents such as methanol.[158]

Asymmetric examples of endoperoxide formation have been reported on substrates bearing chiral auxiliaries. Adam *et al.* showed that dienes bearing chiral oxazolidine auxiliaries gave good to excellent facial selectivity, depending on

the substituents.[159] This can be rationalised by considering the steric interaction of the substituents with the approaching singlet oxygen molecule. More recently, Bach and co-workers reported the use of a chiral hydrogen-bonding templating agent to provide enantioselectivity in the [4+2] photo-oxygenation of 2-pyridones without derivitisation of the substrate. The bulky template complexes to the substrate and selectively blocks one face. This is the furthest towards a catalytic asymmetric singlet oxygen reaction to date, though the template is required in superstoichiometric amounts with only 80-90% recovery after the reaction.[160]

The [2+2] formation of dioxetanes is thought not to proceed through the same perepoxide intermediate as the other two modes described, since the calculated energy barrier for direct rearrangement from perepoxide to dioxetane is high.[161] It has been proposed instead that dioxetane formation proceeds *via* zwitterionic intermediates such as **36** (Scheme 27).[162]

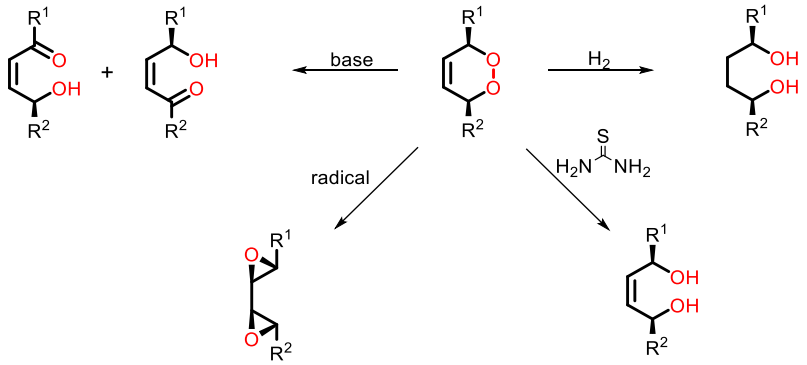


Scheme 27: The accepted zwitterionic mechanism for dioxetane formation in the [2+2] reaction of $^1O_2$.

This is supported by comparatively low rates, and the strong dependence on solvent polarity of the rate of the [2+2] reaction when compared to the Schenck or [4+2] modes of reactivity.[163-164] More polar solvents favour the [2+2] reaction to the point that it can even compete with the much faster Schenck reaction. Like all reactions of $^1O_2$, stereoselectivity is usually controlled by substrate geometry, although Adam *et al.* achieved high diastereoselectivities in the dioxetanes produced from enecarbamate **34** in the study shown previously in Scheme 25, implicating hydrogen bonding as the directing effect.[150]

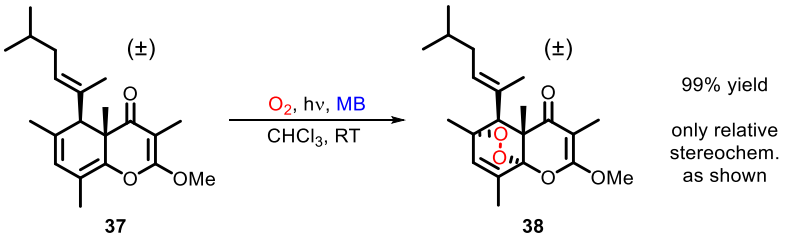
Section 1.2.5: Applications of Singlet Oxygen in Organic Synthesis.

Whilst the reaction of singlet oxygen with organic substrates is mostly limited to the three modes discussed in the previous Section, and modifications thereof, the utility of these reactions to the synthesis of complex molecules is much broader, since the hydroperoxides, endoperoxides and dioxetanes formed can be easily transformed into a wealth of oxygen-containing functional groups, as shown in Schemes 28, 35 and 38.[100, 165-166] This Section serves as a short review of the ways in which singlet oxygen chemistry has been strategically applied to the synthesis of natural products and drug candidates.



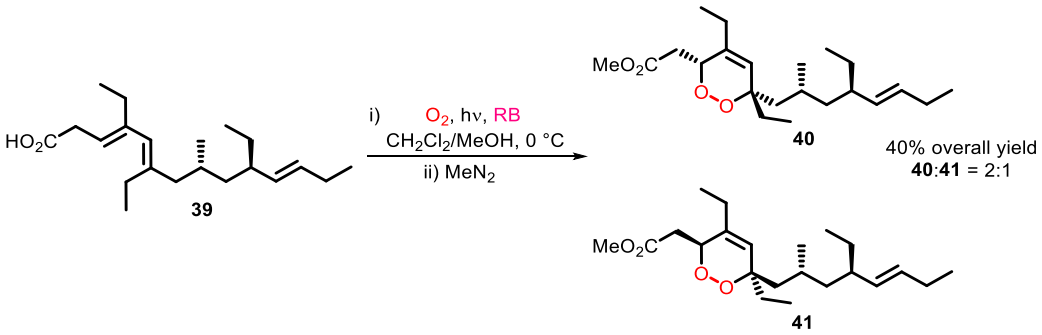
Scheme 28: Synthetically useful transformations of [4+2] photo-oxygenation products.

The most commonly used of the three modes of reactivity discussed here is the [4+2] addition of $^1O_2$ with dienes.[167] The endoperoxide products can be stable and are sometimes the target of a synthesis themselves, for example the photo-oxygenation of racemic (±)-tridachiahydropyrone **37** to (±)-oxytridachiahydropyrone **38** by Moses *et al.* The reaction proceeds in 99% yield in a fully stereoselective manner to give the relative stereochemistry shown in Scheme 29. The stereoselectivity results from steric direction of $^1O_2$ approach by the substrate.[168]



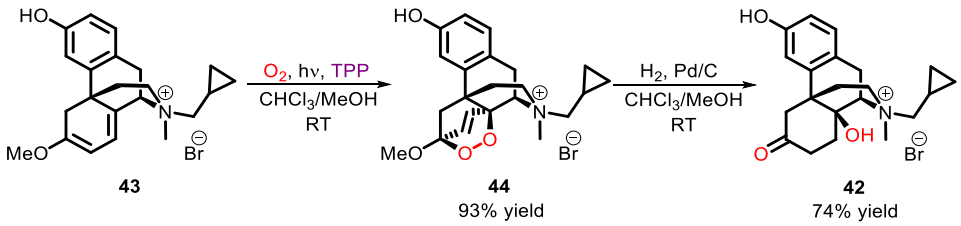
Scheme 29: A stereoselective [4+2] photo-oxygenation in Moses *et al.*'s synthesis of endoperoxide natural product (±)-oxytridachiahydropyrone 38.

In the stereodivergant synthesis of naturally occurring marine sponge endoperoxide **39** (Scheme 30) both endoperoxide isomers **40** and **41** were synthesised and used to assign the stereochemistry of the natural product.[169] Only a slight directing effect from the shape of substrate **39** was seen, resulting in a ratio of 2:1 **40**:**41**. The low yield of 40% was mainly due to further photo-oxygenations of the tail alkene.



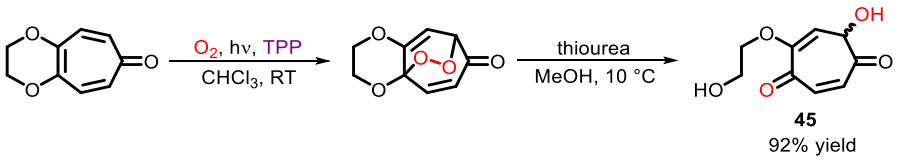
Scheme 30: Non-specific [4+2] photo-oxygenation in the synthesis of two isomeric marine sponge endoperoxides 40 and 41.

Reduction of the unsaturated endoperoxides can yield the corresponding diols with retention of the relative stereochemistry. Examples in synthesis include the synthesis of the opioid *(R)*-methylnaltrexone **42** (Scheme 31).[170] Attack of $^1O_2$ to the more hindered face of diene **43**, possibly directed by electrostatic interaction with the quaternary nitrogen, gave endoperoxide **44** in 93% yield. Hydrogenation of both the endoperoxide and the double bond in **44** using palladium(0) supported on carbon gave *(R)*-methylnaltrexone **42** in 74% yield.



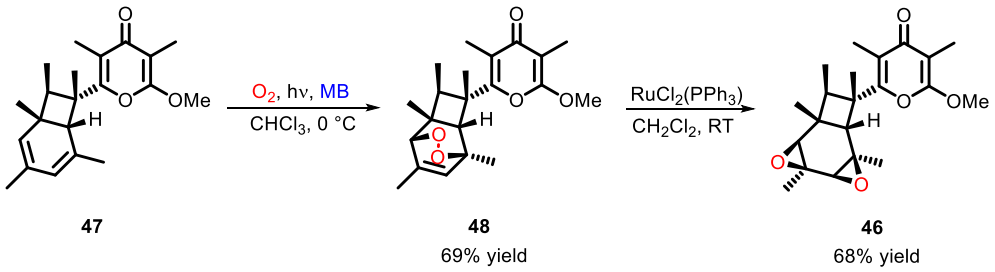
Scheme 31: Synthesis of *(R)*-methylnaltrexone 42 *via* [4+2] photo-oxygenation and reduction using hydrogenation over palladium(0).

Endoperoxides can be reduced selectively under milder conditions using stoichiometric amounts of thiourea, as demonstrated in the synthesis of tropolone compounds such as **45** by Daştan and Balci (Scheme 32). The non-selective nature of the photo-oxygenation was not an issue here due to rapid tautomerisation and racemisation of the product.[171]



Scheme 32: Selective O--O bond reduction using thiourea in the synthesis of tropolone species 45.

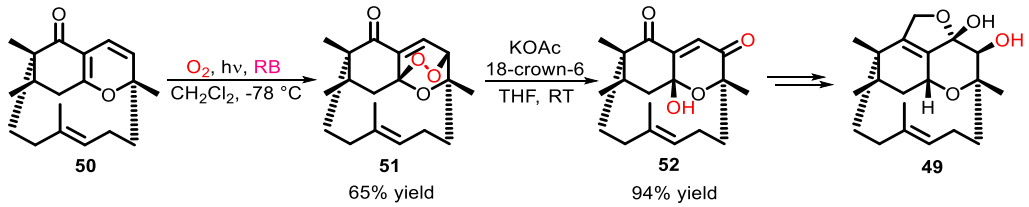
Radical rearrangement of the [4+2] photo-oxygenation products affords *syn*-diepoxides. something which was used to great effect in the synthesis of elysiapyrone A **46** by Barbarow *et al.* shown in Scheme 33:[172]



Scheme 33: Facially selective photo-oxygenation followed by rearrangement to *syn*-diepoxide natural product elysiapyrone A 46.

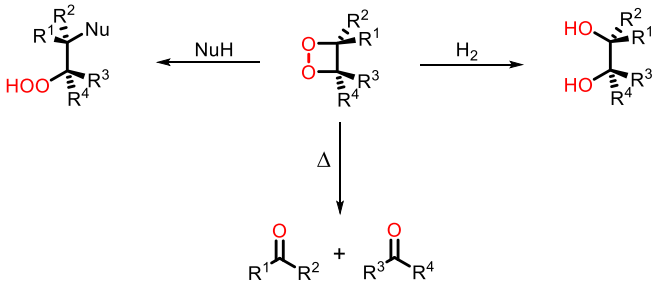
The photo-oxygenation proceeded *via* addition to the least hindered face of diene **47** as expected, and ruthenium(II) catalysed rearrangement of the resulting endoperoxide **48** gave the two epoxides in a suprafacial manner.

The base catalysed Kornblum-DeLaMare rearrangement leads to γ-hydroxy-*cis*-α,β-unsaturated aldehydes or ketones.[173-174] Where there is only one site for deprotonation, this can be regioselective. This rearrangement has been successfully applied to the synthesis of (±)-phomactin A, **49**, shown in Scheme 34. Photo-oxygenation of **50** selectively gave endoperoxide **51**. Deprotonation using potassium acetate / crown ether gave hydroxypyranone **52** in 94% yield. Twenty-four further steps afforded the product **49**.[175]



Scheme 34: Synthesis of (±)-phomactin A 49 *via* [4+2] photo-oxygenation and base-promoted Kornblum-DeLaMare rearrangement.

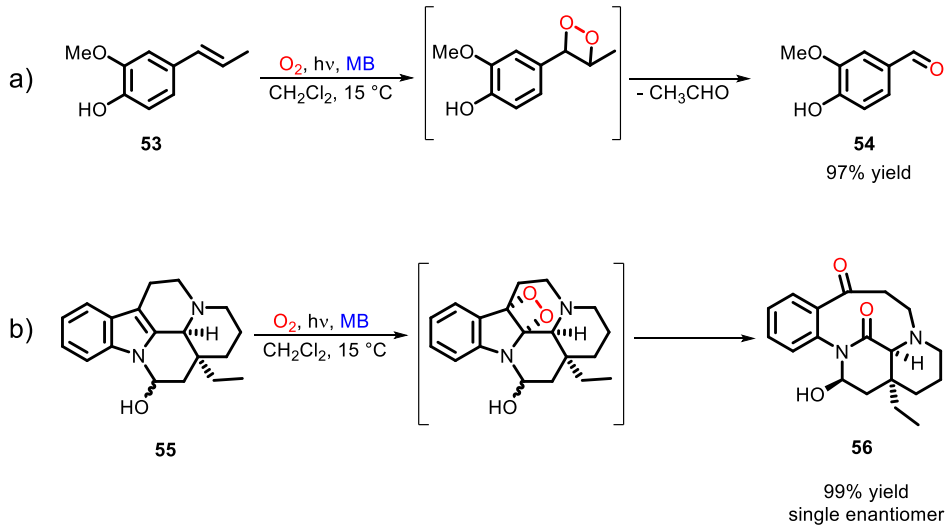
Scheme 35 shows synthetically useful transformations of dioxetanes:[165]



Scheme 35: Synthetically useful transformations of dioxtanes from the [2+2] reaction of $^1O_2$.

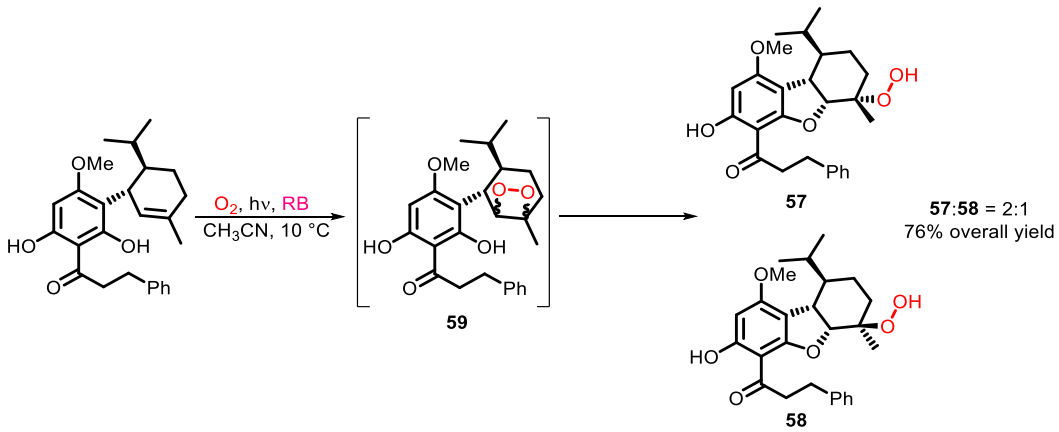
As discussed previously, many dioxetanes are thermally unstable, degrading at raised temperatures *via* a retro-[2+2] reaction to afford two carbonyls. This can provide an alternative methodology to ozonolysis which does not require stoichiometric reductants. Examples of this in synthesis are the conversion of

isoeugenol **53** to vanillin **54** with the expulsion of acetaldehyde (Scheme 36a),[176] as well as the elegant ring expansion of epimeric indoles **55** to (–)-melohenine B **56**, which proceeds with resolution to a single enantiomer of product (Scheme 36b).[177]



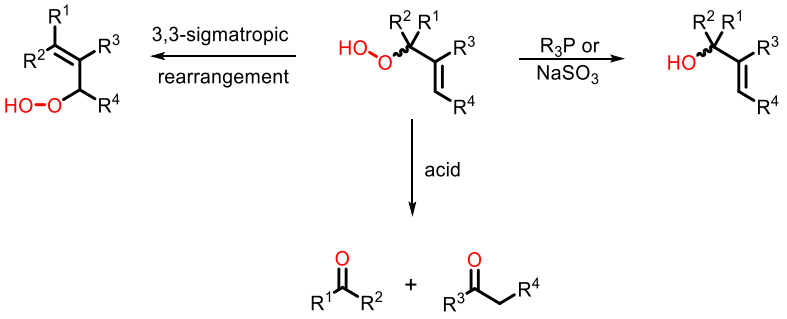
Scheme 36: Examples of the thermal degradation of dioxetanes in a) the formation of vanillin 45 from isoeugenol 53 and b) the synthesis of (–)-melohenine B (56).

Dioxetanes, or intermediates in the formation of dioxetanes, can also be susceptible to nucleophilic attack. In the synthesis of (–)-adunctin E **57**, where the initially formed dioxetane **59** is opened by the nearby phenolic oxygen (Scheme 37).[178] This can also lead to solvolysis in nucleophilic solvents such as methanol.



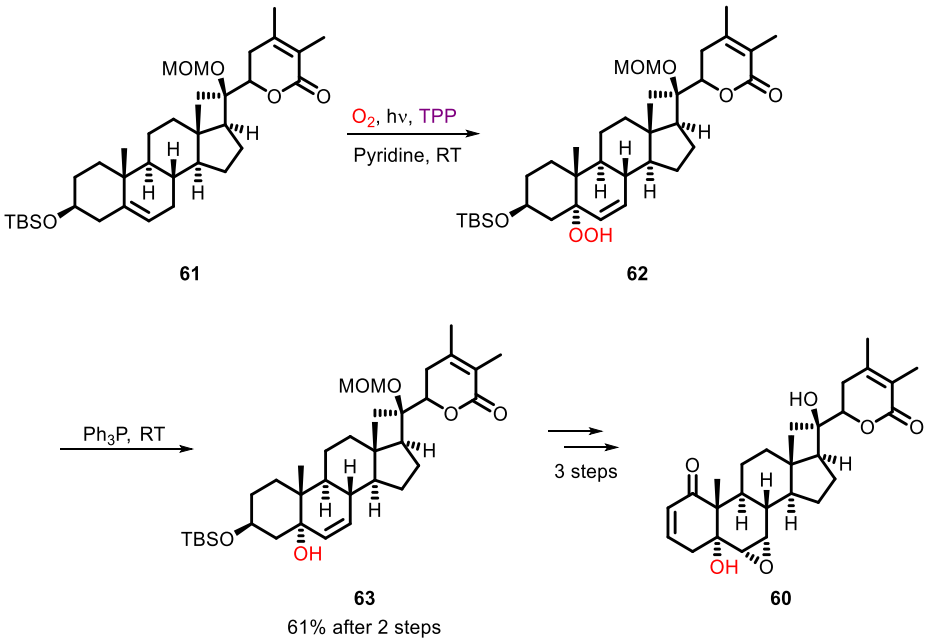
Scheme 37: Synthesis of (–)-adunctin E (57) *via* intramolecular nucleophilic attack on a dioxetane intermediate 59.

Scheme 38 shows synthetically useful transformations of allylic hydroperoxides:[165]



Scheme 38: Synthetically useful transformations of allylic hydroperoxides from the Schenck reaction of $^1O_2$.

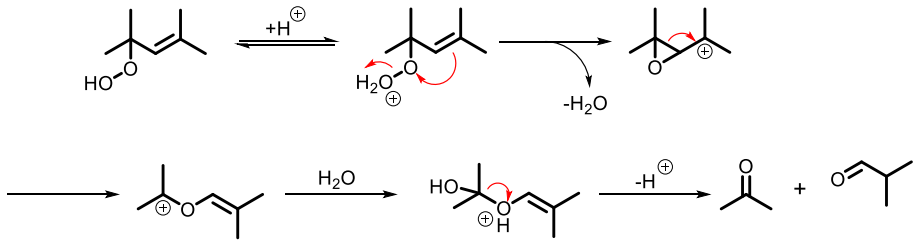
Use of the Schenck reaction in synthesis has been more limited. Reduction of the allylic hydroperoxide products provides allylic alcohols.,[122] which are a very common moiety in synthesis, such as in the synthesis of withanolide A **60** *via* Schenck reaction of steroid precursor **61** to give allylic hydroperoxide **62**, which is then reduced using triphenylphosphine to allylic alcohol **63**.[179]



Scheme 39: Synthesis of withanolide A (60) *via* Schenck reaction and reduction using triphenylphosphine.

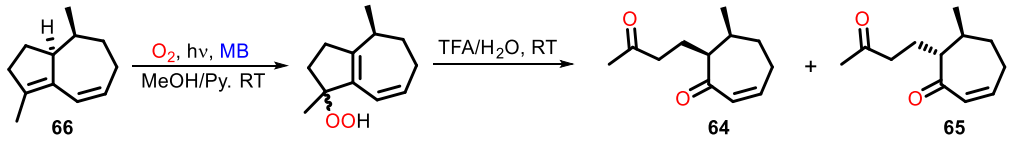
Allylic hydroperoxides can also undergo a 3,3-sigmatropic isomerisation, called the Schenck rearrangement, expanding the utility of this technique.[180]

Finally, another useful reaction of allylic hydroperoxides is the acid catalysed Hock cleavage, which like the decomposition of dioxetanes gives a pair of carbonyl groups along with C—C bond cleavage by the mechanism shown in Scheme 40:[181]



Scheme 40: The mechanism of Hock cleavage, *via* protonation of the distal hydroperoxide oxygen lone pair, elimination of water, ring expansion and hydrolysis.

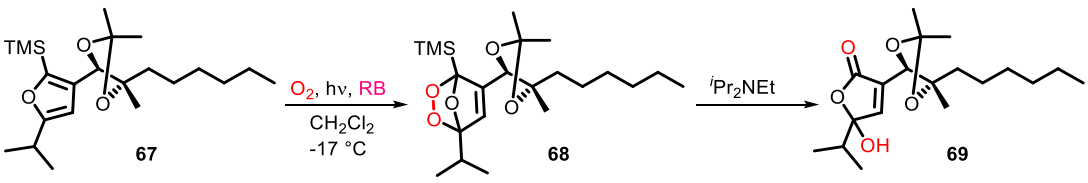
This has been applied to the synthesis of (±)-clavularins A (**64**) and B (**65**) from clavukerin A (**66**) shown in Scheme 41, as well as to the synthesis of the antimalarial natural product artemisinin discussed in Chapters 2 and 3.[182]



Scheme 41: Synthesis of clavularin A (64) and clavularin B (65) from clavukerin A (66).

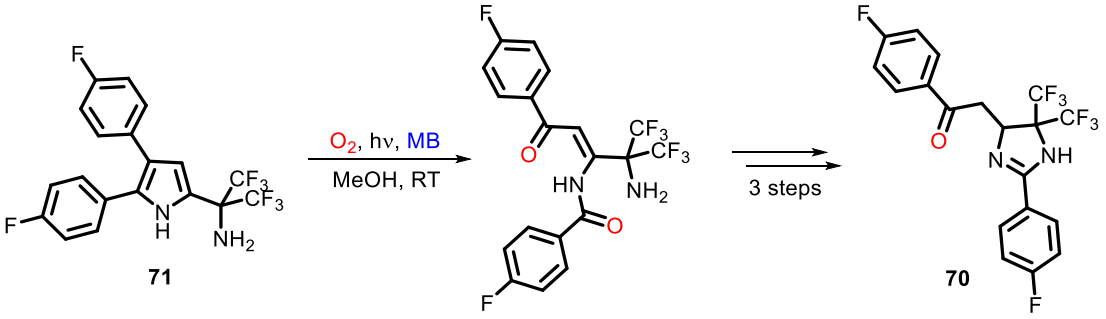
Many electron-rich heterocycles react readily with $^1O_2$, including furans, pyrroles and indoles. For these substrates, the photo-oxygenation products are often unstable and rearrange to give a variety of interesting structures.

Furans react as dienes in the [4+2] reaction, leading to a range of products, depending on the substitution.[183-184] Scheme 42 shows the photo-oxygenation of 2-trimethylsilylfuran **67** to give 1,2,4-trioxane **68**. Base promoted ring opening provides lactone **69**.[185]



Scheme 42: Lactone formation *via* [4+2] photo-oxygenation of furan 67.

Pyrroles and indoles tend to react in the [2+2] mode of reactivity. This is likely due to participation from the nitrogen lone pair encouraging the formation of zwitterionic peroroxyiminium intermediates. Fragmentation of the resulting dioxetanes is rapid and leads to opening of the heterocycle. For example, the synthesis of imidazole **70** is carried out *via* [2+2] photo-oxygenation of pyrrole **71** and subsequent ring-opening and rearrangements.[186] The synthesis of (–)-melohenine B (**56**) shown in Scheme 36b above is an example of a similar indole fragmentation induced by $^1O_2$.



Scheme 43: [2+2] photo-oxygenation of pyrrole 71, subsequent ring opening and rearrangement to dihydroimidazole 70.

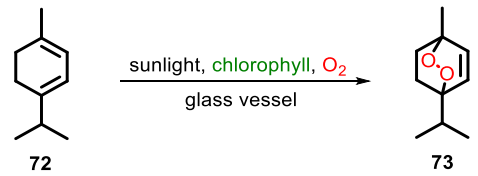
Photo-oxygenation of phenols gives 1,4-peroxyacetals which then ring open and eliminate water to afford qunones. Phenols substituted at the 4-position cannot rearomatise and instead give 4-hydroperoxy quinols, which can also be synthetically useful.[187]

The above review represents only a sample of the broad range of chemistry that can be achieved using singlet oxygen. Forming such complex oxygenated moieties as the ones displayed in this Section by traditional means would in most cases involve extra steps and toxic or dangerous reagents.[165] Thus, photochemically generated singlet oxygen is a versatile and benign oxidant worthy of more widespread use. The following Section discussed the range of enabling technologies which have been developed in the last 20 years for efficient reactions using $^1O_2$.

Section 1.2.6: Technologies for Synthetic Photochemistry

It has been suggested that the two main barriers to wider uptake of photochemistry in the synthesis of complex molecules have been a) the lack of a sufficient 'photoretrosynthetic' strategy and b) the perceived complexity of the experimental setup.[188] The former point was addressed in the previous section, which showed the great utility of singlet oxygen chemistry in a wide range of chemical reactions, forming varied and complex oxygenated molecules from simple alkene substrates. This section discusses the equipment commonly used to perform $^1O_2$ chemistry from a laboratory scale toward large-scale processing.

A photoreactor on any scale has only two critical features – the light source and the window.[189] In short, a light source should be chosen for energy efficiency, ease of use and for the best overlap of the lamp's emission band with the wavelengths required for the chemistry. The window must be transparent at the required wavelengths and ideally should filter undesired wavelengths to achieve greater control over the chemistry performed.



Scheme 44: Schenck and Zeigler's solar photosynthesis of ascaridole 73 from α-terpinene 72.

The earliest examples of photoreactors for singlet oxygen chemistry used simple glass reactors and sunlight, such as Schenck and Zeigler's process for converting α-terpinene **72** to the endoperoxide natural product ascaridole **73** (Scheme 44).[190] This has since been applied in a large scale industrial process.[191] Whilst the direct use of sunlight is perhaps the most energy efficient light source,[192] it is lacking in terms of process control – the intensity and spectrum of light varies greatly day by

day or even hour by hour, which can have a great impact on the rate and selectivity of a reaction.[192] For photochemistry performed using visible light, as is the case for many photosensitised reactions, sunlight presents additional problems from the large amounts of UV light it contains, which is unnecessary to the desired reaction and could cause side reactions or degradation of the product, leading to lower yields. In the specific case of photo-oxygenation reactions, a possible side reaction resulting from the presence of UV light is ozone generation. However, borosilicate (Pyrex) glass absorbs light below 275 nm and so a glass reactor of sufficient thickness should negate this issue.[193]



Figure 9: The immersion-well photoreactor, the most commonly used photochemical apparatus.

Historically, the most commonly used photochemical reactor is the immersion-well reactor shown in Figure 9.[167, 194] These reactors can be made of borosilicate, or if shorter wavelengths are needed, quartz. The immersion-well is double jacketed, containing the reaction solution in the outermost layer, with coolant (typically water) flowing through the second layer to regulate the reaction temperature. At the centre is the light source, commonly a mercury vapour discharge lamp. A

mercury discharge lamp contains mercury vapour through which a current is passed causing emission of light between 350 – 250 nm (UV) depending on the internal pressure.[193] To perform photochemistry using visible wavelengths, a phosphor coating can be applied to the lamp which absorbs the UV and emits broader spectrum visible light.[188] Some tuning of the wavelength is possible by appropriate selection of the phosphor coating. Compact fluorescent lightbulbs which operate on a similar principle but emit in visible wavelengths can be used as an alternative. These light sources are long-lived and widely available, though suffer from problems with large amounts of heat output, hence the requirement for constant cooling. A drawback of the immersion-well reactor as a whole is that illumination of the reaction mixture can be inefficient.[193, 195] In highly absorptive solutions, light intensity drops off rapidly with distance from the lamp, so only a relatively small layer close to the inside of the reactor is illuminated at any one time.[188] Without efficient mixing, rates of reaction are limited by diffusion of unreacted material into the illuminated region. In photo-oxygenation reactions, oxygen gas sparging throughout the reaction can provide some mixing, but the annular shape of the immersion-well reactor makes additional mechanical mixing difficult.

Issues with light penetration have been addressed with the use of falling-film reactors, where a thin flowing film is passed down a glass plate close to a light source. The short path length leads to efficient illumination of the solution, but the low exposure time means that multiple passes through the reactor are often necessary.[196] This is inefficient and can lead to poor selectivity.

Continuous-flow photochemistry is increasingly being used in preference to batch methods. Section 1.1.4. described the many benefits that can be imparted to a reaction by moving to a flow regime, for instance control over selectivity and

efficient mass and heat transfer.[70] This is particularly the case for photochemical reactions where those factors are particularly important.[193, 197] In addition, the illuminated volume of a flow reactor is usually low, which minimises problems with light penetration.[188] The reproducibility of flow conditions and the ease of scale up are also attractive when considering photo-oxygenations on an industrial scale. Another benefit is the simplicity with which multiple step sequences and dual-catalysis strategies can be applied in flow. As shown in the previous Section, these strategies contribute greatly to the synthetic utility of $^1O_2$ chemistry.[167]

Much of the flow photochemistry reported in the literature has been performed in microreactors.[167, 198] These 'lab-on-a-chip' type photoreactors consist of a small channel (<1 mm thickness) cut into a plate of transparent material which is then illuminated as the reaction solution is passed through. An advantage of these systems is the very high degree of control that can be achieved over the reaction conditions and the homogeneity of illumination of the reaction mixture, owing to the small reactor volume. Additionally, the efficiency of gas-liquid reactions like photo-oxygenations is enhanced by the large gas-liquid interface in single-channel slug flow regimes (Figure 10a)[199] or by using a dual-channel system with separate reagent and O_2 channels separated by a gas-permeable membrane (Figure 10b).[200]

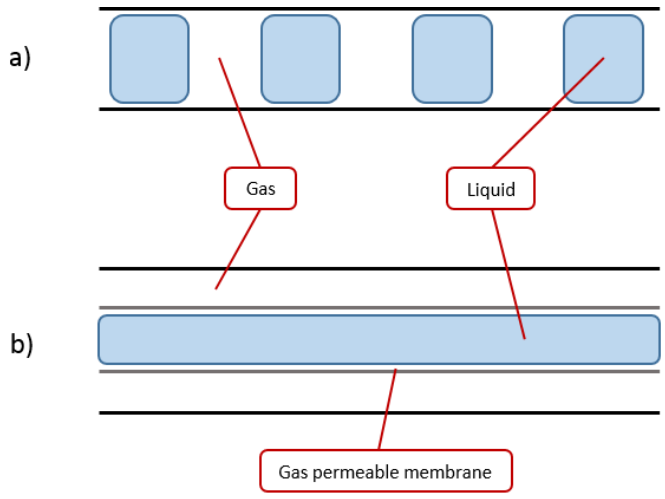


Figure 10: Increased gas-liquid interfacing in microflow in a) single-channel slug flow reactors and b) dual-channel reactors with an O_2 permeable membrane.

When using radial light sources, for example the vapour discharge or fluorescent lamps discussed above, only a small amount of the emitted light is directed at the microreactor, making them poorly energy efficient. Light-emitting diode (LED) light sources have emerged as a more efficient, directional method of illumination for microflow and for batch photochemistry.[193, 201] LEDs are characterised by their narrow emission bands and low heat output compared to the aforementioned radial lamps, though are only available for wavelengths above 350 nm.[197] Their compactness and customisability allow a wider range of reactor geometries and designs to be explored.

The limitation of microreactor chemistry manifests when trying to scale a reaction up for an industrial process.[167] The small channel size means either the residence time will be small, leading to poor conversion, or the flow rate must be very low to compensate, in which case material throughput and productivity will be low. In theory, microreactor chemistry can be 'scaled out' into parallel microreactor arrays. However, the very small channel size also leaves microreactors prone to blockages in the channels and fouling of the windows, so macro-flow reactors are clearly preferable for large scale photochemical production.



Figure 11: The FEP tubing reactor developed by Booker-Milburn and Berry.

A high throughput, versatile reactor for larger scale photochemistry was reported in 2005 by Booker-Milburn and Berry and has now found widespread use.[202] It consists of a length of transparent polymer tubing wrapped around an appropriate light source and illuminated from within (Figure 11). The material most commonly used for the tubing is fluorinated ethylene propylene (FEP) which is highly chemical resistant and transparent to both visible and UV light.[197] The simple design of this reactor means that it is highly customisable – light penetration can be tailored by using tubing of different diameters and residence time can be controlled easily by changing the length of tubing without having to compromise on flow rate. The utility of this reactor for large scale chemical processing was demonstrated by Booker-Milburn and co-workers in their synthesis of pharmaceutically-relevant amides **74** and **75** on a scale of hundreds of grams per day (Figure 12),[202] as well as in their synthesis of *Stemona* alkaloid (±)-neostenine.[203] Seeberger *et al.* have since shown that this type of reactor can be used with a range of photo-oxygenation chemistry, notably the synthesis of the antimalarial natural product artemisinin, discussed throughout Chapters 2 and 3.[204-205]



74 685 g day^{-1} **75** 178 g day^{-1}

Figure 12: Pharmaceutically-relevant amides produced by Booker-Milburn and Berry in hundreds of grams per day using flow photochemistry.

Our group have developed a sapphire tube reactor capable of withstanding pressures exceeding 250 bar.[201] The reactor was originally designed for photo-oxygenations in liquid or supercritical CO_2, but can also be used with conventional solvents.[206] The high pressure tolerance of this reactor allows the reactions to be

performed under higher pressures of O_2, increasing the amount of oxygen in solution. Singlet oxygen chemistry was performed using these reactors at high throughput using both homogeneous and heterogeneous photosensitisers.[207-208] Unlike the FEP reactor described above, the sapphire tube reactor has the reaction volume in the centre and illumination is performed using three inward-facing banks of visible LEDs. Coolant can be flowed between the sapphire tube and the LED units to maintain the reaction temperature. These reactors allow good control of reaction conditions with efficient illumination and are used several times in the work presented in this Thesis.



Figure 13: The sapphire tube photoreactor developed by our group for use with supercritical CO_2. Raised-pressure oxygenations can also be performed in conventional solvents.

In summary, singlet oxygen is a Green alternative reagent for oxygenation reactions in chemical synthesis. Compared to traditional oxidants, $^1O_2$ chemistry is highly atom economical and safe to perform. The scope of structures that can be formed is large, and the potential for synthetic efficiency through 'telescoped' and continuous flow syntheses is large. Improvements in photoreactor technology have facilitated the scale up of these reactions, and examples exist of $^1O_2$ in industrial processes. This Thesis aims to further expand on the industrial relevance and

synthetic utility of singlet oxygen, focussing on its role as an alternative oxidant for Green Chemistry.

Section 1.3: Summary of Thesis Aims and Content.

As shown above, singlet oxygen is finding ever more widespread use in organic synthesis. Clever transformations of the reactive peroxide products allow a wide range of structures to be formed in step and atom economical fashion. For photochemically generated $^1O_2$, catalyst loadings are very low, and with advances in light sources, continuous flow technology and dual-functional catalysis it is now possible to perform these reactions with very little waste and with often very simple purifications required.

In numerous examples provided in Section 1.2.5., with substrates containing a large degree of stereochemical information, high selectivity has been achieved. This selectivity can be predicted accurately using the perepoxide mechanistic model shown in Section 1.2.4. Alternatively, when stereoselectivity is not a requirement, $^1O_2$ can be used to quickly make all possible isomers of a product, just as for the industrial synthesis of rose oxide shown in Section 1.2.3.

Clearly, with all of these things considered, the strategic application of singlet oxygen chemistry is a powerful tool for sustainable synthesis and for sustainable process development. The overriding aim and general theme of this thesis is the use of the photochemical Schenck reaction as a key step in the development of Green and efficient syntheses of natural products.

Chapter 2 describes work performed towards improving the large-scale synthesis of an industrially important antimalarial natural product, artemisinin, using a Schenck reaction of singlet oxygen. In collaboration with the French pharmaceutical company Sanofi we wanted to develop a more productive, cheaper and Greener process. The Chapter details our strategy of using aqueous mixtures

of organic solvents, including fundamental studies on the Schenck reaction in these mixtures, process optimisation in a batch regime and application in continuous flow.

Chapter 3 describes mechanistic studies on the same synthesis of artemisinin. Work is presented towards the development of a method for the continuous monitoring of photo-oxygenation reactions using nuclear magnetic resonance spectroscopy, using a bespoke recirculating continuous photoreactor/ spectrometer system.

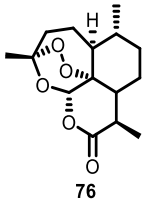
Chapter 4, the final results chapter, describes work towards the total synthesis of the glaciapyrrol family of natural products. We aimed to use a divergent strategy to synthesise multiple members of the family from a common precursor using a non-selective Schenck reaction. In addition, we wanted to develop a route that adhered to the principles of Green chemistry and was as efficient, in the process sense, as possible. The synthetic strategy is described in detail, a scaled-up and telescoped synthesis of the common precursor is reported, and the use of the Schenck reaction to install the oxygen-containing functionality present in the natural products.

An important criterion for all the synthetic routes, reactions and processes developed as part of this body of work is Sustainability. At all points, the potential for scale-up is considered. The principles and strategies detailed in Section 1.1. have been followed as often as possible. By demonstrating the process benefits that can be achieved by following said strategies, we aim to show how the aspirational goals of Green Chemistry and the more pragmatic goals of Industrial Process Chemistry are compatible and even complementary.

Chapter 2: Improving the Synthesis of the Antimalarial Natural Product Artemisinin.

Section 2.1: Introduction and Project Aims.

Malaria is an infectious disease caused by several species of protozoan parasites of the genus *Plasmodium*, the most virulent of which is *Plasmodium Falciparum*. The disease is spread to humans through bites from infected mosquitoes, making infection very difficult to prevent. Vaccines are in development,[209] but in the meantime, treatment remains the only effective option. Even with the advance of modern medicine, malaria still causes a large number of deaths per year. The latest available figures, from 2015, estimate that over 429 thousand people died of malaria that year, with infection numbers surpassing 200 million cases.[209] The vast majority – over 90% in 2015 – of these cases are in Africa, and are concentrated in less economically developed countries, making it important that treatments for the disease, antimalarials, are available at low cost. The high volume of cases means that production of these antimalarials is a large scale industrial undertaking, thus it is also important that they be made via a process with low environmental impact.



76

Figure 14: The antimalarial sesquiterpene, artemisinin 76.

Many current frontline treatments for malaria are derived from the sesquiterpene natural product artemisinin **76**. This compound is so vital to the treatment of malaria that the 2015 Nobel Prize in medicine was awarded for its 1972 discovery. Providing artemisinin at low cost and in large enough amounts to treat the millions of cases is a pressing problem both in academia and in industry.[210] The following Chapter presents work done towards the application of Green Chemistry to a semi-

synthetic process for the production of artemisinin. Our objective for this project was to improve the material throughput whilst reducing the environmental impact of production, in accordance with the principles of Green Chemistry discussed previously. More specifically our criteria for an improved process were as follows:

a) **Environmental Impact** – We sought to develop a process that was low waste, low energy and proceeded under milder conditions than those in the literature, in order to reduce the cost and environmental impact of producing large quantities of artemisinin.

b) **Efficiency** – To more easily meet the global demand, we wanted to maximise yield and selectivity as well as material throughput, allowing us to make the most artemisinin possible per unit time.

c) **Cost** – The cost of medicines derived from the artemisinin produced by our process should be low enough that treatment for malaria is available to all who need it. A process that is low waste and high efficiency should be inherently cheap to run, so we expected that through adhering to the principles of Green chemistry we would develop a less costly process as a matter of course.

Section 2.2: Background.

Section 2.2.1: Sources and Syntheses of Artemisinin.

Most malaria treatments currently recommended by the World Health Organisation are Artemisinin-based Combination Therapies (ACTs),[209] which all contain a prodrug derivative of artemisinin – usually an ether or ester of dihydroartemisinin **77** – together with a secondary antimalarial.[211-212] The most commonly prescribed derivatives are artemether **78**, artemotil **79** and sodium artesunate **80**.

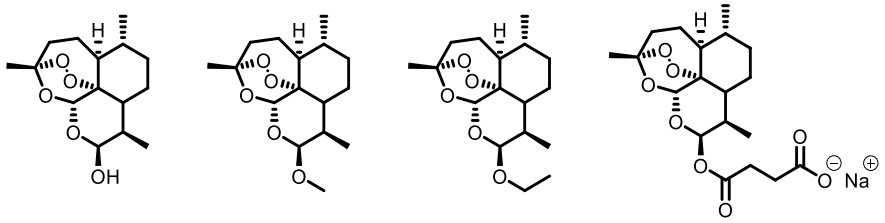


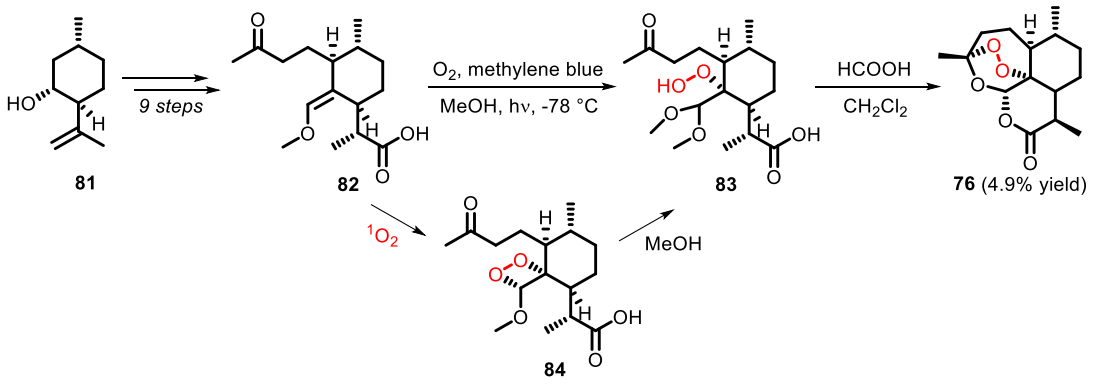
Figure 15: Some prominent artemisinin-derived clinical antimalarials. All are synthesised from naturally acquired artemisinin 76.

This combination strategy reduces the survival rate of artemisinin-resistant *Plasmodia* and so helps to prevent the spread of resistance. Nevertheless, artemisinin-resistant strains of *P. Falciparum* are increasingly being reported, particularly in Asia. Several cases of malaria resistant to a common ACT were recently reported in the UK, showing that resistance is spreading. It is vital that these drugs are made more widely available without delay, whilst they still represent an effective treatment. The main source of artemisinin **76** provided to the pharmaceutical industry has historically been direct extraction from its natural source, the sweet wormwood *Artemisia Annua*.[213] This is a rather inefficient process, yielding on average around 8 g of artemisinin per kilo of dried plant material.[214-215] The long wait times for production and the potential for poor

harvests can result in significant variability in the price of **76** and it is clear that a more stable supply line is required.[216] Many groups have worked on addressing this problem, either by improving the extraction, by searching for total synthetic routes to the product or, most relevant to this Thesis, by semi-synthetic methods employing both biological and photochemical production techniques.

As it became clear that increasing cultivation of *A. Annua* could not keep up with increasing demand for artemisinin **76**,[213, 215] attempts to increase production by conventional breeding of the plant were made. Early experiments with genotypic selection resulted in a hybrid strain with an artemisinin content of 1.38% w/w of dry plant material (w/dw), compared to 1.07% w/dw from the highest yielding wild strain.[214] Since then, detailed genetic mapping of the traits effecting yields of **76** has been performed, allowing breeding programs to produce crops exceeding 1.6% w/dw of **76**.[217-218]

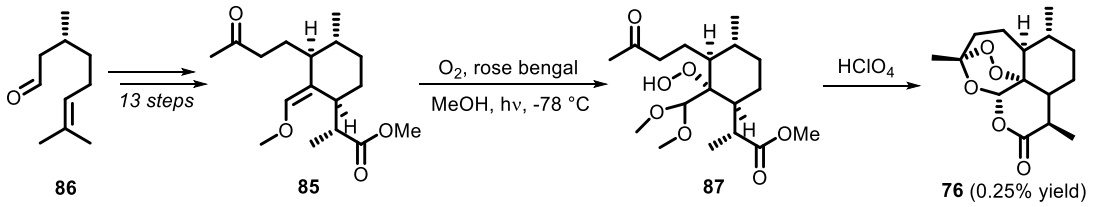
Since its discovery, artemisinin **76** has been synthesised by chemical means a number of times.[219-221] The first total synthesis of **76** was reported in 1983 by Schmid and Hofheinz and gave the product in 11 steps from (–)-isopulegol **81** (Scheme 45).[222]



Scheme 45: Total synthesis of 76 by Schmid and Hofheinz, showing the key photo-oxygenation of an enol ether.

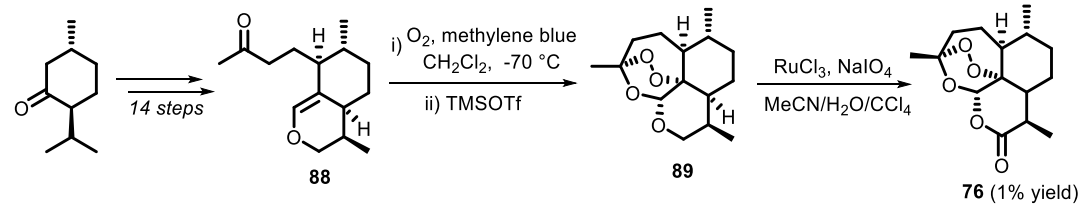
The key step was the photo-oxygenation in methanol of methyl enol ether **82** followed by solvolysis to give the α-hydroperoxy methyl acetal **83**, which upon

deprotection by hydrolysis under acid conditions gave artemisinin **1** in 4.9% yield. The reaction of $^1O_2$ with **82** is likely of the [2+2] type, proceeding *via* dioxetane intermediate **84**.[163]Shortly afterwards, Xu *et al.* published a route to **76** using a similar strategy (Scheme 46).[223] They formed another methyl enol ether **85**, the methyl ester of Schmid's precursor **82**, in 13 steps from *R*-(+)-citronellal **86**. They then applied the same singlet oxygen chemistry to afford peroxide **87**, giving **76** in 0.25% yield after hydrolytic deprotection with perchloric acid.



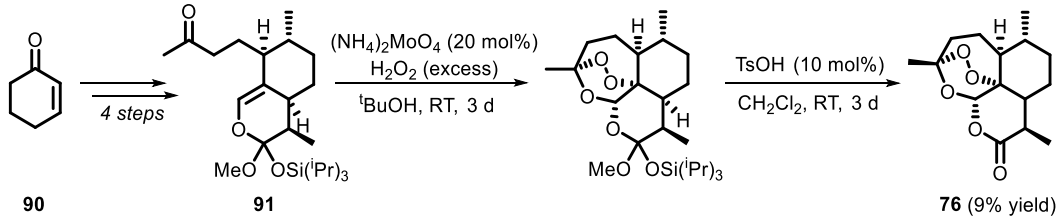
Scheme 46: Synthesis of 76 reported by Xu *et al.*

Several groups – those of Ravindranathan in 1990,[224] Bhonsle in 1994[225] and Yadav in 2003[226] – used this [2+2] photo-oxygenation of an enol ether to construct the hydroperoxide ring. The routes presented by both Ravindranathan and Yadav proceeded *via* the same methyl enol ether **85** as Xu, receiving **76** in 0.5% and 0.3% yield, respectively. Bhonsle *et al.* constructed the 6-membered cyclic enol ether **88** over 14 steps, which provided deoxyartemisinin **89** on photo-oxygenation. Final conversion to **76** was afforded using sodium periodate with a catalytic amount of ruthenium(III) chloride, with 1% overall yield (Scheme 47).



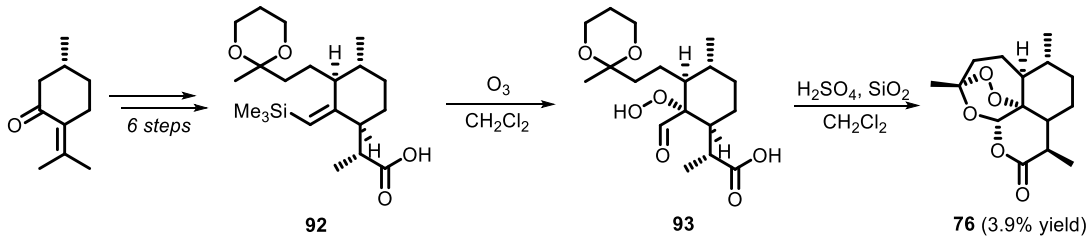
Scheme 47: Bhonsle *et al.*'s synthesis of 76 via cyclic enol ether 88.

Most recently, Zhu and Cook completed the most concise and highest yielding total synthesis of **76** to date – performed in only five steps and giving an overall yield of 9%.[227] Starting from cyclohexenone **90** they made enol ether **91** over their first four steps. They elected to use a 'dark' reaction of chemically generated $^1O_2$ rather than a photo-oxygenation for the final step, using the molybdate catalysed disproportionation of hydrogen peroxide described in Section 1.2.3. Acid hydrolysis with *p*-toluenesulfonic acid (TsOH) gave **76**.



Scheme 48: Concise synthesis of 76 from Zhu and Cook, using a 'dark' singlet oxygen reaction.

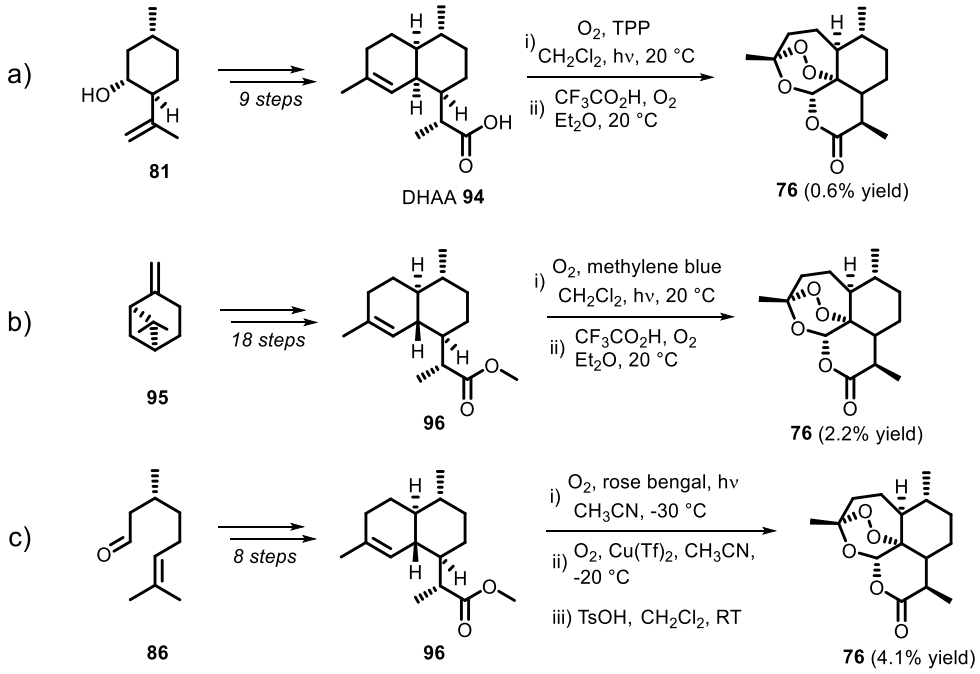
An alternative strategy for the formation of the peroxide bridge was presented by Avery *et al.* as part of a more concise, seven step synthesis in 1992.[228] As shown in Scheme 49, vinyl silane **92** was subjected to an atypical Beckmann-type ozonolysis,[229] giving artemisinin on acid workup in 3.9% yield, *via* the α-hydroperoxy aldehyde **93**.



Scheme 49: Avery's route to 76 using ozonolysis of a vinyl silane 17.

Another frequently used route to **76** has been *via* the synthesis of structures related to another sesquiterpene natural product dihydroartemisinic acid (DHAA,

94). Final conversion to **76** can then be effected by reaction with $^1O_2$ in the presence of acid (Scheme 50).

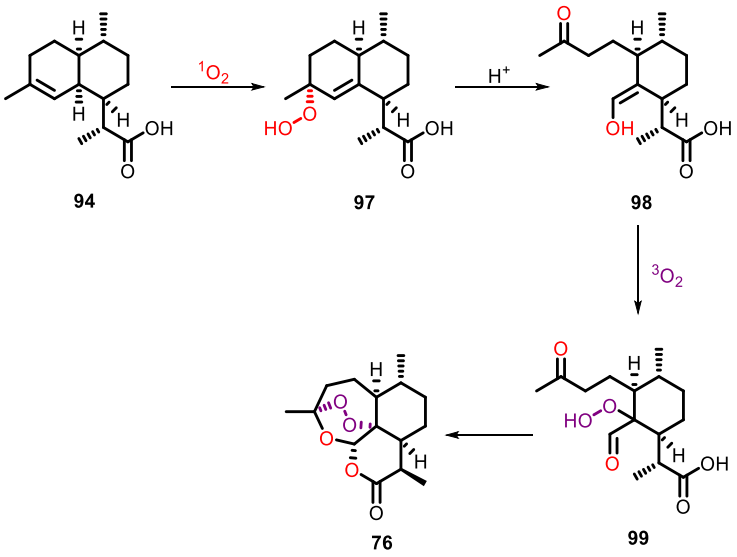


Scheme 50: Synthesis of 76 by photo-oxgenation of DHAA 94 and its analogue 96, reported by a) Constantino *et al.*, b) Liu *et al.* and c) Yadav *et al.*

The first total synthesis in this class was published in 1993 by Liu *et al.*, who synthesised **76** in 2.2% yield *via epi*-DHAA methyl ester **96**.[230] Their synthesis had a total of nineteen steps starting from ß-pinene **83**. Constantino and coworkers synthesised DHAA **84** in nine steps from (–)-isopugelol **81**,[231] whilst Yadav *et al.* started from R-(+)-citronellal **86**, achieving the same intermediate structure **96** as Liu in only 8 steps.[232] Yadav's route is notable for being performed in the absence of any protective groups or chiral auxiliaries.

Conversion of **94** (or **96**) to **76** proceeds in a well-known series of reactions first published by Acton and Roth in 1989 (Scheme 51).[233-234] The reaction of DHAA or its derivative with $^1O_2$ is a Schenck reaction leading to hydroperoxide **97**. Acid catalysed rearrangement leads to keto/enol species **98**, which is similar in structure to the intermediates **82** and **85** in the synthetic routes above. Another

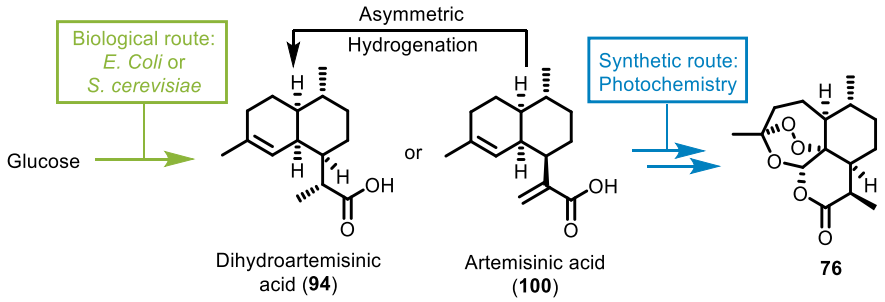
aerobic oxygenation gives hydroperoxide **99**, although unlike in the case of the oxidation of enol ethers **82** and **85** this is not induced by $^1O_2$ but by ground state $^3O_2$.[235] This spin forbidden process is naturally slow and likely limits the overall rate of formation of artemisinin **76**. A series of facile ring closures finishing with the closing of the lactone ring gives **76**. The reaction can be performed in a single pot without intermediate purifications. Detailed consideration of the mechanism and selectivity of this reaction sequence is presented in Section 2.2.2. below.



Scheme 51: Photochemical conversion of DHAA 94 to artemisinin 76 as reported by Acton and Roth.

In all the synthetic routes to **76** described above, the overall strategy has been to first construct the 15-carbon backbone of **76**, including as much of the chirality of the product as possible, then to use oxidations to incorporate the endoperoxide and lactone rings. All routes take many steps and require multiple asymmetric reactions as well as protection and deprotection steps (with the exception of Yadav *et al.*'s 2010 paper above). The long synthetic routes lead to low yields and generate large amounts of waste. This makes them unsuitable for application on an industrial scale since the **76** produced would be too expensive. Shorter, higher yielding and less expensive routes are needed.

Most of the more wasteful steps in these syntheses can be circumvented by applying a semi-synthetic strategy. In general, semi-synthesis is a strategy for the construction of complex targets whereby a late-stage intermediate, containing many of the structural and stereochemical features of the product, is procured from a plant or micro-organism and subsequently transformed into the product by chemical means.



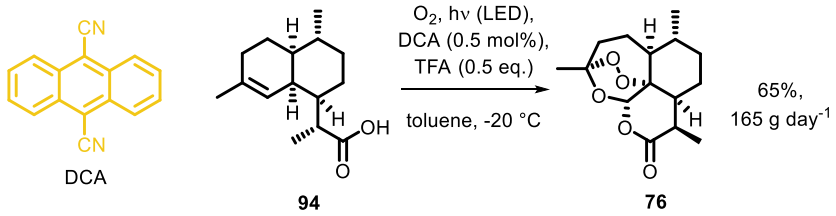
Scheme 52: The semi-synthetic route to artemisinin. 94 and 100 can be obtained from genetically engineered micro-organisms, and converted to 1 using photochemistry.

Scheme 52 shows the specific case of the semi-synthesis of **1**, where the complex intermediate used as the semi-synthetic precursor is DHAA **94**.[236] This contains a closely related sesquiterpene ring system to that found in artemisinin, and of its five chiral centres, four are retained in **76**, providing a high degree of complexity at a very low synthetic cost. The only chemical synthesis that needs to be performed is the one-pot reaction shown in Scheme 51.

DHAA, and the related compound artemisinic acid (AA) **100**, can both be found in *A. Annua* in greater abundance than **76**; both **94** and **100** are thought to be biosynthetic precursors to artemisinin.[237-241] In recent years, advancements in genetic modification have allowed the engineering of micro-organisms containing the metabolic pathway to **100**, specifically *Escherichia Coli* and *Saccharomyces Cerevisiae* (baker's yeast).[242-245] These microorganisms are used in large scale bioreactors to produce **100** *en masse*. This is transformed into **94** *via* asymmetric hydrogenation in quantitative yield and high diastereoselectivity.[246-247] As a result,

94 is available cheaply and in large amounts, and it is now possible to perform the semi-synthesis of **76** on a large enough scale to address the problem of artemisinin supply.[248-249]

Nowadays, the focus of most synthetic work on artemisinin is towards the improvement and optimisation of the conversion of **94** to **76** with a view to scale-up and commercialisation. Several groups have published scalable syntheses of **76** in recent years. The first of these was reported by Seeberger *et al.*, using a continuous flow reactor (Scheme 53).[205, 250]



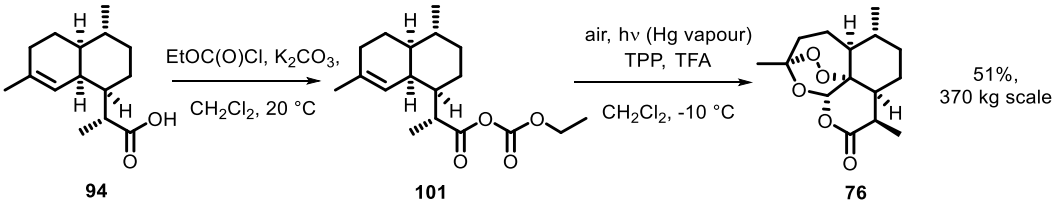
Scheme 53: Continuous flow semi-synthesis of 76 on up to a 200 g scale, reported by Seeberger *et al.*

Their flow rig consisted of a single feed flow containing DHAA **94**, their photosensitiser 9,10-dicyanoanthracene (DCA), and their catalyst trifluoroacetic acid (TFA) dissolved in toluene. O_2 gas was added from a cylinder. The combined streams passed through their photoreactor, of the type described originally by Booker-Milburn and Berry (see Section 1.2.6.). This reactor consists of transparent FEP tubing wrapped around a light source, in this case high-powered LEDs, and immersed in a coolant bath at -20 °C. After photo-oxygenation, the mixture was passed through a tube reactor at 10 °C to warm the mixture, and another at 25 °C to affect the remaining conversion to **76**.

Under their optimised conditions, with a flow rate of 1.25 ml min^{-1}, 0.5 mol% DCA, 0.5 eq. TFA, a 65% yield was achieved, the highest currently in the literature. They predict that their reactor could make 165 g of artemisinin every day, which they calculate to correspond to a space-time yield of 3500 kg m^{-3} day^{-1}. They also

managed to extend their process to the derivitisation of **76** to the active pharmaceutical ingredients **78-80** shown in Figure 15 in a single continuous flow system.[251]

The need to cool their photoreaction then heat afterwards is a source of inefficiency in their process, were it to be implemented on an industrial scale. Additionally, recovery of the artemisinin in pure form required two subsequent crystallisations, which would increase the cost of their process and reduce the space-time yield.

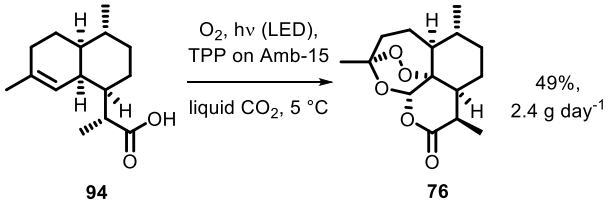


Scheme 54: The Sanofi process for making 76, performed on 600 kg batches of 94.

The only photochemical synthesis of **76** currently applied on an industrial scale belongs to the French pharmaceutical company Sanofi.[249] Sanofi also use TFA as their acid, and dichloromethane as solvent, preferred over toluene for this application since it is non-flammable. They chose TPP as their photosensitiser, citing its ready availability and efficient generation of $^1O_2$ as reasons for the decision. Rather than a fully continuous process, they opted for a semi-batch process where the bulk of the reaction mixture is held in a continuously stirred tank reactor, heated and bubbled with O_2 gas. A small portion of the reaction mixture is constantly circulated through a photoreactor where it is cooled to -15 °C and illuminated with a mercury vapour lamp. In this way, they produce artemisinin with a 51% yield from 600 kg **94**, receiving around 370 kg of **76** per batch. Again, their product must be purified by crystallisation.

Whilst the ability to produce of such a large amount of artemisinin is a great achievement, several inefficiencies remain that will contribute to the price of their

product. The dichloromethane they use as solvent must be tightly contained and recycled as much as possible, as the personal and environmental hazards associated with its use are large. The biggest inefficiency in their process, however, is their derivatisation of **94** to mixed anhydride **101** prior to photo-oxygenation. They claim this extra step is necessary to increase the rate of formation of **76**, and to prevent the formation of side products, though the cost of the extra time and solvent taken for this additional step likely outweighs the increases in rate and yield that they observe.

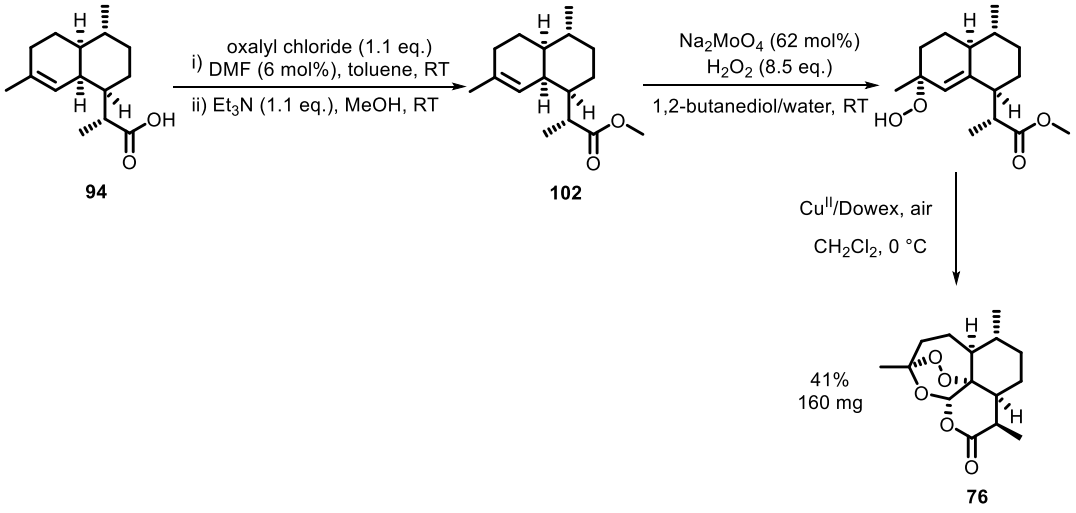


Scheme 55: The continuous process developed on our group, using solid catalysts in liquid CO_2.

In collaboration with Sanofi, we recently developed our own synthesis of **76**, designed to address some of the process inefficiencies described above, and to improve the process in terms of its environmental impact.[206] Because of the very high space-time yield achieved by Seeberger *et al.*, we opted for a fully continuous process. The dichloromethane solvent was replaced with liquid CO_2, which is also non-flammable, and unlike dichloromethane, non-toxic. An additional benefit of using CO_2 as a solvent is that under standard conditions CO_2 is gaseous, meaning recovery of the crude product is as simple as releasing the pressure. However, as solubility of the substrate in CO_2 was low, toluene was added as a co-solvent. Additionally, the requirement for high pressures to retain CO_2 in liquid form necessitates specialist equipment. To this end we developed a sapphire tube photoreactor, capable of withstanding high pressures whilst still being transparent to visible light. The sapphire tube is contained in a cooling jacket and illuminated

from the outside with high-powered LED lamps. To further ease in purification, we employed a heterogeneous dual catalyst consisting of TPP supported on the solid acid resin Amberlyst-15. This single solid catalyst could perform both the photo-oxygenation and rearrangement steps with minimal leeching into the liquid phase. The dual catalyst is retained inside the photoreactor and so does not need to be removed from the product. Using this method, artemisinin was synthesised in 49% yield. The output of the reactor was 2.4 g day^{-1}.

The pharmaceutical company Amyris in collaboration with Keasling *et al.* have developed a process for converting DHAA **94** to artemisinin **76** using chemically generated $^1O_2$, by molybdate catalysed decomposition of hydrogen peroxide (see Section 1.2.3.).[252] They employed a solid supported copper(II) Dowex resin as their acid catalyst, achieving a 41% yield on a 160 mg scale. Like Sanofi, they opted to form an ester of **94** – in this case the methyl ester **102** – in an additional step, again to reduce side product formation. Unlike the three methods described above, Amyris' method requires several solvent switches throughout, using toluene, aqueous methanol and dichloromethane, as shown in Scheme 56.



Scheme 56: Keasling and Amyris' 'dark' synthesis of 1, using chemically generated singlet oxygen.

Finally, another 'dark' process was published by Wu *et al.*, who achieved the same 41% yield as Amyris without derivitisation to the methyl ester.[253]

The argument in favour of chemically generated singlet oxygen rather than photochemical tends to be that scaled-up photochemistry requires specialist equipment. Of course, any dedicated chemical plant for production of **76** would be entirely custom-built regardless of the method used, and as shown in Section 1.2.6. the technology already exists for high-throughput photochemistry on an industrial scale. As discussed in Section 1.1.4., flow methods are inherently scalable. To this date it has only been the photochemical processes developed by Seeberger and by Sanofi that have displayed true scaleability.

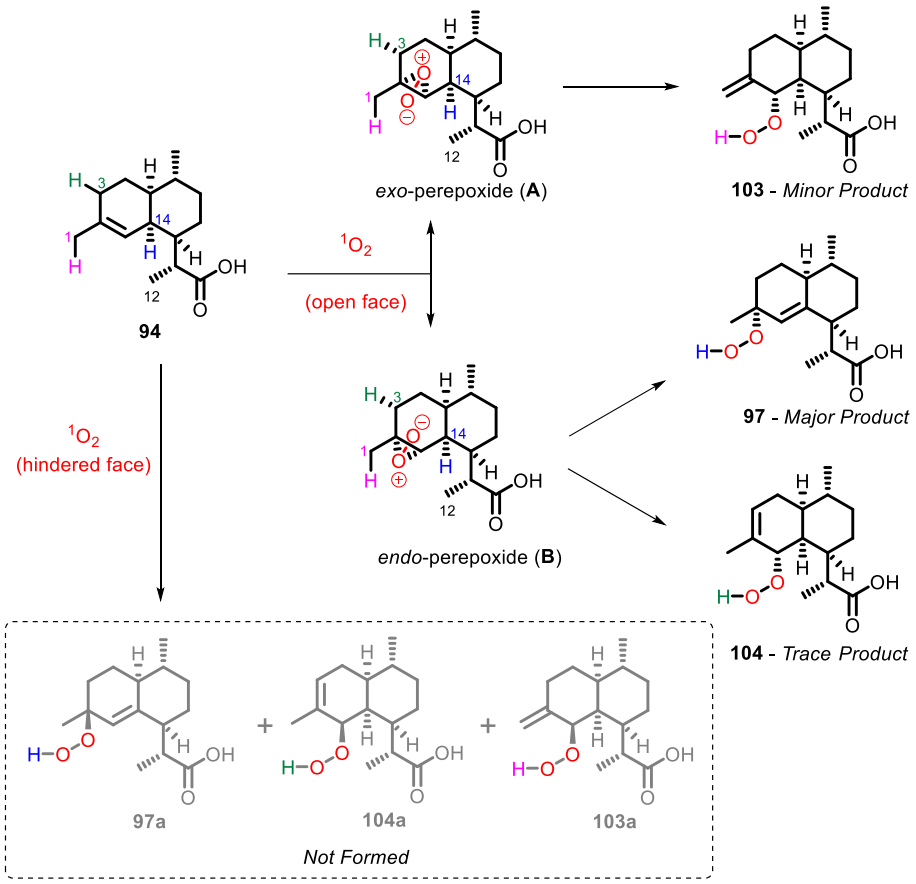
Despite the fact that **76** can now be formed on a large scale, supplementing the naturally sourced material and stabilising the supply, there is still room for improvement. Overall yields are still low, and so the existing processes must be improved upon if the global problem of artemisinin supply is to be addressed. Section 2.3. describes work we have performed towards further improving this process in accordance with the project aims stated in Section 2.1.

Section 2.2.2: Mechanism and Selectivity in the Synthesis of Artemisinin.

The one-pot synthesis of artemisinin **76** from DHAA **94** presented in Section 2.2.1., Scheme 51, is a complex mechanism comprising several distinct chemical transformations. The first step in the reaction sequence is a highly selective Schenck reaction of the alkene bond of **94**. Section 1.2.4 gives a thorough discussion of the factors affecting the selectivity of the Schenck reaction in general. Here, the specific case of the Schenck reaction of **94** is discussed with regards to those factors. Of the six possible allylic hydroperoxides that could form, shown in Scheme 57, tertiary hydroperoxide **97** is produced as the major product, often in very good yields. Secondary hydroperoxides **103** and **104** are formed as minor products, with **103** usually the more abundant of the two. The epimeric structures **97a**, **103a** and **104a** are not seen at all, making this a rare example of an stereoselective Schenck reaction.

As previously discussed, facial selectivity in the Schenck reaction is almost always due to chiral features of the substrate, e.g. one face of the alkene being blocked by a large group. The Schenck reaction of **94** is an extreme example of exactly this – the bicyclic ring system is folded so that the top face of the alkene (as drawn) is blocked, allowing $^1O_2$ to only approach from the bottom face. Thus, hydroperoxides **97a**, **103a** and **104a** cannot form.

The second stereochemical consideration is the side selectivity. Two perepoxide intermediates can be formed, **A** and **B**, with *exo* and *endo* geometry, respectively. *Endo*-perepoxide **B** can lead to hydroperoxides **97** and **104**, whereas *exo*-perepoxide **A** leads only to hydroperoxide **103**. The *endo*-perepoxide is the more stable by virtue of having the peroxide-like oxygen over the more substituted side, as per the cis effect described in Section 1.2.4. As a result, **103** is only produced as a minor product.



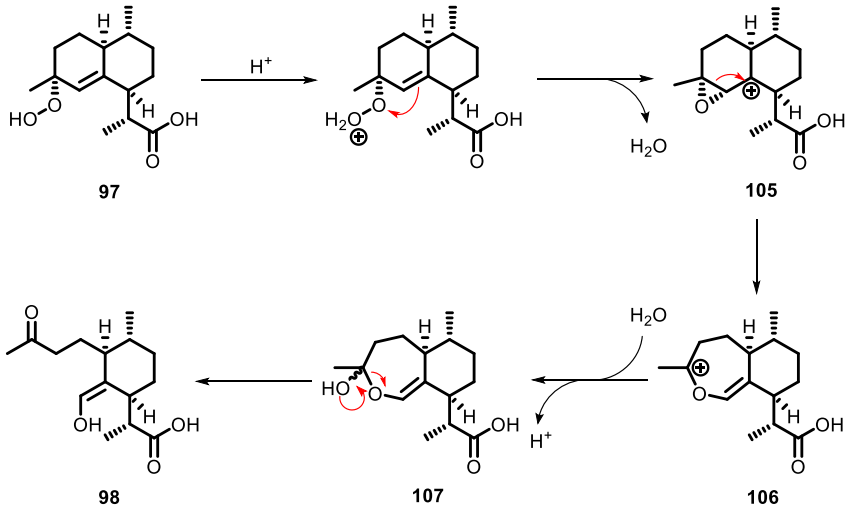
Scheme 57: The stereochemical outcomes of the Schenck reaction of 84, showing the formation of secondary hydroperoxide 103 via the exo-perepoxide, tertiary hydroperoxide 97 and secondary hydroperoxide 104 via the endo-perepoxide, as well as the epimeric structures 97a, 103a and 104a not observed.

Finally, the selectivity between tertiary hydroperoxide **97** and secondary hydroperoxide **104** is a matter of the end selectivity of the reaction. Considerably more **97** forms, which seems to be in line with the large group nonbonding effect, with hydrogen abstraction occurring on the same side as the bulky terpene ring. However, considering the shape of the perepoxide intermediate, it seems unlikely that there is a strong steric interaction between the perepoxide group and the terpene ring, which as previously stated is folded away from the face of attack. The source of the selectivity for **97** over **104** is most likely down to differences in rate of reaction between tertiary and secondary hydrogen abstraction.

The selectivity effects described above become more pronounced as the temperature is lowered, with yields of the desired hydroperoxide **97** reaching

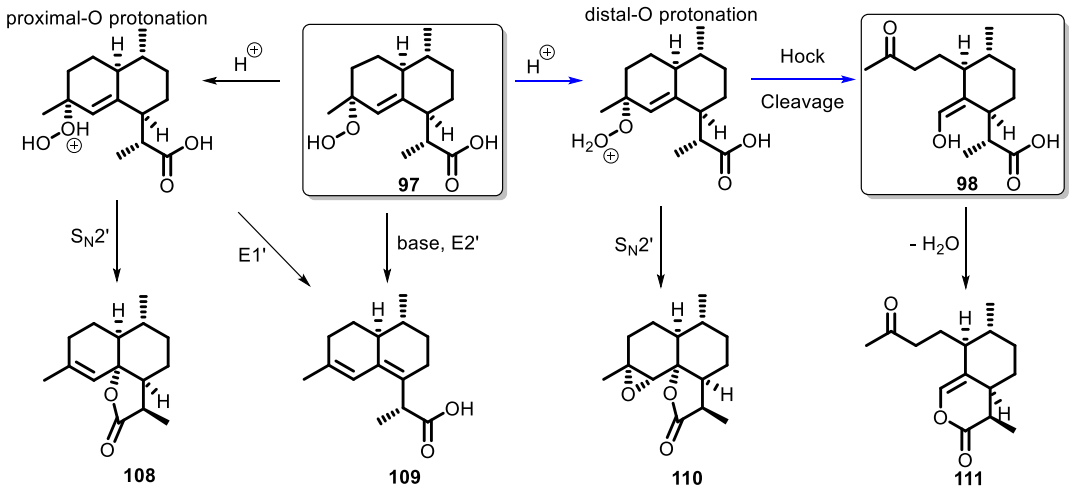
around 84% at -20 °C in studies performed by Seeberger *et al.*[205] This makes it necessary to cool the photo-oxidation step to maximise yields of **76**. Cooling in any case is energy-intensive, but particularly here where the reaction mixture is also being heated by the light source.

The accepted mechanism for conversion of **97** to **98** is shown in Scheme 58.[235, 254] The reaction is thought to be an example of the Hock Cleavage, a known reaction of allylic hydroperoxides described previously in Section 1.2.5.[181] Protonation of **97** at the distal hydroperoxide oxygen leads to elimination of water to give α-epoxide carbocation **105**, which rearranges to the more stable carbocation **106**. Addition of water gives hemiacetal **107** which then ring opens to keto-enol species **98** as shown.



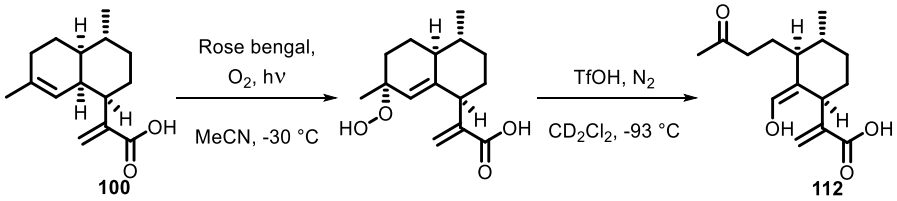
Scheme 58: The Hock cleavage mechanism for the acid catalysed rearrangement of allylic hydroperoxide 97 to keto-enol species 98.

This mechanism was proposed based on the work of several groups, including Acton and Roth who showed that this step was acid-catalysed.[233-235, 255] Brown *et al.* isolated and characterised a wide range of other sesquiterpenes from *A. Annua* and showed that many of them, including lactones **108**, **110** and **111** as well as diene **109**, formed as side products in the conversion of **97** to **98**, suggesting how they might form under the reaction conditions (Scheme 59).[254, 256]



Scheme 59: Brown's mechanisms of side product formation in the Hock cleavage. The pathway eventually leading to artemisinin 76 is shown in blue.

The proposed mechanism fits with the observations of Haynes and Vonwiller, who detected a similar enol intermediate **112** by ^{1}H-NMR when treating the photo-oxygenation product of artemisinic acid **100** with trifluoromethanesulfonic acid (TfOH) under an inert atmosphere (Scheme 60). It is assumed that **112** forms in an analogous fashion to **98** from **97** (Scheme 58, above).

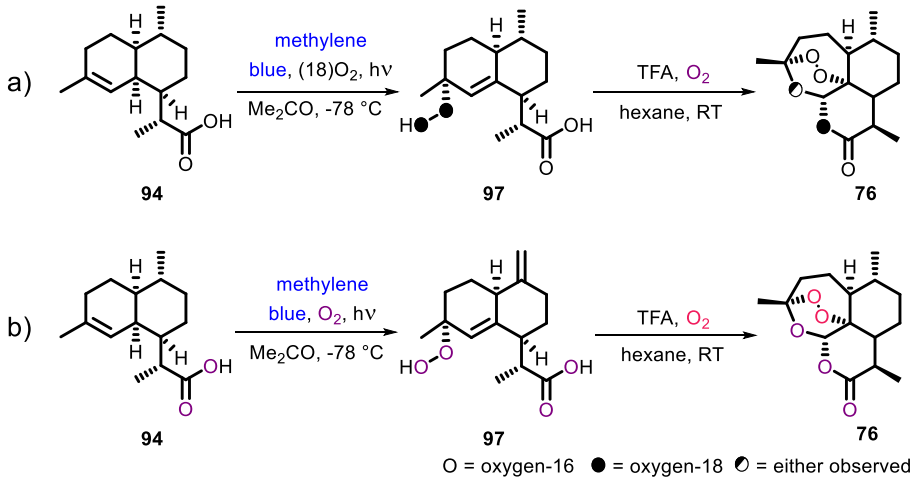


Scheme 60: Haynes and Vonwiller's low temperature ^{1}H-NMR study showing the formation of keto-enol 112, supporting the Hock cleavage mechanism.

In the course of the optimisation of their continuous flow synthesis (Section 2.2.1., Scheme 53), Seeberger *et al.* studied the effect of acid strength, acid quantity and temperature on the yield of the Hock cleavage step.[205] They found a pronounced sensitivity of the yield of artemisinin to the strength and amount of acid used. Originally, they used very strong sulfonic acids, both solid supported and homogenous. They found that the weaker, but still quite strong trifluoroacetic acid (TFA), pK_a = -0.25, outperformed any of the sulfonic acids, as well as the Lewis

acid copper(II) trifluoromethanesulfonate. Increasing the pK_a further led to a loss of selectivity, as shown by the low yield of **76** when using acetic acid, pK_a = 4.75. This indicates that there is an optimal pH range for this reaction. This is further demonstrated in the dependence of the same step on acid concentration and temperature. The researchers found that low concentrations of TFA gave a large relative increase in artemisinin yield as the temperature was raised, which was not observed for higher concentrations.[250]

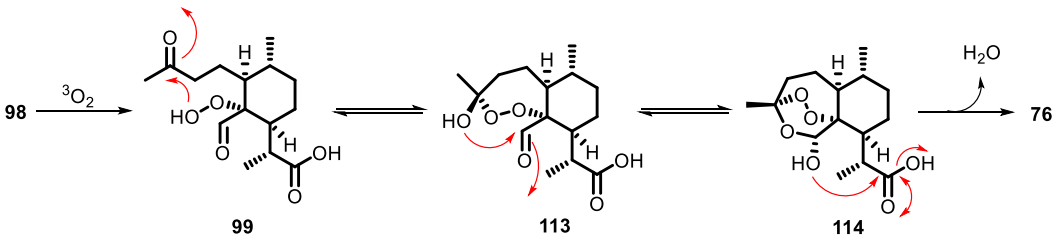
The nature of the oxidation of enol **98** to hydroperoxide **99** was determined by Acton and Roth using oxygen-18 labelling experiments (Scheme 61).[235] They saw that whilst the first oxidation of **94** to **97** requires light and photosensitiser, the second oxidation proceeds at the same rate in the presence or absence of light, indicating a spin forbidden reaction with $^3O_2$. When performing the former oxidation using oxygen-18 labelled O_2, they observed nearly total incorporation of the heavier isotope mainly in the lactone ring, with partial incorporation in the ether bridge of the trioxane ring (Scheme 61a). When they used their labelled O_2 for the latter oxidation instead, they saw the heavier isotope exclusively in the peroxide bridge of the trioxane (Scheme 61b).



Scheme 61: Acton and Roth's oxygen-18 labelling studies, with heavy O_2 used in a) the photo-oxygenation step and b) the second oxidation step.

This provides evidence supporting the Hock Cleavage mechanism shown in Scheme 58, and also shows the order of ring closure to **76**, shown in Scheme 62.

The oxidation of **98** to **99** is not yet fully understood, but enol oxidations with $^3O_2$ proceeding *via* electron transfer mechanisms have been reported for similar substrates, and it is conceivable that a related process is occurring here.[257-258]

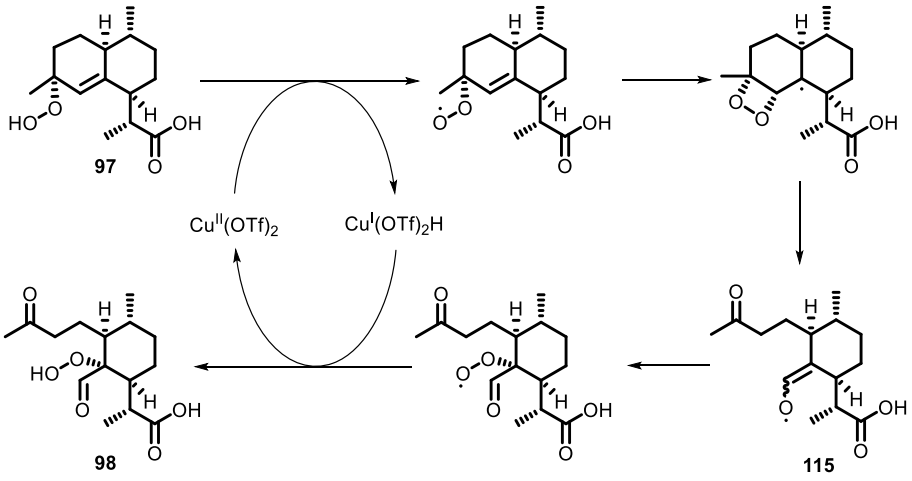


Scheme 62: The stereospecific cascade of ring closures leading to artemisinin 76.

The final ring closure cascade to provide artemisinin **76** is shown below in Scheme 62. This sequence of ring forming reactions is stereospecific, leading only to the naturally occurring diastereomer of **76**. Formation of the acetal species **113** and **114** are likely to be reversible, with the driving force for the reaction being the elimination of water to form the lactone ring in **76**. In the presence of water and under acid catalysis, lactone formation is reversible and may lead to lower yields. Whilst the acetal formation steps can form diastereomers of **113** and **114**, only structure **114** with the stereochemistry shown has the correct geometry for lactone ring formation, explaining the stereospecificity of the cascade.[254]

Another mechanistic pathway has been proposed based on radical intermediates. Early on, Haynes and Vonwiller concluded that the conversion of DHAA **97** to artemisinin **76** must be radical in nature, based on the observation that ground state dioxygen is required.[259] By their mechanism, shown in Scheme 63, the reaction is initiated by abstraction of the peroxy hydrogen by their copper(II) triflate catalyst, giving a peroxy radical. Ring closure gives an α-radical dioxetane which rearranges to give **115**, the enol radical analogue of **98**. Unlike enol **98**,

reaction of **115** with $^3O_2$ is spin allowed and would be expected to proceed rapidly, giving the observed intermediate **99** after back-hydrogen transfer and turnover of the copper catalyst.



Scheme 63: Haynes and Vonwiller's proposal for a radical-mediated rearrangement of allylic hydroperoxide 97, initiated by catalytic copper(II) triflate.

However, they later retracted this mechanism based on the similarities to Acton and Roth's work.[260] The fact that Acton and Roth achieved the same results using TFA, which has no redox capabilities, led them to concede that their copper catalyst was actually acting as a Lewis acid. They noted that the means by which enol **98** reacts with $^3O_2$ remained unclear.

Another indication of the intermediacy of radicals can be seen in the work of Roth and Acton themselves.[234] When leaving a solution of hydroperoxide **97** in hexane to stand under oxygen, they observed slow conversion to artemisinin, in the absence of any acid catalyst. However, this is not conclusive as the amount of artemisinin formed was low, and could also be explained by action of the weakly acidic carboxylic acid of **97**.[261] The true mechanism of this reaction may still yet to be revealed.

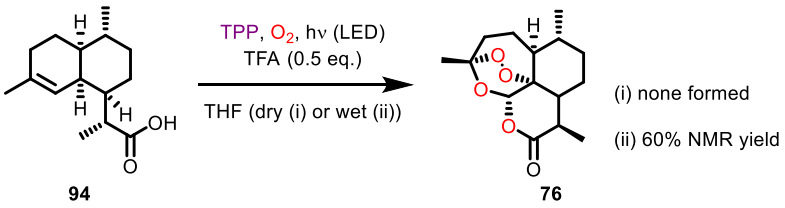
Section 2.3: The Synthesis of Artemisinin in Aqueous Solvent Mixtures.

The work presented in the following sections is part of a collaborative effort towards the development of a cheaper, more sustainable process for the semi-synthesis of artemisinin **76** by the route described above. Where significant contributions have been made by other parties to the studies described below, credit has been given.

Section 2.3.1: The Role of Water in the Artemisinin Synthesis.

Water is considered by many to be the ideal solvent for Green Chemistry, though its use in organic synthetic processes is limited. This is mostly due to problems with the physical properties of water, specifically its high boiling point and the poor solubility in water of many organic substrates. An additional problem for singlet oxygen chemistry is that water is a highly efficient quencher of $^1O_2$, as discussed in Section 1.2.4.

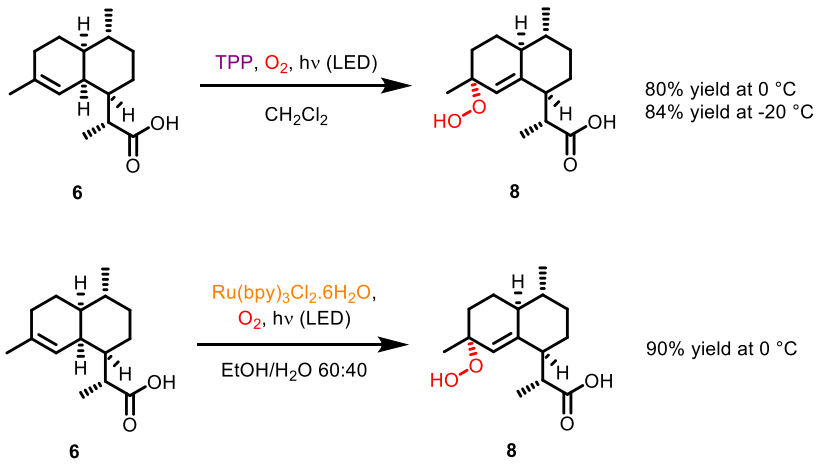
However, early experiments in this project showed that at least a small amount of water is not only beneficial, but vital to the synthesis of artemisinin **76**. Scheme 64 shows the one-pot synthesis of **76** from DHAA **94** in THF, one where the THF has been dried and distilled (Scheme 64, (i)) and another in which THF was used directly from the bottle without drying (Scheme 64, (ii)). Under anhydrous conditions, no artemisinin was formed, instead giving a complex mixture of side products. Based on this result, we began work towards a process for the synthesis of artemisinin in aqueous mixtures of organic solvents.



Scheme 64: One-pot synthesis of 76 from DHAA 94 using meso-tetraphenylporphyrin (TPP) as photosensitiser, in i) sodium dried, distilled THF and ii) THF as supplied commercially

Section 2.3.2: Studies on the Schenck Reaction of DHAA in Aqueous Solvents.

Previous work on the photochemical synthesis of **76** from **94** all showed a significant effect of temperature on the selectivity of the initial photo-oxygenation step. Good selectivity for the desired hydroperoxide isomer **97** over the major side product **103** was only at lower temperatures, and so published syntheses of **76** have all been cooled to well below 0 °C. We observed that in a 60:40 mixture of ethanol and water, the selectivity of the photo-oxygenation towards **97** was increased by comparison to dry organic solvents, even at 0 °C (Scheme 65).

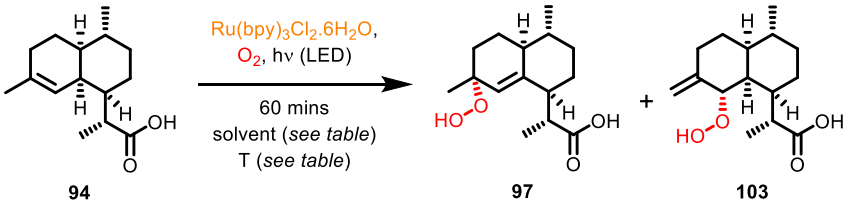


Scheme 65: The yields of hydroperoxide 97 obtained by photo-oxidation of 9 a) in CH_2Cl_2 by Seeberger et al. and b) in water/ethanol by our group.

Cooling is an energy intensive and therefore costly process, and it would be to the benefit of any industrial process to be run as close to ambient temperature as possible. For this reason, we studied the variation in selectivity between the

tertiary hydroperoxide **97** and the secondary hydroperoxide side product **103** with temperature when the photo-oxygenation of DHAA **94** was carried out in ethanol/water mixtures. Because the solubility of DHAA varies greatly in these solvents depending on the amount of water present, the effect of solvent composition on selectivity was also studied. The greater proportion of ethanol would mean higher solubility of DHAA and allow the process to run at a higher concentration, increasing throughput and productivity.

All reactions were performed on 50 mg **94** in 10 mL solvent, with 2 mg $Ru(bpy)_3Cl_2.6H_2O$ as photosensitiser. All reactions were illuminated with white LED light for exactly 1 hour, then stopped before full completion. Formation of the third hydroperoxide isomer **104** was seen to be negligible. Selectivities were calculated from the ratio of peak areas for the characteristic ^{1}H-NMR peaks of hydroperoxides **97** and **103**, δ = 5.25 and 5.08 ppm, respectively (in $CDCl_3$ relative to TMS). Exact conditions and results are shown in Table 3.

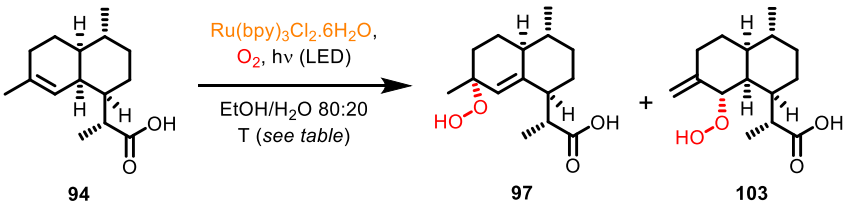


Entry	Solvent	Temperature / °C	Selectivity / 97:103
1	$EtOH/H_2O$ 60:40	30	90:10
2		0	90:10
3		-15	92:8
4	$EtOH/H_2O$ 70:30	30	89:11
5		0	90:10
6		-15	90:10
7	$EtOH/H_2O$ 80:20	30	87:13
8		0	90:10
9		-15	92:8
10		-30	92:8

Table 3: The temperature dependence of the photo-oxygenation of 94 in aqueous solvent mixtures. All reactions were performed at a concentration of 2.12 x 10^{-3} mol dm^{-3} and illuminated for 1 hour using white LED light. $Ru(bpy)_3Cl_2.6H_2O$ was used as photosensitiser.

The above study showed very little dependence of the selectivity between hydroperoxides **97** and **103** on either temperature or solvent composition. Furthermore, selectivity for **97** remained high across the range of temperatures studied.

To corroborate the results of this study, two further reactions were performed in ethanol/water 80:20, differing only in reaction temperature. Unlike the previous study, these reactions were regularly monitored and stopped at full completion. Additionally, to avoid problems with degradation of **97** in $CDCl_3$, acetone-d_6 was used for the NMR analysis. Again, no change of selectivity was observed despite the 40 °C difference in temperature (Table 4). The expected variation with rate was seen, with the higher temperature taking place in a shorter time. This means that a process in aqueous solvent mixtures running at or just above room temperature can give increased yield, higher throughput and improved energy efficiency compared to a process in conventional solvents, in accordance with all of our stated aims.



Entry	Temperature / °C	Time to completion / h	Selectivity / 8:9
1	-8	5	83:17
2	32	3	83:17

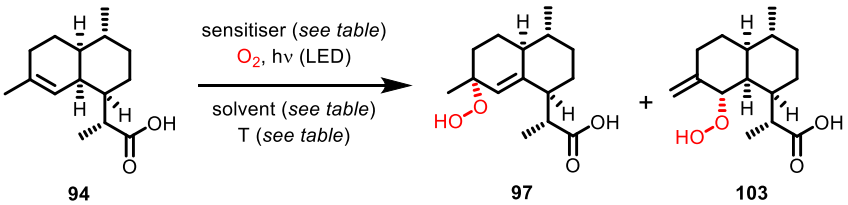
Table 4: Photo-oxygenation of 6 in EtOH/H_2O 80:20, showing no temperature dependence. All reactions were performed at a concentration of 2.12 x 10^{-3} mol dm^{-3} and illuminated using white LED light. $Ru(bpy)_3Cl_2.6H_2O$ was used as photosensitiser.

Since the observed effect only manifests in the presence of bulk quantities of water and does not seem to have a linear relationship to the concentration of water, it can be assumed that it results from a bulk property of water as a solvent, rather than direct participation of water in the reaction mechanism. A reasonable

rationalisation could be the strong hydrogen-bonding potential of water. Selectivity in reactions of $^1O_2$ has been known to arise from hydrogen-bond donating groups on organic substrates, such as the 'mode switching' between the Schenck and [2+2] reactions in the photo-oxygenation of enecarbamates reported by Adam *et al.*[150] and the facial selectivity for the Schenk reaction of allylic alcohols discussed in Section 1.2.4. Furthermore, this selectivity is removed when these reactions are performed in hydrogen-bonding solvent. These results show that hydrogen-bonding can affect reactions of $^1O_2$. If hydrogen-bonding were significant to the stability of the perepoxide intermediates, it would be expected that the less hindered *exo*-perepoxide would have more room for water molecules to co-ordinate, and so be stabilised to a greater extent than the *endo*-perepoxide. This would be expected to raise the activation energy for rearrangement to hydroperoxide **103**, lowering the rate for this pathway and increasing the selectivity for **97**.

To find out if hydrogen-bonding affects the selectivity of the reaction, another strong hydrogen-bond donor was used in place of water – the fluorous alcohol 1,1,1,3,3,3-hexafluoropropan-2-ol (HFIP). If the hydrogen bonding hypothesis were correct then an increase of selectivity at high temperatures would be expected for mixtures of HFIP and organic solvents compared to these solvents alone.

The solvents used were acetonitrile, with $Ru(bpy)_3Cl_2.6H_2O$ as photosensitiser, and toluene, for which meso-tetraphenylporphyrin (TPP) was used instead of $Ru(bpy)_3Cl_2.6H_2O$ due to the insolubility of the latter in pure toluene. For these experiments a known amount of biphenyl was added as an internal standard to help quantify the NMR results, allowing us to report a yield of tertiary hydroperoxide **97** rather than a relative selectivity. Full conditions and results are shown in Table 5.



Entry	Solvent	Sensitiser	Reaction Time / min	Yield of 97 / %
1	MeCN	$Ru(bpy)_3Cl_2$	40	59
2	MeCN/HFIP 90:10	$Ru(bpy)_3Cl_2$	60	59
3			1000+	29
4	Toluene	TPP	40	68
5	Toluene/HFIP 90:10	TPP	60	62
6			1000+	6

Table 5: Study on the effect of the strongly hydrogen-bonding species HFIP on the selectivity of the photo-oxidation of 94. All experiments were carried out at 30 °C on 50 mg 94 in 10 mL solvent. 0.1 eq biphenyl was added to each reaction as an internal standard.

The experiments were carried out in acetonitrile and acetonitrile/HFIP 90:10 showed no difference in yield of **97** (Table 5, Entries 1 and 2). Experiments in toluene and toluene/HFIP 90:10 showed a detrimental effect of adding HFIP, contrary to the expected outcome (Entries 4 and 5). However, when either of the reaction mixtures containing HFIP were left to stand overnight, considerable degradation of **97** was observed, which could account for the lower yields (Entries 3 and 6).

Further information about the role of water in the photo-oxygenation of DHAA **94** can be obtained by considering the rate of quenching of $^1O_2$ by **94** in the presence of water. To see how the lifetimes of $^1O_2$ compared in mixtures of water and ethanol, fluorescence lifetime measurements were performed by group member Dr Raphael Horvath in collaboration with the University of Durham. Lifetime measurements were taken by exciting an air-equilibrated sample with a 5 ns laser pulse at 355 nm (UV), then measuring the near-IR emission spectrum at the characteristic $^1O_2$ emission wavelength of 1270 nm. The intensity of the emission was measured over time and fitted to a monoexponential decay to extract the

lifetime, τ. Measurements were taken in pure dichloromethane, pure ethanol and ethanol/water 50:50. The measurements were repeated with varying concentrations of **94** and the the rate of quenching was calculated using the Stern-Volmer relationship:

$$\frac{1}{\tau} = k_q[\mathbf{94}] + \frac{1}{\tau_0}$$

According to this equation, a plot of the reciprocal of the lifetime against concentration of **94** would give a straight line with a gradient equal to k_q, the quenching constant for **94**, which can be related to the rate of the first step (perepoxide formation) of photo-oxygenation. Interestingly, the quenching constant of reaction in ethanol/water is more than twice that in DCM, and six times that in ethanol without water (Figure 16). This is further evidence of participation of water in the reaction mechanism and shows that there are benefits to these aqueous systems above and beyond the sustainability and safety benefits of moving away from dichloromethane.

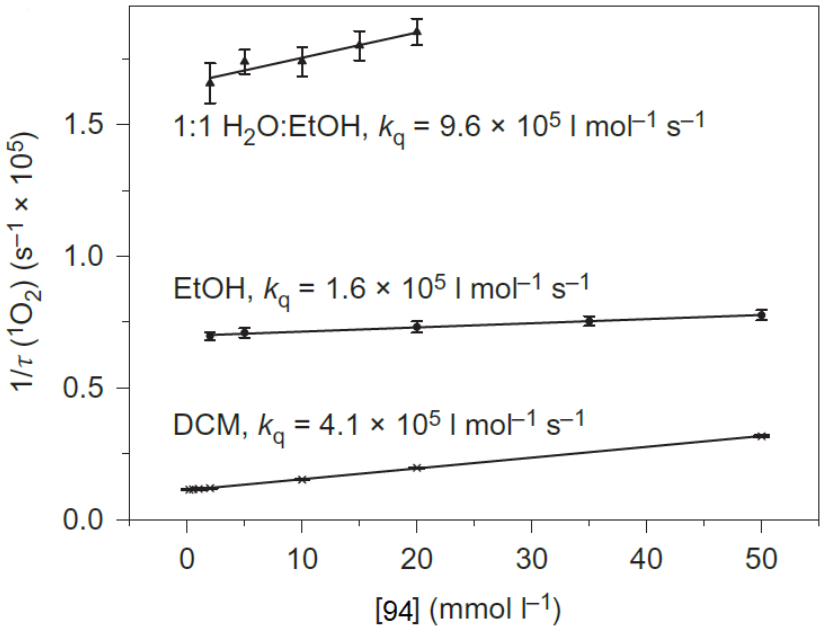


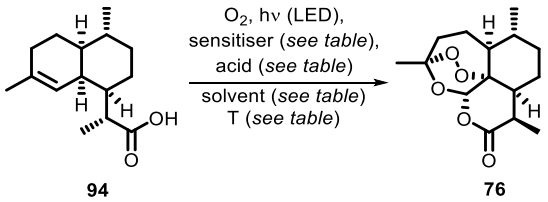
Figure 16: Quenching constants of $^1O_2$ by DHAA 94 in various solvents measured as the concentration dependence of the $^1O_2$ fluorescence lifetime according to the Stern-Volmer equation.

Selectivity between hydroperoxides **97** and **103** is a result of the side selectivity of the Schenck reaction of **94**, as previously discussed in Sections 1.2.4. and 2.2.2., which results from competition between the *endo* and *exo* isomers of the perepoxide intermediate. The preference for the *endo* perepoxide at low temperatures is in line with the *cis*-effect, since it is stabilised by more allylic C—H bonds than the *exo*. The steep reduction in selectivity as the temperature is raised indicates that the difference in energy between the two perepoxide isomers is not large. The demonstrated lack of a strong temperature dependence of the selectivity in aqueous mixtures indicates an interaction between water molecules and the perepoxide intermediate or related transition states that further stabilises the *endo* perepoxide over the *exo*. The strength of this interaction shows that it must be more significant than the temperature dependant *cis* effect. Such an effect is as yet unreported in the literature.

Section 2.3.3: Process Development in Aqueous Mixtures.

In light of the benefits to selectivity in aqueous mixtures that are presented in the above section, we began work on developing a full process for the synthesis of artemisinin **76** in aqueous mixtures. Initial screening of reaction conditions was performed using standard batch methods, with a view to applying our best conditions to continuous flow. As well as cosolvent and concentration, we studied the effect of acid catalyst and photosensitiser.

A solution of DHAA, acid and photosensitiser in the stated solvents at concentrations shown in Table 6 were illuminated with constant O_2 bubbling for 7 hours, then stirred for a further 48 hours in the dark to effect full conversion to artemisinin **76**. Yields were calculated from the crude ^{1}H-NMR mixtures against 10 mol% biphenyl as an internal standard.



Scheme 66: The one-pot conversion of DHAA 94 to artemisinin 76 in aqueous solvent mixtures. A range of conditions were screened and are shown in Table 6.

Several water-miscible organic solvents were used in the course of this study. As well as ethanol (EtOH), which was used in the previous studies on the selectivity of the Schenck photo-oxygenation step, isopropanol (^{i}PrOH) and tetrahydrofuran (THF) were screened to see if the yields of artemisinin **76** were affected. In comparable reactions with solvent/water ratios of 60:40, THF outperformed both alcoholic solvents, giving a yield of 66% compared to 59% for ^{i}PrOH and 50% for EtOH (Figure 17). This trend of decreasing yield corresponds to the increasing nucleophilicity of the organic solvent used.

Entry	Solvent	[94] / mol dm^{-3}	Photosensitiser	T / °C	Acid	Eq. Acid	Yield / %
1	THF/H_2O 60:40	5.3 x 10^{-2}	TPP	10	TFA	0.5	56
2	THF/H_2O 60:40	5.3 x 10^{-2}	$[Ru(bpy)_3]Cl_2$	10	TFA	0.5	66
3	THF/H_2O 60:40	5.3 x 10^{-2}	$[Ru(bpy)_3]Cl_2$	10	TFA	6.3	58
4	THF/H_2O 60:40	5.3 x 10^{-2}	$[Ru(bpy)_3]Cl_2$	10	H_3PO_4	0.5	52
5	^{i}PrOH/H_2O 60:40	5.3 x 10^{-2}	$[Ru(bpy)_3]Cl_2$	10	TFA	0.5	59
6	EtOH/H_2O 60:40	5.3 x 10^{-2}	$[Ru(bpy)_3]Cl_2$	10	TFA	0.5	50
7	EtOH/H_2O 60:40	2.1 x 10^{-2}	$[Ru(bpy)_3]Cl_2$	10	TFA	0.5	50
8	EtOH/H_2O 60:40	5.3 x 10^{-2}	$[Ru(bpy)_3]Cl_2$	10	TFA	1.0	55
9	EtOH/H_2O 60:40	5.3 x 10^{-2}	TPP	10	TFA	0.5	0
10	EtOH/H_2O 60:40	2.1 x 10^{-2}	$[Ru(bpy)_3]Cl_2$	10	H_2SO_4	0.5	47
11	THF/EtOH/H_2O 5:75:20	2.1 x 10^{-2}	$[Ru(bpy)_3]Cl_2$	10	TFA	0.5	62

Table 6: Process optimisation studies on the synthesis of artemisinin 76 in aqueous solvent mixtures.

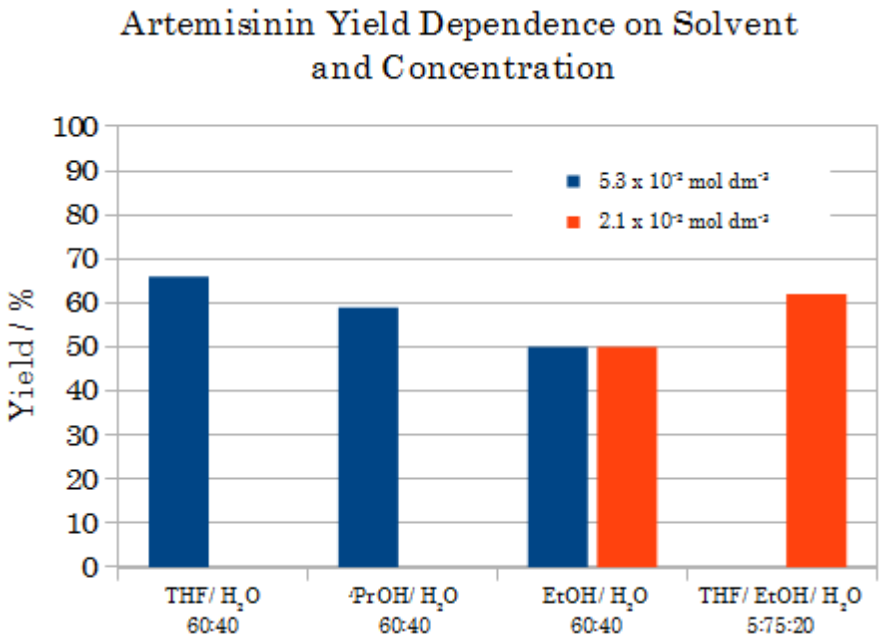


Figure 17: Trends in yield with reaction solvent and concentration. All reactions were performed using $Ru(bpy)_3Cl_2.6H_2O$ (0.5 mol%) as sensitiser and TFA (0.5 eq.) as acid catalyst. Photo-oxygenations were performed at 0 °C with addition steps performed at room temperature.

Many of the known or proposed intermediates discussed in Section 2.2.2. could be expected to be susceptible to nucleophilic attack, particularly under the acidic reaction conditions. Additionally, Brown and other groups have reported artemisinin itself to be unstable in acidic solutions of nucleophilic solvents such as methanol, undergoing solvolysis and ring opening. The long reaction times of 2-3 days mean that even a slow degradation of the product under the reaction conditions could lead to a significant lowering of the yield. We tested the stability of samples of commercially acquired artemisinin in acidic solutions with dichloromethane (DCM), THF, EtOH, THF/water 60:40 and EtOH/water 60:40. Two acids, trifluoroacetic acid (TFA), used by Seeberger *et al.* and by Sanofi in their industrial scale process, and sulfuric acid. After standing in these solutions for 24 hours, considerable degradation of artemisinin was observed in DCM and EtOH by both acids. Slight degradation was seen in EtOH/water, whilst on the timescale of this experiment artemisinin was stable in both THF and THF/water. These observations were in line with the trend in yields shown in Figure 17.

Participation of the solvent in the reaction mechanism could lead to reduction in yield in several ways; the solvent could react with the product as above, with intermediates in an irreversible way leading to the formation of new side products, or with the intermediates in a reversible way, affecting the position of equilibria and lowering the rate of product formation, allowing pre-existing side products to form with higher selectivity. However, when performing the reaction in a three-component mixture of THF, EtOH and water in a 5:75:20 ratio artemisinin was received in a 62% yield. The loss of yield in this reaction compared to in THF/water was less than that observed previously when changing from THF/water to EtOH/water, despite the fact that the three-component mixture has a greater overall proportion of ethanol than the two-component EtOH/water experiment shown. This indicates that the action of the organic solvent as a nucleophile is a minor factor in explaining the observed trend in yields.

Another possible contributing factor to the increased yields achieved in THF is the buffering of the strong acid catalysts by the solvent. Solvent molecules are present in a huge excess compared to substrate or catalyst and so can have a substantial effect on the solution pH. Seeberger *et al.* saw that their yields of artemisinin varied with acid strength (pk_a) at a constant catalyst loading and with catalyst loading at a constant acid strength, which suggests a dependence of the reaction outcome on pH. If the higher yield in THF was down to a buffering effect of the solvent, this would explain why only 5% THF in the three-component mixture provided some of the same benefits as 60% THF. From a Green process point of view, the three-component mixture may be preferable due to the lower cost of ethanol compared to THF, and its ready availability on a large scale from biomass. On the other hand, solubility of DHAA and related compounds is much higher in THF than in ethanol, which would allow the reaction to be performed at higher

concentrations, reducing solvent waste, as well as allowing higher proportions of water to be used, lowering the flammability of the mixture and making the process safer to perform.

The use of aqueous mixtures opens up the possibility of using less toxic, water soluble acid catalysts instead of TFA used by Seeberger and by Sanofi. Since we also believe acid strength to be an important factor in determining the overall yields, several different acid catalysts were tested with a range of pK_a values. Acids were tested in both THF/water and EtOH/water mixtures and are shown in Table 7 compared to TFA in either solvent.

Entry	Solvent	Acid	Equivalents	pK_a	Yield 76 / %
1	THF/water	TFA	0.5	-0.25	66
2		H_3PO_4	0.5	2.12, 7.21	52
3	EtOH/water	TFA	0.5	-0.25	50
4		H_2SO_4	0.5	-3.0, 1.99	47
5		py.TfOH	0.5	5.21	55
6		py.H_2SO_4	0.5	1.99, 5.21	59
7		pyr.TfOH	0.5	11.31	0
8		Et_2N.TfOH	0.5	11.09	0

Table 7: Variation of yield with acid in both THF/water and EtOH/water mixtures. All reactions were performed at a concentration of 5.3 x 10^{-2} mol dm^{-3} with $Ru(bpy)_3Cl_2.6H_2O$ (0.5 mol%) as sensitiser. Photo-oxygenations were performed at 0 °C with addition steps performed at room temperature.

The mineral acid H_2SO_4 showed a decrease in yield compared to TFA in EtOH/water, suggesting that higher pK_a catalysts are not ideal. However, a weaker mineral acid H_3PO_4 was tested in THF/water and also showed a lowering of the yield.

In addition, several amine salts were screened to see if better selectivity could be achieved using catalysts with a considerably higher pK_a. The pyridinium salt of sulfuric acid (py.H_2SO_4, Entry 6) with a primary pK_a of 1.99 gave the highest yields in EtOH/water, 59% compared to 50% when using TFA. The pyridinium salt of

trifluoromethanesulfonic acid (py.TfOH, Entry 5) with a pK_a of 5.21 also showed an increased yield compared to TFA, giving artemisinin in 55% yield. TFA salts of secondary amines pyrrolidine (pyr.TfOH, Entry 7) and diethylamine (Et_2NH.TfOH, Entry 8) did not induce the Hock cleavage step, which is unsurprising since the pK_a values for these salts are around 11, so the parent amines are more basic than the expected values for either of the allylic hydroperoxide oxygens.

Several photosensitisers were screened: TPP, $Ru(bpy)_3Cl_2$ and methylene blue (Figure 18). Methylene blue would be preferable from a Green Chemistry standpoint – it is non-hazardous, water soluble, cheap and easy to make, and contains no toxic metals. However, it was seen to be unstable under the reaction conditions, degrading over the course of the reaction.

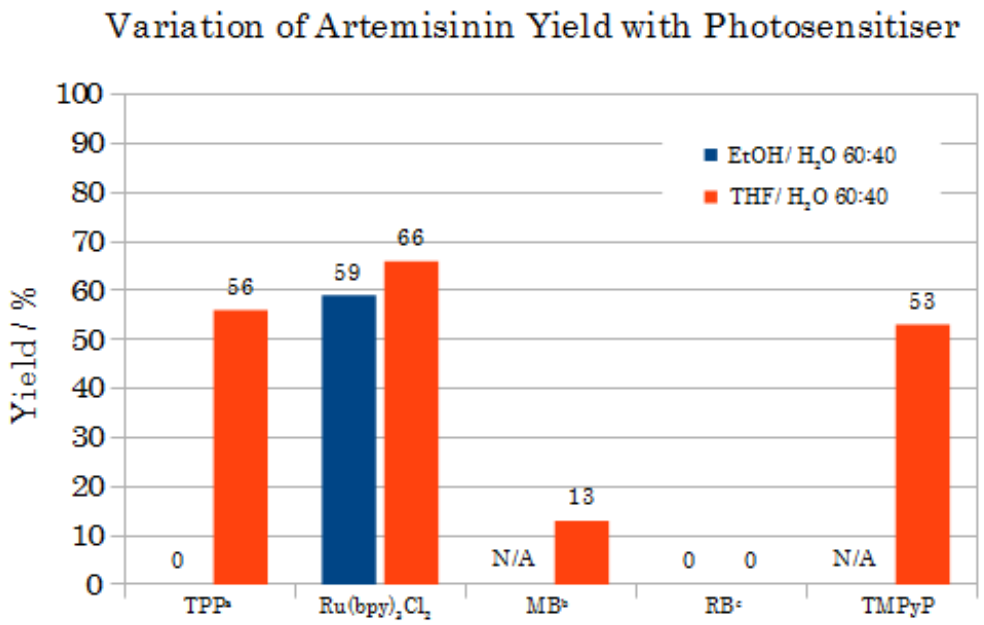


Figure 18: Sensitiser screenings in both THF/water and EtOH/water mixtures. All reactions were performed at a concentration of 5.3 x 10^{-2} mol with TFA (0.5 eq.) as acid catalyst. Photo-oxygenations were performed at 0 °C with addition steps performed at room temperature. [a]TPP was not soluble in EtOH/H_2O. [b]MB bleached over the course of the reaction. [c]RB degraded rapidly on exposure to the acidic reaction conditions.

Full conversion was not achieved, and the overall yield was low. The xanthone lactone Rose Bengal, another cheap and non-toxic organic photosensitiser, was

tested but degraded rapidly under the acidic reaction conditions before illumination was commenced.Of the two other photosensitisers that were screened, the ruthenium(II) salt outperformed TPP in a direct comparison in THF/water. In EtOH/water TPP was not soluble and no conversion was observed at all. The downside to using the metal-based sensitiser is that it is comparatively expensive and both more toxic and less sustainable than the three organic sensitisers tested. An unforeseen benefit of our aqueous system was the ease with which the product could be recovered from the reaction mixture. By concentrating the mixture under vacuum and in doing so increasing the proportion of water in the solvent mixture, **76** can be recovered by fractional crystallisation from the reaction mixture. Artemisinin recovered in this way is of very high purity, and a crystal structure could be obtained using x-ray crystallography without any need for recrystallisation.

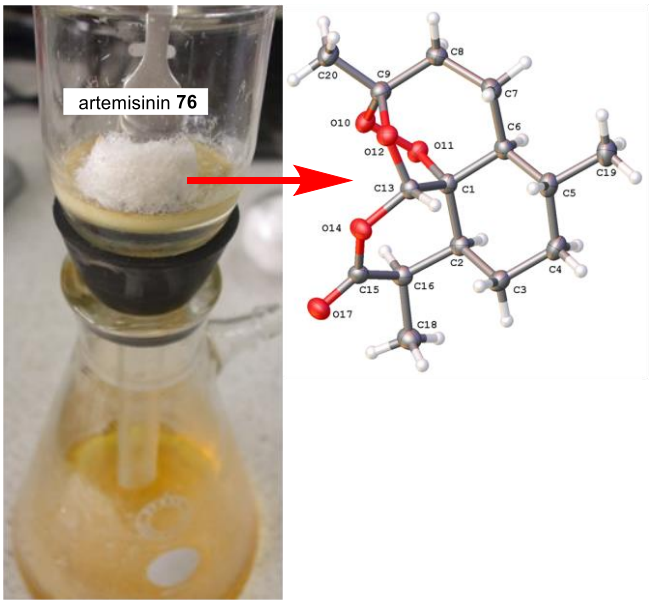
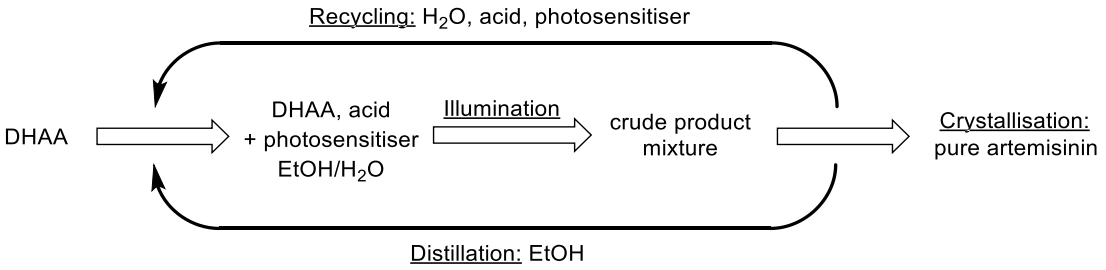


Figure 19: High purity artemisinin received directly from the reaction mixture by evaporation of the co-solvent and crystallisation.

Optical rotation measurements on the crystallised product gave an $[\alpha]_D^{25} = +66.7°$ (c 1, $CHCl_3$), identical to naturally sourced artemisinin. The process benefits

provided by this are clear – in not requiring an additional recrystallisation step to receive high-purity product we save on both reaction time and solvent waste, increasing the productivity and lowering the environmental impact of our process. An experiment was performed by group member Dr Zacharias Amara to assess whether the mother liquor from these crystallisations could be recycled (Scheme 67). The reaction was performed on a gram scale initially, then after reaction and crystallisation of the product, the aqueous phase containing photosensitiser and acid were added to a solution of fresh DHAA **94** in a mixture of fresh and recycled ethanol. The amount of DHAA **94** needed to be increased with each subsequent use to maintain the same concentration due to growing reaction volumes (Table 8). It was shown that catalyst mixture could be used at least 3 times with no change in yield for the individual run, though side products accumulating in the reaction mixture would be expected to cause a lowering of yields on further use. Table 8 also shows the yields for individual steps as well as the overall yield of 37%.



Scheme 67: The recycling protocol allowing reuse of the aqueous catalysts and the organic cosolvent, in this case ethanol.

Pass	Total Volume / mL	DHAA / mol	artemisinin / mol	Yield / %
1	200	4.24×10^{-3}	1.60×10^{-3}	38
2	300	6.36×10^{-3}	2.45×10^{-3}	39
3	438	9.33×10^{-3}	3.38×10^{-3}	36
Total	438	19.93×10^{-3}	7.43×10^{-3}	37

Table 8: The recycling experiment showing volume, quantities and yields for each subsequent pass. Concentration was kept constant at 2.12 mol dm^{-3}. $Ru(bpy)_3Cl_2.6H_2O$ (10 mg) was added as sensitiser with H_2SO_4 (112 µL) as acid catalyst.

By removing the need for extra purification steps, and by reusing the catalysts and solvents, we reduce the waste produced by our process and as a result, the environmental impact and the cost. The time taken to produce pure, saleable artemisinin will also be reduced by crystallising the product directly from the reaction mixture rather than isolating the crude and recrystallizing, further increasing the efficiency and throughput of the process.

A general observation on the synthesis of artemisinin in aqueous mixtures was that compared to conventional organic solvents the rate of artemisinin production was low. The following Section details work performed with the aim of increasing artemisinin productivity using continuous flow processing.

Section 2.3.4: Continuous Flow Reactions.

A continuous flow reactor ('rig') was built for performing the synthesis of artemisinin **76** in aqueous mixtures. Continuous flow chemistry is discussed in Section 1.1.4., and provides many benefits to a process such as this, in particular the high throughput that can be achieved with relatively small reactors, in accordance with our aim to produce large amounts of artemisinin in the shortest possible time. Other benefits include finer control over the reaction temperature and pressure, giving a finer control of the reaction and reducing the likelihood of an accident, and the relatively short amount of time the products are kept under reactive conditions, leading to a higher yielding and more efficient process.

In the specific case of our synthesis of artemisinin in aqueous solvent mixtures, described in the previous section, the use of continuous flow could help to avoid degradation of the product under the acidic reaction conditions by removing it from the system as it forms.

The rig used for this study was built around the sapphire tube photoreactor discussed in Section 1.2.6., with a 6-port switching valve configured as an O_2 dosing system for precise control of the amount of oxygen present. The sapphire tube reactor provides efficient lighting and temperature control, and is filled with glass beads to minimise the optical path length of the solution, as well as to provide good mixing of the reaction mixture, since the large diameter of the tube means the plug flow approximation cannot be reliably applied to this reactor (see Section 1.1.4.). Its high pressure tolerance allowed the use of raised pressures of O_2. A detailed description of the rig can be found in experimental Section 5.2.4.

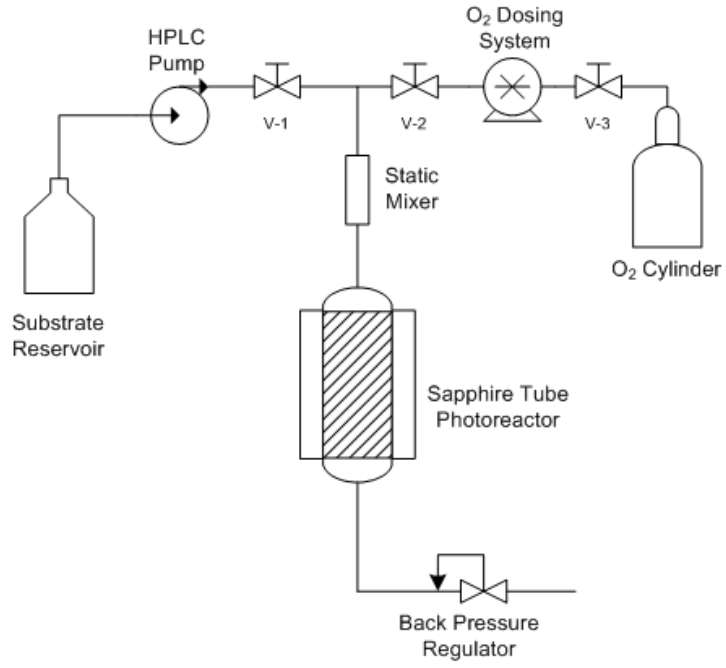


Figure 20: Schematic diagram of the continuous flow rig used for the reactions described below.

The synthesis of artemisinin **76** using the continuous flow rig shown above was performed in a semi-batch manner, rather than as a purely continuous reaction, due to the low rate of final conversion of enol **98** to **76**. A reaction mixture was prepared in the desired solvent, containing DHAA **94**, $[Ru(bpy)_3Cl_2]$ and H_2SO_4 (0.5 eq.). This was then fed into the reactor as described above. For each separate set of conditions, the reaction was begun at a high flow rate which was lowered in a stepwise manner until the maximum conversion from DHAA **94** was achieved.

	Solvent	[DHAA] / mol dm^{-3}	[$Ru(bpy)_3Cl_2$] / mol dm^{-3}	pO_2 / bar	Flow rate / mL min^{-1}	Conversion / %	Yield / %
1	EtOH/water 60:40	2.0×10^{-2}	1.0×10^{-4}	1	0.25	99	
2					0.5	93	
3					2	69	
4	EtOH/water 60:40	2.0×10^{-2}	2.0×10^{-4}	1	0.25	99	38
5					0.5	96	
6					1	80	
7					2	69	
8	EtOH/water 60:40	2.0×10^{-2}	1.0×10^{-4}	10	0.5	100	28
9					1	96	
10					2	90	
11					4	68	
12	EtOH/water 80:20	2.0×10^{-2}	1.0×10^{-4}	1	0.25	96	29
13					0.5	90	
14					1	84	
15					2	80	
16					4	38	
17	EtOH/water 80:20	4.0×10^{-2}	1.0×10^{-4}	1	0.25	94	23
18					0.5	67	
19					1	61	
20					2	43	
21					4	33	
22	EtOH/water 80:20	4.0×10^{-2}	1.0×10^{-4}	10	0.25	98	21
23					0.5	98	
24					1	93	
25					2	77	
26					4	56	
27	THF/EtOH/ water 5:75:20	2.0×10^{-2}	1.0×10^{-4}	10	0.25	99	46
28					0.5	98	
29					1	96	
30					2	92	
31					4	54	
32[a]	THF/EtOH/ water 5:75:20	2.0×10^{-2}	1.0×10^{-4}	10	0.25	99	16
33	THF/water 60:40	2.1×10^{-1}	1.0×10^{-4}	1	0.12	98	38
34					0.25	92	
35					0.5	87	
36	THF/water 60:40	2.1×10^{-1}	1.0×10^{-4}	10	0.12	98	36
37					0.25	98	
38					0.5	90	

Table 9: Optimisation studies on the synthesis of artemisinin in continuous flow. Experiments in green are used below in comparisons of productivity. [a]The reaction mixture was held under 10 bar O_2 for 16 hours after exiting the rig.

The flow rate at maximum conversion could be used as an indirect measurement of how the rate of the photo-oxygenation step varied with parameters such as concentration of **94**, concentration of photosensitiser and pressure. Results are shown in Table 9. After photo-oxygenation, the reaction mixture was collected and stirred under oxygen at standard pressure for 24 hours. Artemisinin **76** was then crystallised from the solution by evaporating away the co-solvent as described in Section 2.3.3. The variable we wanted to maximise in our flow process optimisation study was throughput rather than yield. For the sake of productivity, it may be beneficial when designing a process to accept a slightly reduced yield for the sake of material throughput. Therefore, a set of conditions (temperature, pressure, flow rate) which gave a conversion of greater than 95% is considered acceptable.

The initial test run using the rig described above was carried out in EtOH/water 60:40, with a substrate concentration of 2.0×10^{-2} M, a sensitiser concentration of 1.0×10^{-4} M (0.5 mol%) and a system pressure of 1 bar. The photoreactor was kept at 5 °C. The crude rig output was analysed by ^{1}H-NMR. At maximum conversion, a bulk collection was performed and the mixture was stirred overnight under air at room temperature before isolation of the product by crystallisation.

Under the initial conditions, an acceptable conversion was not achieved above 0.25 mL min^{-1}. Increasing the amount of photosensitiser to 1 mol% allowed faster conversion, and a 96% conversion was achieved at 0.5 mL min^{-1}. On crystallisation, 38% yield of artemisinin was recovered.

Decreasing the proportion of water in the solvent mixture was expected to increase the rate of photo-oxygenation by reducing the extent of quenching of singlet oxygen by water, though when the reaction was performed in EtOH/water 80:20, only 96% conversion from DHAA **94** was achieved at a flow rate of 0.25 mL min^{-1}. One possible explanation for this is that the extinction coefficient for $Ru(bpy)_3Cl_2$ is

lower in ethanol than in water and so less $^1O_2$ is generated for the same amount of irradiation. At this higher proportion of ethanol, more DHAA was soluble and the concentration could be increased to 4 x 10^{-2} M. The concentration of photosensitiser was kept the same, so the loading was effectively reduced to 0.25 mol%. This lowered the rate of photo-oxygenation to the point that an acceptable conversion was not possible, with only 94% DHAA conversion at 0.25 mL min^{-1}. Additionally the yield of artemisinin was reduced to 23% compared to 29% for the previous experiment.

In THF/water 60:40, the solubility of DHAA **94** was much greater and so the reaction could be ran at a much higher concentration of 2.1 x 10^{-1} M, a greater than tenfold increase. Because of this the conversion dropped and the flow rate needed to be reduced to 0.12 mL min^{-1} to achieve a 98% conversion. Respectable isolated yields of 38% were achieved, reflecting the findings of the batch optimisation experiments in the previous section. Since the yields are comparable to the reactions at lower concentration in EtOH/water, moving to THF as solvent still represents a fivefold increase in productivity.

This flow rig was originally designed for use with supercritical CO_2 and is resistant to high pressures. It was thought that the rate of photo-oxygenation could be increased by using higher system pressures and so increasing the amount of O_2 in solution. In both EtOH/water and THF/water the rate of photo-oxygenation was observed to increase, with a 96% conversion achieved at 1 ml min^{-1} for the former, and a 98% conversion achieved at 0.25 mL min^{-1} for the latter. In both cases the yield was only slightly reduced. This can be expected to greatly improve the productivity of the flow reactor in terms of space-time-yield.

The highest yields achieved were found in the three-component solvent mixture of THF, EtOH and water at a 5:75:20 ratio. Under 10 bar O_2, a 96% conversion from

DHAA was achieved at 1 mL min^{-1}, resulting in a 46% isolated yield of artemisinin. The 16% loss in yield between this experiment and the similar experiment performed in batch, whilst significant, may be outweighed by the 90% saving in solvent and tenfold increase in productivity, both in terms of cost and environmental impact. The effect on cost would depend on the relative prices of the solvent and substrate.

Finally, the factor limiting the productivity of our process is the rate of the spin-forbidden auto-oxidation step. Since increasing the pressure of O_2 drastically improved the rate of the photo-oxygenation step, it was thought that the same might apply to this second oxygenation. The rig output from an identical reaction to the three-component experiment described above, performed at 0.25 mL min^{-1}, was held in a 316 stainless steel autoclave under 10 bar O_2 for 16 hours. Surprisingly, the yield of artemisinin from this reaction was much lower than all previous runs at only 16%. Clearly this was not a feasible strategy for improving the throughput of this reaction.

Comparison of the various conditions in terms of productivity is enlightening as to exactly the parameters that have the greatest effect on material throughput. Table 10 shows the projected grams of artemisinin that could be produced per day, from a single rig of the size used in this study, for several of the conditions screened. For each system which gave an acceptable conversion (<95%) and yield (<20%), the productivity was calculated at the maximum flow rate that gave an acceptable conversion. The experiments used are coloured in green in Table 9. These calculations can be found in full in Experimental Section 5.2.

The highest rate of artemisinin production we achieved is 7.68 g day^{-1}. Whilst this is not competitive with the larger flow rig reported by Seeberger *et al.*, there are

some interesting points highlighted by this study with regards to improving the material throughput of artemisinin production.

Entry	Solvent	[DHAA] / mol dm^{-3}	pO_2 / bar	Flow rate / mL min^{-1}	Adjusted yield / %	Productivity / g day^{-1}
1	EtOH/ water 60:40	0.02	1	0.5	37	1.50
2	EtOH/ water 60:40	0.02	10	1	27	2.19
3	EtOH/ water 80:20	0.02	1	0.25	29	0.59
4	EtOH/ water 80:20	0.04	10	0.5	21	1.71
5	THF/ EtOH/ water 5:75:20	0.02	10	1	45	3.66
6	THF/ water 60:40	0.21	1	0.12	38	4.05
7	THF/ water 60:40	0.21	10	0.25	36	7.68

Table 10: Calculations of the projected productivity for selected flow experiments, shown in green in Table 9.

Somewhat surprisingly, the greatest contributing factor to the throughput of the reaction was not yield but concentration, followed by flow rate. Unfortunately, over the course of the study we have had to compromise between these two parameters, since running a reaction at high concentration necessitates a lower flow rate to achieve high conversion.

The two most highly productive sets of conditions, Entries 6 and 7, were high concentration and low flow rate, though our highest flow rate and highest yielding conditions (Entry 5) are still competitive. The ability to perform the photo-

oxygenation at higher than atmospheric pressures of O_2 is a great advantage, allowing the flow rate to be increased despite higher concentrations. In the following Section, several of the systems described in Sections 3.3.3. and 3.3.4. are compared in terms of their environmental impact, then compared to the method currently employed by Sanofi.

Section 2.3.5: Comparison of New and Existing Processes.

The systems evaluated here are the highest yielding experiments from the batch optimisation study in Section 2.3.3. the batch process in ethanol/water with solvent and catalyst recycling shown in Scheme 67 and the most productive flow process from Section 2.3.4. (Table 10, Entry 7). These processes are shown again in Table 11 and denoted processes **A**-**D**:

Entry	Process	Regime	Solvent	DHAA / mol dm^{-3}	Yield / %	PMI
1	A	Batch	THF/water 60:40	5.3 x 10^{-2}	66	56
2	B	Batch	THF/EtOH/water 5:75:20	2.1 x 10^{-2}	62	139
3	C	Batch	EtOH/water (varying proportions)	6.9 x 10^{-2}	37	105
4	D	Flow	THF/water 60:40	2.1 x 10^{-1}	36	28
5	Sanofi	Semi-batch	dichloromethane	1[a]	54	23

Table 11: Comparison of selected processes in terms of their process mass intensities. [a]photo-oxygenation step only – extra solvent used in subsequent recrystallisations.

Again, concentration appears to be the greatest contributing factor here, and – as stated many times throughout this thesis – it is the solvent that contributes most to the waste of a process. Since the mass of water is not included in PMI calculations by convention, a higher proportion of water in the solvent mixture also improves the PMI. This is evident when comparing the PMI values for the two

standard batch processes **A** and **B** (Entries 1 and 2). The latter has a PMI more than 2.5 times that of the former, which can be mostly attributed to the extra 20% of the solvent volume made up with water. This validates our assumption that aqueous solvent mixtures are a sustainable option. The reaction yield is much more significant here than when determining the throughput of the flow rig above, since PMI is calculated from the mass of product. Thus, despite the higher overall concentration of the recycling experiment (process **C**, Entry 3), the PMI is higher than the non-recycled process **A**. The best PMI is received in the flow experiment **D** (Entry 4), though this can be accounted for almost solely by the higher reaction concentration. Still, it is the only process developed with a PMI comparable to that of Sanofi's existing process (Entry 5). The fact that it achieves this at one-fifth of the concentration shows the value of our new, Greener system.

To understand the environmental impact of a process it is not only important to consider the amount of waste produced, but also the hazards associated with that waste. As previously stated in Section 2.2.1., a major drawback of the Sanofi process is the dichloromethane solvent, which is classified as a category 2B carcinogen, and requires careful containment. Replacing this with THF or EtOH would make the containment requirements less stringent, saving money, as well making disposal easier and reducing the risk of a large-scale environmental disaster. The same can be said for replacing the volatile and toxic acid TFA with H_2SO_4. In this regard, all of our processes are improved compared to the existing Sanofi process.

Whilst productivity and waste are important considerations in process chemistry, the most important factor is cost. Information on the costs involved in running Sanofi's current process is not available, though it is likely that the substrate DHAA **94** is the most expensive material per unit mass. Perhaps then the higher

yielding but more wasteful processes **A** or **B** would be more profitable overall, and therefore more sustainable economically. Certainly, ethanol is cheaper than either dichloromethane or THF and is more easily obtained from renewable sources, so the processes **A** and **C** which use mainly ethanol as solvent may be preferred.

Section 2.5: Chapter Summary.

The above Chapter presented work towards improving the industrial scale process currently applied by Sanofi to the synthesis of the antimalarial drug artemisinin. Or criteria for an improved process were

a) A more productive and efficient synthesis, giving higher yields and a greater rate of production for artemisinin.
b) A Greener process, replacing the undesirable solvent dichloromethane as well as substituting the photosensitiser and acid catalyst for less hazardous alternatives and increasing the material and energy efficiency of the process.
c) Low cost. Addressing the two above points was predicted to lead to lower cost to the manufacturer, which in turn would lead to cheaper and more widely available artemisinin-derived malaria medicines and so increase their availability in the economically poor regions where they are most needed.

Our strategy was to use an aqueous system combining a large proportion of water with a cheap organic co-solvent. Systems were described above in both batch and flow regimes which fulfilled the above aims and provided additional unforeseen process benefits.

Firstly, studies on the Schenck photo-oxygenation in mixtures of water and ethanol showed a previously unknown effect of water on the reaction outcome (Section 2.3.2.). Greater selectivity for the desired allylic hydroperoxide isomer was achieved without a requirement for cryogenic temperatures during photo-oxygenation, which had been assumed by previous research groups. It was shown that the selectivity in these solvent mixtures was much less dependent on the temperature than in dichloromethane or toluene, and that the proportion of water in the mixture did not directly affect the selectivity either. This effect was proposed to result from a bulk property of water, and whilst studies on the effect of hydrogen bonding on the selectivity of the Schenck reaction were inconclusive, fluorescence lifetime measurements on $^1O_2$ showed a higher rate constant for substrate quenching in our ethanol/water system compared to dichloromethane or ethanol alone. This indicates a stabilisation of the perepoxide intermediate or related transition states which could lead to the observed selectivity.

This discovery helps to further our stated aims in several ways: It shows that there are process benefits to the use of aqueous solvent mixtures above and beyond the Green Chemistry benefits from using a less hazardous solvent, and so validates our process. Increased selectivity gives an opportunity for higher overall yields, and the reduced requirement for reactor cooling gives a more energy efficient process, leading to higher efficiency and lower cost.

Our process development studies in batch, given in Section 2.3.3., further displayed the power of these aqueous systems. Optimisation of the reaction conditions led to greater yields than the Sanofi process without derivatisation of the substrate, removing an entire synthetic step and thus saving a large amount of material. Studies on the role of acid and solvent with regards reaction yield emphasised the importance of pH to the reaction outcome, and could lead to fine

tuning of the system for maximum output. Our system additionally allowed isolation of the pure product using simple evaporation of the cosolvent, avoiding extra crystallisation steps and saving on the associated time and material costs. This in turn led to opportunities for easy catalyst recycling that are not possible in conventional solvent systems.

These batch optimisation studies contribute to the fulfilment of our aims in several ways. The systems presented in Section 2.3.3. are high yielding, which can lead to greater productivity. They are more sustainable in many ways. As stated above, the material efficiency is much higher than the Sanofi process due to the removal of entire derivatisation and purification steps. The solvents used, ethanol and tetrahydrofuran, are considerably less hazardous than dichloromethane, and in the case of ethanol, particularly cheap and renewable. Recycling of the aqueous phase after crystallisation of the product reduces acid and photosensitiser waste. All of these points can be expected to contribute to a lower cost of the artemisinin produced in these systems.

Studies performed towards a continuous system for artemisinin production highlighted several factors that lead to a more productive, efficient process (Section 2.3.4). It was shown that concentration has the greatest effect on material throughput, and that in our laboratory scale reactor a compromise had to be reached with flow rate to achieve maximum productivity with high conversion. This issue could be addressed upon scale up, since a larger photoreactor would allow greater conversion at high flow rates.

A major benefit of using our sapphire tube photoreactors was the ability to perform the photo-oxygenation step at high pressures of O_2. This improved the rate of reaction, negating the low $^1O_2$ lifetime in aqueous mixtures. These factors will be

important upon scale up and optimisation thereof is expected to lead to further fulfilment of our aims.

In general, our strategy for the production of artemisinin using aqueous solvent mixtures is greatly improved compared to the process currently in place at Sanofi. We use less hazardous solvents and catalysts, perform our synthesis in fewer unit operations with fewer overall steps and a greater energy efficiency. Therefore, we predict that application of this system on an industrial scale would lead to cheaper, more sustainable artemisinin and help to address the problem of global supply.

Section 2.6: Future Directions

Further work towards industrial production of artemisinin in aqueous solvent mixtures would be best carried out at Sanofi. Our solvents and catalysts could be applied in their existing semi-batch reactor leading to immediate benefits to material cost and process efficiency. Further, precise optimisation of several factors would need to be performed to ensure the best reaction parameters for use with their reactor – the maximum concentration in their solvent would need to be found, as well as the correct balance of pH, perhaps using a sulfate or phosphate buffer solution. Optimisation of temperature, pressure and flow rate would give the best rate of photo-oxygenation.

The greatest inefficiency in the synthesis of artemisinin using aqueous solvent mixtures is the low rate of the auto-oxidation of enol intermediate **98** with ground state $^{3}O_{2}$. The precise nature of this transformation is unknown, though since it has been proposed that electron-transfer mechanisms are involved, an appropriate direction of study may be to research electrochemical redox processes or the use of superoxide ($O_{2}^{\cdot -}$) to increase the rate of this reaction.

In terms of a general research strategy, the process optimisation studies presented in this Chapter use a trial-and-error method of optimisation. This is due to an incomplete knowledge of the reaction mechanism and kinetics. More efficient and reliable directed optimisations would be possible if the reaction mechanism were better understood, which would require precise reaction monitoring experiments. The next Chapter presents work we have performed on the development of a continuous monitoring technique using nuclear magnetic resonance, and its use in studying the mechanism of the artemisinin synthesis.

Chapter 3: NMR Reaction Monitoring of the Synthesis of Artemisinin

Section 3.1: Introduction and Project Aims.

The photochemical semi-synthesis of artemisinin **76** presented in the previous Chapter is a complex multi-step sequence with a great deal of mechanistic intricacy. The contributions of many groups to our knowledge of the mechanism of the reaction, including the work of Brown *et al.* on the formation of side products, are described in Section 2.2.2.[233-235, 240-241, 254-256, 259-263] Many factors contribute to the yield of **76** with varying importance. The effect of parameters such as temperature, concentration and solvent can be completely different from step to step, and yet it can be difficult to separate the individual steps in order to know where and how these parameters contribute to an increase or loss of yield. This creates a barrier to performing a directed, rational optimisation of a process. Knowledge of a reactions mechanism enables informed decisions about process optimisation to be made, and can lead to a more optimal process in a shorter time than trial-and-error methods.

Therefore, we intended to study the mechanism and kinetics of the process described throughout Chapter 2, with a view to applying the knowledge gained to further optimising the yield and rate of our process. In particular, we were interested in a) assessing which points in the reaction sequence contribute most to loss of yield, b) probing the rearrangement and cyclisation steps, and c) investigating the parameters affecting side product formation. Additionally, we sought to identify and characterise any previously unknown intermediates leading to **76**, and any previously unreported side products.

An ideal reaction monitoring technique would be quantitative, non-invasive and would provide structural information about the species present.[264] We considered that reaction monitoring by nuclear magnetic resonance (NMR) would fulfil these criteria, as discussed in Section 3.2.2. We aimed to develop a method for the

continuous monitoring of photo-oxygenation reactions by NMR and to use said method to study the synthesis of artemisinin **76**.

Section 3.2: Background.

Section 3.2.1: Process Analytics and Reaction Monitoring for Green Chemistry.

Process analytical technology (PAT) – tools for the monitoring of chemical reactions and processes – is a vital part of the design and operation of Greener, more sustainable chemistry.[265] The 11th Principle of Green Chemistry recommends 'continuous monitoring for real-time waste prevention'. Optimisation of a process requires fundamental understanding of the effects of the various parameters under the operators control *i.e.* temperature, pressure, concentration, *etc*. In the previous Chapter, it was shown how a trial-and-error approach could be used to improve yields and productivity in our process for the synthesis of artemisinin **76**. This approach requires a considerable input of operator time and materials and it is difficult to be sure that the set of reaction conditions arrived at is truly optimal. Directed, expedient optimisation requires quantitative information on the progression of the reaction under the experimental conditions, not just its output. An understanding of where along the reaction co-ordinate the mechanistic pathways for product and side-product formation diverge provides points of attack where the reaction outcome can be influenced in favour of the desired product. Measuring rates of product formation rather than yields alone can aid in finding ways to increase yield without compromising on productivity, as was necessary in the processes described in Chapter 2.

Reaction monitoring with the intent of extracting kinetic information requires a method for collecting data on the rate of change of reagent and intermediate

concentrations which is **quantifiable**, **reproducible** and **sensitive**.[264] An ideal technique would additionally allow monitoring of the reaction *in situ*, under reaction conditions, in a non-invasive manner (Figure 21). A wide range of chromatographic, calorimetric and spectroscopic methods have been applied to the real-time analysis of chemical reactions in pharmaceutical development and are discussed below.

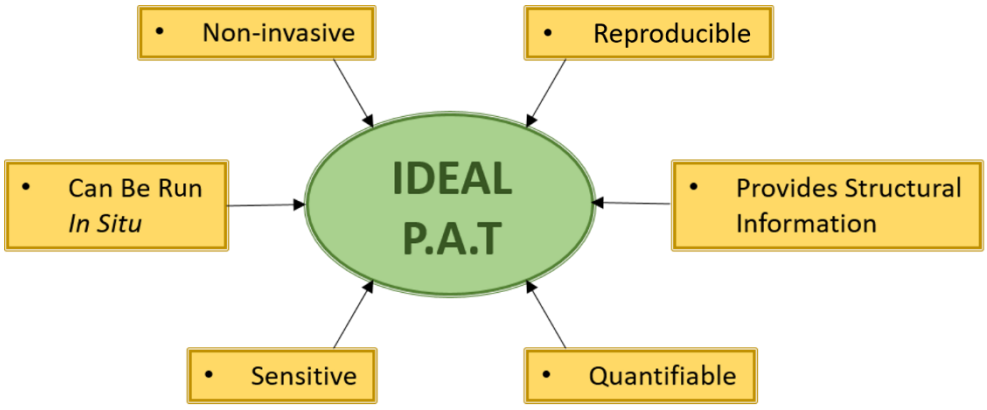


Figure 21: The qualities of an ideal process analytical technology (PAT).

Chromatographic methods such as gas chromatography (GC) or high-performance liquid chromatography (HPLC) are amongst the most widely used PAT. They can be used on-line or off-line, but in either mode are sample based *i.e.* aliquots must be removed from the reaction and injected into the analytical apparatus. This adds an unnecessary risk of contamination or degradation of the sample. The chromatograph separates the reaction mixture into its individual components either by applying a temperature gradient in the gas phase (in the case of GC) or by selective adsorption onto a solid phase (in HPLC). Time-resolved detection of the material as it exits the chromatograph gives an intensity *vs.* time trace, a chromatogram, with individual peaks for each component of the mixture. This is a simple and rapid way of determining the number of products formed in a reaction, and using the peak areas, the selectivity between them. However, chromatographic methods alone can rarely provide any structural data on the compounds in

question. HPLC is commonly coupled to mass spectrometry (LC-MS) which allows identification of the eluting product from their mass to charge ratios. The detectors commonly used for GC or HPLC are UV absorption, flame ionisation/conductivity or refractive index detectors, which are all only quantitative if the individual **response factors** are known for the analytes. Chromatographic methods are mostly useful if every component has previously been isolated and characterised, which is not always possible, particularly early in a process' development.

Spectroscopic or calorimetric methods of analysis have the advantage that they can be performed *in situ*, giving real-time feedback on a reaction as it progresses.[265] Methods based on attenuated total reflectance infrared spectroscopy (ATR-IR) have become a common tool for process chemists, and Mettler Toledo now produce a commercial ReactIR™ ATR probe which can be used off the shelf for this purpose.[266-267] The IR spectrum of the sample is measured over time, and the change in intensity of characteristic peaks from the products and intermediates are recorded. An IR spectrum shows peaks dependent on the functional groups present in the mixture, so there is inherent structural information in this method. The limitation for reaction monitoring is that for complex mixtures overlap of peaks is common and so measurement of the kinetics of the reaction can be difficult.

A common PAT for kinetic analysis is calorimetry.[268] Heat flow between the reaction and surroundings at a constant temperature is measured, and so the production or consumption of energy can be calculated and related to the rate of reaction. No structural data can be extracted from a calorimetry study, but it provides a simple and accurate method for analysing the kinetics of a process, and has been used to great effect by Donna Blackmond and others.

Both GC and ATR-IR have been used to great effect in our group for the automated self-optimisation of continuous flow reactors, where feedback from the on-line PAT into a computer algorithm allows rapid optimisation without the aforementioned material and operator input.[269-270] Any major or minor product in a mixture can be selected as the target of optimisation and its yield maximised. So far, these self-optimisation techniques have only been applied to relatively simple systems such as the methylation of amines using dimethyl carbonate.[270]

The one-pot synthesis of artemisinin is a particularly complex process, with multiple reactions occurring subsequently and many closely related species present. To acquire real-time kinetic and structural data for use in the optimisation of this reaction would require a technique which is simultaneously high resolution, quantitative, non-invasive and can provide structural information on any unknown intermediates and side products. High field nuclear magnetic resonance (NMR) spectroscopy is an incredibly powerful spectroscopic technique but is less commonly used for reaction monitoring than the above methods. NMR combines the structural analysis of IR with the accuracy of calorimetry and is quantifiable without the need to calculate response factors. The following section provides the theoretical background to this technique.

Section 3.2.2: Nuclear Magnetic Resonance Spectroscopy.

Nuclear magnetic resonance (NMR) spectroscopy is a structural analytical technique based upon the absorbance of electromagnetic radiation by atomic nuclei in strong magnetic fields.[271-272] Many atomic nuclei possess an intrinsic angular momentum known as **spin**, and are referred to as **spin-active**. The number of spin states available to a nucleus depends on that nucleus' **spin quantum number**, *I*. Spin-active nuclei also have another intrinsic property, the **magnetogyric ratio** γ,

a scalar quantity related to the strength of a nucleus' interaction with a magnetic field. The nuclear magnetic moment of a spin state, $\boldsymbol{\mu}$, is given by:

$$\boldsymbol{\mu} = \gamma \boldsymbol{I}$$

All nuclear spin states are degenerate in energy in the absence of an external magnetic field. In a magnetic field $\boldsymbol{B}$, the energies E of the spin states vary depending on their orientation in respect to the direction of the field. The separation between the states depends on the strength of the magnetic field, B, and the projection of $\boldsymbol{\mu}$ onto the magnetic field axis z, μ_z:

$$\begin{aligned} E &= -\mu_z B \\ &= -\gamma I_z B \end{aligned}$$

Usually, γ is positive, and so the lowest energy spin state is that whose nuclear magnetic moment aligns most closely with the applied magnetic field.
This gives a resonance condition of:

$$\Delta E = \hbar|\gamma|B$$

And a resonant frequency of:

$$\nu_{NMR} = \frac{|\gamma|B}{2\pi}$$

So the resonant frequency of a nucleus in a magnetic field, also called the **Larmor frequency**, depends only on the strength of the magnetic field and the magnetogyric

ratio of the nucleus. For magnetic fields in the range of 8-20 T, the common range for commercially available NMR spectrometers, this will fall into the shortwave radio (MHz) region of the electromagnetic spectrum, so does not interact with rotational, vibrational or electronic transitions. At these high field strengths, the separation between resonant frequencies for different spin-active nuclei (^{1}H, ^{13}C, ^{19}F) is in the kHz range so NMR experiments can be easily tuned to detect a specific element in a molecule. Inducing and measuring the transitions between nuclear spin states does not cause any chemical change in a molecule so NMR is a non-invasive technique.

For isolated NMR-active nuclei of the same type in a uniform magnetic field, the resonant frequencies would be identical and a single NMR signal would be detected. However, real world atoms are surrounded by electrons in orbitals. In a strong magnetic field, these electrons circulate within their orbitals, generating a current. This current in turn generates a magnetic field which opposes the applied field, altering the effective field experienced by the nucleus. In molecules, the situation is more complex, involving bonding orbitals and neighbouring atoms. The result of this is that nuclei of the same element can give differing NMR signals dependant on their chemical environment. The environment-dependant change in a resonant frequency ν_0 is called the **chemical shift**, δ. Using prior knowledge, simple additive algorithms or *ab initio* calculations the chemical shift of a nucleus' NMR signal can be used to characterise that nucleus' chemical environment, giving information on the functional groups present similar to infrared (IR) spectroscopy.

Nuclear magnetic moments also interact with each other. For nuclei in identical chemical environments, this leads to no change in resonance and the signals are additive. In this case integration of the peak areas provides the relative number of nuclei in a particular environment. When the interacting nuclear magnetic

moments have different resonant frequencies, this leads to multiple absorption frequencies for each nucleus, and a splitting of the signals. This **coupling** of NMR signals for different chemical environments gives of additional information about the structure of the molecule being studied. Scalar, through bond coupling shows closeness between two nuclei in a molecule. The **splitting pattern** of a signal provides information on the nuclei with which it is coupled, so can be used to help determine the structure of the molecule. The separation of these peaks, *J*, in Hz, is mutual between the two signals being split and can also be characteristic of the two environments involved.

The interaction of nuclear magnetic moments can also be taken advantage of by applying two-dimensional (2D) NMR techniques. Very generally, 2D-NMR experiments work by allowing transfer of magnetisation from one nucleus to another, measuring the resulting cross peaks.

The 2D-NMR experiments used in this work are:

COSY – **Co**rrelation **S**pectroscop**y**, which measures the same scalar J-coupling described above between two nuclei of the same type, usually ^{1}H. Where a scalar through-bond coupling occurs, a cross peak can be seen between the coupled nuclei on a COSY spectrum. This can deconvolute the patterns of scalar coupling, making it easier to see which hydrogen nuclei are interacting, but can make it much more difficult to measure the coupling constants.

HSQC – **H**eteronuclear **S**ingle **Q**uantum **C**oherence Spectroscopy is a technique measuring the transfer of spin information between nuclei of different elements. In this case, the transfer being measured takes place across a single bond. Most commonly, and exclusively in the work presented in this Thesis, ^{1}H-^{13}C HSQC experiments are performed to correlate a proton signal to the carbon nucleus to which it is directly bound.

HMBC – **H**eteronuclear **M**ulti-**B**ond **C**ohesion Spectroscopy, another heteronuclear technique, shows longer-distance ^{1}H-^{13}C couplings, through two to four chemical bonds. This can be used to establish connectivity more widely in a molecule and provide conclusive information on chemical structure.

Additionally, using a 2D heteronuclear technique can deconvolute overlapping signals in a ^{1}H spectrum by separating the signals along more than one axis. In Section 3.3.4., HSQC and HMBC experiments are used to help to identify different components of a mixture of compounds.

Finally, an advantage that NMR has over many other techniques is that it is easily quantifiable. The peak area of an NMR signal is proportional to the number of nuclei resonating at that frequency. For spin-active nuclei of high abundance, e.g. ^{1}H, this can be used to tell the relative number of nuclei in a chemical environment, and with the addition of a standard of known concentration, this can be related to an absolute quantity of material present. For mixtures of compounds, the amount of each compound present can be calculated by integrating a signal from each component of the mixture resulting from a known number of nuclei and comparing against a standard. Unlike chromatographic techniques (HPLC or GC) there is no need to calculate a response factor for each molecule, since isotopic abundances are consistent.

As shown, NMR fulfils all the requirements laid out in the previous Section for a reaction monitoring technique. It is reproducible, directly quantifiable, and simple experiments can provide detailed structural information. Whilst it is not inherently sensitive, the sensitivity is dependent on the equipment and experiment design and modern high-field NMR gives more than satisfactory detection limits and signal-to-noise ratios. Most of all, NMR is entirely non-invasive. However, as shown in the following Section the use of NMR can be limited

in scope by the equipment, particularly for the monitoring of photochemical reactions.

Section 3.2.3: Reaction Monitoring using NMR in Continuous Flow.

The simplest method of monitoring a chemical reaction with NMR spectroscopy is by placing a standard glass tube containing a static sample into the spectrometer immediately after initiation of the reaction, and holding it there whilst acquiring spectra until the reaction is complete. It is also, unsurprisingly, the most common method used. This has the advantage of requiring no specialist equipment as well as not perturbing the reaction mixture once the analysis has started. Clearly, this method can only be used for thermally activated chemistry or for chemistry requiring a single initiation event. Monitoring of photochemical reactions by static mode NMR must be done in a stop-flow or point-by-point manner, since illumination within the spectrometer is not possible, nor is gas bubbling in the specific case of photo-oxygenations. This creates a need for constant operator input throughout the monitoring experiment, and leads to considerable perturbation of the sample. For multi-step reactions, where one step is photochemical and others are thermal (*i.e.* all photosensitised and photocatalytic reactions) the relative kinetics of the different steps is altered by the discontinuous illumination, and any kinetic measurements are not representative of the reaction under standard conditions. Therefore, static mode NMR must be considered invasive in these cases.

Continuous flow NMR experiments can be used for the analysis of chemical reactions under conditions closer to the actual reaction conditions.[273-275] A bulk reactor can be set up with a small amount of reaction mixture passed continually through the spectrometer. If the volume in the reactor is large compared to the

volume in the spectrometer and the flow rate is sufficiently high, the average monitored rates are close to the true kinetics under reaction conditions. The requirements for NMR spectroscopy of flowing samples are slightly different to those for static samples, though the underlying theory is well known. Understanding the unique properties of flow NMR requires a brief discussion of how an NMR spectrum is acquired, and the hardware involved.

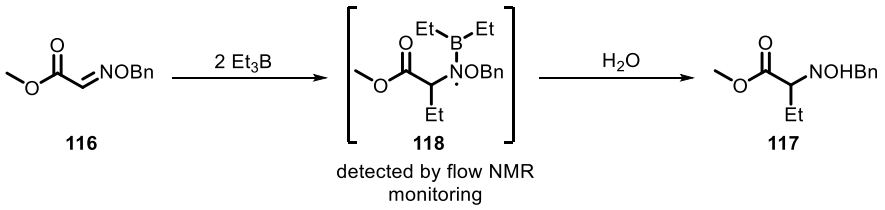
In a standard static NMR experiment, the sample in a glass tube is held at the centre of the magnet. The magnetic spin states of the nuclei in the sample are split in energy dependant on their alignment relative to the applied magnetic field as described in the previous Section.[271] The sample will reach an equilibrium bulk magnetisation in the direction of the magnetic field z, due to the slightly higher population of the lower energy state. The magnetic moments of the individual nuclei **precess** around z in the x-y plane at their Larmor frequency, with random orientations. Around the sample there is a coil, the **probe**, through which a radiofrequency current is passed to generate an oscillating magnetic field perpendicular to the bulk field. This induces a transient magnetisation away from the z axis and causes the magnetic moment to line up in phase. After the pulse, the magnetic moments continue to precess in the x-y plane at their individual resonant frequencies, but now generate a coherant, measurable signal, which can be detected using the same probe coil. The transient magnetisation dies away as the magnetic moments re-orient themselves with the bulk field, and the signal received is a free induction decay (FID). Fourier transform of this time-domain signal gives the frequency-domain spectrum. The complete sequence of equilibration, pulse and detection is referred to as a **scan**. A single NMR experiment is usually made up of multiple scans, with the FIDs added together to improve the signal-to-noise ratio of the resultant spectrum.

For our proposed reaction monitoring experiment, we require that the very small steady-state concentrations of our reaction intermediates be measurable, so our NMR experiments need to have high sensitivity. NMR is not inherently a sensitive technique and relies upon the equipment and experiment design.[271] The important factors for high sensitivity are a) strong bulk magnetisation of the sample at equilibrium b) good homogeneity of the magnetic field and c) a high quality probe. In static NMR experiments, the largest bulk magnetisation is achieved by using the strongest possible magnetic field, and by giving the sample enough time to reach equilibrium between scans.[272] In flow NMR, fresh sample is constantly entering and leaving the detection volume, and for the maximum sensitivity the flow rate must be low enough to ensure that the sample entering the detection volume is fully magnetised.[273] When sufficiently low flow rates are used, it is well reported that a signal enhancement occurs compared to static NMR. This was first reported by Suryan in 1951 who saw a 5-fold increase in the intensity of a water ^{1}H-NMR spectrum.[273]

The homogeneity of the magnetic field is important because the signal strength and thus sensitivity depends on the phasing and coherence of the signal. Within the probe, the magnetic field varies by less than 1 ppb for a properly set up experiment. This is achieved using smaller, secondary electromagnet (**shimming**) coils to which the power can be varied until maximum signal output is obtained.[272] In static samples, this is sufficient to provide strong signals, since the temperature in the detection volume is constant and homogeneous. In flow NMR, temperature gradients caused by the moving sample can mimic the effects of a poorly shimmed magnetic field and destroy sample coherence, leading to poor sensitivity. Again, lower flow rates can allow temperature equilibration prior to the sample entering the detection volume. Additionally, the reactor and the transfer lines should be

kept as close as possible to the probe temperature to decrease the time taken for the temperature to equilibrate.

The coils that make up an NMR probe need to have a very low electrical resistance and a precise geometry to generate the strongest signal possible, and the best probes are very expensive. The majority of process and reaction monitoring experiments using NMR have been performed with a specialised flow probe which is installed in the spectrometer in place of the standard probe and shimming assembly. Nakakoshi *et al.* used a commercially available flow probe with a 500 mHz spectrometer to elucidate the mechanism of the radical addition of triethylborane **116** to oxime ether **117** by detecting small amounts of unstable intermediate **118**.[276] Several other groups have since used the combination of a commercial flow probe and high field NMR to similar success.



Scheme 68: Nakakashi et al. determined the mechanism of the radical addition of boranes to oximes using flow NMR monitoring.

Low field (<300 mHz) spectrometers have also been used for the monitoring of chemical reactions, notably by the groups of Cronin,[277] Duchateau[278] and Milburn.[279] Smaller low field spectrometers are simpler and easier to work with, though as highlighted by Duchateau they have the downsides of lower resolution and poorer detection limits when compared to high field spectrometers. For our purposes, we require the maximum achievable sensitivity and resolution, and therefore high field spectrometers.

Several flow cells have been developed that can be used in conjunction with a standard NMR probe at high field.[280-283] The advantage of this is that standard

probes are available with much higher sensitivity and better shimming than their flow counterparts.[282] One such cell, reported originally by Foley and Marquez has now been commercialised by Bruker and is available under the name 'InsightMR'.[283] They reported good stability and temperature control, and emphasise the flexibility with regards to probe and spectrometer choices. This apparatus was used for the NMR monitoring studies presented in Sections 3.3.3. and 3.3.4. and is described in more detail in Section 3.3.3.

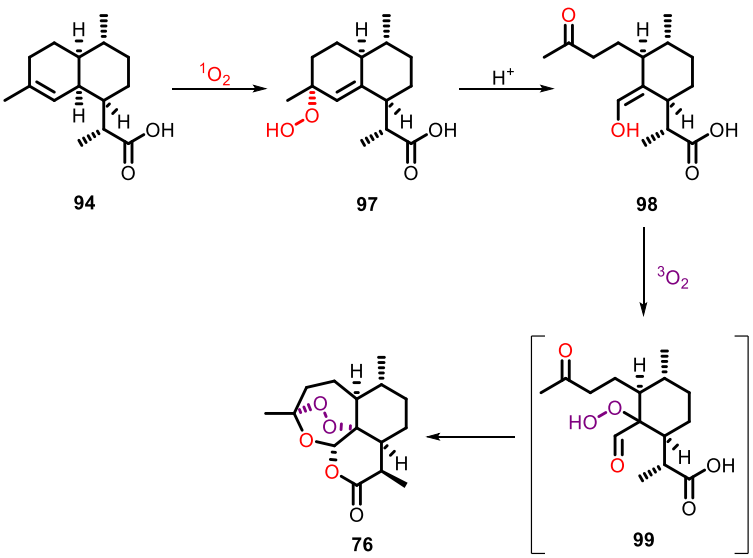
As a technique for the characterisation of organic molecules, continuous flow NMR is unparalleled. In theory, it fulfils all the criteria for an ideal process analytical technology outlined in Figure 21 – Experiments can be performed that give information about elemental composition, functionality, connectivity and even the shape of a molecule, and absolute quantities can be easily measured. Sensitivity and signal quality depend on easily controlled experimental parameters and on the properties of the spectrometer.

The continuous flow monitoring apparatus that we sought to develop must fulfil all the above requirements for a high quality spectrum, and also be stable enough that reliable kinetic data can be extracted from the experiment.

Section 3.3: NMR Monitoring of the Synthesis of Artemisinin.

Section 3.3.1: Preliminary Studies Assessing Yield Loss.

Experiments were undertaken to determine at which point in the reaction sequence material was being lost. Scheme 69 again shows the major steps in the sequence: the Schenck reaction of DHAA **94** to allylic hydroperoxide **97**, the Hock cleavage to give keto-enol **98** and the auto-oxidation/cyclisation cascade to the final product artemisinin **76**.



Scheme 69: The reaction sequence by which DHAA 94 converts to artemisinin 76.

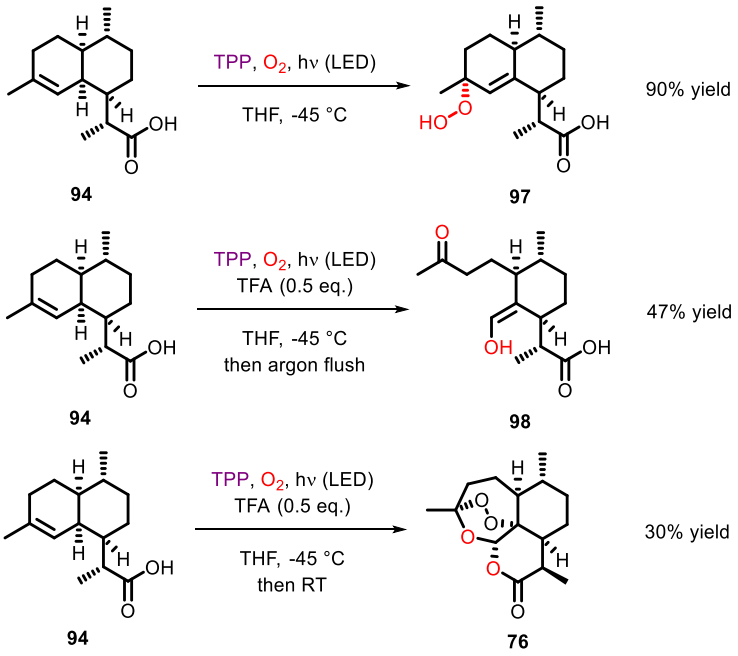
In Section 2.3.2. it was shown that the Schenck reaction in aqueous mixtures gave consistently high yields of 87-92% for the required tertiary hydroperoxide **97**. Overall reaction yields of **76** using these same solvent mixtures were between 30-60%, meaning that considerable material loss occurs during the two subsequent steps. To determine the distribution of material loss between the two steps, the yield of keto-enol intermediate **98** needed to be measured. The issue with this is that intermediate **98** cannot easily be isolated under the high-oxygen environment used for the preceding steps. It is, however, stable at low temperatures, as shown by the work of Haynes and Vonwiller discussed in Section 2.2.2.[260] It was planned

to halt the reaction sequence at enol **98** by performing the photo-oxygenation and Hock cleavage steps at low temperature then removing oxygen from the reaction mixture before warming to room temperature for analysis.

This intermediate trapping experiment was carried out at -45 °C. The freezing point of most aqueous solvent mixtures is well above this temperature, and so the experiment was performed in THF using tetraphenylporphyrin (TPP) as photosensitiser. Biphenyl was added as an internal standard to quantify the yields of species of interest. Two reactions were performed: the first without acid to gauge the yield of hydroperoxide **97** under these conditions and the second with acid to form the keto-enol intermediate **98**. The reactions were monitored by taking aliquots and analysing their ^{1}H-NMR spectra in degassed benzene-d_6. The Schenck reaction was considered complete when the signal for DHAA **94** at 5.08 ppm had disappeared. Likewise, the Hock cleavage was complete when the signal for hydroperoxide **97** at 5.26 ppm was gone. At this point in the acid-containing reaction ii), the oxygen atmosphere was replaced with argon and a final aliquot was taken, contained in a sealed, argon-filled NMR tube and analysed by ^{1}H-NMR, giving a yield for intermediate **98** of 47% against internal standard biphenyl (Scheme 70). The conversion of enol **98** to artemisinin **76** was then initiated by replacing the O_2 in the reaction mixture and stirring under an oxygen atmosphere overnight. No **98** remained, and artemisinin was formed in around a 30% yield. This shows that there may be additional pathways to side product formation in the auto-oxidation or cyclisation steps.

The results of this experiment suggest that the main source of material loss in the sequence of reactions shown in Scheme 70 is the acid-catalysed Hock cleavage step, which is shown to be around 50% selective for enol **98**. This is likely due to the formation of side products **108-110** reported by Brown *et al.* The later steps (auto-

oxidation and cyclisation) are around 65% selective for artemisinin **76**. Assessment of the factors influencing the formation of each side product will be the most significant way to impact the overall yield of artemisinin.



Scheme 70: Intermediate trapping experiments in benzene-*d*6, showing that the greatest loss of yield occurs in the Hock cleavage step.

The fact that some yield was lost in the auto-oxidation/cyclisation step was intriguing, since no side products had been reported as forming in this step. After the catalyst recycling experiment in ethanol/water described in Section 2.3.3., a highly polar oligomeric by-product was isolated in greater than 30% mass yield, which was analysed by matrix assisted laser desorption/ionisation time of flight mass spectrometry (MALDI-TOF) showing a strong mass peak at M/Z = 1213. The ketone and enol groups on intermediate **98** may be prone to Aldol-type oligomerisation, and the mass peak at M/Z = 1213 corresponds to $[M+H]^+$ where M is formed from five units of enol **98** condensing together with the loss of five molecules of water. This could explain the formation of these products and account for the loss of yield in the final step.

Whilst this experiment was a good indication that the Hock cleavage was the least selective step of this synthesis, it involved a large amount of sample perturbation, and the conditions under which it was performed are so different to those used by our process described in the previous Chapter that it is difficult to be certain whether a direct comparison is valid.

Direct, non-invasive monitoring of the progression of the reaction is only possible using spectroscopy, so we began work on the development of methods to monitor this reaction using NMR, the benefits of which have been discussed in detail in Section 3.2.

Section 3.3.2: Static Monitoring of the Artemisinin Synthesis by NMR.

Most monitoring of reactions by NMR for mechanistic purposes is carried out on static samples which can be held inside the spectrometer and analysed regularly for the duration of the reaction. This presents difficulties for the monitoring of photo-oxygenations since neither illumination nor oxygen sparging are possible inside the magnet of an NMR spectrometer. We considered that the sample could be illuminated between the acquisition of spectra and either sparged with or sealed under a static atmosphere of O_2.

Initial monitoring experiments were carried out using static samples in a standard 5 mm borosilicate NMR tube. Early attempts showed that the Schenck photo-oxygenation of DHAA **94** did not proceed under a static atmosphere of O_2 and required constant sparging to achieve efficient conversion. During illumination the tube was fitted with an O_2 bubbler and allowed to vent to atmosphere. Solvent loss due to evaporation became a major problem and the sample required regularly topping up to avoid issues associated with changing concentration, such as migration and broadening of the acid peak.

For the first full monitoring experiment, a 0.042 M solution of DHAA **94** in THF-d_8/D_2O 80:20 was prepared, containing 0.5 mol% TPP. 5 mL was added to a borosilicate NMR tube fitted with a Young tap head. TFA-*d* was added along with biphenyl as an internal standard. The tube was fitted with a needle and septum as shown in Figure 22, and bubbled with O_2 gas whilst illuminating with white LED light. The tube was sealed and a ^{1}H-NMR spectrum was run on a Bruker (iii)400. After the spectrum was acquired, illumination and bubbling were resumed. Once all the DHAA **94** was consumed, illumination and gas bubbling were ceased and the tube was sealed under a static atmosphere of O_2 gas.

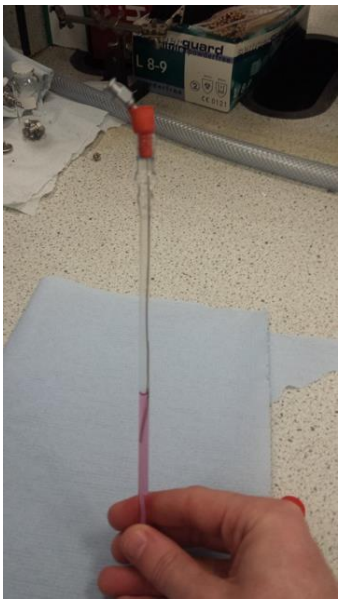


Figure 22: The equipment used for static mode NMR monitoring

Integration of the crude spectra allowed a timecourse plot to be generated (Figure 23). The progression of the reaction can be seen clearly, with DHAA **94** consumed rapidly during the photo-oxygenation step. Concurrent formation of secondary hydroperoxide **103** is seen, reaching a maximum at around 13% yield in accordance with the selectivities measured in EtOH/H_2O mixtures on a preparative scale. Interestingly, tertiary hydroperoxide **97** is not observed, which could mean that the steady-state concentration of this intermediate is lower than the detection limit of the apparatus under these conditions.

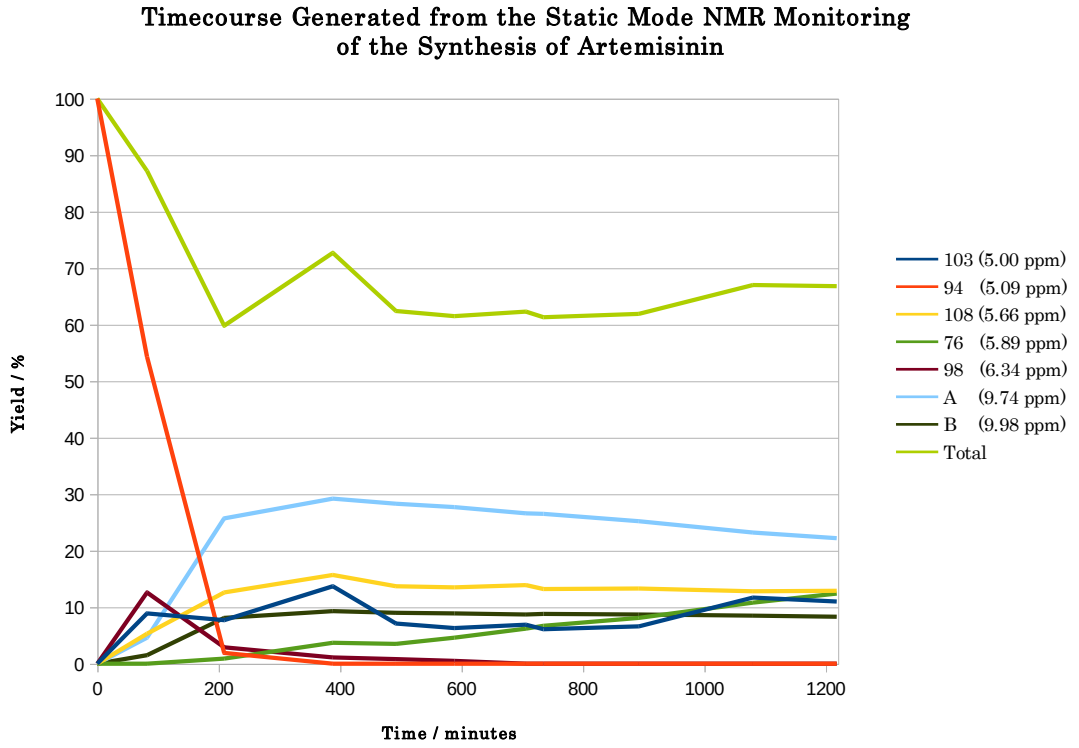
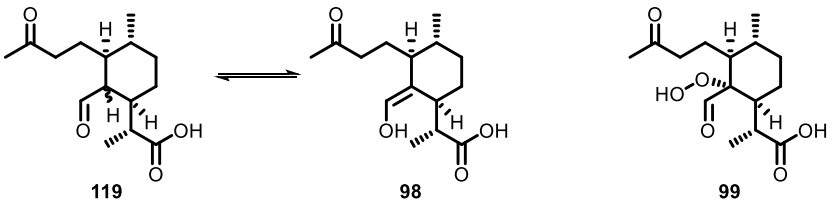


Figure 23: Timecourse plot derived from integration of the static mode ^{1}H-NMR monitoring experiment.

The major side product from the Hock cleavage step, lactone **108**, was formed in 13% yield which plateaued as DHAA **94** was depleted, at which point the formation of tertiary hydroperoxide **97** would be expected to cease. Enol intermediate **98** reached a maximum yield of 12% after 90 minutes as conversion to other species outpaced its rate of formation. Interestingly, consumption of enol **98** was not concurrent with formation of artemisinin **76**, but appeared to convert first to two aldehyde species, denoted **A** and **B**. Formation of artemisinin **76** continued after enol **98** was entirely consumed, so one or both of these aldehydes must be intermediates between **98** and **76**. The sum total of the yields of the species present decreased over the course of the reaction by 35%, which could not be accounted for by the growth of any one species in the NMR spectrum, but may be attributed to the formation of oligomers reported in Section 3.3.1. The rate of total yield loss

plateaued as the enol intermediate **98** was consumed, supporting the hypothesis presented earlier that these oligomers were produced as by-products of the final step of the reaction sequence.

The accumulation of large amounts of aldehyde intermediates under the experimental conditions is unusual, and not observed in conventional organic solvents. Brown *et al.* reported several aldehyde species, of which the most likely candidates for those observed here are the aldehyde tautomer **119** of enol **98** and the hydroperoxy-aldehyde **99** proposed by several groups as the intermediate resulting from auto-oxidation of **98**. Separation of these unstable compounds for the purpose of characterisation was not successful, and deconvolution of the crude NMR spectra was not possible due to limited resolution and spectrum quality.



Scheme 71: Possible structures of the aldehyde species A and B observed in the static monitoring experiment: Aldehyde tautomer 119 of enol 98, and hydroperoxyl-aldehyde 99 from auto-oxidation of 98.

Section 3.3.3: Continuous Monitoring of the Artemisinin Synthesis by NMR.

Work presented in this Section involved considerable contributions to the development of the reactor and data processing from Dr Zahra Abada and to the design and programming of the NMR experiment by Dr Huw Williams.

A recirculating reactor with on-line NMR analysis was designed for the purpose of monitoring the photochemical synthesis of Artemisinin. The currently understood

mechanism of this reaction is shown in Scheme 69 and discussed in detail in Section 2.2.2.

For the NMR analysis, the InsightMR flow apparatus produced by Bruker was used. This consists of a capillary-fed 5 mm diameter borosilicate NMR tube held in a plastic holder which can be inserted into the probe of a NMR spectrometer in the same way as a normal NMR sample tube. This means the apparatus can be used with a standard probe, rather than a dedicated flow probe. In this way we remove the need to change the probe before every run, avoiding lengthy experiment set up times. Additionally, the standard probe available was more powerful than any commercially available flow probe, giving us better sensitivity and thus lower detection limits and shorter spectrum acquisition times.

The inlet and outlet capillaries of the sample tube are held in coaxial cooling tubes and surrounded by foam insulation, to minimise changes in temperature between reactor and spectrometer. The capillaries terminate at a four-port manual switching valve to allow the spectrometer to be bypassed or for stop-flow experiments. The length of tubing from switching valve to probe is approximately seven metres.

The initial apparatus used with the InsightMR was based on the equipment used for batch photo-oxygenations in Section 2.3.3. The reaction mixture was stirred in standard borosilicate glassware and bubbled with O_2 *via* syringe whilst illuminating with a fan-cooled block of white light LEDs. An HPLC pump was used to transfer the material from the flask to the InsightMR, which fed back into the flask after NMR analysis. Full details of the apparatus are provided in experimental Section 5.3.

Our greatest concern when beginning this study was preserving the homogeneity (shimming) of the applied magnetic field and maintaining the signal quality when

measuring a moving sample. Magnetic field and temperature gradients lead to a loss of signal cohesion and can prevent the data from being fully quantitative, as well as causing peak broadening which can lead to difficulties with integration when signals overlap. The use of a high field 19 T magnet helps to achieve high resolution but poorly shimmed and inhomogeneous samples can negate this entirely. The flow rate must be low enough that the sample flowing through the spectrometer has appropriate time to equilibrate to the temperature and field before entering the probe. On the other hand, very low flow rates would increase the transfer time from reactor to spectrometer which could lead to temperature changes in the transfer lines and reduce the reliability of any kinetic information extracted from the experiment. A flow rate of 3 mL min^{-1} was found to give a good balance of transfer time, signal strength and resolution.

The loss of solvent from the reaction mixture was a huge drawback to this reactor design. Changes in concentration and solvent composition preclude the extraction of any meaningful kinetic data from the system, and lead to problems with signal lock and shimming. Additionally, the need to top up solvent regularly over a two- or three-day reaction presents a logistical problem, and deuterated THF is expensive. A sealed system was not possible as continuous O_2 bubbling was required. Perceived solutions were to reduce solvent loss by a) minimising the surface area open to atmosphere, b) separating the illuminated portion and open portion of the reaction mixture spatially, c) cooling the illuminated mixture more efficiently and d) controlling O_2 addition more closely.

To address the issues found in the previous experiment, a sapphire tube photoreactor identical to that used for the preparative artemisinin flow synthesis (Section 2.3.4.) was used. Again, the new rig design used the Bruker InsightMR apparatus described in the previous section. The sapphire tube photoreactor has

more efficient cooling and illumination than the batch equipment used previously. The excess oxygen gas is released from the system after the reactor by a small airlock, which is not illuminated and was kept small to minimise the evaporating surface area. The airlock acts as a reservoir from which solution is drawn by the Gilson 306 HPLC pump and pumped through the spectrometer. Oxygen gas was added from the bottom of the reactor through a one-way check valve and maintained at the minimum flow rate required to open the valve. We predicted that this new rig design would greatly reduce the rate of evaporation of the solvent, as well as the overall reactor volume, reducing the amount of expensive deuterated solvent required and providing better stability for the monitoring experiments.

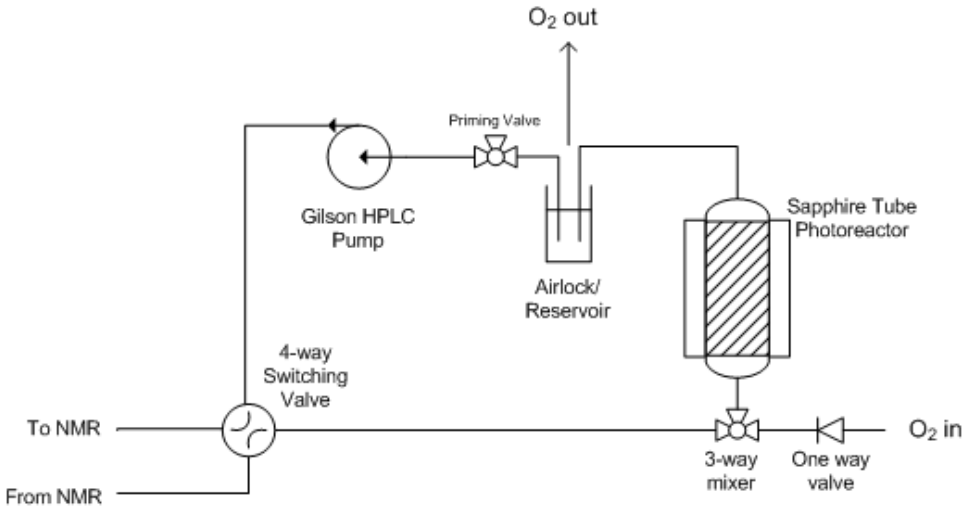


Figure 24: Schematic diagram showing the recirculating NMR monitoring rig based ona sapphire tube photoreactor.

A schematic of the new monitoring apparatus is shown in Figure 24. The reaction mixture is drawn from the airlock/reservoir by the Gilson 306 HPLC pump and pushed through the InsightMR apparatus to the probe to be analysed. On leaving the spectrometer, the mixture passes through the sapphire tube photoreactor where it is oxygenated and illuminated before being released back into the airlock. Unlike the preparative experiments presented in Section 2.3.4., a high rate of conversion was not a requirement, so the flow rate was kept high at 3 mL min^{-1}

and the LED lamps used on their lowest power setting. Figure 25 shows the apparatus under operation.

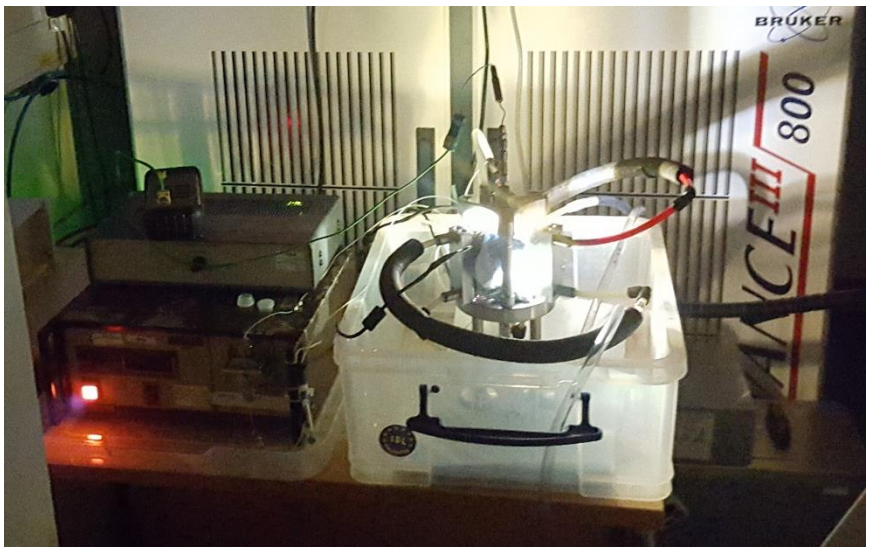


Figure 25: The equipment used for the continuous NMR monitoring of the synthesis of artemisinin, showing the sapphire tube reactor (right), HPLC pump (lower left) and LED control module (upper left). The NMR spectrometer and InsightMR apparatus are not shown.

The NMR spectrometer was programmed to constantly acquire spectra, alternating one-dimensional proton spectra, for quantitative data on the reaction's progression, with two-dimensional heteronuclear experiments HSQC and HMBC (see Section 3.2.2.) for structural information on the species present. The two-dimensional experiments could be run as frequently or infrequently as necessary. A solution of DHAA **94**, TPP and the biphenyl internal standard in THF-d_6/D_2O 60:40 was added to the monitoring rig, and cycled through the photoreactor and spectrometer as described above. The TFA-*d* acid catalyst was added and the photoreactor was continually sparged with O_2 and illuminated. 1D ^{1}H-NMR spectra (64 scans each) were acquired constantly for the duration of the photo-oxygenation step. When all DHAA **94** had been consumed, the following sequence of spectra were acquired: 64 scan 1D, 1024 scan HSQC, 4096 scan HMBC, repeat. This was continued until no change in the reaction mixture was seen, a duration of approximately three days. Unlike the batch setup described above, the reactor remained stable throughout the experiment. Some solvent loss was still observed

but was greatly reduced compared to either the static experiments or the previous continuous experiments. Generally, the spectrum quality was good, though the homogenisation (shimming) of the magnetic field needed to be repeated periodically to ensure sharp peaks and good resolution.

Just as in the static mode monitoring experiment, the one-dimensional spectra could be integrated and used to generate a timecourse plot of the reaction as it progressed, shown in Figure 26.

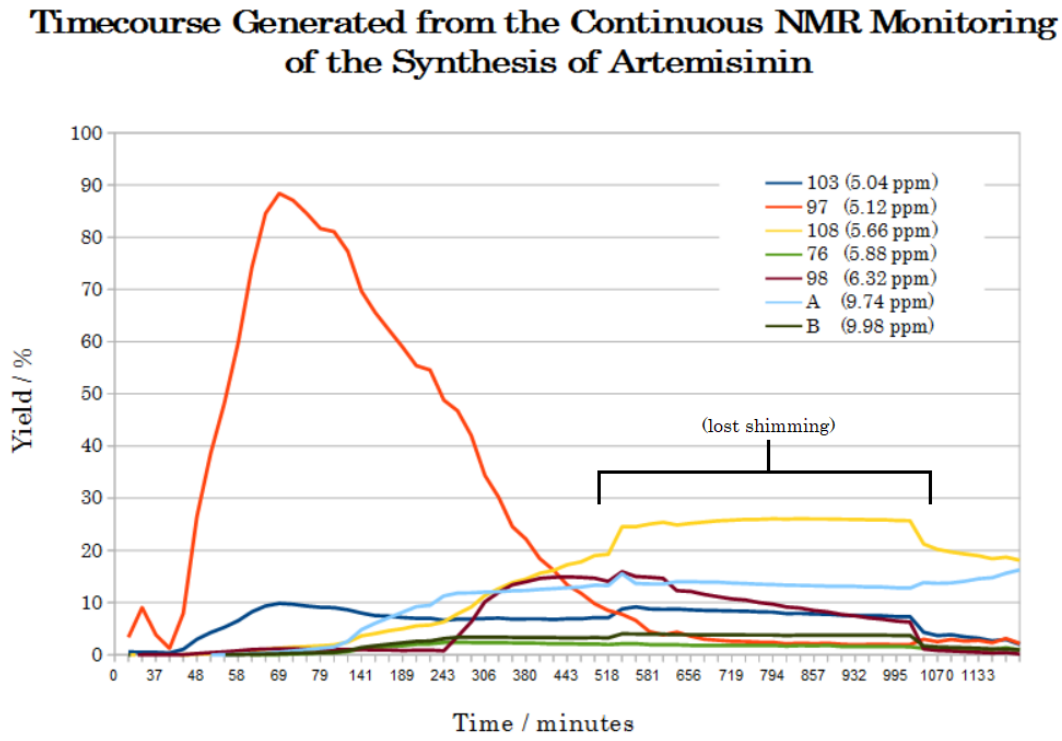


Figure 26: Timecourse plot derived from integration of the ^{1}H-NMR spectra acquired during the continuous monitoring experiment. The trace for the starting material, DHAA 94 has been omitted for clarity.

The continuous monitoring experiment showed similar results to the static experiment presented in Section 3.3.2. Unlike the static mode monitoring experiment, the hydroperoxide product **97** of the Schenck reaction was observed, forming in close to 90% yield before the addition of the acid catalyst. Lactone **108** was formed in 20% yield, considerably higher than in the static monitoring. Again, steady formation of artemisinin **76** was seen throughout the experiment, although

at the point that the reaction was deemed complete the yield of artemisinin was only 2% and considerable amounts of aldehydes **A** and **B** were still present. It could be that under a more oxygen-rich environment further conversion to artemisinin **76** would occur, as was observed for the preparative flow experiments in Section 2.3.4.

Whilst the quality of the spectra in general was greater for the continuous monitoring experiment than the static, and many more data points could be taken in a short amount of time, the quality of the timecourse shown in Figure 26 was lowered by the loss of shimming at the probe partway through the experiment. Broadening and overlap of the reference peaks made quantification of the product yields difficult, hence the 'jump' seen in several traces around t = 518 minutes, leading to higher yields being measured until the shimming was fixed at around t = 1070 minutes. This unfortunately precluded the extraction of any kinetic data. The two-dimensional heteronuclear experiments (HSQC and HMBC) could be used to confirm or assign the structures of intermediates formed *in situ*. We were particularly interested in the aldehydes that were accumulating in our aqueous solvent system, since their formation in such large amounts had not been previously reported. Even with the high sensitivity and high resolution equipment being used, assignment of the structure of these compounds was difficult, due to the complexity of the reaction mixture. An interesting observation from the 2D spectra was the appearance of cross-species correlations between the enol hydroxy proton resonance of enol **98** and carbon atoms attributed to the more downfield shifted (^{1}H at 9.98) aldehyde species **B**. For this to be observed must mean the two species are interconverting on a similar timescale to that of the NMR experiment, and it can be concluded that these two species are directly adjacent in the reaction mechanism. Reverse couplings were also observed, which suggests that the two

species are in equilibrium. The obvious explanation for this is the expected aldehyde-enol tautomerisation between enol **98** and aldehyde **119** (Figure 27). This observation would strongly support the idea that the aldehyde species **B** with a resonance at 9.98 ppm is due to aldehyde **119**. The other aldehyde species **A** that was observed could be either of the previously suggested intermediates, peroxy-aldehyde **99** or cyclised equivalent **113** (Section 2.2.2., Scheme 62), or a previously unknown intermediate.

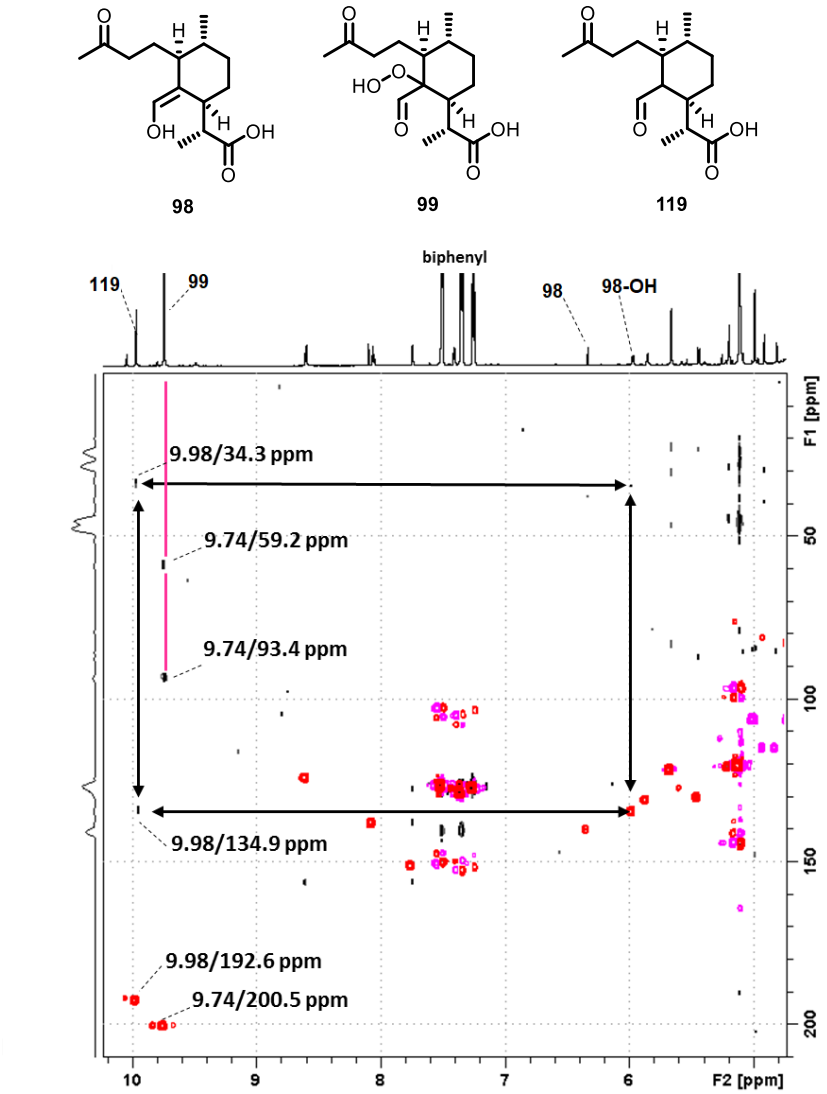


Figure 27: Overlaid HSQC (pink/red) and HMBS (black) spectra showing the cross-species correlation between the hydroxy proton of enol 98 and the aldehyde carbon of 119. Chemical exchange must be occurring between these two species on the NMR experiment timescale.

To confirm whether these aldehyde peaks were due to any of the known structures mentioned above, the ^{13}C-NMR spectra of the aldehydes **99**, **119** and the cyclised structure **113** were simulated using computational chemistry. The predictions were carried out by group member Dr Magnus Hanson-Heine using the EDF2/6-31G(d) level of density functional theory. The calculated chemical shifts for **99** and **119** were consistent with the peaks observed in the 2D-NMR spectra for the aldehydes **A** (at 9.74 ppm) and **B** (at 9.98 ppm), respectively, confirming our predictions. The full table of calculated and experimental assignments is given in experimental Section 5.3.

The presence of large amounts of aldehyde **119** in our aqueous system, something that is not observed in conventional organic solvents, indicates that the position of the tautomeric equilibrium between aldehyde **119** and enol **98** shifted in favour of **119** by the presence of large amounts of water. This shift in the equilibrium can be expected to impede the formation of artemisinin **76**, since enol **98** is thought to be the direct mechanistic precursor to **76**, with aldehyde **119** representing a mechanistic 'dead end'. This may go some way to explaining the lower rate of formation of artemisinin **76** in our aqueous system compared to in conventional solvents. Similarly, the accumulation of peroxy-aldehyde **99** in our aqueous system may suggest that the cyclisation steps are similarly impeded. Further work, including reliable kinetic studies, is required to understand how the reaction parameters affect the rate of reaction and to find a vector for additional improvement to our process.

Section 3.4: Chapter Summary.

The main aim of the work presented in this Chapter was to study the mechanism of the synthesis of artemisinin from Chapter 2. We believed that a proper

understanding of the reaction mechanism would enable a more directed optimisation of our process. In particular, we wanted to better understand the formation of side products in this reaction.

We envisioned that this could be achieved by developing a method for monitoring this reaction by NMR. NMR is a powerful characterisation technique as shown throughout Section 3.2., but is incompatible with illumination and oxygen sparging, which presents a barrier to the monitoring of photo-oxygenation reactions. We sought to overcome that barrier by working towards a continuous recirculating reactor which incorporated a high field NMR spectrometer.

Initial probing of side product formation in the synthesis of artemisinin was performed by trapping and measuring the yields of key intermediates. Assessing the yield of enol **98** which accumulated at low temperatures showed that the major source of material loss was the acid-catalysed Hock cleavage step (Section 3.3.1). Many side products have been reported from this step, so this result was not unexpected, but the same experiments also showed yield loss in the later steps, for which no side products had been characterised. This was rationalised based on the observation of oligomeric by-products in the recycling experiment presented in Section 2.3.3., which could result from Aldol condensations of enol **98**. This furthered our knowledge of how material was being lost in our process.

Static mode NMR monitoring experiments were performed in mixtures of deuterated tetrahydrofuran and D_2O, and also showed a loss of yield over the final steps, corroborating the results of the previous study (Section 3.3.2.). This experiment also showed the formation of aldehyde species from enol **98**, further adding to our knowledge of side product formation.

The development of a continuous recirculating reactor for monitoring photo-oxygenations by NMR was performed using the commercial Bruker InsightMR

apparatus. This was originally attempted using standard laboratory glassware, *i.e.* in a semi-batch manner. We managed to achieve high sensitivity in the spectrometer using this equipment whilst minimising the volume of reaction mixture in the spectrometer. However, considerable issues arose with solvent evaporation, which in turn affected the lock and shim of the spectrometer and the quality of the spectra acquired later in the experiment. This precluded the extraction of reliable kinetic data. However, these experiments showed that photo-oxygenation reactions could be monitored by NMR in a continuous manner.

By using a sapphire tube photoreactor we were able to build a fully continuous reaction monitoring rig. Advantages of using this reactor with an additional airlock/reservoir to release excess O_2 were improved temperature stability and minimal solvent evaporation, which would allow more reliable kinetic data to be produced. Using this improved rig, we could follow the entire course of the reaction sequence from dihydroartemisinic acid to artemisinin. The inclusion of two-dimensional NMR experiments allowed characterisation of the aldehyde species reported previously *in situ*, with the help of *ab initio* chemical shift calculations. We showed that in aqueous systems, enol **98** is in tautomeric equilibrium with its aldehyde form, which could both contribute to the low rate of the later steps of this reaction and the formation of the observed oligomeric by-products. This knowledge may lead to further improvements to the process described in Chapter 2.

Overall, the work presented in this Chapter has fulfilled our aims to probe the formation of side products in this reaction, providing specific insight to our aqueous system which would not be possible without the use of the continuous NMR monitoring rig that we have developed. It represents a step towards the acquisition of reliable kinetic data on this process, which could in turn lead to a comprehensive understanding of the reaction mechanism and a directed optimisation of further

processes. We have demonstrated the powerful combination of NMR spectroscopy and continuous flow technology for the monitoring of photochemical reactions. A combination of reactor and experiment design has allowed the apparent incompatibility of photochemistry and NMR to be overcome, and we have shown how the wealth of data available can be used to determine mechanistic details of the photochemical synthesis of artemisinin.

Section 3.5: Future Directions.

The work detailed in the above Chapter represents significant steps towards our aim of developing a recirculating rig for the monitoring of photochemical reactions by nuclear magnetic resonance spectroscopy. However, if this work is to be taken forward to a general monitoring technique, further refinement, testing and optimisation of both the reactor system and experiment design is necessary.

Solvent loss was still an issue, albeit a smaller one, even with our improved second design using the sapphire tube reactor. This stems from the necessity to vent the reactor to atmosphere to remove any O_2 bubbles before the spectrometer. For the monitoring of other types of photochemical reaction in oxygen free conditions, the same problem may arise if the system requires sparging with an inert gas. A potential solution to this problem could be found by inserting a dual-channel or tube-in-tube system such as the one shown in Section 1.2.6., Figure 10b, in which a gas-permeable membrane allows the movement of O_2 to the surroundings but retains the reaction mixture, including solvent, inside. The back-pressure from the transfer capillary is expected to be high enough to ensure all the oxygen would be either dissolved or expelled to the atmosphere. If this is not the case, a slight vacuum could be applied to the outside of the gas-permeable tubing to increase the rate of O_2 transfer through the membrane.

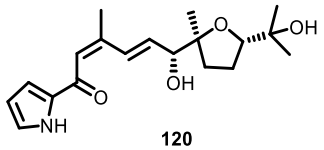
The second major issue with the continuous monitoring experiment was the loss of field homogeneity (shimming) partway through the run. This can result from temperature gradients or changes in flow rate or solvent composition during the experiment and leads poor sensitivity and line broadening in the NMR spectrum. The data extracted from the spectra with poor shimming are not suitable for the extraction of kinetic data. Automatic shimming programs are an integral part of all spectrometer software, and could be added to the automated cycle of operations performed by the spectrometer, such that the spectrometer re-shims itself periodically without operator input.

Another improvement to the rig for the monitoring of photo-oxygenation reactions would be the addition of an oxygen dosing system such as the one used in the preparative continuous flow rig described in Section 2.3.4. This allowed precise control over the amount of oxygen gas entering the reactor, and if a similar system could be included here, the overall safety and stability of the rig could be improved. Once a stable reactor design has been built and tested, experiments can be performed on the artemisinin synthesis with the aim of extracting kinetic data. Varying parameters such as temperature, concentration and acid strength between runs would provide information on how these parameters affect the rate of artemisinin formation, allowing us to improve the productivity of our process.

Chapter 4: Studies Towards the Synthesis of the Glaciapyrrol Family of Natural Products.

Section 4.1: Introduction and Project Aims.

The search for new bioactive compounds is a major undertaking in the scientific community. There is a constant demand for new medicines displaying increased specificity or efficacy (in the case of anticancer drugs) or that circumvent growing resistance (in the case of antimicrobials). The bacterial genus *Streptomyces* has been and continues to be one of the most fruitful sources of novel bioactive structures, including antibiotics, anticancer agents and immunosuppressants. Many of the bioactive compounds in these *Streptomyces* species are only present in very small amounts, and it can be difficult to isolate them in the quantities needed for full characterisation and activity screening. These compounds must often be made synthetically before it can be determined for certain whether they have any potential for use as pharmaceuticals.



120
glaciapyrrol A

Figure 28: The potential anti-cancer natural product glaciapyrrol A, isolated from a Streptomyces bacterium.

The work described in the following Chapter is a collection of studies towards the synthesis of a novel family of pharmaceutically relevant natural products, the glaciapyrrols, isolated from a range of *Streptomyces* species.[284-288] The glaciapyrrols have displayed a range of promising biological activity, as explained in more detail in Section 4.2.1. Only glaciapyrrol A (**120**) shown in Figure 28 has been synthesised to date.[289] Many members of the family are only characterised in terms of their connectivity and relative stereochemistry, with the absolute stereochemistry still unknown.

All compounds in the family consist of a pyrrole-fused terpenoid backbone bearing a range of oxygen-containing functionality. The aim of this project was to develop a process for the synthesis of these compounds using singlet oxygen to install the functionality in an efficient and divergent manner. By our strategy, given in greater detail in Section 4.2.2., a common precursor is synthesised, which gives access to the whole family *via* simple non-selective Schenck photo-oxygenation and a series of rearrangements of the peroxide products. We wanted the synthesis to be high yielding, operationally simple and as efficient as possible. It would need to be performed on a mid-to-large scale to provide enough of each potential product for testing and characterisation.

Section 4.2: Background.

Section 4.2.1: The Glaciapyrrol Family of Natural Products.

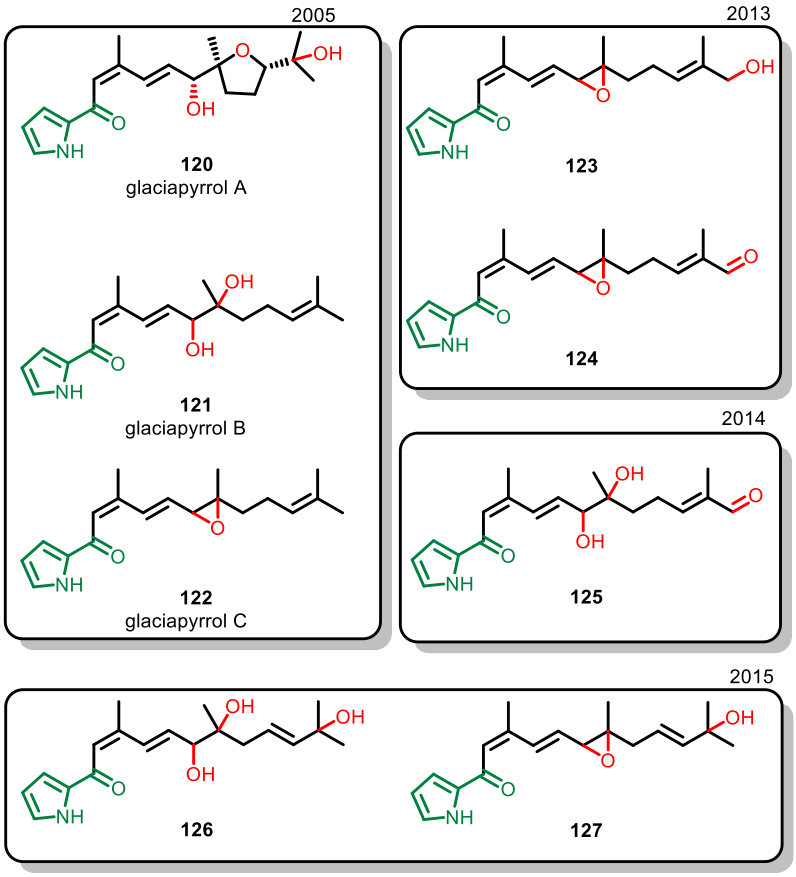


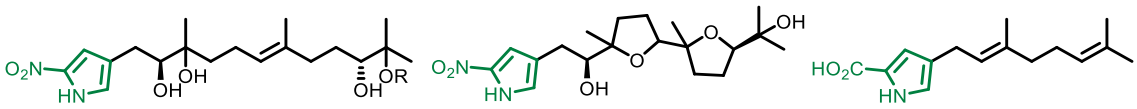
Figure 29: The glaciapyrrol family of natural products, showing the unique 2-acylpyrrol moiety in green, and the oxygen functionality in red.

The glaciapyrrols are a family of pyrrolosesquiterpene natural products that have been isolated from various strains of *Streptomyces*. Several members of the family have exhibited biological activity as either antibiotic or anticancer lead compounds.[284-288]

The first of these compounds to be discovered were isolated in 2005 from cultures of a *Streptomyces* strain found in an arctic marine sediment, earning them the names glaciapyrrol A (**120**), B (**121**) and C (**122**). Glaciapyrrol A was tested for anti-cancer activity against both colorectal adenocarcinoma and melanoma tumour cell lines and showed inhibition of both with an IC_{50} (half maximal inhibitory

concentration) of 180 μM.[284] This is only weak activity but shows potential for these unique structures as starting points for the discovery of new drugs. Two related structures, **123** and **124**, were isolated in 2013, this time from a soil bacterium from Daxinganling forest, China. The relationship to compounds **120-122** is clear. Compounds **123** and **124** were also tested for anti-cancer activity and showed greater efficacy than compound **120**, in the region of 20 μM.[285] The same group later isolated compound **125** from the same *Streptomyces* culture, which showed moderate cytotoxic activity against several tumour cell lines[286-287] Finally, compounds **126** and **127** were isolated in 2015 from yet another *Streptomyces* species. They were characterised but not screened for biological activity.[288] Whilst the therapeutic potential of these natural products is interesting, further exploration of the biological activity has not been possible due to the very small amounts of these products made by the bacteria.

The classification of these compounds as pyrrolosesquiterpenes refers to their unusual pyrrole-fused 15-carbon terpene backbone, of which very few examples are known.[290] The glaciapyrrols are unique even amongst this select group in that they contain a 2-acylpyrrole moiety whereas all previously known pyrroloterpenes bear their terpene fragment at the pyrrole 3-position, e.g. the herronapyrrols A-C (**128-130**) and pyrrolostatin **131**.[291-298]



heronapyrrole A (**128**) R = Me
heronapyrrole B (**129**) R = H

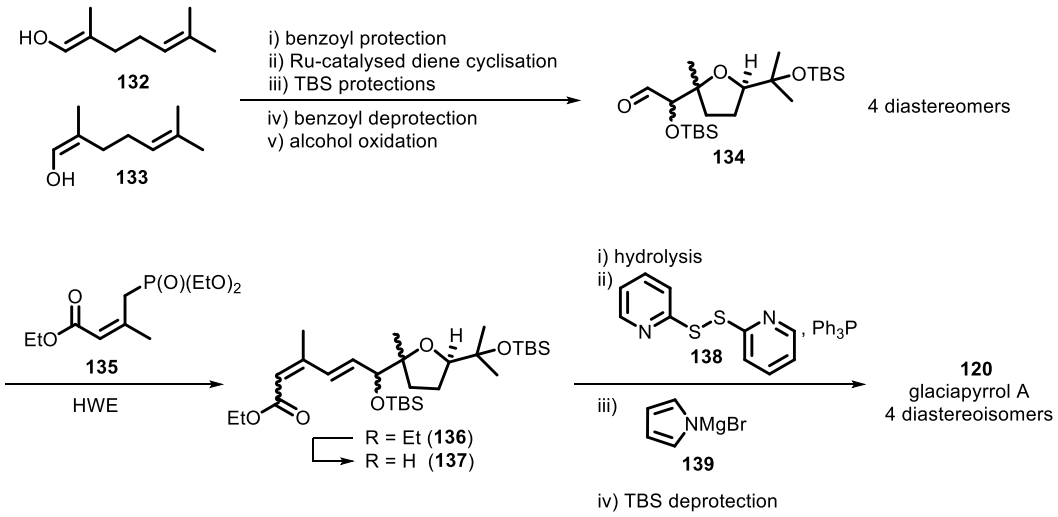
130
heronapyrrole C

131
pyrrolostatin

Figure 30: Other naturally occurring pyrrolosesquiterpene compounds, showing the 3-substituted pyrrole moiety in green.

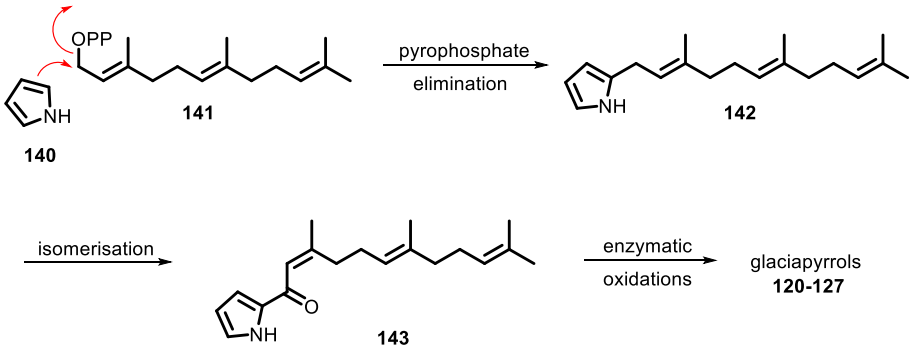
The sesquiterpene 'tails' of the glaciapyrrols are highly oxidised and contain a variety of oxygen containing functional groups, including allylic alcohols, diols,

epoxides and tetrahydrofuran rings. All members of the glaciapyrrol family have several stereochemical elements, including multiple chiral centres. In many cases the relative configuration of these chiral centres can be difficult to determine by spectroscopic methods, and the absolute configuration can only be determined by crystallography. So far, absolute assignment of the stereochemistry has only been possible for glaciapyrrol A (**120**). This is also the only member of the glaciapyrrol family to have been synthesised to date, by Riclea and Dickschat.[289] Dickschat *et al.* approached the synthesis of glaciapyrrol A (**120**) in a stereochemically divergent manner, reasoning that if they could make and characterise all possible isomers of **120**, they would be able to compare spectroscopic data to that of the natural material and assign the absolute structure. Their synthesis (Scheme 72) was centred on Roth *et al.*'s ruthenium catalysed oxidative cyclisation of dienes to tetrahydrofurans.[299-300] Starting from the isomeric terpene alcohols geraniol **132** and nerol **133**, they were able to form the four possible isomers of tetrahydrofuran **134**. Chain extension using an isoprenoid phosphonate **135** in a Horner-Wadsworth-Emmons (HWE) reaction gave the functionalised sesquiterpene ester **136**. The crucial 2-acylpyrrole bond was formed *via* hydrolysis of **136** to the corresponding carboxylic acid **137**, followed by activation as the thioester using 2,2'-dipyridyldisulfide **138** and coupling to the pyrrole Grignard reagent **139**. Removal of the protecting groups from the resulting pyrollosesquiterpene gave the four possible isomers of glaciapyrrol A (**120**). Comparison of their synthetic compounds to the natural material confirmed the structure of glaciapyrrol A with the *(11R,12S,15S)* stereochemistry shown in Figures 28 and 29.



Scheme 72: The total synthesis of glaciapyrrol A 1 in 10 steps by Riclea and Dickschat, including a ruthenium-catalysed THF ring formation, HWE chain extension and coupling to the pyrrole Grignard reagent 20.

In their discussion of the biosynthesis of the glaciapyrrols, Dickschat *et al.* highlight the likelihood that all members of the glaciapyrrol family share a biosynthetic pathway. One possible pathway that they suggest is shown in Scheme 73. They propose a biosynthesis whereby pyrrole **140** is coupled to *(2E,6E)*-farnesyl diphosphate **141**, the known biosynthetic precursor to the sesquiterpene natural products, giving *(2E,6E)*-pyrrolosesquiterpene **142**. Isomerisation of the (2*E*)-double bond of **142** to the *(2Z)* isomer gives *(2Z,6E)*-pyrrolosesquiterpene **143** which is the proposed biosynthetic progenitor to the entire family. They suggest that a series of enzymatic oxidations, epoxidations and hydrolyses convert this single biosynthetic progenitor to the various glaciapyrrols. A synthetic route based on this proposed biosynthesis would be much more step, atom and redox economic than the one published by Riclea and Dickschat, and be much closer to Hendrickson's ideal synthesis discussed in Section 1.1.2.[12]

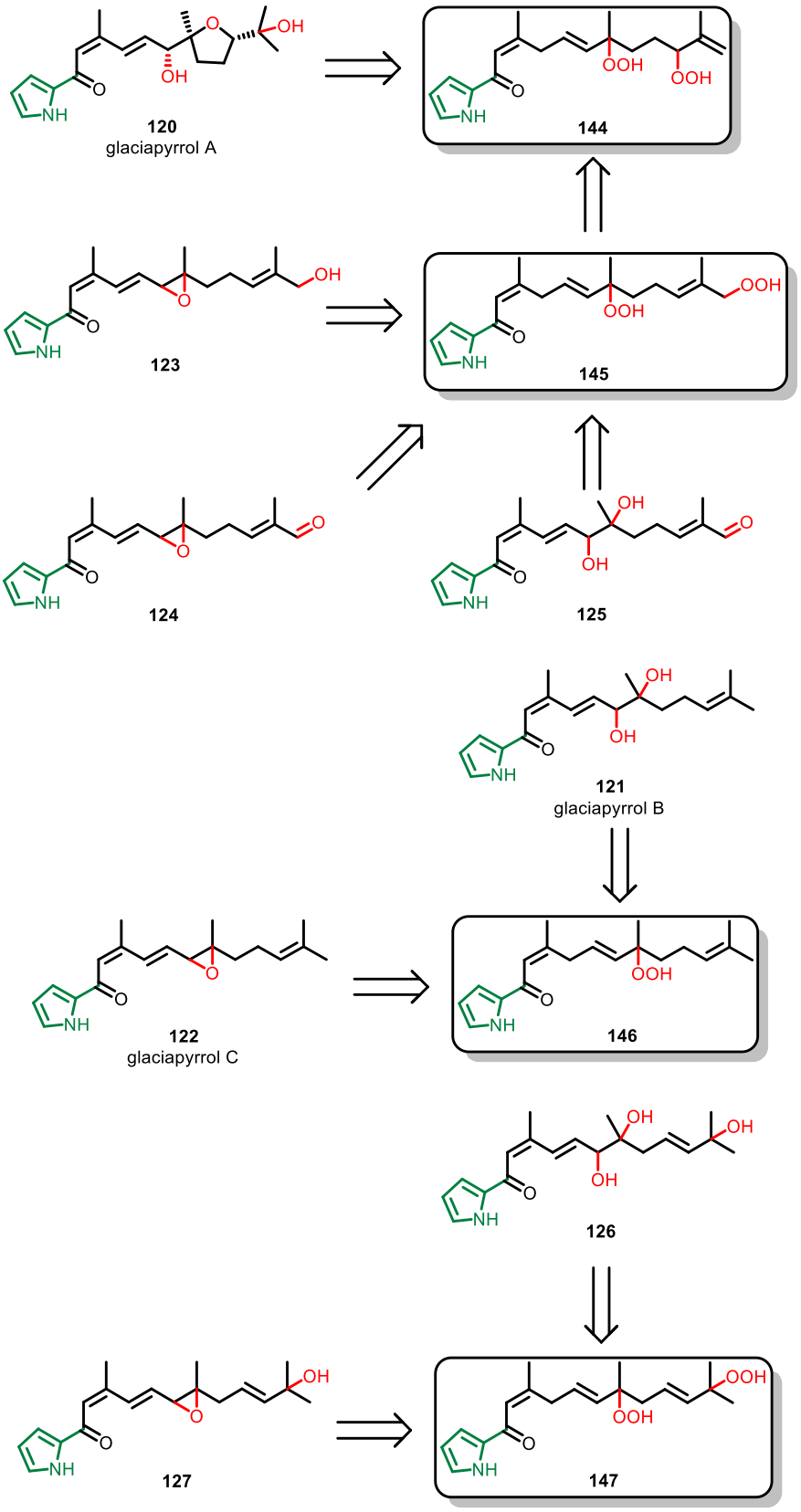


Scheme 73: One possible route for the biosynthesis of the glaciapyrrols, as proposed by Riclea and Dickschat.

Our approach to these compounds, described in the following Section, is biomimetic in that we propose to form the same precursor **143** then using singlet oxygen to install the additional functional groups.[301-302]

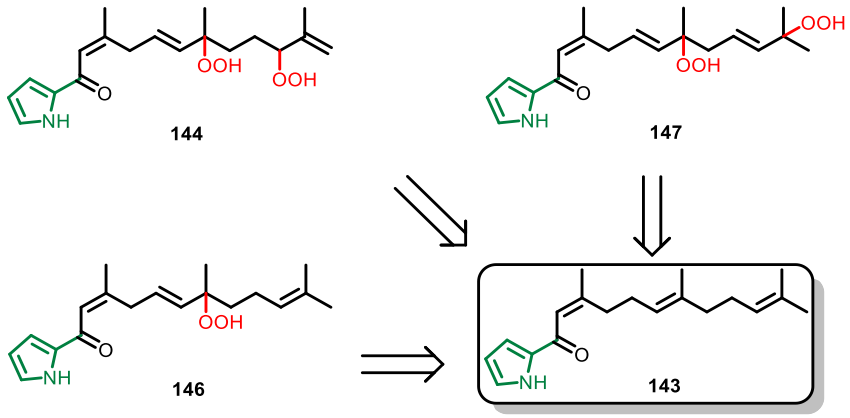
Section 4.2.2: Synthetic Strategy.

A strategy was developed for the synthesis of the glaciapyrrol family of natural products, based on the biosynthetic route proposed by Dickschat *et al.* We aimed to make the various members of the family in a stereodivergent manner, intending to separate and individually characterise the isomers, then to assign the stereochemistry of the naturally occurring isomers by comparison to the synthesised compounds. Amounts in the order of 10-100 mg of each compound would be required to allow a full screen of the compounds' pharmaceutical activity to be performed. We envisioned that many of the oxygen-containing functional groups could be installed from the photo-oxygenation of a sesquiterpene backbone and rearrangement of the resulting peroxides. Retrosynthetic analysis of the glaciapyrrols with this in mind provided allylic hydroperoxides **144**-**147** as the precursors to the entire family.



Scheme 74: Retrosynthetic analysis showing that glaciapyrrol A (120) and unnamed glaciapyrrols 123, 124 and 125 can be formed from di-allylic hydroperoxides 144 and 145, glaciapyrrols B (121) and C (122) can be formed from allylic hydroperoxide 146, and unnamed glaciapyrrols 126 and 127 can be formed from di-allylic hydroperoxide 147.

The hydroperoxides themselves could be formed in a single non-selective Schenck reaction of pyrrolosesquiterpene precursor **143**, the same species proposed by Dickschat as the biosynthetic progenitor of the family. Pyrrolosesquiterpene **143** could be formed in a biomimetic fashion from a farnesyl fragment, synthon **A** and a pyrrole fragment, synthon **B**.



Scheme 75: Hydroperoxides 144, 146 and 147 are all expected photo-oxygenation products of pyrrolosesquiterpene 143.

As such, the synthesis could be divided into two distinct parts – a mid-to-large scale synthesis of the common pyrrolosesquiterpene precursor **143** followed by a series of photo-oxygenations and transformations of peroxides to install the various functionality of the glaciapyrrols, *i.e.* the epoxide and allylic alcohol functionalities of **121**-**127** and the THF ring of **120**.



Scheme 76: Disconnection of pyrrolosesquiterpene 143 into pyrrole and farnesyl fragments A and B.

The synthesis of pyrrolosesquiterpene **143** could proceed *via* several routes. We aimed to develop a synthetic process for production of **143** on the mid-to-large scale which was sustainable in the way that was outlined throughout Section 1.1: atom economical, avoiding bulky or wasteful reagents, step and redox economical and

operationally simple, requiring few unit operations and a small amount of ancillary materials. If these goals are achieved, the synthesis should have a high productivity and a low environmental impact. Section 4.3. describes the development of this process.

Elaboration of pyrrolosesquiterpene **143** would require the development of simple protocols for the formation of the epoxide and THF functionality displayed by the glaciapyrrol natural products from the hydroperoxides available through photo-oxygenation of **143**. Preferably these transformations would avoid stoichiometric reagents. Section 4.4. describes the development of these transformations and their application in work towards the synthesis of the glaciapyrrols.

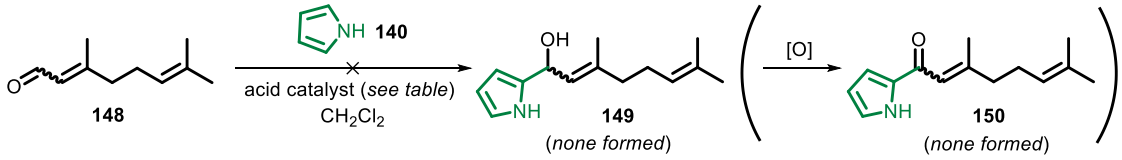
Section 4.3: Synthesis of the Common Pyrrolosesquiterpene Precursor.

Section 4.3.1: Exploration of Aldehyde-Pyrrole Couplings.

The first strategy that was attempted was the acid catalysed addition of pyrrole **140** to an aldehyde. Citral **148** was used as a model substrate due to its lower price and greater availability. Citral was purchased as a 1:1 mixture of two isomers, the *trans*-isomer geranial **148a** and the *cis*-isomer neral **148b**. These two isomers interconvert easily, though were expected to react in a similar manner and so were used together without separation.

The secondary alcohol **149** that was expected to form from reaction of citral with pyrrole could be oxidised afterwards to give desired pyrroloterpene **150**. A range of Brønsted and Lewis acids were tested. The catalyst screenings were performed in dichloromethane with an initially high catalyst loading of 60 mol%, with a view to optimising the conditions and loadings for any successful hits. Results are shown

in Table 12. None of the conditions that were tested gave the desired secondary alcohol product **149**, instead giving mixtures of overaddition products and considerable amounts of a brown/black tar. As a result, isolation of the reaction products was not achieved, and assumptions about the reaction outcome were made based on the crude HRMS results. Some of these assumed products are shown in Figure 31. The tar was taken to be oligomers of pyrrole. Reaction of the starting aldehyde was only observed at all when strong acid trifluoroacetic acid (TFA) was used. In these cases, HRMS indicated that the product was dipyrromethane **151**. Weaker phosphoric acid gave no reaction of the aldehyde but still produced a small amount of oligomeric tar.



Entry	Catalyst	Eq.	Temperature	Time	Outcome
1	-	-	RT	18 h	No reaction
2	-	-	50 °C	18 h	No reaction
3	TFA	0.6	RT	30 s	**151**, oligomers
4	TFA	0.1	RT	30 s	**151**, oligomers
5	TFA	0.1	-20 °C	15 m	**151**, oligomers
6	H_3PO_4	0.6	RT	18 h	Oligomers only
7	ZnO	0.6	RT	18 h	No reaction
8[a]	TFA	0.1	-20 °C	10 m	**151**, **152**, oligomers
9[b]	TFA	0.1	-20 °C	30 m	**153**, oligomers

Table 12: Screening of catalysts and conditions for acid-catalysis addition of pyrrole 140 to citral 148. All reactions were carried out in dichloromethane at a concentration of 0.2 M. Temperatures, reaction times, catalysts and equivalents are given in the Table. [a]0.5 eq. of pyrrole 140 was used. [b]Reaction performed in the presence of 2 eq. para-benzoquinone.

The formation of dipyrromethanes from aldehydes and pyrroles is well known and is commonly applied to the formation of porphyrin and dipyrromethene (dipy) dyes.[303] It was thought that by adding an excess of citral **148**, the formation of dipyrromethane **151** could be reduced in favour of alcohol **149**. Again, the major

products were pyrrole oligomers and unreacted aldehyde, with the HRMS of the minor product corresponding to the 2,5-diacylpyrrole **152**. The reaction with TFA was carried out in the presence of *para*-benzoquinone in an attempt to oxidise alcohol **149** before it could dehydrate (Entry 9). The reaction mixture turned a vivid blue colour, and the HRMS showed the mass of the dipyrromethene **153**.

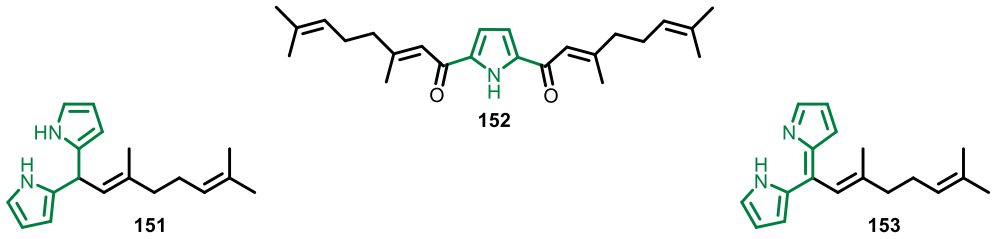


Figure 31: The presumed products of the acid-catalysed addition of pyrrole 140 to citral 149, based on HRMS results and literature precedent.

Based on the results shown in Table 12, and the existing literature surrounding dipyrromethane formation, several things were concluded: Activation of the aldehyde towards nucleophilic attack requires strong acid, whilst oligomerisation of pyrrole takes place under much milder conditions. This means that the latter will always be a competitive pathway under acidic conditions. The formation of the dipyrromethane could not be stopped by adding an excess of citral **148**, nor by trapping the alcohol intermediate **149** by oxidation, which suggests that dehydration of **149** is rapid. It was therefore decided that direct addition under acidic conditions was not a viable route.

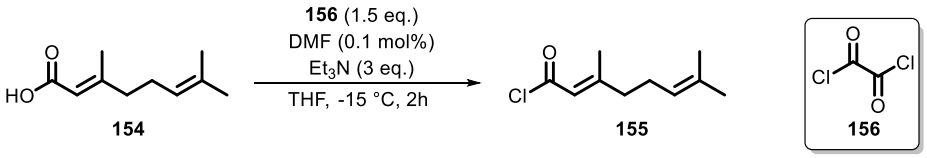
Nucleophilic coupling of pyrrole to citral was also attempted under basic conditions, using the pyrrole Grignard reagent **139** used by Riclea and Dickschat to make glaciapyrrol A.[289] Again, none of the desired product was formed and the major products were assumed to be dipyrromethane **151** and pyrrole oligomers.

Section 4.3.2: Exploration of Carboxylic Acid-Pyrrole Couplings.

It was decided that addition of pyrrole derivatives to an activated carboxylic acid may provide access to 2-acylpyrroles without the tendency of the intermediates to dehydrate. This strategy adds a 'concession' step to the synthesis in that a functional group transformation must be performed prior to the acyl-pyrrole bond formation.

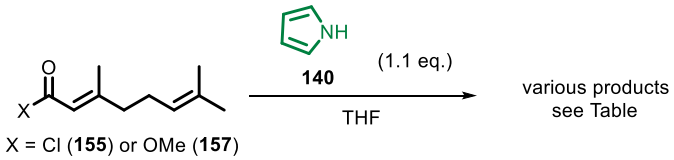
Couplings of carboxylic acid derivatives to pyrrole were again modelled using a smaller terpene substrate, this time the *trans*-α,β-unsaturated acid geranic acid, **154**. The acid does not have the same tendency to isomerise as the citral aldehydes **148** used previously, and so **154** could be used pure. The *trans*-isomer was used due to its greatly reduced cost compared to the *cis*, and the fact that the reactivity of the two compounds was not expected to differ greatly.

Table 13 shows the results of pyrrole coupling reactions using simple electrophilic derivatives of geranic acid **154**. Initially, the acid was activated as the acyl chloride **155**. Chlorination was performed using oxalyl chloride **156**, which was seen as a relatively benign and atom economic chlorinating agent. The mass of the reagent is small compared to other chlorinating agents e.g. thionyl chloride or *N*-chlorosuccinimide. Additionally, the only side products are the gases carbon dioxide and carbon monoxide, as well as hydrochloric acid, which can be removed easily by addition of an organic base such as triethylamine. This makes recovery of the products of the reaction very simple. The conditions used for chlorination of geranic acid are shown in Scheme 77. A catalytic amount of *N,N*-dimethylformamide (DMF) was added to increase the activity of the oxalyl chloride.



Scheme 77: Chlorination of geranic acid 154 to geranyl chloride 155 using oxalyl chloride 156, with *N,N*-dimethylformamide (DMF) as catalyst.

The coupling reactions with acyl chlorides were not successful. All showed addition of multiple equivalents of pyrrole to the acyl chloride, as well as large amounts of the same oligomeric tar received previously. Lowering the temperature reduced conversion without improving the selectivity for geranylpyrrole **150**. Zinc(II) oxide was added as a catalyst based on the work of Ji *et al.*[304] The rate was increased but still the desired product was not formed.



Entry	X	Catalyst (eq.)	Temperature / °C	Major Product
1	Cl	--	RT	Multiple additions
2	Cl	ZnO (0.5)	-15 °C	Multiple additions
3	Cl	ZnO (0.5)	-15 °C	Multiple additions
4	OMe	--	RT	No reaction
5	OMe	ZnO (0.5)	RT	No reaction

Table 13: Screening of coupling reactions of pyrrole 140 to geranyl chloride 155 or methyl geranate 157. All reactions were performed in tetrahydrofuran (THF) at a concentration of 0.2 M. Catalysts, equivalents and temperatures are given in the Table.

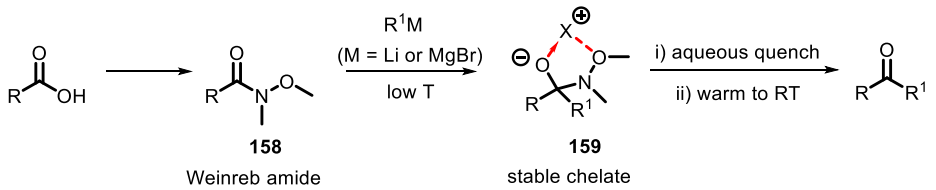
Couplings to the less reactive methyl ester, methyl geranate **157** were also attempted. It was theorised that the lower reactivity of the substrate and lower acidity of the methanol side product would enable a more controlled addition under

milder reaction conditions. However, the reactivity of ester **157** proved to be too low and it did not react at all with pyrrole **140**, even on addition of zinc(II) oxide as a catalyst.

It was concluded from this study that a milder, more controlled method was needed to form the required 2-acylpyrrole bond. This would require a formal derivitisation of geranic acid in an additional concession step, moving further away from the ideal synthesis.

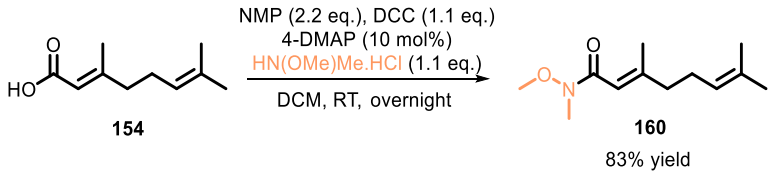
Section 4.3.3: Formation of Weinreb Amides from Carboxylic Acids using DCC.

More controlled addition of organometallics to carbonyl compounds is possible using the Weinreb ketone synthesis.[305] This protocol uses *N,O*-dimethylhydroxamates **158**, referred to as Weinreb amides, as the electrophile. Whilst less electrophilic than esters and acyl chlorides, as well as the ketone products, addition of an organometallic reagent to these species gives chelated tetrahedral intermediates **159**, which are usually stable below -15 °C.[306] This intermediate is not electrophilic, so multiple additions of organometallics is not possible. When addition to the aldehyde is complete, the organometallic can be quenched at low temperature and the temperature raised to give the ketone product. Whilst this adds an extra concession step to the reaction sequence, failure of the more ideal methods presented above led to the decision that this concession was necessary and beneficial.



Scheme 78: A generalised Scheme showing the Weinreb ketone synthesis. Addition of strong nucleophiles, e.g. organometallic species, to the Weinreb amides 158 gives stable chelated tetrahedral intermediates 159, which do not react further with the organometallic nucleophile.

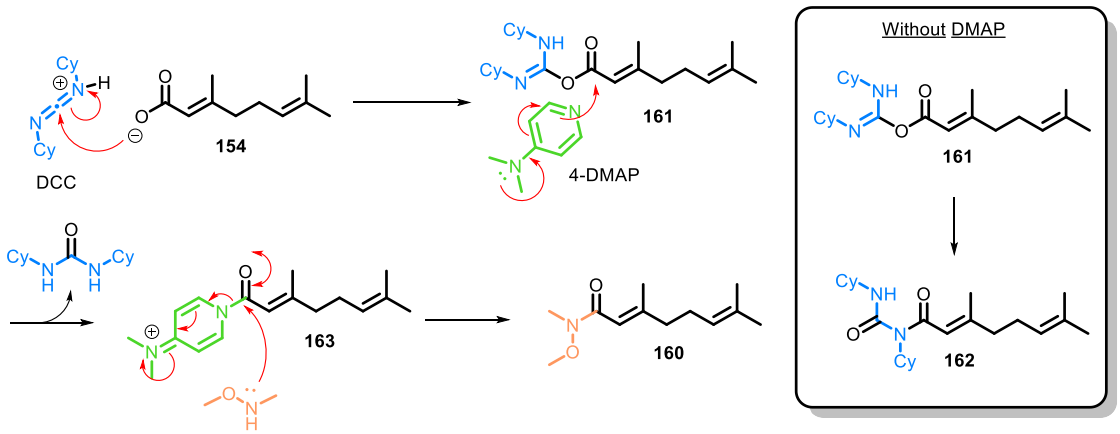
Weinreb amide formation from geranic acid **154** was performed under literature conditions using *N,N*-dicyclohexylcarbodiimide (DCC) as a coupling reagent.[307] One drawback to this reaction is the formation of a stoichiometric amount of urea waste, which can often be difficult to remove from the product mixture. Typically, column chromatography is required to achieve clean product. Additionally, the literature procedure used dichloromethane as solvent, a potential carcinogen and undesirable material. The reaction was carried out in dichloromethane at a concentration of 0.5 M, using 1.1 eq. DCC, 10 mol% 4-(*N,N*-dimethylamino)pyridine (4-DMAP) as a catalyst and 1.1 eq. of the Weinreb salt *N,O*-dimethylhydroxylamine hydrochloride. *N*-methylpyrrolidine (NMP, 2.2eq) was added to deprotonate the Weinreb salt to the more active and soluble free base form. The reaction was stirred at room temperature overnight. After purification by column chromatography, Weinreb amide **160** was isolated in 83% yield.



Scheme 79: Synthesis of Weinreb amide 160 by peptide coupling of geranic acid 154 using *N,N*-dicyclohexyl carbodiimide as coupling reagent.

The mechanism of the DCC-mediated amidation reaction is as follows.[308] The carboxylic acid **154** is deprotonated under basic conditions, and the mildly nucleophilic carboxylate attacks the electrophilic carbodiimide carbon to give *O*-acyl isourea intermediate **161**. This could be attacked directly by strong nucleophiles at the carbonyl carbon to give the desired product, but for weaker nucleophiles such as *N,O*-dimethylhydroxylamine used above there is a competing 1,3-acyl migration to *N*-acylurea **162**, which is not strongly electrophilic and leads

to loss of yield. This side reaction is suppressed in the presence of the 4-DMAP catalyst. 4-DMAP rapidly attacks the carbonyl carbon of **161** before rearrangement can take place, giving activated aminopyridinium ester **163**, which can react quickly with the amine nucleophile, to give the product amide **160**.



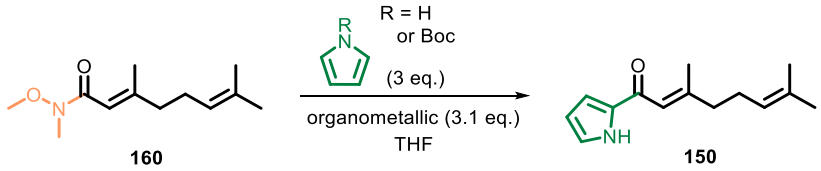
Scheme 80: The mechanism of DCC-mediated peptide coupling of geranic acid 154 to form Weinreb amide 160. Also shown is the rearrangement of *O*-acyl isourea 161 to *N*-acylurea 162 in the absence of the 4-DMAP catalyst.

Section 4.3.4: Screening of Organometallic Couplings to Weinreb Amides.

Weinreb amide **160** was subjected to several coupling reactions with organometallic pyrrole reagents. Two such reagents were used, pyrrole-1-magnesium bromide (**139**) and 1-tertbutyloxycarbamate-pyrrole-2-lithium (**164**). Unprotected pyrrole-1-lithium was not used as it is reported as being nucleophilic at the 1 position, unlike Grignard reagent **139** which is a softer nucleophile, reacting at the 2- (5-) position.[309]

All reactions proceeded to give the pyrroloterpene product **150** with varying yields. Results are shown in Table 14. In general, pyrrole-magnesium bromide **139** was a poorer coupling partner than Boc-pyrrole-lithium **164**. The yield of pyrroloterpene **150** when using ethylmagnesium bromide (EtMgBr, Entry 1) to generate **139** was only 22%. Even in the presence of LiCl (Entry 2), known to increase the reactivity

of Grignard reagents,[310] yields of product **150** were low. The Grignard reagent was observed to be less stable than the organolithium reagent **164**, forming larger amounts of polymeric side product. This, in addition to the lower rate of addition expected for the less nucleophilic Grignard, can explain the lower observed yields.



Entry	Organometallic	R (reagent)	Temperature / °C	Yield / %
1	EtMgBr	H (**139**)	-15 → 0	22
2	EtMgBr / LiCl	H (**139**)	-15 → 0	24
3	LDA	Boc (**164**)	-45	12
4	TMP-Li	Boc (**164**)	-45	80
5	^{t}BuLi	Boc (**164**)	-45	78

Table 14: Screening of organometallic reagents and conditions for pyrrole coupling to Weinreb amide 160. All reactions were performed in THF at a concentration of 160 of 0.2M. Reactions were monitored by TLC.

The organolithium reagent **164** was generated *in situ* from several different lithium bases. When lithium diisopropylamide (LDA, Entry 3)) was used, **150** formed in only 12% yield, along with large amounts of a side product which was not isolated, but which based on a strong HRMS peak at M/Z = 320 was attributed to nucleophilic addition of LDA to Weinreb amide **160**. Another amide base, lithium 2,2,6,6-tetramethylpiperidide (TMP-Li, Entry 4) was used. The forward-facing methyl groups hinder this base and its parent amide from acting as a nucleophile and so the yield of **150** increased to 80%. The pyrrole Boc group was removed under the mildly acidic work-up conditions. Repeating the reaction using ^{t}BuLi directly showed only a slight decrease in yield.

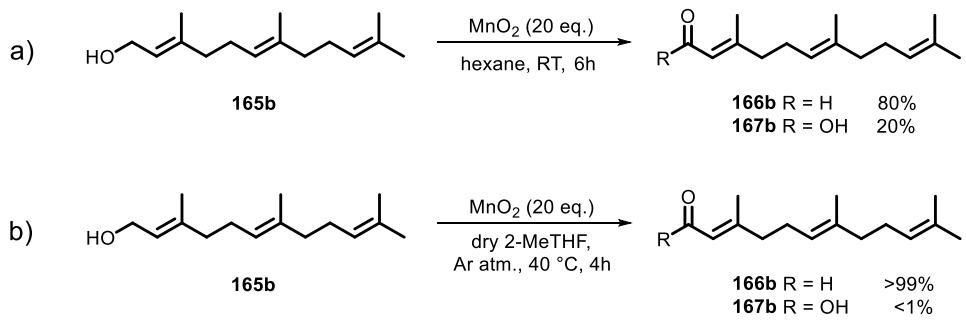
Section 4.3.5: Synthesis of the Pyrrolosesquiterpene Precursor.

Now that a validated method for the formation of the required 2-acylpyrrole bond had been found, it could be applied to the synthesis of the actual precursor to the glaciapyrrols, pyrrolosesquiterpene **143**. The starting point chosen for this synthesis was (2*Z*,6*E*)-farnesol **165a**, although the high price of the pure material compared to the mixture of (2*Z*,6*E*)- and (2*E*,6*E*)- isomers meant that the mixture would be used and separation performed afterwards.

Initially, the pure (2*E*,6*E*)- isomer **165b** was used to see if conversion between the isomers took place at any point along the proposed route.

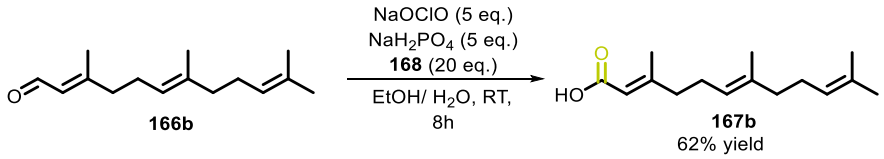
The (2*E*,6*E*)- isomer of farnesal, **166b** was obtained by oxidation of (2*E*,6*E*)-farnesol **165b** using manganese(iv) dioxide. This reagent was chosen as a reliable and selective oxidation of allylic and benzylic alcohols, giving high yields of aldehydes.[311] The reaction is heterogenous as the manganese reagent is insoluble in organic solvents, allowing easy removal by filtration. However, a large excess of manganese dioxide is required for full conversion, and overoxidation is possible to the carboxylic acid.

The reaction was performed using literature conditions:[312] 20 equivalents of manganese(iv) dioxide suspended in hexane, at room temperature. Full conversion was achieved in 6 hours, giving (2*E*,6*E*)-farnesal **166b** in 80% with (2*E*,6*E*)-farnesic acid **167b** as the minor product (Scheme 81a). This could be improved upon by performing the reaction under inert conditions and heating the reaction to 40 °C. Since hexane is an undesirable solvent from a Green Chemistry standpoint it was substituted for the biomass-derived sustainable solvent 2-methyltetrahydrofuran (2-MeTHF). Under these conditions on a 1 mmol scale the yield was quantitative and the reaction time was reduced to 4 hours (Scheme 81b).



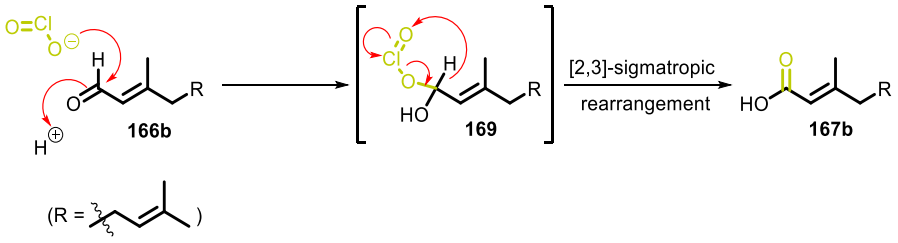
Scheme 81: Oxidation of allylic alcohol farnesol 165b using manganese(iv) dioxide under a) literature conditions, giving a mixture of farnesal 166b and farnesic acid 167b and b) optimised conditions giving almost exclusively farnesal.

Oxidation of (2*E*,6*E*)-farnesal **166b** to (2*E*,6*E*)-farnesic acid **167b** was affected using the known reaction of aldehydes with chlorous acid, the Pinnick oxidation.[313] This reaction generally gives good yields of carboxylic acids under mild conditions, with high atom economy and low toxicity compared to other commonly applied reactions, for example the use of 2,3-dichloro-5,6-dicyano-1,4-benzoquinone (DDQ) or pyridinium chlorochromate (PCC). The reagents are water-soluble and the reaction is commonly performed in water/alcohol mixtures. Chlorous acid is unstable so is generated *in situ* from the stable sodium salt and a weak acid. One thing that detracts from the atom economy of this reaction is the formation of the reactive hypochlorite by-product which degrades the chlorite reagent and can react with alkene bonds in the substrates or products. This necessitates the addition of large amounts of a scavenger, commonly 2-methyl-2-butene **168**, to ensure high yields and clean product mixtures. The Pinnick oxidation of **166b** was performed using literature conditions: 5 equivalents of sodium chlorite, 5 equivalents of monosodium orthophosphate and 20 equivalents of **168**. Farnesic acid **167b** was obtained in 62% yield as a mixture of isomers. The isomers could not be separated by column chromatography and were used directly in the following step.



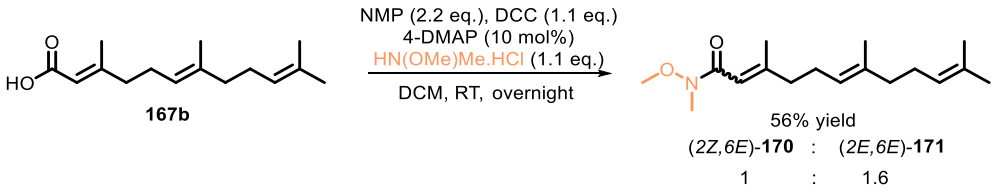
Scheme 82: Pinnick oxidation of farnesal 166b to farnesic acid 167b under literature conditions.

The mechanism of the Pinnick oxidation is shown in Scheme 82. Chlorite adds to aldehyde **166b** under acidic conditions to give intermediate **169**, which undergoes a [2,3]-sigmatropic rearrangement to expel hypochlorite and provide carboxylic acid **167b**.



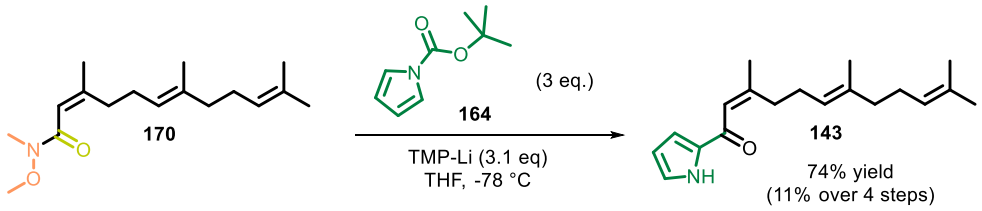
Scheme 83: The mechanism of the Pinnick oxidation of 166b, via nucleophilic addition of chlorite to the aldehyde followed by rearrangement to give the carboxylic acid product 167b.

Weinreb amides **170** and **171** were formed from the corresponding carboxylic acid **167b** using an identical protocol to that described in Section 4.3.3. The reaction proceeded smoothly to give a 1:1.6 mixture of (2*Z*,6*E*)- and (2*E*,6*E*)-isomers, **170** and **171** respectively. These could be separated using column chromatography and were received in a 56% overall yield.



Scheme 84: DCC coupling of farnesic acid 167b to give the farnesoyl Weinreb amides 170 and 171.

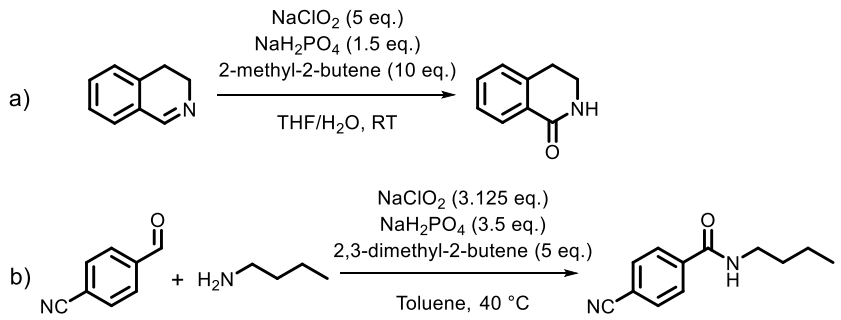
(2*Z*,6*E*)-farnesoyl Weinreb amide **170** was coupled to the Boc-pyrrole organolithium reagent **164** as described in Section 4.3.4., using freshly prepared TMP-Li to form the organometallic pyrrole reagent. The reaction proceeded much as for Weinreb amide **160**, giving pyrrolosesquiterpene **143** 74% yield. Over the four steps from farnesol the glaciapyrrol precursor **143** was made in 11% overall yield.



Scheme 85: Organolithium coupling to form pyrrolosesquiterpene 143.

Section 4.3.6: Direct Pinnick-type Amidation of Farnesal.

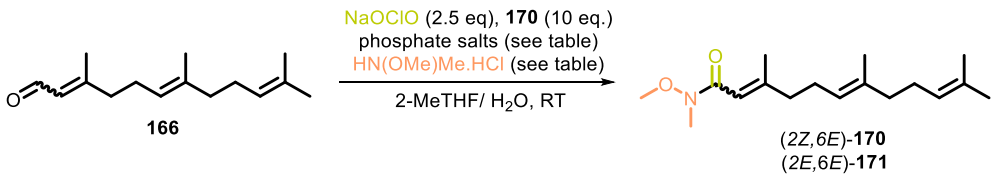
Literature precedent exists for the formation of amides using a Pinnick type protocol. This was originally reported with a limited scope by Tomioka *et al.* who used imines rather than aldehydes as substrate under standard Pinnick conditions (Scheme 86a).[314] Tan *et al.* later showed that the same amidation could be performed as a one-pot reaction from aldehydes and amines, with a large substrate scope and good yields (Scheme 86b).[315] They proposed a mechanism based on initial formation of an imine followed by reaction with chlorous acid analogous to the Pinnick oxidation mechanism shown previously in Scheme 18. It was thought that a similar protocol could be developed for the direct amidation of farnesal **166** (as a mixture of (2*Z*,6*E*)- and (2*E*,6*E*)-isomers **166a** and **166b**) to Weinreb amides **170** and **171**.



Scheme 86: Literature precendent for the Pinnick-type formation of amides by a) Tomioka et al. from imines and b) Tan et al from aldehydes and amines.

Tan *et al.* had found that better yields were obtained for less water-miscible co-solvents toluene, ethyl acetate and ^{t}BuOH compared to acetonitrile or 1,4-dioxane. Because of this, the biomass derived sustainable solvent 2-methyltetrahydrofuran (2-MeTHF), which is immiscible with water, was chosen for this reaction. The amount of sodium chlorite was reduced to 2.5 equivalents, and the amount of 2-methyl-2-butene scavenger **168** reduced to 10 equivalents. Because the amine would be added as the hydrochloride salt, a mixture of 1.0 eq. NaH_2PO_4 and 1.5 eq. Na_2HPO_4 was used to balance the pH, rather than the 2.5 eq. NaH_2PO_4 used in the synthesis of farnesic acid **167**.

The one pot reaction of farnesal **166** and *N,O*-dimethylhydroxylamine with sodium chlorite under the conditions shown in Table 15, Entry 1 gave only a moderate yield of 21% for the desired amides, with the carboxylic acids **167** making up the remaining 79%. No side reactions with hypochlorite were observed despite the lower amount of scavenger present.



Entry	NaOClO Addition time / min	Amine / eq.	NaH_2PO_4 / eq.	Na_2HPO_4 / eq.	Yield amides / %	Yield acids / %
1	0 (180)	1.5	1	1.5	21	79
2	140 (180)	1.5	1	1.5	38	62
3	300	1.5	1	1.5	64	36
4	300	2.5	0	2.5	95	5

Table 15: Optimisation of the yield of Weinreb amides 170 and 171 from farnesal 166. All reactions were performed at room temperature, Where total reaction time is different to the time for chlorite addition the former is given in brackets.

It was thought that the low yield of this reaction compared to those typically acheived by Tomioka or Tan might be because condensation of an aldehyde with a secondary amine gives a charged iminium species rather than a neutral imine. Formation of the former is less favourable than the latter and so the aldehyde-iminium equilibrium is more in favour of the aldehyde. Tan *et al.* also observed lower yields of amides when using secondary amines.

It was predicted that a slow addition of sodium chlorite solution to the reaction mixture might improve the selectivity of the reaction and increase yields of amide. Adding the chlorite solution dropwise over 140 minutes increased the yield to 38% (Table 15, Entry 2), and a 300 minute addition raised it further to 64% (Entry 3). By increasing the amount of amine to 2.5 equivalents the yield was increased to an excellent 95% (Entry 4).

This change in selectivity is thought to be an example of thermodynamic *versus* kinetic control, and can be rationalised based on the rates of the competing reactions (Figure 32). Whilst the rate constant for iminium formation (k_1) is expected to be lower than that for imine hydrolysis (k_{-1}), giving a higher concentration of aldehyde **172** compared to iminium **173**, the rate constant for

chlorite addition to aldehyde **172** (k_2) is expected to be smaller than for chlorite addition to the more electrophilic iminium **173** (k_3). Where chlorite is present in excess, as in Table 15, Entry 1, the product distribution is dependent on the relative concentrations of **172** and **173**, and will reflect the position of the aldehyde/iminium equilibrium – thermodynamic control. Thus, carboxylic acid **174** is the major product. Where chlorite concentration is rate-limiting, as in the case of slow addition (Entries 3 and 4), the relative rates of reaction v_2 and v_3 depend more on the size of the rate constants k_2 and k_3 – kinetic control. In this case amide **175** is the major product. However, the reaction is clearly not under full kinetic control at the rates of addition used in the above study, since adding another equivalent of *N,O*-dimethylhydroxylamine – shifting the equilibrium in favour of iminium formation – also improved the yield.

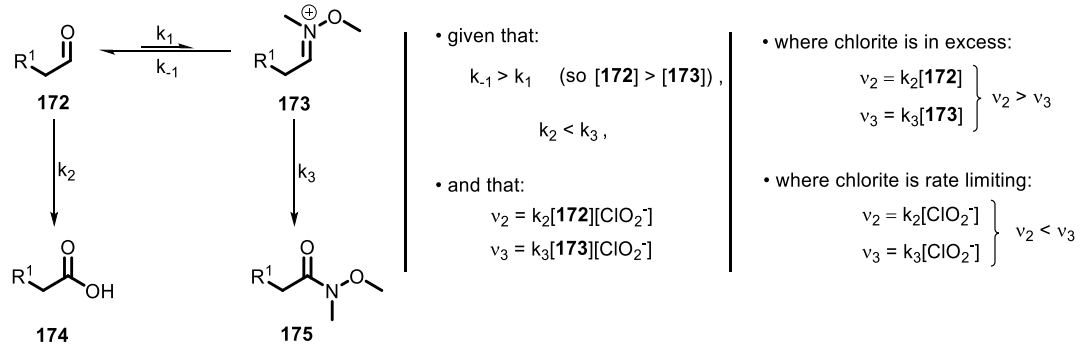


Figure 32: Rationalisation of the increased amide yields with slow addition of chlorite.

The use of this direct, multicomponent aldehyde amidation is a huge benefit to the efficiency and sustainability of this synthesis. Not only does it remove an entire step from the reaction scheme, with all the savings in time, energy and materials that come with it, but the 95% yield is considerably better than the combined 35% over two steps for the Pinnick/DCC coupling route. Several problems with the standard Pinnick oxidation have been addressed – the use of a biphasic solvent mixture seems to greatly reduce the side reactions of substrate or product with

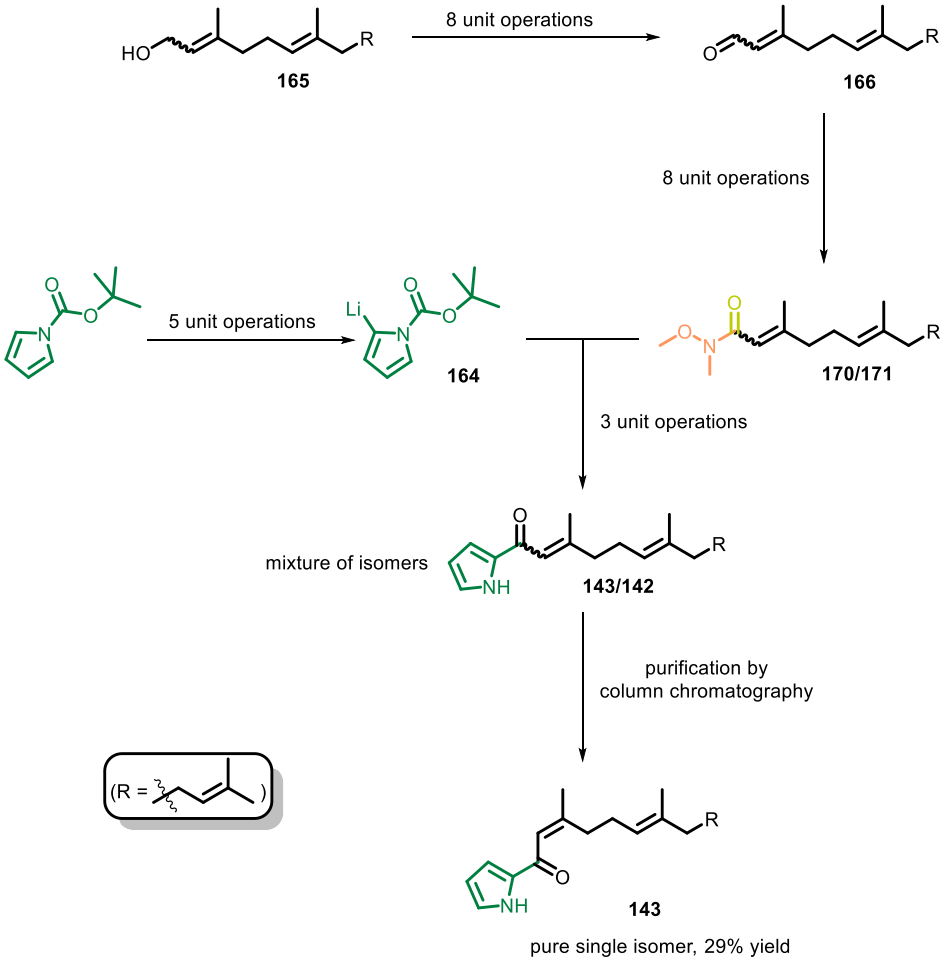
hypochlorite, reducing the amount of scavenger required. Additionally, lower amounts of sodium chlorite are needed for this reaction, which could be due to the lower amount present compared to scavenger 2-methyl-2-butene **168**, reducing degradation by hypochlorite. Finally, the workup of this reaction is simple – all excess reagents and by-products can be removed by removal of the aqueous phase and washing with mild aqueous acid. This is greatly improved compared to the difficult chromatographic workup required for the amide coupling using DCC described in Section 4.3.5.

The high yield and easy work-up make this reaction a good choice for use in a telescoped synthesis, as described in the following Section.

Section 4.3.7: Scale-up and Telescoping of Reaction Steps.

As discussed in Section 1.1.3., the efficiency of a process can be improved and the amount of waste generated can be reduced by performing several steps consecutively without purification or solvent switching, a strategy referred to as telescoping. The synthesis of pyrrolosesquiterpene **143** from farnesol **165** *via* the direct amidation presented in the previous Section was ideal for telescoping since the first two of three steps used biphasic reagents, and already used the same solvent, 2-MeTHF. The solvent used in the final organometallic coupling step was THF, which has similar properties to 2-MeTHF, and it was thought that the two could be interchanged with very little effect on the yield. The reaction was scaled up and telescoped through as shown in Scheme 87. The reactions were performed on a 35 mmol scale, starting from 7.8 g of mixed farnesol isomers **165**, at a concentration of 0.2M. The manganese dioxide oxidation reaction proceeded exactly as described in Section 4.3.5. to give a mixture of farnesal isomers in 96% yield by ^{1}H-NMR. At full completion, the manganese dioxide was removed by

filtration and washed with more 2-MeTHF, bringing the concentration to 0.14M. The combined organic solution was added to a stirred solution of phosphates and the Weinreb salt as described in Section 4.3.6. The scavenger 2-methyl-2-butene was added, followed by slow addition of aqueous sodium chlorite. On completion, the aqueous layer was removed and washed with additional solvent, further reducing the concentration to 0.1 M. After drying, the combined organic phases were cooled and treated with a pre-prepared solution of the pyrrole organolithium reagent **164** to give a crude mixture containing pyrrolosesquiterpenes **143** and **142**. This mixture was purified by column chromatograpy to give species **143** and **142** in a 29% and 43% yield, respectively. In total, the three synthetic steps require 25 unit processes and 250 mL organic solvent to make 2.9 g of product **143** in a greatly improved 29% overall yield from the mixed isomer of farnesol.

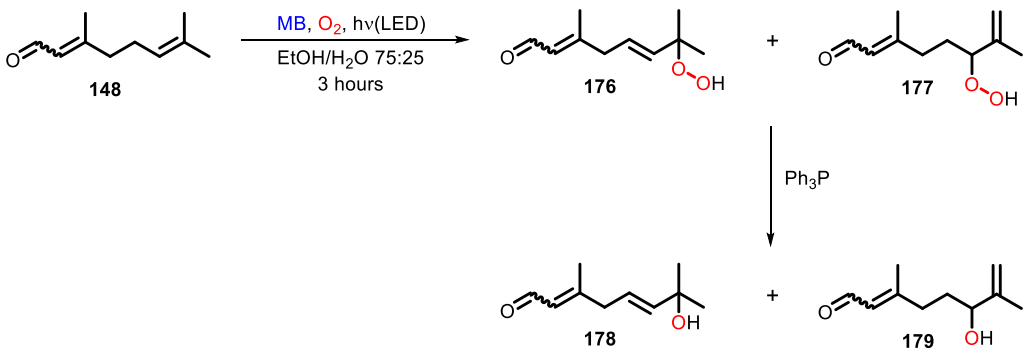


Scheme 87: Telescoped synthesis of glaciapyrrol precursor 143.

Section 4.4: Synthesis of Glaciapyrrol Moieties Using Singlet Oxygen.

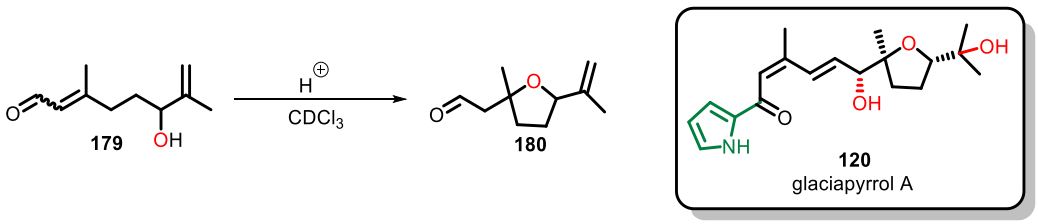
Section 4.4.1: Model Studies on the Photo-Oxygenation of Citral.

The use of citral **148** as a model substrate was continued in studies towards the functionalisation of the precursor formed in the previous section. Under standard photo-oxygenation conditions, using methylene blue (MB) as photosensitiser in a 75:25 mixture of ethanol and water, citral **148** showed the expected Schenck reaction of the tail alkene bond (Scheme 88). A 1:1 mixture of tertiary hydroperoxide **176** and secondary hydroperoxide **177** was obtained, which were reduced to the corresponding allylic alcohols **178** and **179** using triphenylphosphine (Ph_3P) before characterisation. Only the *trans*- isomer of **178** was formed, as predicted by the abstraction selectivity rules described in Section 1.2.4.



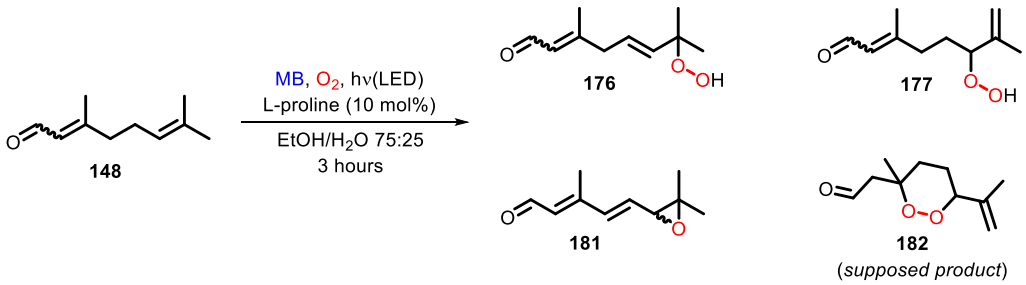
Scheme 88: Photo-oxygenation of citral 148.

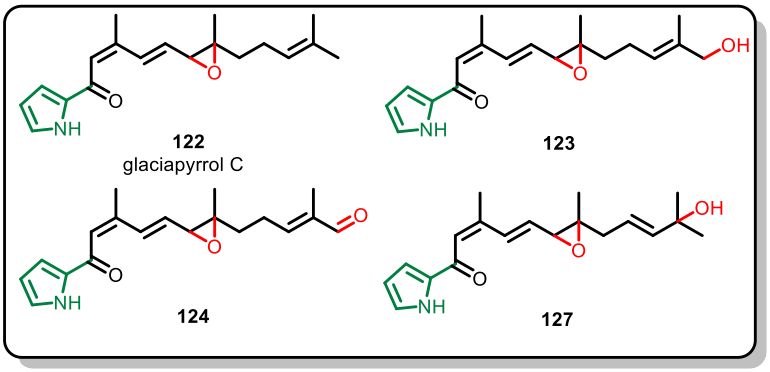
Secondary alcohol **179** was unstable on silica and in the presence of acid – instead, substituted tetrahydrofuran **180** was formed (Scheme 89). This tetrahydrofuran moiety is similar to that found in glaciapyrrol A **120**.



Scheme 89: Cyclisation of allylic alcohol 179 to tetrahydrofuran 180.

Photo-oxygenation of citral in the presence of 10 mol% L-proline was found to give two additional products (Scheme 90). One of these was isolated by column chromatography and characterised as epoxide **181**, with a similar structure to glaciapyrrol C **122** and to the unnamed glaciapyrrols **123**, **124** and **127**. The second new product was unstable on silica but based on HRMS and the crude ^{1}H-NMR spectrum was tentatively assigned as endoperoxide **182**.

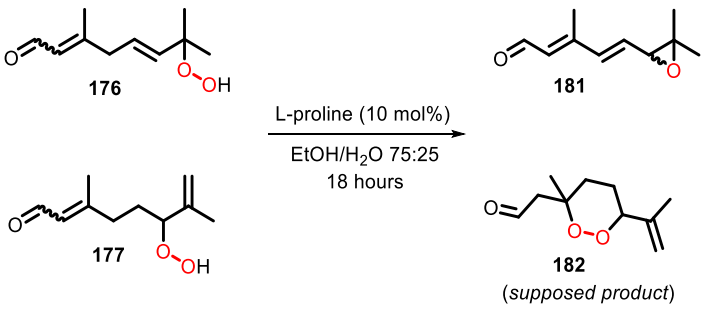




Scheme 90: Photo-oxygenation of citral 148 in the presence of L-proline.

Control experiments were performed to probe the nature of the proline-catalysed transformation. In the absence of light and/or photosensitiser, no conversion from citral **148** was observed by TLC, mass spectroscopy or ^{1}H-NMR, showing that the

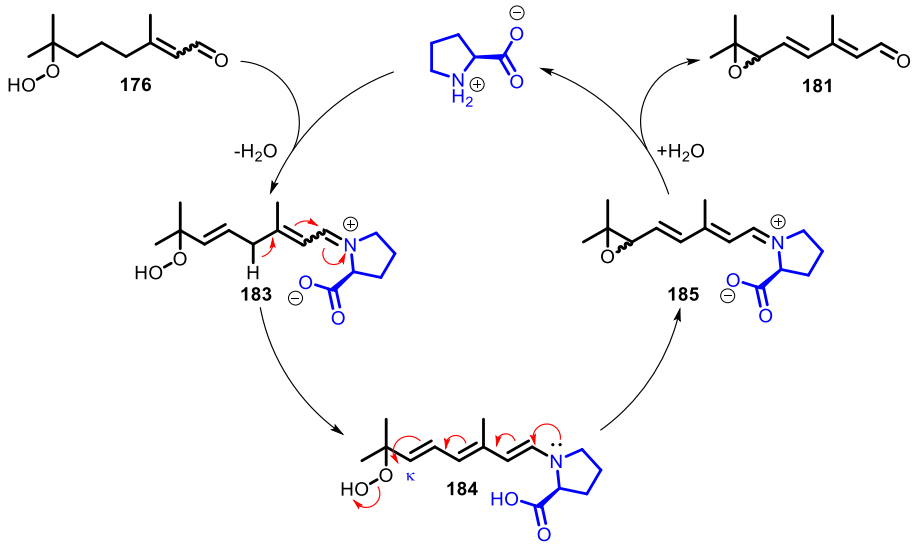
reaction was at least in part photochemical. Addition of L-proline to a pre-prepared solution of hydroperoxides **176** and **177** gave the same two products **181** and **182**, indicating a two-step transformation *via* an initial Schenck reaction of citral. Stirring with L-proline overnight gave full conversion to epoxide **181** and endoperoxide **182** (Scheme 91). Since the second step did not require light or oxygen gas, so it was proposed that **181** and **182** were forming *via* Schenck reaction of **148** to give hydroperoxides **176** and **177**, which then undergo proline-catalysed cyclisations – tertiary hydroperoxide **176** to epoxide **181** and secondary hydroperoxide **177** to the supposed endoperoxide **182**. Likely mechanisms for these cyclisations are discussed below.



Scheme 91: Treatment of hydroperoxides 176 and 177 with L-proline led to formation of epoxide 181 and hydroperoxide 182.

A proposed catalytic cycle leading to epoxide **181** is shown in Scheme 92. Condensation of L-proline onto hydroperoxide **176** is expected to give vinyliminium species **183**. This would be in tautomeric equilibrium with trienamine **184**. This equilibrium can be expected to greatly favour the trienamine side as this is the lower energy structure. This is supported by the fact that no addition products of water or ethanol to vinyliminium **183** were observed. Trienamine **184** would be nucleophilic at the κ-position and could attack the proximal hydroperoxide oxygen to eliminate hydroxide, closing the epoxide ring in a 3-*exo*-tet cyclisation and forming another iminium ion **185**. Hydrolysis of the iminium would provide the

product epoxide **181** and regenerate the proline catalyst. A similar homoallylic epoxidation was reported by Griesbeck *et al.* in 2009.[316]



Scheme 92: Proposed catalytic cycle for the proline-catalysed transformation of allylic hydroperoxide 176 to epoxide 181.

Proline is chiral, and is used frequently in asymmetric organocatalytic reactions. An asymmetric vinylogous epoxidation would potentially allow simple access to the glaciapyrrols and related natural products. No such methodology currently exists in the literature. Thus, to determine whether the chiral proline catalyst imparted any enantioselectivity to the formation of epoxide **181**, the reaction was repeated using racemic DL-proline. Since hydroperoxide **176** is achiral, any selectivity between enantiomers of the epoxide products must occur during the epoxide ring closure. A difference in enantioselectivity between reactions using L- or DL-proline would show an inductive effect from the catalyst. Samples of epoxide **181** isolated from reactions with chiral and racemic proline were analysed using chiral HPLC by Reach Separations Inc. The HPLC traces (UV detection) showed that two enantiomeric products did indeed form. Table 16 shows the retention times and peak areas for the two enantiomers for samples of **181** prepared using chiral L-proline and racemic DL-proline. The enantiomeric excess measured for the chiral catalyst was 1.6%. The racemic catalyst gave fully racemic product, as expected.

Catalyst	Retention Time / mins	Peak Area / %	Enantiomeric excess / %
L-proline	1.76	49.2	1.6
	2.10	50.8	
DL-proline	1.80	50.0	0
	2.15	50.0	

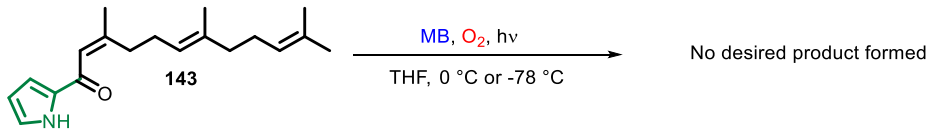
Table 16: The results of chiral separation of enantiomers of epoxide 181 by Reach separations. Where a chiral catalyst L-proline was used, only a slight enantioselectivity was seen.

Whilst disappointing, the lack of chiral induction by L-proline was unsurprising since the distance between the chiral centre and the reaction centre in the trienamine intermediate **184** is large compared to the chiral acid group on proline. It may be that a larger chiral amine catalyst could induce some enantioselectivity in this reaction, though this was not studied further.

Additionally, it was found that the epoxidation could be performed in the absence of an amine catalyst under basic conditions. Treatment of a solution of hydroperoxides **176** and **187** with 30% aqueous potassium hydroxide gave the same two products as the above reaction with proline in identical yield.

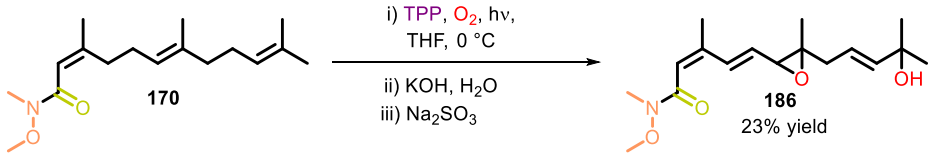
Section 4.4.2: Photo-oxygenation of Precursors to the Glaciapyrrols.

The photo-oxygenation of pyrrolosesquiterpene precursor **143** was performed at 0 °C in THF, using methylene blue (MB) as photosensitiser. After 2 hours of illumination, all of the starting material was consumed. Crude ^{1}H-NMR showed that under these conditions, the acylpyrrole moiety had reacted with singlet oxygen as well as the terpene backbone. None of the desired products could be isolated from the complex mixture. The reaction was repeated at -78 °C showing the same result. The sensitivity of pyrrole groups to photo-oxygenation was discussed in Section 1.2.5.



Scheme 93: Photo-oxygenation of pyrrolosesquiterpene precursor 143 leading only to degradation products.

Due to the instability of the pyrrole group of pyrrolosesquiterpene **143** to photo-oxygenation conditions, it was necessary to attempt installation of the oxygen-containing functionality at an earlier step. The photo-oxygenation of Weinreb amide **170** was performed in THF using TPP as photosensitiser, forming a mixture of hydroperoxide products. The reaction mixture was then treated with 30% aqueous potassium hydroxide to effect ring closure, then any remaining hydroperoxides were reduced with saturated aqueous sodium sulfite. Separation of the product mixture was attempted using column chromatography but only one compound was isolated. This was characterised as epoxide **186**, which is a precursor to the unnamed glaciapyrrol **127** and was received in 23% yield from the Weinreb amide.



Scheme 94: Photo-oxygenation of Weinreb amide 170 leading to a glaciapyrrol analogue.

The pyrrole coupling of epoxide under the conditions used previously to give glaciapyrrol **127** was attempted at a range of temperatures. Unfortunately, none of the reactions performed gave the desired product, instead showing no reaction at temperatures below -30 °C and a mixture of addition products at higher temperatures. This difference in reactivity compared to the unsubstituted Weinreb amide **170** could be down to the extra degree of conjugation in the former reducing the electrophilicity of the already poorly reactive amide carbon. Due to time

constraints, further coupling reactions were not attempted. Clearly a reworking of the applied strategy is necessary if the glaciapyrrol family of compounds are to be synthesised in this way.

Section 4.5: Chapter Summary.

Even though the work presented in this Chapter towards the synthesis of the glaciapyrrol family of natural products was ultimately unsuccessful, it has led to the development and application of some interesting methodology and highlighted some interesting points regarding the execution of a total synthesis in a sustainable manner.

Our original assumption that the glaciapyrrol family can be synthesised in a divergent way using singlet oxygen seems to be justified, as the model studies performed using citral as a substrate have shown that the allylic alcohol, tetrahydrofuran and epoxide moieties present in the glaciapyrrols can all be formed from the photo-oxygenation of terpenes as predicted.

The exact substitution pattern of one member of this family of compounds was installed in a one-pot reaction from Weinreb amide **170**, using only very simple and abundant reagents, and without the need for expensive metal catalysts or complex ligands.

The synthesis of the common pyrrolosesquiterpene precursor **143** has shown the application of several of the strategies for sustainable processes described in Section 1.1.3. Primarily among these is the multicomponent Pinnick-type amidation reaction that was used to form Weinreb amides **170** and **171**. By applying this reaction an entire step could be removed from the reaction sequence. It was shown that this reaction, reported previously for the formation of secondary amides in good yields, could be extended to the formation of tertiary amides using

a biphasic reaction system and keeping the concentration of the chlorite reagent low. An increase in yield from 20% under the initial screening conditions to greater than 95% was achieved.

The mass efficiency of the route was greatly improved by telescoping the reaction mixture through several steps without purification. The use of high yielding, biphasic reactions, both solid-liquid and liquid-liquid, allowed the three-step synthesis of **143** to be performed on a 3 g scale using only 250 mL of organic solvent.

Section 4.6: Future Directions.

The work described above towards the synthesis of the glaciapyrrol family of natural products has several loose ends. Principal among these is the fact the total synthesis is incomplete, although the general strategy seems to be valid. Two issues have been highlighted that must be overcome – the pyrrolosesquiterpene substrate **143** cannot be reacted with singlet oxygen without degrading the pyrrole moiety, and the oxygenated Weinreb amide **186** could not be coupled to pyrrole by the same method as used for the unsubstituted Weinreb amide **170**. Overcoming either of these obstacles would allow synthesis of the glaciapyrrols.

The sensitivity of the pyrrole moiety could potentially be overcome by modifying the electronics of the aromatic ring by adding an electron-donating or withdrawing *N*-substituent. Since singlet oxygen is generally considered to be an electrophilic reagent, the latter is a more reasonable line of investigation – reducing the nucleophilicity of the pyrrole double bonds may allow the alkene bonds of the terpene 'tail' to react preferentially. Alternatively, milder conditions for pyrrole coupling would need to be found that allow the terpene oxygenation and rearrangement to be performed first and the acyl-pyrrole bond formed afterwards.

In the course of the attempted synthesis of the glaciapyrrols, some interesting methodologies have been developed – the multicomponent amidation from aldehydes and the vinylogous epoxidation using singlet oxygen. Both of these methodologies could find synthetic use outside of this synthesis if the extent of the substrate scope were known, for example, the range of amines and aldehydes that can be used in the amidation reaction or the types of internal nucleophile that can effect the conjugate elimination of water from an allylic hydroperoxide. Lactone or lactam cyclisations would be an interesting starting point.

A considerable inefficiency in the synthesis of pyrrolosesquiterpene **143** is the fact that an equal amount of all-*trans*-isomer **142** is also formed. The yield of **143** could be doubled if a stereoselective way to form the compound could be found, or if **142** could be isomerised to **143** rather than discarded.

Finally, a question that should be addressed is whether the efficiency and scalability of the telescoped process for the synthesis of pyrrolosesquiterpene **143** could be further increased with the use of continuous flow chemistry, as was the case for the synthesis of artemisinin in Chapter 2. The high local concentration of solid reagents compared to substrate in a PFR may be beneficial to the MnO_2 oxidation of farnesol to farnesal, and might allow the required excess of reagent to be reduced. On the other hand, the amidation reaction with chlorite does not seem well suited to flow chemistry, as the slow addition of chlorite is not possible in a PFR-based rig. Potentially, a semi-batch process with continuous addition of chlorite and aldehyde to a stirred tank containing high concentrations of amine in phosphate buffer solution could be the way forward.

Chapter 5: Experimental Methods and Data

Section 5.1: General Experimental Information.

All reagents and solvents used in this Thesis were obtained from commercial suppliers and used without additional purification unless stated otherwise. Dihydroartemisinic acid used in Chapters 2 and 3 was kindly provided by Sanofi-Aventis in >95% purity and >99% enantiomeric excess.

Column chromatography was performed on slurry packed silica gel (pore size 60 angstroms, particle size 63 – 200 µm mesh) provided by Merck. Thin layer chromatography (TLC) was carried out on aluminium-backed plates pre-coated with silica (0.2 mm depth, 60 Å, F_{254}) also provided by Merck. Preparative TLC experiments were carried out using glass-backed plates pre-coated with silica (1.5 mm depth, 60 Å, F_{254}) supplied by Analtech.

^{1}H-NMR spectra for the purpose of characterisation were recorded at 300 MHz on a Bruker DPX300, at 400 MHz on a Bruker DPX400, Bruker AV400 or Bruker AV(III)400. ^{13}C-NMR spectra were recorded using the same instruments at a frequency ¼ of the ^{1}H resonance frequencies. All NMR Chemical shifts (δ) are reported in parts per million (ppm) relative to TMS using the residual solvent peak as an internal standard. All coupling constants (J) are reported in Hertz (Hz) and the multiplicity of each signal are designated by the following abbreviations: s = singlet, br = broad, d = doublet, t = triplet, dd = double doublet, m = intractable multiplet.

High resolution mass spectra were recorded on a Bruker TOF spectrometer using electrospray ionisation (EI) and are reported to four decimal places with error limits for acceptance of ±5.0 ppm.

Section 5.2: Experimental Methods and Data for Chapter 2.

Section 5.2.1: General Procedure for Batch Photo-oxygenation:

The following are the standard equipment and procedures for photo-oxygenations performed in batch in this Thesis, and are used throughout unless otherwise stated.

Equipment for Batch Photo-oxygenations

Batch photo-oxygenation experiments were performed in a standard two-necked borosilicate round bottomed flask with a water-cooled reflux condenser fitted to the upright neck. The flask was maintained at reaction temperature using either an oil bath/hotplate for elevated temperatures or an appropriate solvent based cooling bath for low temperatures. The reaction mixture was oxygenated by bubbling *via* a needle through a septum on the diagonal neck. Excess oxygen was released from the system *via* a second needle at the top of the condenser. Illumination of the reaction was performed using a fan cooled bank of five x 1000 lumen white light LEDs (Citizen Electronics Co. Ltd., part code: CL-L233-C13N1-C, each array consists of 36 diodes).

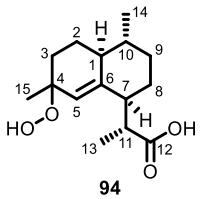
General Procedure for Batch Photo-oxygenations

1. Prepare the desired reaction mixture in a two-necked round bottomed flask with stirrer bar.
2. Fit the vertical neck with a reflux condenser and the diagonal neck and top of the condenser with Suba seals.
3. Pierce the seal at the top of the condenser with two short needles.
4. Attach a long needle to the O_2 line and insert into the reaction mixture through the seal on the diagonal neck, ensuring the tip of the needle sits at the bottom of the flask.

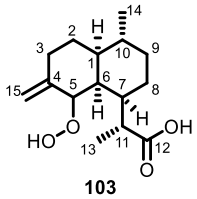
5. Flow water slowly through the condenser.
6. Gently open the O_2 regulator so that a slow, constant stream of bubbles flows through the reaction mixture. Allow the solution to saturate with O_2 for at least 5 minutes before commencing the reaction.
7. Clamp the LED unit close to the reaction mixture and loosely cover the reaction with aluminium foil.
8. Commence illumination by turning the LED unit to full.

Section 5.2.2: Studies on the Selectivity of the Schenk reaction of DHAA.

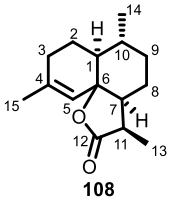
Synthesis of *(R)*-2-((*1S,4R,4aS,7R)*-7-hydroperoxy-4,7-dimethyl-1,2,3,4,4a,5,6,7-octahydronaphthalen-1-yl)propanoic acid (97) and *(R)*-2-((*1R,4R,4aS,8S,8aS)*-8-hydroperoxy-4-methyl-7-methylenedecahydronaphthalen-1-yl)propanoic acid (103) and *(3R,3aS,6R,6aS)*-3,6,9-trimethyl-3,3a,4,5,6,6a,7,8-octahydro-*2H*-naphtho[8a,1-b]furan-2-one (108):



94



103



108

Dihydroartemisinic acid **94** (250 mg, 1.06 x 10^{-3} mol) was dissolved in ethanol (20 mL). A solution of $Ru(bpy)_3Cl_2.6H_2O$ (1 mg, 1.34 x 10^{-6} mol) in deionised water (2 mL) was added. The mixture was reacted per the general photo-oxygenation procedure above, at 0 °C (ice/water bath). After 7 hours, analysis by TLC showed full depletion of the starting material, so illumination and oxygen bubbling were ceased. The mixture was concentrated under vacuum then diluted with brine (20 mL) and extracted with diethyl ether (3 x 30 mL). The combined ether fractions

were washed with brine (50 mL) and dried over $MgSO_4$. Removal of the solvent under vacuum gave a 9:1 mixture of tertiary hydroperoxide **97** and secondary hydroperoxide **103** which were not separated. Attempts to purify tertiary hydroperoxide **97** by column chromatography afforded mainly lactone **108** in addition to secondary hydroperoxide **103**. NMR resonances of tertiary hydroperoxide **103** reported below are taken from the crude mixture, and are consistent with the reported data.

Tertiary hydroperoxide 97:

^{1}H-NMR (400 MHz, $CDCl_3$): (from crude) δ = 5.25 (s, 1H, H5), 2.73 (dq, not resolved, 1H, H11), 1.31 (s, 3H, H15), 1.28 (d, J = 6.4 Hz, 3H, H13), 0.93 (m, 3H, H14) ppm. *In agreement with reported data.*

Selectivity studies on the Schenk photo-oxygenation of dihydroartemisinic acid (94) in water/ ethanol mixtures:

Dihydroartemisinic acid **94** (50 mg, 2.12 x 10^{-4} mol) was dissolved in an amount of ethanol given in Section 2.3.2, Table 3 (x mL). A solution of $Ru(bpy)_3Cl_2.6H_2O$ (1 mg, 1.34 x 10^{-6} mol) in deionised water ((10 – x) mL) was added and the reaction mixture was reacted per the general photo-oxygenation procedure above. After 1 hour, illumination and oxygen bubbling were ceased, then an aliquot (0.2 mL) was taken and removed of solvent under vacuum before re-dissolving in chloroform-*d* (0.5 mL) and analysis using ^{1}H-NMR.

Selectivities were calculated from the crude ^{1}H-NMR spectra using the integration values for characteristic peaks of compounds **97**, **103** and **108** given in Table 17:

Compound	δ ($CDCl_3$) / ppm
97	5.25
103	4.90
108	5.63

Table 17: Characteristic peaks used to quantify the selectivity of the Sckenck reaction of DHAA 94.

Since lactone **108** is known to form through acid-catalysed degradation of tertiary hydroperoxide **97**, its yield was also taken into account as shown below:

$$Selectivity\ (\mathbf{97}:\mathbf{103}) =$$

$$\frac{\mathrm{I}(\mathbf{97}) + \mathrm{I}(\mathbf{108})}{\mathrm{I}(\mathbf{97}) + \mathrm{I}(\mathbf{103}) + \mathrm{I}(\mathbf{108})} \times 100 \ : \ \frac{\mathrm{I}(\mathbf{103})}{\mathrm{I}(\mathbf{97}) + \mathrm{I}(\mathbf{103}) + \mathrm{I}(\mathbf{108})} \times 100$$

Study on the selectivity of the Schenk photo-oxygenation in ethanol/water 80:20 at full completion:

At 32 °C:

Dihydroartemisinic acid **94**, (50 mg, 2.12 x 10^{-4} mol) and biphenyl (3.2 mg, 2.12 x 10^{-5} mol) were dissolved in ethanol (8 mL). A solution of $Ru(bpy)_3Cl_2.6H_2O$ (1 mg, 1.34 x 10^{-6} mol) in deionised water (2 mL) was added and the mixture was sonicated until fully dissolved. The reaction mixture was reacted per the general photo-oxygenation procedure above, at 32 °C (water bath). The reaction was monitored by TLC until the dihydroartemisinic acid was consumed, then illumination and oxygen bubbling were ceased and an aliquot (0.2 mL) was taken. The aliquot was removed of solvent under vacuum and re-dissolved in acetone-d_6, then analysed using ^{1}H-NMR. Selectivities were calculated as above.

At -8 °C:

The reaction was performed as above with the exception that the temperature was maintained at -8 °C using a Stir-Kool electronic cooling unit.

Study on the selectivity of the Schenk photo-oxygenation in solvent mixtures containing HFIP:

Dihydroartemisinic acid **94** (50 mg, 2.12 x 10^{-4} mol), biphenyl (3.2 mg, 2.12 x 10^{-5} mol) and either $Ru(bpy)_3Cl_2.6H_2O$ or *meso*-tetraphenylporphyrin (1 mg) were dissolved in the appropriate solvent mixture (10 mL), as stated in Section 2.3.2., Table 5. The reaction mixture was reacted per the general photo-

oxygenation procedure above, at 30 °C (water bath). Aliquots were taken every 20 minutes and analysed by ^{1}H-NMR in chloroform-*d*. When dihydroartemisinic acid **94** was entirely consumed, illumination and oxygen bubbling were ceased and another aliquot was taken, removed of solvent under vacuum and analysed by ^{1}H-NMR in acetone-d_6. Selectivities were calculated as above.

Singlet oxygen fluorescence lifetime measurements:

(Performed by Dr Raphael Horvath)

Fluorescence lifetime measurements on singlet oxygen were carried out in air-equilibrated solutions of $Ru(bpy)_3Cl_2.6H_2O$ and varying amounts of dihydroartemisinic acid **94** in dichloromethane, ethanol and ethanol/water 50:50. Concentration of photosensitizer was adjusted to give an absorbance of 0.3 at the excitation wavelength.

The samples in a quartz cuvette were irradiated using a 355 nm laser pulse (GCR150-10, 10 Hz, approx. 1 mJ per pulse). Emission at 1270 nm was recorded at a 90° angle after a delay time t. The recorded wavelength was selected with a monochromator (TRIAX-320) and measured with a NIR-PMT (Hamamatsu H10330A-45) controlled by LabVIEW. The intensity of emission was plotted against the delay time t and fitted to a monoexponential decay (approx. 10000 shots per decay). The lifetimes τ extracted from the exponential fits were plotted against concentration of dihydroartemisinic acid **94** to determine the rate constant for substrate quenching k_q according to the Stern-Volmer equation:

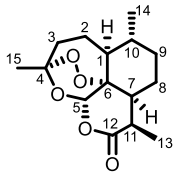
$$\frac{1}{\tau} = k_q[\mathbf{94}] + \frac{1}{\tau_0}$$

Where τ_0 is the lifetime in the absence of substrate **94**.

The quenching constant k_q was assumed to be equivalent to the rate constant for photo-oxygenation.

Section 5.2.3: Studies on the One-pot Batch Synthesis of Artemisinin in Aqueous Solvent Mixtures.

One-pot synthesis of artemisinin (76) from dihydroartemisinic acid (94) in THF:



76

Dihydroartemisinic acid **94** (250 mg, 1.06 x 10^{-3} mol) and *meso*-tetraphenylporphirin (1 mg, 1.63 x 10^{-6} mol) were dissolved in THF (20 mL). The solution was cooled to -20 °C and bubbled with oxygen gas for 10 minutes. Trifluoroacetic acid (40 μL, 5.28 x 10^{-4} mol) was added and the reaction mixture was reacted per the general photo-oxygenation procedure above, at -20 °C (ice/acetone bath). After 3 hours, analysis by TLC showed full depletion of the starting material, so illumination was ceased. The mixture was stirred for a further 4 hours at room temperature with continued oxygen bubbling.

Solvent was removed under vacuum, and the crude mixture was purified by column chromatography (silica gel, cyclohexane/ ethyl acetate 90:10 as eluent) to give a white crystalline solid which was identical by ^{1}H- and ^{13}C- NMR to commercially sourced artemisinin **76** (179 mg, 60% yield):

^{1}H-NMR (400 MHz, $CDCl_3$): δ = 5.87 (s, 1H, H5), 3.41 (dq, *J*= 7.3, 5.4 Hz, 1H, H11), 2.48 to 2.40 (m, 1H, H3), 2.09 to 1.97 (m, 2H, H2/H3), 1.93 to 1.86 (m, 1H, H8), 1.81 to 1.74 (m, 2H, H7/H9), 1.53 to 1.35 (m, 2H, H2/H10), 1.45 (s, 3H, H15), 1.21 (d, *J* = 7.3 Hz, 3H, H13), 1.12 to 1.04 (m, 2H, H8/H9), 1.00 (d, *J*= 5.9 Hz, 3H, H14) ppm.

^{13}C-NMR (100 MHz, $CDCl_3$): δ = 172.0 (C12), 105.4 (C4), 93.5 (C5), 79.9 (C6), 49.9 (C1), 44.8 (C7), 37.4 (C10), 35.8 (C3), 33.6 (C9), 33.0 (C11), 25.3 (C15), 24.8 (C2), 23.4 (C8), 19.8 (C14), 12.5 (C13) ppm.

HRMS (ESI+) $[M+Na]^+$: Expected M/Z = 305.1359, Measured M/Z = 305.1351.

Procedure for process optimisation of the one-pot batch synthesis of artemisinin (76) in aqueous solvent mixtures:

A solution was prepared containing DHAA **94**, photosensitiser, acid and biphenyl as internal standard in an aqueous solvent mixture, according to the conditions given in Section 2.3.3., Table 6. The mixture was reacted as per the general photo-oxygenation procedure above. When TLC showed all starting material to be consumed, illumination was ceased (approx. 7 hours). Stirring and oxygen bubbling was continued for a further 2 days or until the yield of artemisinin was no longer increasing. Yields were measured from the crude ^{1}H-NMR spectra by integration against the biphenyl internal standard.

Scaled up batch synthesis of artemisinin (76) with catalyst and solvent recycling:

(Performed by Dr Zacharias Amara)

First Pass:

DHAA **94** (1.0 g, 4.24 x 10^{-3} mol) was dissolved in ethanol (120 mL) in a 3-necked round bottomed flask fitted with thermometer and reflux condenser. A solution of $Ru(bpy)_3Cl_2.6H_2O$ (10 mg, 1.34 x 10^{-5} mol) in deionised water (80 mL) was added and the resulting solution was cooled to 0 °C. H_2SO_4 (98%, 112 μL, 2.12 x 10^{-3} mol) was added dropwise and the mixture was bubbled with oxygen gas for 10 minutes. The reaction was illuminated with white LED light and bubbled with oxygen gas for 9 hours, at which point ^{1}H-NMR showed full consumption of the starting material. Illumination was ceased and the mixture was bubbled with oxygen gas at room temperature for a further 24 hours.

The mixture was concentrated under vacuum until a white precipitate formed, then allowed to stand at room temperature overnight. White crystalline needles of

artemisinin **76** formed and were collected by filtration. Further concentration and crystallisation yielded a total of 450 mg **76**.

Second Pass:

The mother liquor from the first pass (120 mL) was diluted with a mixture of fresh and recycled ethanol (180 mL). DHAA **94** (1.5 g, 6.36 x 10^{-3} mol) was added and the reaction mixture was oxygenated and illuminated with white LED light at 0 °C as before. After 10 hours illumination and a further 25 hours bubbling at room temperature, fractional crystallisation was performed as before to yield a further 690 mg artemisinin **76**.

Third Pass:

The mother liquor from the previous experiment (175 mL) was again diluted with fresh and recycled ethanol (263 mL). DHAA **94** (2.2 g, 9.33 x 10^{-3} mol) was added and the reaction mixture was oxygenated and illuminated with white LED light for 17 hours at 0 °C. The reaction was stirred at room temperature with oxygen bubbling for a further 31 hours. Fractional crystallisation as above yielded a further 954 mg artemisinin **76**.

^{1}H-NMR (400 MHz, $CDCl_3$): as reported above.

^{13}C-NMR (100 MHz, $CDCl_3$): as reported above.

X-ray Crystallography Data: Single crystals of $C_{15}H_{22}O_5$ artemisinin were taken directly from the reaction vessel. A suitable crystal was selected and mounted in fomblin film on a micromount on a GV1000, Atlas diffractometer. The crystal was kept at 120(2)K during data collection. Using Olex2,43 the structure was solved with the olex2.solve structure solution program using Charge Flipping and refined with the ShelXL44 refinement package using Least Squares minimization.

Crystal Parameters (M = 282.32): orthorhombic, space group $P2_12_12_1$ (no. 19), a = 6.32081(9) Å, b = 9.31057(18) Å, c = 23.9696(4) Å, V = 1410.62(4) Å^3, Z = 4,

T = 120(2) K, μ(CuKα) = 0.817 mm^{-1}, D_{calc} = 1.329 g/mm^3, 35814 reflections measured (7.376 ≤ 2Θ ≤ 152.53), 2925 unique (R_{int} = 0.0317, R_{sigma} = 0.0119) which were used in all calculations. The final R_1 was 0.0252 (I > 2σ(I)) and wR_2 was 0.0668 (all data). Absolute structure parameter - 0.01(3).

Melting Point: 155-156 °C. (Commercial: 158-159 °C).

$[\alpha]_D$: +66.7° (c = 1, $CHCl_3$). (Commercial: +66.8° (c = 1, $CHCl_3$).

Isolation of highly polar oligomeric side product:

Column chromatography of the mother liquor of the recycling experiment (silica gel, cyclohexane/ ethyl acetate 90:10 → 40:60 as eluent) afforded no further artemisinin from the crude material. On washing the column with EtOH, a highly polar oligomeric material was recovered which was analysed using MALDI spectrometry.

MALDI-TOF $[M+H]^+$: M/Z = 1213

Section 5.2.4: Studies on the Continuous Flow Production of Artemisinin in Aqueous Solvent Mixtures.

Equipment and Standard Procedure for Continuous Flow Photo-oxygenation:

The following is a description of the continuous flow rig and operating procedure used for the experiments described in Section 2.3.4.

Equipment for Continuous Flow Photo-oxygenation

The reactor system for continuous flow photo-oxygenations was built around a sapphire tube photoreactor, designed previously within the group for use with supercritical carbon dioxide. Sapphire was chosen as the window material because of its high pressure tolerance and transparency to visible light. The sapphire tube itself (Saint-Gobain Crystals, 10 mm outer diameter, 1 mm wall thickness, 12.0 cm

length) is housed in a metal frame and held in place at either end with an O-ring (ethylene-propylene diene monomer, EPDM) to provide a pressure seal. Around the tube is a Lexan sheath (18 mm outer diameter, 2 mm wall thickness, 9.5 cm length) with an approximately 2 mm gap between the sapphire and Lexan tubes. Coolant can be flowed through the gap from a recirculating cooling bath to maintain the reactor at a desired temperature. The internal reactor temperature is monitored using a K-type thermocouple attached to the outlet of the reactor. The inside of the sapphire tube is filled with glass beads to reduce the optical path length of the solution, maximising light penetration, and to ensure good mixing within the reactor.

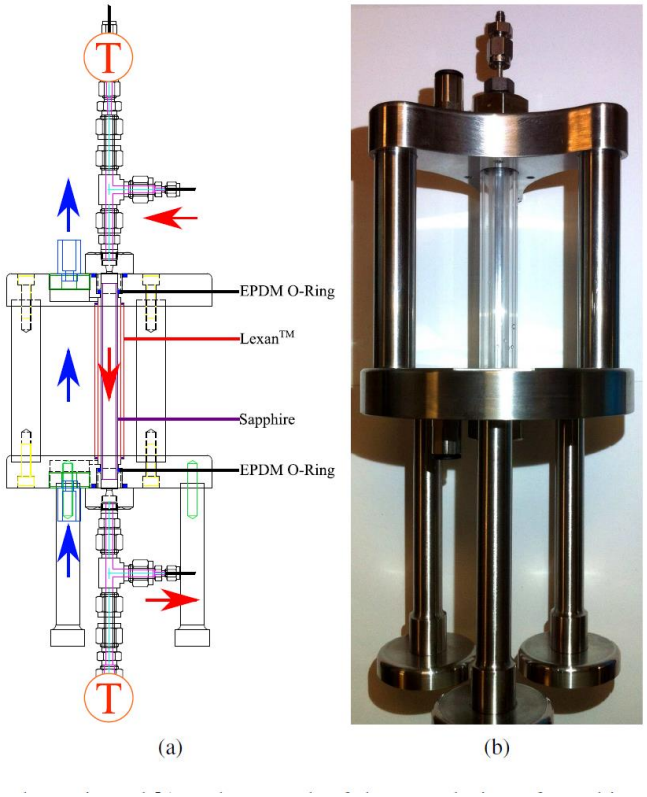


Figure 33: The sapphire tube photoreactor as: a) cross-sectional schematic showing the construction of the reactor and b) photograph showing the sapphire tube inside the Lexan cooling sheath and stainless steel frame.

The metal frame of the sapphire tube reactor can hold three inward-facing banks of five x 1000 lumen white light LEDs (Citizen Electronics Co. Ltd., part code:

CL-L233-C13N1-C, each array consists of 36 diodes). The three banks of LEDs are controlled from a single variable power supply.

Oxygen gas is added to the rig using a modified Rheodyne 70 series 2-position 6-port switching valve configured as a dosing unit. By using a switching valve rather than directly feeding O_2 from a gas cylinder we control the precise amount of oxygen gas entering the rig. In the event of an accident, power to the switching valve can be cut, immediately isolating the oxygen cylinder from the reactor The Rheodyne unit is configured as shown in Figure 34, in such a way that the two sample loops empty and fill alternatingly, giving a very even flow of gas into the rig:

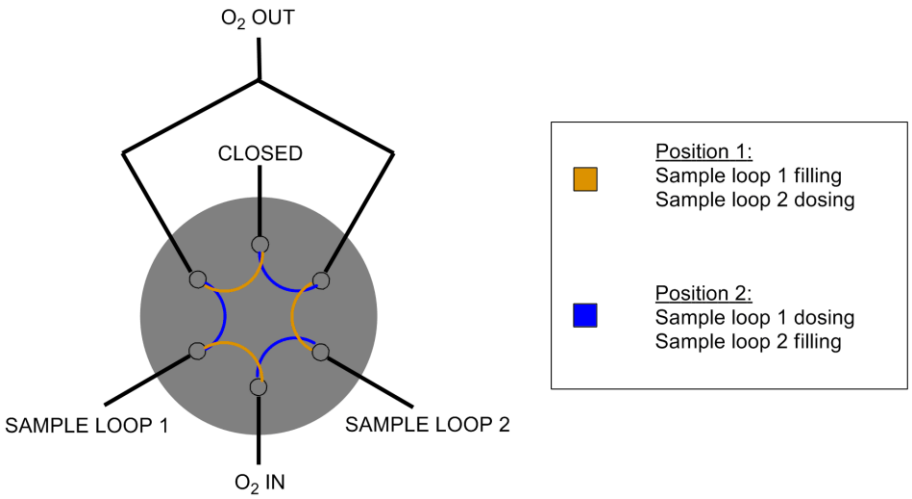


Figure 34: The Rheodyne 70 series 2-position 6-port switching valve, configured for oxygen gas dosing as used in this experiment. In either position, one sample loop is filling from the cylinder whilst the other doses into the system.

The amount of O_2 can be controlled by varying the following parameters:

- Cylinder O_2 pressure, p_c,
- Sample loop volume, V, and
- Rheodyne switching time, t_R.

With the rate of addition of O_2 varying as shown:

$$v_{O_2} \propto \frac{p_c V}{t_R}$$

Thus, the amount of O_2 entering the rig per unit time can be increased by either increasing the cylinder pressure, increasing the sample loop volume or decreasing the switching time. The latter is preferred since transferring a large quantity of O_2 ($q_{O2} = p_c V$) with a long switching time causes an uneven pulsed flow of O_2. This causes pressure spikes and can reduce the homogeneity of the reactor. Conversely, there is a low limit to switching time at higher q_{O2} as t_R must be long enough to allow the gas to fully discharge from the sample loops. For the sake of safety and reliability of the reaction it is important to have the smallest amount of O_2 whilst still being above the solubility limit in the solvent used.

The rig is configured as shown in Figure 35. Reagents are added to the rig in solution using a Jasco PU-980 dual-piston HPLC pump. The solution is combined with the O_2 stream dosed *via* Rheodyne as described above, and passed through a static mixer to ensure saturation before being introduced to the sapphire tube photoreactor from the bottom and illuminated. After illumination the reaction mixture exits the reactor and passes through a Jasco BP-1580-81 back pressure regulator which allows raised pressures inside the reactor whilst still allowing continuous transfer of material through the rig. All tubing is 1/16" outer diameter 316 stainless steel and is connected using 316 stainless steel fittings procured from Swagelok.

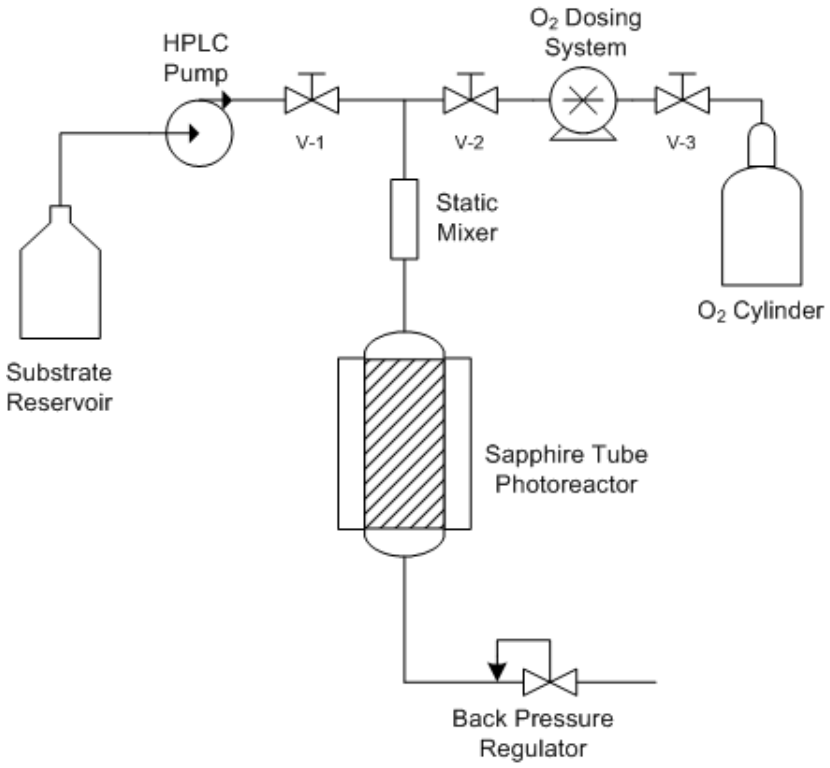


Figure 35: The continuous flow rig used for the synthesis of artemisinin.

Standard Operating Procedure

1. Set the system high pressure, O_2 low pressure, and temperature trips to the appropriate levels. The O_2 low pressure trip should be set 10 bar above the desired reaction pressure. The system and HPLC pump high pressure trips should be set 10 bar above the O_2 low pressure trip. The high temperature trips should be set to 10 °C above the desired reaction temperature. All trips should be below the maximum pressure and temperature ratings for the rig.
2. Attach the appropriate sample loops to the Rheodyne O_2 dosing unit.
3. Set the BPR to the desired reaction pressure.
4. Prime the HPLC pump with reaction solvent and begin pumping at 5 mL min^{-1}. Open valve V1 to allow solvent to enter the rig.
5. Start the reactor cooling bath. Adjust the temperature control so that the reactor is at the desired temperature.

6. Open valve V3 and turn on the Rheodyne dosing unit. Gently open valve V2 to allow oxygen gas to enter the rig. Adjust the switching time so that a continuous stream of small bubbles flows through the photoreactor.
7. Set the pump to the experiments initial flow rate. Replace the feed with the reaction mixture.
8. Turn the LED power supply to full. Adjust the level of the recirculating cooling bath if necessary.
9. The rig is now under starting conditions.

Calculations of productivity:

Productivities in grams of artemisinin per day were calculated for several of the higher-yielding conditions from the continuous flow synthesis of artemisinin described above. The productivity for a set of conditions was expressed as a function of concentration, flow rate and yield, as described below:

$$Productivity = Flow\ rate \times Concentration \times Yield \times M_r(Artemisinin)$$

Table 18 shows the calculations in full. Conditions can be found in Section 2.3.4., Table 10:

Entry	Adjusted yield[a] / %	Flow rate / $dm^3\ day^{-1}$	Concentration / $mol\ dm^{-3}$	Productivity / $mol\ day^{-1}$	Productivity / $g\ day^{-1}$
1	37	0.72	0.02	0.005328	1.502496
2	27	1.44	0.02	0.007776	2.192832
3	29	0.36	0.02	0.002088	0.588816
4	21	0.72	0.04	0.006048	1.705536
5	45	1.44	0.02	0.01296	3.65472
6	38	0.18	0.21	0.014364	4.050648
7	36	0.36	0.21	0.027216	7.674912

Table 18: Calculations of productivity for the continuous flow synthesis of artemsinin 76. [a]The yield of artemisinin for each individual continuous flow experiment was calculated at the lowest flow rate assessed. Where the flow rate for which the rig productivity has been calculated is higher, yields have been adjusted to account for any lower conversion observed. Flow rates and conversions are given in Section 2.3.4., Table 10.

Calculations of Process Mass Intensity:

Assessment of the waste generated by selected batch and flow processes for the synthesis of artemisinin from throughout Chapter 3 was carried out by calculating the Process Mass Intensities (PMI) as the total mass of material used divided by the mass of artemisinin produced:

$$PMI = \frac{Mass\ of\ material\ consumed}{Mass\ of\ product\ produced}$$

	Process				
	A	**B**	**C**	**D**	**Sanofi[249]**
Regime	Batch	Batch	Batch	Flow	Semi-Batch
DHAA (mol)	1.06×10^{-3}	1.06×10^{-3}	1.99×10^{-2}	7.56×10^{-2}	-
DHAA (g)	0.25053	0.25053	4.71046	17.8681	6×10^{5}
EtOH (mL)	0	30	273	0	-
EtOH (g)	0	23.679	215.479	0	-
THF (mL)	12	2	0	216	-
THF (g)	10.704	1.784	0	192.024	-
water[a] (g)	8	8	215	144	-
acid (mol)	5.3×10^{-4}	5.3×10^{-4}	0.00212	0.0378	-
acid (g)	6.04×10^{-4}	6.04×10^{-4}	0.20793	3.70739	-
photosensitiser (mol)	1×10^{-6}	1×10^{-6}	0.000013	0.00038	-
photosensitiser (g)	7.5×10^{-4}	7.5×10^{-4}	0.00973	0.24212	-
yield (%)	66	62	37	36	54
artemisinin (mol)	0.0006996	0.0006572	0.0073741	0.0272	-
artemisinin (g)	0.19729	0.18533	2.0795	7.6704	370000
total mass (g)	11.0157	25.7747	220.407	213.842	8568300
PMI	**55.8359**	**139.074**	**105.991**	**27.8788**	**23.1576**

Table 19: Calculations of process mass intensity. The total mass used to calculate the PMI for the Sanofi process is taken from reference 249.

Section 5.3: Experimental Methods and Data for Chapter 3.

Procedure for the trapping of enol intermediate *(R)*-2-((*1S,3S,4R,E*)-2-(hydroxymethylene)-4-methyl-3-(3-oxobutyl)cyclohexyl)propanoic acid (98):

DHAA **94** (500 mg, 2.12 x 10^{-3} mol), biphenyl (32.7 mg, 2.12 x 10^{-4} mol) and TPP (2.0 mg, 3.25 x 10^{-6} mol) were dissolved in THF (25 mL). TFA (0.08 mL, 1.05 x 10^{-3} mol) was added and the green mixture was reacted per the photo-oxygenation general procedure given in Section 5.2.1, at -45 °C. After 2.5 hours, O_2 bubbling and illumination were ceased and the mixture was frozen using liquid nitrogen. The O_2 atmosphere was replaced with argon using the freeze-pump-thaw method (3 cycles) and the mixture was allowed to warm to room temperature. Integration of the C5 resonance in the ^{1}H-NMR spectrum of the crude mixture showed the enol intermediate **98** to be present in 47% yield.

^{1}H-NMR (300 MHz, C_6D_6): δ = 5.8 (d, *J* = 1.3 Hz, 1H, H5) ppm.

Procedure for static-mode NMR monitoring of the synthesis of artemisinin (76):

In a Young tap NMR tube, DHAA **94** (5.0 mg, 2.12 x 10^{-5} mol) and biphenyl (3.3 mg, 2.12 x 10^{-}) were dissolved in THF-d_8 (0.6 mL). To this was added 0.4 mL of a solution of $Ru(bpy)_3Cl_2.6H_2O$ (1.5 mg, 2.12 x 10^{-7} mol) and TFA-*d* (0.81 mL, 1.05 x 10^{-5} mol) in D_2O (4.0 mL). The reaction mixture was bubbled with O_2 gas and illuminated with white LED light at 0 °C. After 1 hour, 2.5 hours and 4 hours illumination, the NMR tube was sealed and a ^{1}H-NMR spectrum was ran using a Bruker (iii)400 MHz NMR spectrometer. After 4 hours, all the DHAA **94** was consumed. The reaction mixture was then analysed by ^{1}H-NMR every hour with intermittent O_2 bubbling. Yields of species present were measured by comparison of the integration values of the characteristic peaks shown in Table 20 to the internal standard biphenyl.

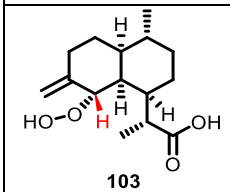
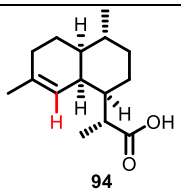
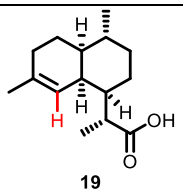
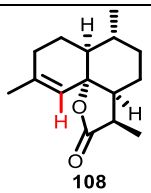
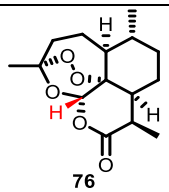
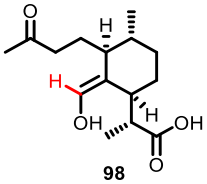
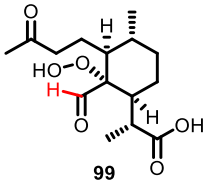
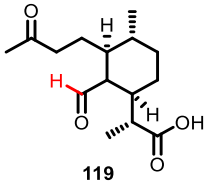
δ = 5.00 ppm	δ = 5.08 ppm	δ = 5.25 ppm	δ = 5.66 ppm
 103	 94	 19	 108
δ = 5.89 ppm	**δ = 6.34 ppm**	**δ = 9.78 ppm[a]**	**δ = 9.99 ppm[a]**
 76	 98	 99	 119

Table 20: Chemical shifts of the characteristic ^{1}H-NMR resonances used to follow various species present in the synthesis of artemisinin 76. Chemical shift values for the protons shown in red are given in THF-*d*$_8$/D$_2$O 60:40. [a]structure assigned later by DFT calculation of ^{13}C-NMR chemical shifts – see below.

'Batch-type' Reactor System for Continuous NMR Monitoring Experiments.

The following is a description of the equipment and procedures for the initial 'batch-type' monitoring experiment described in Section 3.3.3.

Equipment

Initial continuous monitoring experiments were carried out using a recirculating reactor based on the batch photo-oxygenation apparatus described above. The reaction mixture was stirred in a 5 mL test tube which was held in an ice/water/acetone bath at approximately 0 °C (internal temperature measured using a K-type thermocouple). The reaction mixture was drawn from the test tube using a Gilson 306 single-piston HPLC pump (5 mL pump head) and fed into the Bruker InsightMR apparatus contained inside a Bruker 800 MHz NMR spectrometer. The outlet of the InsightMR was fed back into the test tube. The reaction mixture was saturated with oxygen gas at atmospheric pressure by bubbling *via* needle directly from an oxygen cylinder. The test tube was illuminated with white light using a fan-cooled bank of five x 1000 lumen white light LEDs (Citizen Electronics Co. Ltd., part code: CL-L233-C13N1-C, each array

consists of 36 diodes). All tubing is 1/16" outer diameter PTFE and is connected using either 316 stainless steel fittings procured from Swagelok or polyether ether ketone (PEEK) fittings procured from Upchurch Scientific.

Standard Operating Procedure

1. Prepare the reaction solution in the test tube and cool to 0 °C.
2. Prime the HPLC pump by syringe and begin pumping at 3 mL min^{-1}.
3. When the solution begins to circulate back into the test tube, run solvent lock and automatic shim programs on the spectrometer.

'Flow-type' Reactor System for Continuous NMR Monitoring Experiments.

The following is a description of the equipment and procedures for the 'flow-type' monitoring experiment described in Section 3.3.3.

Equipment

The 'flow-type' NMR monitoring rig contains a sapphire tube photoreactor identical to the one described above. O_2 is dosed into the rig through a non-return valve. A small vial acts as a vent for excess O_2 and a reservoir for reaction mixture. The reaction mixture is drawn from the airlock/reservoir using a Gilson 306 single-piston HPLC pump (5 mL pump head) and fed into the Bruker InsightMR apparatus contained inside a Bruker 800 MHz NMR spectrometer The outlet of the InsightMR apparatus was connected to the bottom of the sapphire tube reactor, where it was mixed with the incoming O_2 stream and illuminated with three banks of five x 1000 lumen white light LEDs. On exiting the photoreactor the reaction mixture is fed back into the reservoir.

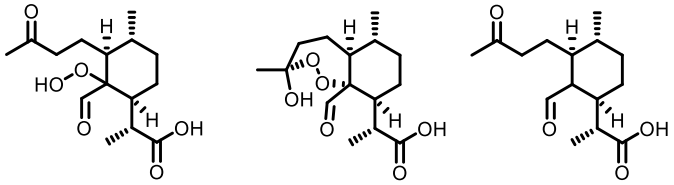
All tubing is 1/16" outer diameter PTFE and is connected using either 316 stainless steel fittings procured from Swagelok or polyether ether ketone (PEEK) fittings procured from Upchurch Scientific.

Standard Operating Procedure

1. Prepare the reaction solution and feed into the sapphire tube reactor from below until the reservoir is full.
2. Prime the HPLC pump by syringe and begin pumping at 3 mL min^{-1}.
3. When the solution begins to circulate back into the reservoir, run solvent lock and automatic shim programs on the spectrometer.
4. Gently open the O_2 regulator so that a slow, constant stream of bubbles flows through the reaction mixture. Allow the solution to saturate with O_2 for at least 5 minutes.
5. Begin acquiring one-dimensional ^{1}H-NMR spectra (1D).
6. Commence illumination by turning the LED unit to full.
7. At full conversion from the starting material, begin acquiring the following sequence of spectra: 1D (64 scans), HSQC (1024 scans), HMBC (4096 scans), repeat.

Prediction of ^{13}C-NMR chemical shifts using density functional theory:

(performed by Dr Magnus Hanson-Heine)



The ^{13}C NMR shifts of known aldehyde **119**, peroxyl aldehyde **99** and the open ring endoperoxide aldehyde **113** have been calculated at the EDF2/6-31G(d) level theory. Aldehyde **119** has already been characterized and simulated and is here as a fully assigned control. A large number of conformations are likely to be accessible at experimental timescales due to the conformational flexibility of the molecules.

These results support the assignment of the hydro-peroxyl aldehyde **99** at as the species observed in the monitoring experiments at 9.78 ppm and denoted aldehyde **A**. The calculation chemical shifts were in excellent agreement with those determined experimentally in the 2D-NMR spectra.

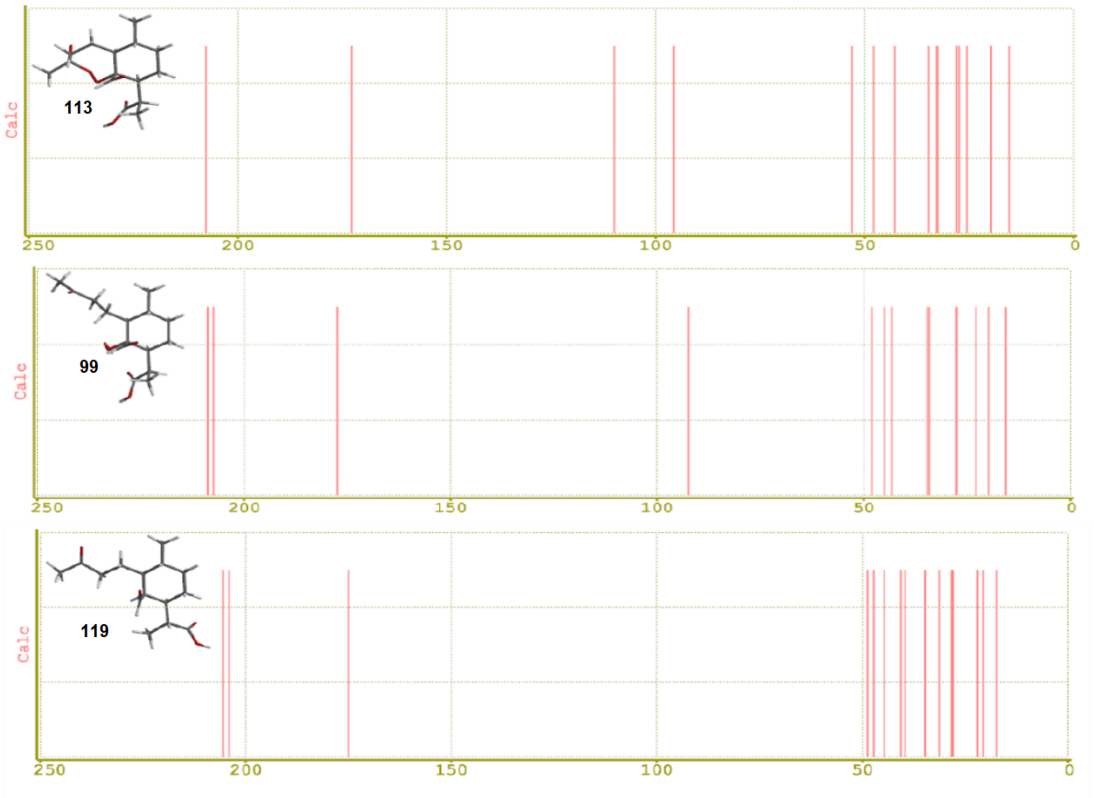


Figure 36: Simulated ^{13}C-NMR spectra for aldehydes 99, 113 and 119, used to assign the species seen in monitoring experiments.

Full chemical shifts and assignments are given in Table 21 on the next page.

	Aldehyde A	119			99	113
Atom	δC exp. (ppm)	δC calc. (ppm)	δC calc. lit. (ppm)	Δ δC (ppm)[d]	δC calc. (ppm)	δC calc. (ppm)
1	59.1	48.9	46.1	-2.8	49.6	49.5
2		23.3	24.4	-26	24.2	26.9
3		40.7	41	0.3	44.3	34.0
4		194.3	208.6	14.4	195.9	107.7
5		193.2	206.1	12.9	198.7	197.4
6	93.4	50.4	49.9	-0.46	92.3	95.4
7		46.3	43.1	-3.2	46.6	54.6
8		29.6	27.3	-2.3	28.8	28.7
9		36.0	35.5	-0.5	35.8	35.9
10		33.2	33.4	0.2	35.9	34.3
11		42.4	42.9	0.5	44.9	44.5
12		165.6	181	15.4	168.7	163.4
13		18.1	15.1	-3	16.5	16.3
14		21.4	20.2	-1.2	20.6	20.6
15		28.7	29.7	0.99	28.3	28.7

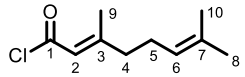
Table 21: Computation simulations of ^{13}C-NMR spectra. [a]experimentally determined chemical shifts for aldehyde A. [b]calculated chemical shifts. [c]chemical shifts from a simulation performed by Brown *et al.*[317] [d]Δ δc= (δc Cal. Lit. - δc cal.).

Section 5.4: Experimental Methods and Data for Chapter 4

Representative procedure for acid-catalysed reactions of citral with pyrrole:

To a solution of citral, as mixed *cis*- and *trans*- isomers (0.34 mL, 1 x 10^{-3} mol) in dichloromethane (6 mL) was added freshly distilled pyrrole (0.07 mL, 1 x 10^{-3} mol). TFA (0.08 mL, 6 x 10^{-4} mol) was added and the reaction rapidly turned a dark brown colour. After 30 seconds, the reaction was quenched by addition of saturate aqueous $NaHCO_3$ (2 mL), washed with brine (2 mL) and the organic phase removed of solvent to give a brown tar-like substance. This could not be purified by column chromatography, but HRMS indicated the formation of a dipyrromethane or related substance. For other conditions screened, see Section 4.3.1., Table 12.

Formation of *(E)*-3,7-dimethylocta-2,6-dienoyl chloride (155):



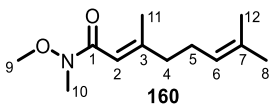
155

Geranic acid (1.04 mL, 6 x 10^{-3} mol) was dissolved in dry tetrahydrofuran (20 mL) and cooled to -15 °C in an ice/acetone bath. Oxalyl chloride (0.52 mL, 6 x 10^{-3} mol) was added followed by dry *N,N*-dimethylformamide (1.5 µL, 2 x 10^{-5} mol), causing slow effervescence. When effervescence halted after approximately 30 minutes, the reaction mixture was allowed to warm to 0 °C in an ice/water bath and stirred for a further 2 hours. The colourless solution gradually turned yellow over the course of the reaction. This yellow solution was used directly in further coupling reactions.

General procedure for reactions of pyrrole with activated carbonyl compounds:

Either the solution of geranyl chloride **155** in tetrahydrofuran prepared as above (5 mL, 1.5 x 10^{-3} mol) or a solution of methyl geranate (0.286 mL, 1.5 x 10^{-3} mol) in tetrahydrofuran (5 mL) was brought to the desired reaction temperature as stated in Section 4.3.2., Table 13. Freshly distilled pyrrole (0.11 mL, 1.65 x 10^{-3} mol) was added dropwise by syringe. Where stated in Table 13, ZnO (61 mg, 7.5 x 10^{-4} mol) was added to catalyse the addition. The reaction mixture was stirred for 2 hours, then brought to room temperature and removed of solvent and excess pyrrole under vacuum. None of the conditions screened gave the desired product.

Synthesis of *(E)*-*N*-methoxy-*N*,3,7-trimethylocta-2,6-dienamide (160):



160

N,N'-dicyclohexylcarbodiimide (2.27 g, 1.1 x 10^{-2} mol) and geranic acid (85% with neric acid, 1.73 mL, 1 x 10^{-2} mol) were dissolved in dichloromethane (30 mL). To

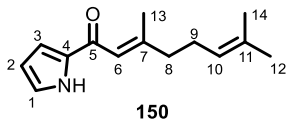
this was added a solution of *N,O*-dimethylhydroxylamine hydrochloride (1.07 g, 1.1 x 10^{-2} mol) and *N*-methylpyrrolidine (2.29 mL, 2.2 x 10^{-2} mol) in dichloromethane (30 mL), followed by a solution of 4-(*N,N*-dimethylamino)pyridine (122 mg, 1 x 10^{-3} mol) in dichloromethane (20 mL). The mixture was stirred at room temperature overnight. The reaction mixture was washed with 1M aqueous HCl (30 mL), water (2 x 20 mL) then brine (20 mL) and the organic phase was dried over $MgSO_4$ and removed of solvent under vacuum to give a crude yellow oil. The crude oil was purified using column chromatography on silica (cyclohexane/ ethyl acetate 90:10 → 80:20 as eluent) to give *(E)*-*N*-methoxy-*N*,3,7-trimethylocta-2,6-dienamide **160** as a pale yellow oil (1.49 g, 83% yield).

^{1}H-NMR (500 MHz, $CDCl_3$): δ = 6.11 (s, 1H, H2), 5.17 (tt, *J* = 7.1, 1.3 Hz, 1H, H6) 3.68 (s, 3H, H9), 3.21 (s, 3H, H10), 2.61 (t, *J* = 8.0 Hz, 2H, H4), 2.19 (dt, *J* = 8.0, 7.2 Hz, 2H, H5), 1.91 (d, *J* = 1.3 Hz, 3H, H11), 1.68 (s, 3H, H8/12), 1.63 (s, 3H, H8/12) ppm.

^{13}C-NMR (100 MHz, $CDCl_3$): δ = 167.8 (C1), 156.7 (C3), 131.8 (C7), 124.0 (C6), 114.6 (C2), 61.3 (C9), 33.5 (C4), 31.9 (C10), 26.9 (C5), 25.7 (C11), 25.4 (C8/12), 17.7 (C8/12) ppm.

HRMS (ESI+) $[M+Na]^+$: Expected M/Z = 234.1464, Measured M/Z = 234.1469.

Synthesis of *(E)*-3,7-dimethyl-1-(1*H*-pyrrol-2-yl)octa-2,6-dien-1-one (150):



150

To a flame-dried round bottomed flask was added dry THF (10 mL) and freshly distilled pyrrole (0.308 µL, 4.45 x 10^{-3} mol). The solution was cooled to -78 °C in a dry ice/acetone bath. Ethylmagnesium bromide (3.0 M in diethyl ether, 1.5 mL, 4.5 x 10^{-3} mol) was added gradually by syringe over 30 minutes, maintaining the

temperature below -70 °C. After addition, the solution was stirred at -78 °C for 2 hours, displaying gentle effervescence and a colour change from colourless to deep orange.

(E)-*N*-methoxy-*N*,3,7-trimethylocta-2,6-dienamide **160** (211 mg, 1 x 10^{-3} mol) was dissolved in dry THF (5 mL) in a 2-necked, flame-dried round bottomed flask and cooled to -45 °C. The orange solution of pyrrolemagnesium bromide prepared above was added at this temperature and stirred for 5 hours, turning a dark brown colour. The reaction mixture was quenched by addition of saturated aqueous ammonium chloride (5 mL) at -45 °C and brought slowly to room temperature over a further hour.

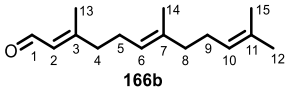
Purification using column chromatography on silica (cyclohexane/ethyl acetate 97:3 → 80:20) provided a pale brown gum which was recrystallised from pentane/diethyl ether to give a white solid (174 mg, 80% yield).

^{1}H-NMR (400 MHz, $CDCl_3$): δ = 9.45 (b, 1H, NH), 7.03 (m, 1H, H3), 6.88 (m, 1H, H1), 6.58 (s, 1H, H6), 6.30 (m, 1H, H2), 5.15 (m, 1H, H10), 2.27 (d, J = 1.3 Hz, 3H, H13), 2.26 (b, 2H, H8), 2.25 (b, 2H, H9), 1.72 (s, 3H, H12/14), 1.65 (s, 3H, H12/14) ppm.

^{13}C-NMR (100 MHz, $CDCl_3$): δ = 181.1 (C5), 159.0 (C7), 134.8 (C4), 132.5 (C11), 124.2 (C3), 123.2 (C10), 120.3 (C6), 114.9 (C1), 110.5 (C2), 41.5 (C9), 26.3 (C8), 25.7 (C12/14), 19.6 (C13), 17.8 (C12/14) ppm.

HRMS (ESI+) $[M+H]^+$: Expected M/Z = 218.1539, Measured M/Z = 218.1538.

Formation of *(2E,6E)*-3,7,11-trimethyldodeca-2,6,10-trienal (166b) by oxidation with manganese(IV) dioxide:



166b

Method A):

To a stirred suspension of manganese dioxide (7.82 g, 9.00 x 10^{-2} mol) in hexane (100 mL) was added *(2E,6E)*-farnesol (1.14 mL, 4.50 x 10^{-3} mol). The mixture was stirred for 6 hours at room temperature. The crude reaction mixture was filtered through celite, and the pale yellow solution was concentrated under vacuum to give a yellow oil. Purification by column chromatography gave *(2E,6E)*-3,7,11-trimethyldodeca-2,6,10-trienal **166b** (792 mg, 80% yield) and *(2E,6E)*-3,7,11-trimethyldodeca-2,6,10-trienoic acid **167b** (212 mg, 20% yield).

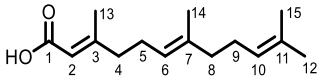
Method B):

To a stirred suspension of manganese dioxide (3.92 g, 4.50 x 10^{-2} mol) in dry 2-methyltetrahydrofuran (100 mL) under an argon atmosphere was added *(2E,6E)*-farnesol (1.14 mL, 4.50 x 10^{-3} mol). The reaction mixture was heated to 40 °C for 4 hours. The crude mixture was filtered through celite and the pale yellow solution was concentrated under vacuum to give a yellow oil. Purification by column chromatography gave *(2E,6E)*-3,7,11-trimethyldodeca-2,6,10-trienal **166b** (983 mg, <99% yield) as the sole product.

^{1}H-NMR (400 MHz, $CDCl_3$): δ = 10.01 (d, *J* = 8.2 Hz, 1H, H1), 5.93 – 5.88 (m, 1H), 5.15 – 5.05 (m, 2H), 2.30 – 2.21 (m, 4H), 2.19 (d, *J* = 1.3 Hz, 3H), 2.14 – 1.95 (m, 4H), 1.70 (d, *J* = 0.8 Hz, 3H), 1.62 (s, 3H), 1.61 (s, 3H) ppm. *In agreement with reported data.*

HRMS (ESI+) $[M+Na]^+$: Expected M/Z = 243.1725, Measured M/Z = 243.1729.

Formation of *(2E,6E)*-3,7,11-trimethyldodeca-2,6,10-trienoic acid (167b) and by oxidation with sodium chlorite (the Pinnick oxidation):



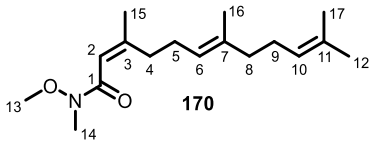
167b

(2E,6E)-3,7,11-trimethyldodeca-2,6,10-trienal **166b** (1.00 g, 4.54 x 10^{-3} mol) and 2-methyl-2-butene (9.62 mL, 9.08 x 10^{-2} mol) were dissolved in ethanol (240 mL). A solution of sodium chlorite (2.05 g, 2.27 x 10^{-2} mol) and sodium dihydrogen orthophosphate (3.54 g, 2.27 x 10^{-2} mol) in deionised water (60 mL) was added and the reaction was stirred at room temperature for 8 hours, turning a yellow/green colour. 30% aqueous hydrogen peroxide was added dropwise to decolourise the reaction mixture, then brine (100 mL) and diethyl ether (100 mL) were added to form two phases. The aqueous phase was washed with diethyl ether (2 x 200 mL) and the combined organic fractions were washed with brine (200 mL), dried over $MgSO_4$ and removed of solvent under vacuum to give a pale yellow oil. The crude mixture was purified using column chromatography on silica (cyclohexane/ ethyl acetate) to afford *(2E,6E)*-3,7,11-trimethyldodeca-2,6,10-trienoic acid **167b** as a colourless oil (658 mg, 62% yield).

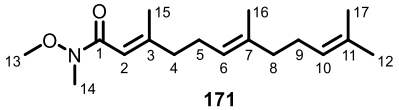
^{1}H-NMR (400 MHz, $CDCl_3$): δ = 10.77 (br, 1H), 5.72 (d, *J* = 0.9 Hz, 1H, H2), 5.16 – 5.05 (m, 2H, H6/H10), 2.24 – 2.18 (m, 7H), 2.14 – 2.94 (m, 4H), 1.70 (d, *J* = 0.9 Hz, 3H), 1.62 (s, 6H) ppm. *In agreement with reported data.*

HRMS (ESI+) $[M+H]^+$: Expected M/Z = 235.1704 Measured M/Z = 235.1698.

Formation of *(2Z,6E)*-*N*-methoxy-*N*,3,7,11-tetramethyldodeca-2,6,10-trienamide (170) and *(2E,6E)*-*N*-methoxy-*N*,3,7,11-tetramethyldodeca-2,6,10-trienamide (171) *via* amide coupling with *N,N'*-dicyclohexylcarbodiimide:



170

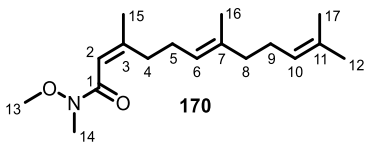


171

N,N'-dicyclohexylcarbodiimide (384 mg, 1.84 x 10^{-3} mol) and farnesic acid (400 mg, 1.69 x 10^{-3} mol) were dissolved in dichloromethane (2 mL). To this was added a solution of *N,O*-dimethylhydroxylamine hydrochloride (181 mg, 1.86 x 10^{-3} mol) and *N*-methylpyrrolidine (0.387 mL, 3.72 x 10^{-3} mol) in dichloromethane (2 mL), followed by a solution of 4-(*N,N*-dimethylamino)pyridine (21 mg, 1.69 x 10^{-4} mol) in dichloromethane (1 mL). The mixture was stirred at room temperature overnight. The reaction mixture was washed with 1M aqueous HCl (2 mL), water (2 x 2 mL) then brine (2 mL) and the organic phase was dried over $MgSO_4$ and removed of solvent under vacuum to give a crude yellow oil.

The crude oil was purified using column chromatography on silica (cyclohexane/ ethyl acetate 90:10 → 80:20 as eluent) to give Weinreb amides **170** (102 mg, 22% yield) and **171** (163 mg, 35% yield) as pale yellow oils.

***(2Z,6E)*-Weinreb amide 170:**



170

^{1}H-NMR (400 MHz, $CDCl_3$): δ = 6.10 (s, 1H, H2), 5.21 – 5.15 (m, 1H, H6), 5.12 – 5.06 (m, 1H, H10), 3.68 (s, 3H, H13), 3.20 (s, 3H, H14), 2.65 – 2.57 (m, 2H, H4), 2.22 – 2.16 (m, 2H, H5), 2.08 – 2.02 (m, 2H, H9), 2.00 – 1.94 (m, 2H, H8), 1.70 (b,

3H, H12/17), 1.67 (d, *J* = 1.1 Hz, 3H, H16), 1.64 (s, 3H, H15), 1.59 (s, 3H, H12/17) ppm.

^{13}C-NMR (100 MHz, $CDCl_3$): δ = 167.8 (C1), 156.9 (C3), 135.5 (C7), 131.3 (C11), 124.4 (C10), 123.9 (C6), 114.6 (C2), 61.4 (C13), 39.7 (C8), 33.7 (C4), 32.3 (C14), 32.0 (C9), 26.9 (C5), 25.9 (C12/17), 23.4 (C16), 17.7 (C12/17), 16.1 (C15) ppm.

HRMS (ESI+) $[M+H]^+$: Expected M/Z = 280.2271, Measured M/Z = 280.2269.

***(2E,6E)*-Weinreb amide 171:**

^{1}H-NMR (400 MHz, $CDCl_3$): δ = 6.12 (s, 1H, H2), 5.15 – 5.09 (m, 1H, H6), 5.12 – 5.06 (m, 1H, H10), 3.67 (s, 3H, H13), 3.21 (s, 3H, H14), 2.22 – 2.11 (m, 4H, H5/H8), 2.08 – 2.03 (m, 2H, H9), 2.00 – 1.96 (m, 2H, H4), 1.69 (s, 3H, H16), 1.68 (s, 3H, H12/17), 1.61 (s, 3H, H15), 1.60 (s, 3H, H12/17) ppm.

^{13}C-NMR (100 MHz, $CDCl_3$): δ = 168.2 (C1), 156.4 (C3), 135.9 (C7), 131.5 (C11), 124.2 (C10), 123.2 (C6), 113.9 (C2), 61.4 (C13), 41.4 (C8), 40.0 (C4), 32.4 (C14), 26.7 (C9), 25.1 (C5), 25.9 (C12/17), 23.5 (C16), 17.8 (C12/17), 16.4 (C15) ppm.

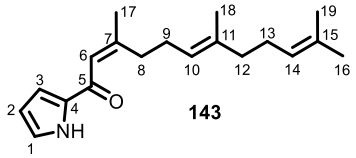
HRMS (ESI+) $[M+H]^+$: Expected M/Z = 280.2271, Measured M/Z = 280.2272.

Synthesis of *(2E,6E)*-*N*-methoxy-*N*,3,7,11-tetramethyldodeca-2,6,10-trienamide (170) and *(2Z,6E)*-*N*-methoxy-*N*,3,7,11-tetramethyldodeca-2,6,10-trienamide (171) using a Pinnick-type amidation protocol:

(2E,6E)-3,7,11-trimethyldodeca-2,6,10-trienal **166b** (440 mg, 2 x 10^{-3} mol) and 2-methyl-2-butene (2.15 mL, 2 x 10^{-2} mol) were dissolved in 2-methyltetrahydrofuran (30 mL). A solution of *N,O*-dimethylhydroxylamine hydrochloride (500 mg, 5 x 10^{-3} mol) and disodium hydrogen orthophosphate (710 mg, 5 x 10^{-3} mol) in water (10 mL) was added and the biphasic mixture was

stirred vigorously at room temperature. A solution of sodium chlorite (904 mg, 5 x 10^{-3} mol) in water was added dropwise by syringe over a period of 5 hours. The reaction was quenched by addition of saturated aqueous $NaHSO_3$ (20 mL). The biphasic mixture was brought to pH 3 by addition of 1M aqueous HCl and the aqueous phase was washed with 2-methyltetrahydrofuran (2 x 50 mL). The combined organic fractions were washed with brine (30 mL) and dried over $MgSO_4$. Removal of the solvent gave a yellow oil, which was purified by column chromatography on silica (cyclohexane/ ethyl acetate 90:10 → 80:20 as eluent) to give Weinreb amides **170** (230 mg, 41% yield) and **171** (300 mg, 54% yield) as well as *(2E,6E)*-3,7,11-trimethyldodeca-2,6,10-trienoic acid **167b** (24 mg, 5% yield).

Synthesis of *(2Z,6E)*-3,7,11-trimethyl-1-(1H-pyrrol-2-yl)dodeca-2,6,10-trien-1-one (143):



143

Dry, distilled TMP (0.57 mL, 3.30 x 10^{-3} mol) was dissolved in dry THF (6 mL) under an argon atmosphere and cooled to -78 °C. ^{t}BuLi (1.6 M in THF/Ethylbenzene, 2.06 mL, 3.30 x 10^{-3}) was added dropwise. The mixture was stirred at -78 °C for 10 minutes, then warmed to -10 °C for 15 minutes before cooling again to -78 °C. Freshly purified *N*-Boc-pyrrole (0.50 mL, 3.00 x 10^{-3} mol) in dry THF (4 mL) was added slowly by syringe and the mixture was stirred for 2 hours.

A solution of *(2Z,6E)*-*N*-methoxy-*N*,3,7,11-tetramethyldodeca-2,6,10-trienamide **170** (280 mg, 1 x 10^{-3} mol) in dry THF (5 mL) was cooled to -78° C and the solution of *N*-Boc-pyrrole lithium prepared above was added slowly by syringe. Once addition was complete the mixture was warmed to -45 °C and stirred for 5 hours.

The reaction mixture was then quenched by addition of saturated aqueous NH_4Cl (2 mL) and allowed to warm to room temperature. The organic phase was washed with 1M aqueous HCl (5 mL), brine (5 mL) and dried over anhydrous $MgSO_4$. Purification by column chromatography on silica (cyclohexane/ethyl acetate 95:5 → 80:20) gave pyrrolosesquiterpene **143** as a colourless oil (210 mg, 74% yield).

^{1}H-NMR (400 MHz, $CDCl_3$): δ = 7.35 (t, *J* = 1.6 Hz, 1H, H1), 7.23 – 7.21 (m, 1H, H2), 6.99 (s, 1H, H6), 6.30 – 6.28 (m, 1H, H3), 5.18 (tq, *J* = 7.1, 1.1 Hz, 1H, H10), 5.08 (m, 1H, H14), 2.46 (t, *J* = 7.9 Hz, 2H, H8), 2.31 – 220 (m, 2H), 2.12 – 2.04 (m, 2H), 2.03 – 1.96 (m, 2H), 1.69 (d, *J* = 1.1 Hz, 3H, H18), 1.61 (s, 3H), 1.60 (s, 3H), 1.27 (s, 3H) ppm.

^{13}C-NMR (100 MHz, $CDCl_3$): δ = 167.9 (C1), 142.5, 138.8, 135.8, 131.9, 125.6, 124.3, 123.7, 111.1 (C6), 30.3, 29.7, 28.4, 26.7, 25.7, 25.0, 17.7, 16.0 ppm.

HRMS (ESI+) $[M+H]^+$: Expected M/Z = 285.2114, Measured M/Z = 285.2099.

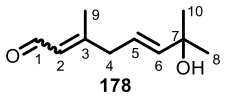
Procedure for the telescoped synthesis of *(2Z,6E)*-3,7,11-trimethyl-1-(1H-pyrrol-2-yl)dodeca-2,6,10-trien-1-one (143):

A 1:1 mixture of *(2Z,6E)*-3,7,11-trimethyldodeca-2,6,10-trienal **166a** and *(2E,6E)*-3,7,11-trimethyldodeca-2,6,10-trienal **166b** (7.8 g, 3.51×10^{-2} mol) was dissolved in 2-methyltetrahydrofuran (180 mL). Manganese(IV) dioxide (30.4 g, 3.50×10^{-1} mol) was suspended in this solution which was stirred under an argon atmosphere at 40 °C overnight. The mixture was filtered through a plug of celite and the solid retentate washed with 2-methyltetrahydrofuran (70 mL). The combined organic fractions were washed with saturated aqueous $NaHCO_3$ (200 mL).

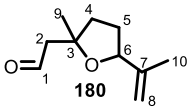
To the organic phase was added 2-methyl-2-butene (37.1 mL, 3.50×10^{-1} mL), followed by a solution of *N,O*-dimethylhydroxylamine hydrochloride (5.2 g, 5.25×10^{-2} mol), sodium dihydrogen orthophosphate dihydrate (5.46 g, 3.50×10^{-2} mol) and disodium hydrogen orthophosphate (7.46 g, 5.25×10^{-2} mol) in water (100 mL). The biphasic mixture was stirred vigorously at room temperature. A saturated solution of sodium chlorite (7.91 g, 8.75×10^{-2} mol) in water was added dropwise by syringe over a period of 14 hours. The reaction was quenched by addition of saturated aqueous $NaHSO_3$ (50 mL). The biphasic mixture was brought to pH 3 by addition of 1M aqueous HCl and the organic phase was washed with saturate aqueous $NaHCO_3$. The organic phase was washed with brine and dried over $MgSO_4$.

A solution of ^{t}BuLi in hexanes (3.0 M, 35 mL, 1.05×10^{-1} mol) was cooled to -78 °C in a dry ice/acetone bath. This was slowly added to a solution of *N*-bocpyrrole (16.7 mL, 1.00×10^{-1} mol) in dry 2-methyltetrahydrofuran (15 mL) at -78 °C. After addition was complete (*ca.* 30 minutes) the reaction was stirred for a further hour at -45 °C. The solution of Weinreb amides from the previous steps was then added over a period of 2 hours, then the mixture was stirred for a further 3 hours. The mixture was quenched by addition of saturated aqueous NH_4Cl and allowed to warm to room temperature. Evaporation of the solvent and purification by column chromatography on silica (cyclohexane/ethyl acetate 95:5 → 80:20) gave pyrrolosesquiterpene **143** as a colourless oil (2.89 g, 29% yield), along with isomeric pyrrolosesquiterpene **142**.

Synthesis of *(5E)*-7-hydroxy-3,7-dimethylocta-2,5-dienal (178) and 2-(2-methyl-5-(prop-1-en-2-yl)tetrahydrofuran-2-yl)acetaldehyde (180):



178



180

Citral (0.34 mL, 2 x 10^{-3} mol) was dissolved in ethanol (7.5 mL) and deionised water (2.5 mL). Methylene blue (3.2 mg, 1 x 10^{-5} mol) was added and the solution was cooled to 0 °C. The mixture was reacted per the photo-oxygenation general procedure given in Section 5.2.1. After 3 hours TLC showed no remaining citral and illumination and oxygen bubbling were ceased. The reaction was concentrated by removal of the solvent under vacuum, then extracted with diethyl ether (3 x 20 mL).

Triphenylphosphine (1.04 g, 4 x 10^{-3} mol) was added to the combined ether fractions and the mixture was stirred overnight. Removal of the solvent under vacuum gave a yellow oil which was purified by column chromatography (silica, cyclohexane/ethyl acetate 80:20) to give allylic alcohol **178** (74 mg, 22% yield (50% in crude by ^{1}H-NMR) as an interchanging mixture of *2Z*- and *2E*-isomers as well as tetrahydrofuran **180** (91 mg, 27% yield) as a mixture of diastereomers.

Allylic alcohol 178:

^{1}H-NMR (400 MHz, $CDCl_3$): δ = 9.98 (d, *J* = 8.1 Hz, 1H, H1), 5.91 (dd, *J* = 8.1, 1.2 Hz, 1H, H2), 5.01 – 4.96 (m, 1H, H6), 4.91 – 4.87 (m, 1H, H5), 2.80 – 2.53 (m, 1H, H7), 2.36 – 2.22 (m, 1H, H4), 1.99 (d, *J* = 1.2 Hz, 3H, H9), 1.74 (b, 6H, H8/10) ppm.

^{13}C-NMR (100 MHz, $CDCl_3$): δ = 191.1 (C1), 141.1 (C3), 128.6 (C6), 127.5 (C5), 111.6 (C2), 36.5 (C7), 33.4 (C9), 28.8 (C4), 24.9 (C8/10), 17.8 (C8/10) ppm.

HRMS (ESI+) $[M+Na]^+$: Expected M/Z = 191.1043, Measured M/Z = 191.1047.

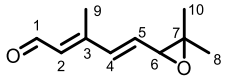
Tetrahydrofuran 180:

^{1}H-NMR (400 MHz, $CDCl_3$): δ = 9.85 (t, *J* = 3.0 Hz, 1H, H1), 5.05 – 5.02 (m, 1H, H8),4.84 – 4.81 (m, 1H, H8), 4.41 (t, *J* = 6.8 Hz, 1H, H6), 2.63 (dd, *J* = 7.7, 3.0 Hz, 2H, H2), 2.17 – 2.04 (m, 1H, H4), 1.96 – 1.82 (m, 3H, H4/5), 1.73 (s, 3H, H10), 1.38 (s, 3H, H9) ppm.

^{13}C-NMR (100 MHz, $CDCl_3$): δ = 202.4 (C1), 145.4 (C7), 110.6 (C8), 82.7 (C6), 81.2 (C3), 54.3 (C2), 37.7 (C5), 30.9 (C4), 27.7 (C9), 17.9 (C10) ppm.

HRMS (ESI+) $[M+Na]^+$: Expected M/Z = 191.1043, Measured M/Z = 191.0863.

Synthesis of *(2E,4E)*-5-(3,3-dimethyloxiran-2-yl)-3-methylpenta-2,4-dienal (181):



181

Citral (0.34 mL, 2 x 10^{-3} mol) was dissolved in ethanol (7.5 mL) and deionised water (2.5 mL). Methylene blue (3.2 mg, 1 x 10^{-5} mol) was added and the solution was cooled to 0 °C. The mixture was reacted per the photo-oxygenation general procedure given in Section 5.2.1. After 3 hours TLC showed no remaining citral and illumination and oxygen bubbling were ceased. L-proline (23 mg, 2 x 10^{-4} mol) was added and the reaction mixture was stirred overnight. The reaction was concentrated by removal of the solvent under vacuum, then extracted with diethyl ether (3 x 20 mL). Purification by column chromatography (silica, cyclohexane/ethyl acetate 80:20) gave epoxide **181** as a pale yellow oil (148 mg, 44% yield).

^{1}H-NMR (400 MHz, $CDCl_3$): δ = 10.13 (d, *J* = 7.9 Hz, 1H, H1), 6.53 (d, *J* = 15.8 Hz, 1H, H4), 6.11 (dd, *J* = 15.8, 7.2 Hz, 1H, H5), 5.97 (d, *J* = 8 Hz, 1H, H2), 3.34 (d, *J* =

7.2 Hz, 1H, H6), 2.27 (d, J = 1 Hz, 3H, H9), 1.41 (s, 3H, H8/10), 1.32 (s, 3H, H8/10) ppm.

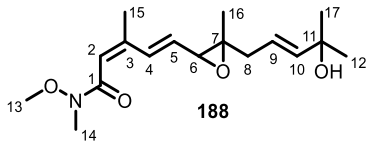
^{13}C-NMR (100 MHz, $CDCl_3$): δ = 191.4 (C1), 152.7 (C3), 137.3 (C4), 132.9 (C5), 130.0 (C2), 63.6 (C6), 61.5 (C7), 24.6 (C8/10), 18.9 (C8/10), 13.0 (C9) ppm.

HRMS (ESI+) $[M+Na]^+$: Expected M/Z = 189.0886, Measured M/Z = 189.0885.

Photo-oxygenation of pyrrolosesquiterpene 143:

Pyrrolosesquiterpene **143** (50 mg, 1.75 x 10^{-4} mol) and methylene blue (0.3 mg, 9 x 10^{-7} mol) were dissolved in tetrahydrofuran (2 mL). The mixture was cooled to -78 °C and reacted per the photo-oxygenation general procedure given in Section 5.2.1. After 1 hour, TLC showed no starting material remained, so the reaction was ceased, though none of the desired product was formed and ^{1}H-NMR of the crude material indicated degradation of the pyrrole moiety.

***(2Z,4E)*-5-(3-((*E*)-4-hydroxy-4-methylpent-2-en-1-yl)-3-methyloxiran-2-yl)-*N*-methoxy-*N*,3-dimethylpenta-2,4-dienamide (188):**



188

Weinreb amide **170** (558 mg, 2.00 x 10^{-3} mol) and *meso*-tetraphenylporphyrin (6 mg, 2 x 10^{-5} mol) were dissolved in tetrahydrofuran (10 mL). The mixture was cooled to -78 °C and reacted per the photo-oxygenation general procedure given in Section 5.2.1. After 5 hours, TLC showed full consumption of the starting material. 30% aqueous NaOH (2 mL) was added and the mixture was stirred overnight. The resulting mixture was quenched with saturated aqueous Na_2SO_3 and purified using column chromatography on silica (cyclohexane/ethyl acetate 95:5 → 50:50) to give glaciapyrrol analogue **188** as a colourless oil (152 mg, 24% yield).

^{1}H-NMR (400 MHz, $CDCl_3$): δ = 6.49 (d, *J* = 15.6 Hz, 1H, H4), 6.28 (s, 1H, H2), 5.92 (dd, *J* = 15.6, 7.0 Hz, 1H, H5), 5.78 – 5.71 (m, 1H, H10), 5.68 – 5.56 (m, 1H, H9), 3.70 (s, 3H, H13), 3.35 (d, *J* = 7.0 Hz, 1H, H6), 3.24 (s, 3H, H14), 2.42 – 2.28 (m, 2H, H8), 2.25 (s, 3H, CH_3), 1.34 (s, 3H, CH_3), 1.33 – 1.28 (m, 6H, 2 x CH_3) ppm.

^{13}C-NMR (100 MHz, $CDCl_3$): δ = 199.4 (C1), 170.9 (C3), 141.9 (C10), 138.8 (C4), 129.2 (C5), 121.2 (C9), 119.1 (C2), 70.7 (C7), 63.1 (C6), 61.8 (C13), 41.1 (C8), 36.2 (C11), 32.1 (C14), 29.7 (CH_3), 22.0 (CH_3), 17.0 (CH_3), 13.9 (CH_3) ppm.

HRMS (ESI+) $[M+C_3H_5N_2]^+$: Expected M/Z = 378.23, Measured M/Z = 378.2399.

Chapter 6: Overall Conclusions

The overarching purpose of the body of work presented in this Thesis has been to show the capacity of singlet oxygen chemistry as a tool for clean, environmentally benign oxygenations as part of a greener, large-scale chemical synthesis. To that end we had two general aims, expressed in Section 1.3. These aims are stated again below, and the extent to which the work in previous Chapters has fulfilled those aims is discussed. Individual project aims and conclusions have been given in the relevant Chapters.

Aim 1: To demonstrate the versatility, simplicity and inherent step and atom economy of singlet oxygen chemistry, and to expand upon the utility of singlet oxygen in large-scale organic synthesis:

Progress: The value of singlet oxygen chemistry to large-scale organic synthesis has been demonstrated in several ways in this Thesis. The synthesis of artemisinin discussed in Chapter 2 and performed on an industrial scale by Sanofi is a well-established application of $^1O_2$, though our research has highlighted several interesting aspects of this chemistry. Despite the reportedly short lifetime of singlet oxygen in water, we have shown that performing singlet oxygen chemistry in aqueous systems is possible, albeit with a reduced rate. Additionally, we observed high selectivity and a high rate constant for quenching of $^1O_2$ by our substrate compared to conventional organic solvents. With our use of a high-pressure flow photoreactor we have shown how the productivity of photo-oxygenations can be increased by applying high partial pressures of O_2, which can help to counteract the low oxygen solubility and short lifetime of singlet oxygen in our aqueous systems. Combined, these developments open up the possibility for greener and more efficient reactions of singlet oxygen by using higher pressures

and higher proportions of water, saving waste and increasing throughput, which would make this chemistry more attractive for large-scale chemical production, in accordance with our stated aim.

Chapter 3 described the development of a reactor-spectrometer system for continuous monitoring of $^1O_2$ reactions by NMR. In this Thesis, a recirculating reactor was used for mechanistic elucidations, but the same general system could be easily adapted for quality control of optimisation of conditions. This provides a way for researchers to very easily acquire quantitative characterisation data on photo-oxygenations. As such, we have provided a way to increase the level of control and understanding over this chemistry so that it can be confidently applied in an industrial setting.

The work presented in Chapter 4 towards a synthesis of the glaciapyrrol family of natural products showed how singlet oxygen chemistry can be applied to install a wide range of oxygen functionality in an atom and step economic manner. A single photo-oxygenation followed by successive reaction of the hydroperoxide products allowed access to the entire complex functionality of a glaciapyrrol precursor in one pot, using benchtop laboratory reagents. This demonstrates the efficiency and versatility of singlet oxygen chemistry for natural product synthesis. Included in this was an interesting and useful vinylogous epoxidation reaction, which could find widespread use in organic synthesis due to the prevalence of epoxides as synthetic intermediates.

Aim 2: To develop syntheses and processes involving singlet oxygen that adhere to the Principles of Green Chemistry and show the synergy between Green Chemistry and Process Chemistry:

Progress: It was our intention that all the synthetic work performed herein be as sustainable as possible, producing minimal waste and requiring the minimal amount of both synthetic steps and unit operations.

The pre-existing synthetic route used in the synthesis of artemisinin is already highly efficient, proceeding as a cascade of reactions that can be performed in one pot. However, several inefficiencies were highlighted in Sanofi's application of this route, particularly the use of hazardous solvent dichloromethane and their aditional derivatisation (esterification) and purification steps, which are costly in both time and material, and the low temperature needed for high selectivities in the photo-oxygenation step, which is costly in energy. The work in Chapter 2 replaces the dichloromethane solvent with more benign aqueous mixtures, reducing the hazards associated with the process. The esterification step is removed with no loss of yield, increasing the step and atom economy of the process. In some conditions that have been tested, yields were in fact higher than in Sanofi's process. In addition, the product could be obtained in high purity directly from the reaction mixture, removing the waste produced by extra recrystallisation steps. As a whole, the process we have developed is demonstrably greener, less wasteful and involving fewer unit operations, completely fulfilling this aim. Furthermore, the continuous NMR monitoring studies in Chapter 3 allow real-time feedback on the reaction as it progresses, in accordance with Anastas' 11th principle of Green Chemistry.

The greatest achievements in this Thesis in terms of sustainable synthesis were made in the course of the attempted synthesis of the glaciapyrrol natural products. The number of synthetic steps was minimised by the development of a one-pot protocol for the amidation/oxidation of aldehydes to form a Weinreb amide for use in organometallic couplings. This reaction was successfully optimised for the desired amide product using slow addition to control selectivity, and a biphasic reaction mixture to minimise side product formation. The biphasic system allowed for simple work-up of the reaction, which was extended to a fully telescoped, scaled-up synthesis of a common precursor to the target family of compounds. This work demonstrates several strategies for maximising step economy and reducing waste and cost, fulfilling our aim for Greener processes.

In both bodies of synthetic work presented in this Thesis, decisions made from a Green Chemistry standpoint have yielded substantial process benefits, examples being the fortuitous discovery of pure artemisinin crystallising from our aqueous solvents in Chapter 2, or the application of the biphasic amidation protocol in Chapter 4 allowing full telescoping of the three-step precursor synthesis. This clearly shows that by aiming for Greener chemistry we can achieve more economic sustainable chemical processing.

To summarise, the work contained within this Thesis has successfully applied singlet oxygen chemistry as part of efficient, sustainable chemical syntheses, showing its value as a clean, versatile oxidant for the oxygenation of organic substrates. It is the sincere hope of the author that this work might contribute to the increased application in the chemical industries of photochemically generated singlet oxygen, and Green synthetic strategy in general.

References.

[1]. Poliakoff, M.; Fitzpatrick, J. M.; Farren, T. R.; Anastas, P. T., *Science* **2002,** *297*, 807-810.

[2]. Kolb, V. M., *Green organic chemistry and its interdisciplinary applications*. CNC Press: Boca Raton, FL, 2016.

[3]. Anastas, P. T.; Warner, J. C., *Green chemistry: Theory and practice*. Oxford University Press: Oxford, UK, 1998.

[4]. Anastas, P.; Eghbali, N., *Chem. Soc. Rev.* **2010,** *39*, 301-312.

[5]. Tang, S. L. Y.; Smith, R. L.; Poliakoff, M., *Green Chem.* **2005,** *7*, 761-762.

[6]. Gani, R., *Comput. Chem. Eng.* **2004,** *28*, 2441-2457.

[7]. Kralisch, D.; Ott, D.; Gericke, D., *Green Chem.* **2015,** *17*, 123-145.

[8]. Anastas, P. T.; Lankey, R. L., *Green Chem.* **2000,** *2*, 289-295.

[9]. Lankey, R. L.; Anastas, P. T., *Ind. Eng. Chem. Res.* **2002,** *41*, 4498-4502.

[10]. Tufvesson, L. M.; Tufvesson, P.; Woodley, J. M.; Borjesson, P., *Int. J. Life Cycle Ass.* **2013,** *18*, 431-444.

[11]. Anastas, P. T.; Zimmerman, J. B., *Environ. Sci. Technol.* **2003,** *37*, 94A-101A.

[12]. Hendrickson, J. B., *J. Am. Chem. Soc.* **1975,** *97*, 5784-5800.

[13]. Newhouse, T.; Baran, P. S.; Hoffmann, R. W., *Chem. Soc. Rev.* **2009,** *38*, 3010-3021.

[14]. Trost, B. M., *Science* **1991,** *254*, 1471-1477.

[15]. Sheldon, R. A., *J. Chem. Technol. Biotechnol.* **1997,** *68*, 381-388.

[16]. Wender, P. A.; Verma, V. A.; Paxton, T. J.; Pillow, T. H., *Acc. Chem. Res.* **2008,** *41*, 40-49.

[17]. Wender, P. A.; Miller, B. L., *Nature* **2009,** *460*, 197-201.

[18]. Burns, N. Z.; Baran, P. S.; Hoffmann, R. W., *Angew. Chem. Int. Ed. Engl.* **2009,** *48*, 2854-2867.

[19]. Richter, J. M.; Ishihara, Y.; Masuda, T.; Whitefield, B. W.; Llamas, T.; Pohjakallio, A.; Baran, P. S., *J. Am. Chem. Soc.* **2008,** *130*, 17938-17954.

[20]. Gaich, T.; Baran, P. S., *J. Org. Chem.* **2010,** *75*, 4657-4673.

[21]. Li, C. J.; Trost, B. M., *P. Natl. Acad. Sci. USA* **2008,** *105*, 13197-13202.

[22]. Sheldon, R. A., *Green Chem.* **2005,** *7*, 267-278.

[23]. Henderson, R. K.; Jimenez-Gonzalez, C.; Constable, D. J. C.; Alston, S. R.; Inglis, G. G. A.; Fisher, G.; Sherwood, J.; Binks, S. P.; Curzons, A. D., *Green Chem.* **2011,** *13*, 854-862.

[24]. Prat, D.; Pardigon, O.; Flemming, H. W.; Letestu, S.; Ducandas, V.; Isnard, P.; Guntrum, E.; Senac, T.; Ruisseau, S.; Cruciani, P.; Hosek, P., *Org. Process Res. Dev.* **2013,** *17*, 1517-1525.

[25]. Diorazio, L. J.; Hose, D. R. J.; Adlington, N. K., *Org. Process Res. Dev.* **2016,** *20*, 760-773.

[26]. Sneddon, H. F., *Green Chem.* **2016,** *18*, 5082-5085.

[27]. Milas, N. A.; Trepagnier, J. H.; Nolan, J. T.; Iliopulos, M. I., *J. Am. Chem. Soc.* **1959,** *81*, 4730-4733.

[28]. Eames, J.; Mitchell, H. J.; Nelson, A.; O'Brien, P.; Warren, S.; Wyatt, P., *J. Chem. Soc. Perk. Trans. 1* **1999**, 1095-1103.

[29]. Jacobsen, E. N.; Marko, I.; Mungall, W. S.; Schroder, G.; Sharpless, K. B., *J. Am. Chem. Soc.* **1988,** *110*, 1968-1970.

[30]. Frontana-Uribe, B. A.; Little, R. D.; Ibanez, J. G.; Palma, A.; Vasquez-Medrano, R., *Green Chem.* **2010,** *12*, 2099-2119.

[31]. Francke, R.; Little, R. D., *Chem. Soc. Rev.* **2014,** *43*, 2492-2521.

[32]. Prier, C. K.; Rankic, D. A.; MacMillan, D. W. C., *Chem. Rev.* **2013,** *113*, 5322-5363.

[33]. Karkas, M. D.; Porco, J. A.; Stephenson, C. R. J., *Chem. Rev.* **2016,** *116*, 9683-9747.

[34]. Yoon, T. P.; Ischay, M. A.; Du, J. N., *Nature Chem.* **2010,** *2*, 527-532.

[35]. Tang, F.; Chen, C.; Moeller, K. D., *Synthesis-Stuttgart* **2007**, 3411-3420.

[36]. Laird, T., *Org. Process Res. Dev.* **2007,** *11*, 783-783.

[37]. Anastas, P. T., *Environ. Sci. Technol.* **2003,** *37*, 423A-423A.

[38]. Butters, M.; Catterick, D.; Craig, A.; Curzons, A.; Dale, D.; Gillmore, A.; Green, S. P.; Marziano, I.; Sherlock, J. P.; White, W., *Chem. Rev.* **2006,** *106*, 3002-3027.

[39]. Azzaro-Pantel, C., Green process design methodology: A multicriteria approach. In *Green process engineering*, Poux, M.; Cognet, P.; Gourdon, C., Eds. CRC Press: Boka Raton, FL, 2015; pp 3-26.

[40]. Dach, R.; Song, J. H. J.; Roschangar, F.; Samstag, W.; Senanayake, C. H., *Org. Process Res. Dev.* **2012,** *16*, 1697-1706.

[41]. Jimenez-Gonzalez, C.; Constable, D. J. C.; Ponder, C. S., *Chem. Soc. Rev.* **2012,** *41*, 1485-1498.

[42]. Auge, J., *Green Chem.* **2008,** *10*, 225-231.

[43]. Calvo-Flores, F. G., *Chemsuschem* **2009,** *2*, 905-919.

[44]. Constable, D. J. C.; Curzons, A. D.; Cunningham, V. L., *Green Chem.* **2002,** *4*, 521-527.

[45]. Sheldon, R. A., *Chem. Ind. - London* **1992**, 903-906.

[46]. Andraos, J., *Org. Process Res. Dev.* **2009,** *13*, 161-185.

[47]. Sheldon, R. A., *Chem. Commun.* **2008**, 3352-3365.

[48]. Clark, J.; Sheldon, R.; Raston, C.; Poliakoff, M.; Leitner, W., *Green Chem.* **2014,** *16*, 18-23.

[49]. Mikami, K.; Shimizu, M., *Chem. Rev.* **1992,** *92*, 1021-1050.

[50]. Kniss, A. R.; Coburn, C. W., *PLOS One* **2015,** *10*.

[51]. Kovach, J.; Petzoldt, C.; Degni, J.; Tette, J., *New York Food Life* **1992**, 1-8.

[52]. McCabe, W. L.; Smith, J. C.; Harriott, P., *Unit operations of chemical engineering 7/e*. McGraw-Hill: New York, NY, 2005.

[53]. Parsons, P. J.; Penkett, C. S.; Shell, A. J., *Chem. Rev.* **1996,** *96*, 195-206.

[54]. Nicolaou, K. C.; Edmonds, D. J.; Bulger, P. G., *Angew. Chem. Int. Ed. Engl.* **2006,** *45*, 7134-7186.

[55]. Desai, A. A.; Molitor, E. J.; Anderson, J. E., *Org. Process Res. Dev.* **2012,** *16*, 160-165.

[56]. Domling, A.; Ugi, I., *Angew. Chem. Int. Ed. Engl.* **2000,** *39*, 3168-3210.

[57]. Vaxelaire, C.; Winter, P.; Christmann, M., *Angew. Chem. Int. Ed. Engl.* **2011,** *50*, 3605-3607.

[58]. Soule, J. F.; Miyamura, H.; Kobayashi, S., *Chem. Asian. J.* **2013,** *8*, 2614-2626.

[59]. Denmark, S. E.; Fan, Y., *J. Org. Chem.* **2005,** *70*, 9667-9676.

[60]. Pando, O.; Stark, S.; Denkert, A.; Porzel, A.; Preusentanz, R.; Wessjohann, L. A., *J. Am. Chem. Soc.* **2011,** *133*, 7692-7695.

[61]. Porta, R.; Benaglia, M.; Puglisi, A., *Org. Process Res. Dev.* **2016,** *20*, 2-25.

[62]. Jimenez-Gonzalez, C.; Poechlauer, P.; Broxterman, Q. B.; Yang, B. S.; Ende, D. A.; Baird, J.; Bertsch, C.; Hannah, R. E.; Dell'Orco, P.; Noorrnan, H.; Yee, S.; Reintjens, R.; Wells, A.; Massonneau, V.; Manley, J., *Org. Process Res. Dev.* **2011,** *15*, 900-911.

[63]. Malet-Sanz, L.; Susanne, F., *J. Med. Chem.* **2012,** *55*, 4062-4098.

[64]. McQuade, D. T.; Seeberger, P. H., *J. Org. Chem.* **2013,** *78*, 6384-6389.

[65]. Anderson, N. G., *Org. Process Res. Dev.* **2012,** *16*, 852-869.

[66]. Gutmann, B.; Cantillo, D.; Kappe, C. O., *Angew. Chem. Int. Ed. Engl.* **2015,** *54*, 6688-6728.

[67]. Fogler, H. S., *Elements of chemical reaction engineering*. Pearson Education Limited: Harlow, UK, 2014.

[68]. Penders, I.; Amara, Z.; Horvath, R.; Rossen, K.; Poliakoff, M.; George, M. W., *RSC Adv.* **2015,** *5*, 6501-6504.

[69]. Kobayashi, S., *Chem. Asian. J.* **2016,** *11*, 425-436.

[70]. Plutschack, M. B.; Pieber, B.; Gilmore, K.; Seeberger, P. H., *Chem. Rev.* **2017**.

[71]. Movsisyan, M.; Delbeke, E. I. P.; Berton, J.; Battilocchio, C.; Ley, S. V.; Stevens, C. V., *Chem. Soc. Rev.* **2016,** *45*, 4892-4928.

[72]. Muller, S. T. R.; Wirth, T., *Chemsuschem* **2015,** *8*, 245-250.

[73]. Pollet, P.; Cope, E. D.; Kassner, M. K.; Charney, R.; Terett, S. H.; Richman, K. W.; Dubay, W.; Stringer, J.; Eckertt, C. A.; Liotta, C. L., *Ind. Eng. Chem. Res.* **2009,** *48*, 7032-7036.

[74]. Maurya, R. A.; Park, C. P.; Lee, J. H.; Kim, D. P., *Angew. Chem. Int. Ed. Engl.* **2011,** *50*, 5952-5955.

[75]. Martin, L. J.; Marzinzik, A. L.; Ley, S. V.; Baxendale, I. R., *Org. Lett.* **2011,** *13*, 320-323.

[76]. Mastronardi, F.; Gutmann, B.; Kappe, C. O., *Org. Lett.* **2013,** *15*, 5590-5593.

[77]. Muller, S. T. R.; Murat, A.; Hellier, P.; Wirth, T., *Org. Process Res. Dev.* **2016,** *20*, 495-502.

[78]. Fuse, S.; Mifune, Y.; Takahashi, T., *Angew. Chem. Int. Ed. Engl.* **2014,** *53*, 851-855.

[79]. Battilocchio, C.; Deadman, B. J.; Nikbin, N.; Kitching, M. O.; Baxendale, I. R.; Ley, S. V., *Chem. Eur. J.* **2013,** *19*, 7917-7930.

[80]. Pierce, M. E.; Parsons, R. L.; Radesca, L. A.; Lo, Y. S.; Silverman, S.; Moore, J. R.; Islam, Q.; Choudhury, A.; Fortunak, J. M. D.; Nguyen, D.; Luo, C.; Morgan, S. J.; Davis, W. P.; Confalone, P. N.; Chen, C. Y.; Tillyer, R. D.; Frey, L.; Tan, L. S.; Xu, F.; Zhao, D. L.; Thompson, A. S.; Corley, E. G.; Grabowski, E. J. J.; Reamer, R.; Reider, P. J., *J. Org. Chem.* **1998,** *63*, 8536-8543.

[81]. Dai, D.; Long, X.; Luo, B.; Kulesza, A.; Reichwagen, J.; Guo, Y. Process for preparation of efavirenz by cyclisation. 2012.

[82]. Tsubogo, T.; Oyamada, H.; Kobayashi, S., *Nature* **2015,** *520*, 329-332.

[83]. Chiroli, V.; Benaglia, M.; Cozzi, F.; Puglisi, A.; Annunziata, R.; Celentano, G., *Org. Lett.* **2013,** *15*, 3590-3593.

[84]. Atodiresei, I.; Vila, C.; Rueping, M., *ACS Catal.* **2015,** *5*, 1972-1985.

[85]. Mak, X. Y.; Laurino, P.; Seeberger, P. H., *Beilstein J. Org. Chem.* **2009,** *5*.

[86]. Mascia, S.; Heider, P. L.; Zhang, H. T.; Lakerveld, R.; Benyahia, B.; Barton, P. I.; Braatz, R. D.; Cooney, C. L.; Evans, J. M. B.; Jamison, T. F.; Jensen, K. F.; Myerson, A. S.; Trout, B. L., *Angew. Chem. Int. Ed. Engl.* **2013,** *52*, 12359-12363.

[87]. Heider, P. L.; Born, S. C.; Basak, S.; Benyahia, B.; Lakerveld, R.; Zhang, H. T.; Hogan, R.; Buchbinder, L.; Wolfe, A.; Mascia, S.; Evans, J. M. B.; Jamison, T. F.; Jensen, K. F., *Org. Process Res. Dev.* **2014,** *18*, 402-409.

[88]. Albini, A.; Fagnoni, M., *Green Chem.* **2004,** *6*, 1-6.

[89]. Kearns, D. R., *Chem. Rev.* **1971,** *71*, 395-&.

[90]. Foote, C. S., *Acc. Chem. Res.* **1968,** *1*, 104-&.

[91]. Hudlicky, T., *Oxidation in organic chemistry*. American Chemical Society: Washington, DC, 1990.

[92]. Clennan, E. L.; Pace, A., *Tetrahedron* **2005,** *61*, 6665-6691.

[93]. DeRosa, M. C.; Crutchley, R. J., *Coord. Chem. Rev.* **2002,** *233*, 351-371.

[94]. Ogilby, P. R.; Foote, C. S., *J. Am. Chem. Soc.* **1982,** *104*, 2069-2070.

[95]. Ogilby, P. R., *Acc. Chem. Res.* **1999,** *32*, 512-519.

[96]. Schweitzer, C.; Schmidt, R., *Chem. Rev.* **2003,** *103*, 1685-1757.

[97]. Bregnhoj, M.; Westberg, M.; Jensen, F.; Ogilby, P. R., *Phys. Chem. Chem. Phys.* **2016,** *18*, 22946-22961.

[98]. Foote, C. S.; Wexler, S.; Ando, W.; Higgins, R., *J. Am. Chem. Soc.* **1968,** *90*, 975-&.

[99]. Shakhashiri, B. Z.; Williams, L. G., *J. Chem. Educ.* **1976,** *53*, 358-361.

[100]. Frimer, A. A., *The chemistry of functional groups: Peroxides*. John Wiley & Sons Ltd.: 1983.

[101]. Schaap, A. P.; Kees, K.; Thayer, A. L., *J. Org. Chem.* **1975,** *40*, 1185-1186.

[102]. Aubry, J. M.; Cazin, B., *Inorg. Chem.* **1988,** *27*, 2013-2014.

[103]. Nardello, V.; Herve, M.; Alsters, P. L.; Aubry, J. M., *Adv. Synth. Catal.* **2002,** *344*, 184-191.

[104]. Csanyi, L. J., *J. Mol. Catal. A: Chem.* **2010,** *322*, 1-6.

[105]. Alsters, P. L.; Jary, W.; Nardello-Rataj, V.; Aubry, J. M., *Org. Process Res. Dev.* **2010,** *14*, 259-262.

[106]. Hong, B.; Lebeuf, R.; Delbaere, S.; Alsters, P. L.; Nardello-Rataj, V., *Catalysts* **2016,** *6*.

[107]. Spikes, J. D., *J. Photochem. Photobiol., B* **1998,** *42*, 1-11.

[108]. Schmidt, R., *Photochem. Photobiol.* **2006,** *82*, 1161-1177.

[109]. Zhao, J. Z.; Wu, W. H.; Sun, J. F.; Guo, S., *Chem. Soc. Rev.* **2013,** *42*, 5323-5351.

[110]. Wayne, C. E.; Wayne, R. P., *Photochemistry*. Oxford University Press: New York, NY, 1996.

[111]. Sivery, A.; Barras, A.; Boukherroub, R.; Pierlot, C.; Aubry, J. M.; Anquez, F.; Courtade, E., *J. Phys. Chem. C* **2014,** *118*, 2885-2893.

[112]. Afshari, E.; Schmidt, R., *Chem. Phys. Lett.* **1991,** *184*, 128-132.

[113]. Rodgers, M. A. J., *J. Am. Chem. Soc.* **1983,** *105*, 6201-6205.

[114]. Merkel, P. B.; Kearns, D. R.; Nilsson, R., *J. Am. Chem. Soc.* **1972,** *94*, 1030-&.

[115]. Smith, W. F., *J. Am. Chem. Soc.* **1972,** *94*, 186-&.

[116]. Young, R. H.; Martin, R. L.; Feriozi, D.; Brewer, D.; Kayser, R., *Photochem. Photobiol.* **1973,** *17*, 233-244.

[117]. Matheson, I. B. C.; Etheridge, R. D.; Kratowich, N. R.; Lee, J., *Photochem. Photobiol.* **1975,** *21*, 165-171.

[118]. Monroe, B. M., *J. Phys. Chem.* **1977,** *81*, 1861-1864.

[119]. Foote, C. S.; Denny, R. W., *J. Am. Chem. Soc.* **1968,** *90*, 6233-&.

[120]. Frimer, A. A., *Chem. Rev.* **1979,** *79*, 359-387.

[121]. Clennan, E. L., *Tetrahedron* **2000,** *56*, 9151-9179.

[122]. Prein, M.; Adam, W., *Angew. Chem. Int. Ed. Engl.* **1996,** *35*, 477-494.

[123]. Clennan, E. L., *Acc. Chem. Res.* **2001,** *34*, 875-884.

[124]. Stephenson, L. M.; Grdina, M. J.; Orfanopoulos, M., *Acc. Chem. Res.* **1980,** *13*, 419-425.

[125]. Stratakis, M.; Orfanopoulos, M., *Tetrahedron* **2000,** *56*, 1595-1615.

[126]. Harding, L. B.; Goddard, W. A., *J. Am. Chem. Soc.* **1980,** *102*, 439-449.

[127]. Yamaguchi, K.; Yabushita, S.; Fueno, T.; Houk, K. N., *J. Am. Chem. Soc.* **1981,** *103*, 5043-5046.

[128]. Davies, A. G.; Schiesser, C. H., *Tetrahedron* **1991,** *47*, 1707-1726.

[129]. Orfanopoulos, M.; Stephenson, L. M., *J. Am. Chem. Soc.* **1980,** *102*, 1417-1418.

[130]. Kopecky, K. R.; Filby, J. E.; Mumford, C.; Lockwood, P. A.; Ding, J. Y., *Can. J. Chem.* **1975,** *53*, 1103-1122.

[131]. Hurst, J. R.; Wilson, S. L.; Schuster, G. B., *Tetrahedron* **1985,** *41*, 2191-2197.

[132]. Foote, C. S.; Denny, R. W., *J. Am. Chem. Soc.* **1971,** *93*, 5162-&.

[133]. Frimer, A. A.; Rot, D.; Sprecher, M., *Tetrahedron Lett.* **1977**, 1927-1930.

[134]. Leach, A. G.; Houk, K. N.; Foote, C. S., *J. Org. Chem.* **2008,** *73*, 8511-8519.

[135]. Luis, J. G.; Andres, L. S.; Fletcher, W. Q., *Tetrahedron Lett.* **1994,** *35*, 179-182.

[136]. Clennan, E. L., Photo-oxygenation of the ene type. In *Synthetic organic photochemistry*, Griesbeck, A. G.; Mattay, J., Eds. Marcel Dekker: New York, NY, 2005; pp 365-390.

[137]. Clennan, E. L.; Chen, X. N.; Koola, J. J., *J. Am. Chem. Soc.* **1990,** *112*, 5193-5199.

[138]. Stratakis, M.; Orfanopoulos, M., *Synth. Commun.* **1993,** *23*, 425-430.

[139]. Orfanopoulos, M.; Grdina, S. M. B.; Stephenson, L. M., *J. Am. Chem. Soc.* **1979,** *101*, 275-276.

[140]. Lerdal, D.; Foote, C. S., *Tetrahedron Lett.* **1978**, 3227-3230.

[141]. Rousseau, G.; Leperchec, P.; Conia, J. M., *Tetrahedron Lett.* **1977**, 2517-2520.

[142]. Inagaki, S.; Fujimoto, H.; Fukui, K., *Chem. Lett.* **1976**, 749-752.

[143]. Houk, K. N.; Williams, J. C.; Mitchell, P. A.; Yamaguchi, K., *J. Am. Chem. Soc.* **1981,** *103*, 949-951.

[144]. Jefford, C. W.; Boschung, A. F.; Laffer, M. H., *J. Am. Chem. Soc.* **1972,** *94*, 8904-&.

[145]. Adam, W.; Wirth, T., *Acc. Chem. Res.* **1999,** *32*, 703-710.

[146]. Adam, W.; Bottke, N.; Krebs, O.; Lykakis, I.; Orfanopoulos, M.; Stratakis, M., *J. Am. Chem. Soc.* **2002,** *124*, 14403-14409.

[147]. Wieringa, J. H.; Wynberg, H.; Strating, J.; Adam, W., *Tetrahedron Lett.* **1972**, 169-&.

[148]. Adam, W.; Brunker, H. G., *Synthesis-Stuttgart* **1995**, 1066-&.

[149]. Adam, W.; Degen, H. G.; Krebs, O.; Saha-Moller, C. R., *J. Am. Chem. Soc.* **2002,** *124*, 12938-12939.

[150]. Adam, W.; Bosio, S. G.; Turro, N. J., *J. Am. Chem. Soc.* **2002,** *124*, 14004-14005.

[151]. Rajeev, R.; Sunoj, R. B., *J. Org. Chem.* **2012,** *77*, 2474-2485.

[152]. Kuroda, Y.; Hiroshige, T.; Sera, T.; Shiroiwa, Y.; Tanaka, H.; Ogoshi, H., *J. Am. Chem. Soc.* **1989,** *111*, 1912-1913.

[153]. Kuroda, Y.; Sera, T.; Ogoshi, H., *J. Am. Chem. Soc.* **1991,** *113*, 2793-2794.

[154]. Joy, A.; Robbins, R. J.; Pitchumani, K.; Ramamurthy, V., *Tetrahedron Lett.* **1997,** *38*, 8825-8828.

[155]. Iesce, M. R., Photo-oxygenation of the [4+2] and [2+2] type. In *Synthetic organic photochemistry*, Griesbeck, A. G.; Mattay, J., Eds. Marcel Dekker: New York, NY, 2005; pp 299-364.

[156]. Delogu, G.; Fabbri, D.; Fabris, F.; Sbrogio, F.; Valle, G.; Delucchi, O., *J. Chem. Soc. Chem. Commun.* **1995**, 1887-1888.

[157]. Adam, W.; Prein, M., *Acc. Chem. Res.* **1996,** *29*, 275-283.

[158]. Adam, W.; Saha-Moller, C. R.; Schambony, S. B.; Schmid, K. S.; Wirth, T., *Photochem. Photobiol.* **1999,** *70*, 476-483.

[159]. Adam, W.; Guthlein, M.; Peters, E. M.; Peters, K.; Wirth, T., *J. Am. Chem. Soc.* **1998,** *120*, 4091-4093.

[160]. Wiegand, C.; Herdtweck, E.; Bach, T., *Chem. Commun.* **2012,** *48*, 10195-10197.

[161]. Maranzana, A.; Ghigo, G.; Tonachini, G., *J. Am. Chem. Soc.* **2000,** *122*, 1414-1423.

[162]. Jefford, C. W., *Chem. Soc. Rev.* **1993,** *22*, 59-66.

[163]. Asveld, E. W. H.; Kellogg, R. M., *J. Am. Chem. Soc.* **1980,** *102*, 3644-3646.

[164]. Greer, A.; Vassilikogiannakis, G.; Lee, K. C.; Koffas, T. S.; Nahm, K.; Foote, C. S., *J. Org. Chem.* **2000,** *65*, 6876-6878.

[165]. Yaremenko, I. A.; Vil, V. A.; Demchuk, D. V.; Terent'ev, A. O., *Beilstein J. Org. Chem.* **2016,** *12*, 1647-1748.

[166]. Ohloff, G., *Pure Appl. Chem.* **1975,** *43*, 481-502.

[167]. Ghogare, A. A.; Greer, A., *Chem. Rev.* **2016,** *116*, 9994-10034.

[168]. Sharma, P.; Lygo, B.; Lewis, W.; Moses, J. E., *J. Am. Chem. Soc.* **2009,** *131*, 5966-5972.

[169]. Yao, G.; Steliou, K., *Org. Lett.* **2002,** *4*, 485-488.

[170]. Machara, A.; Werner, L.; Leisch, H.; Carroll, R. J.; Adams, D. R.; Haque, D. M.; Cox, D. P.; Hudlicky, T., *Synlett* **2015,** *26*, 2101-2108.

[171]. Dastan, A.; Balci, M., *Tetrahedron* **2006,** *62*, 4003-4010.

[172]. Barbarow, J. E.; Miller, A. K.; Trauner, D., *Org. Lett.* **2005,** *7*, 2901-2903.

[173]. Kornblum, N.; Delamare, H. E., *J. Am. Chem. Soc.* **1951,** *73*, 880-881.

[174]. Schultee.Kh; Willhalm, B.; Ohloff, G., *Angew. Chem. Int. Ed. Engl.* **1969,** *8*, 985-&.

[175]. Tang, Y.; Cole, K. P.; Buchanan, G. S.; Li, G.; Hsung, R. P., *Org. Lett.* **2009,** *11*, 1591-1594.

[176]. DellaGreca, M.; Iesce, M. R.; Previtera, L.; Purcaro, R.; Rubino, M.; Zarrelli, A., *Photoch. Photobio. Sci.* **2008,** *7*, 28-32.

[177]. Lancefield, C. S.; Zhou, L. N.; Lebl, T.; Slawin, A. M. Z.; Westwood, N. J., *Org. Lett.* **2012,** *14*, 6166-6169.

[178]. Dethe, D. H.; Dherange, B. D., *J. Org. Chem.* **2015,** *80*, 4526-4531.

[179]. Liffert, R.; Hoecker, J.; Jana, C. K.; Woods, T. M.; Burch, P.; Jessen, H. J.; Neuburger, M.; Gademann, K., *Chem. Sci.* **2013,** *4*, 2851-2857.

[180]. Schenck, G. O.; Neumuller, O. A.; Eisfeld, W., *Angew. Chem. Int. Ed. Engl.* **1958,** *70*, 595-595.

[181]. Hock, H.; Kropf, H., *Angew. Chem. Int. Ed. Engl.* **1957,** *69*, 313-321.

[182]. Kim, S. K.; Pak, C. S., *J. Org. Chem.* **1991,** *56*, 6829-6832.

[183]. Montagnon, T.; Tofi, M.; Vassilikogiannakis, G., *Acc. Chem. Res.* **2008,** *41*, 1001-1011.

[184]. Merkushev, A. A., *Chem. Heterocycl. Compd.* **2016,** *52*, 359-361.

[185]. Shiraki, R.; Sumino, A.; Tadano, K.; Ogawa, S., *Tetrahedron Lett.* **1995,** *36*, 5551-5554.

[186]. Li, H. Y.; Drummond, S.; DeLucca, I.; Boswell, G. A., *Tetrahedron* **1996,** *52*, 11153-11162.

[187]. Tong, G. H.; Liu, Z.; Li, P. F., *Org. Lett.* **2014,** *16*, 2288-2291.

[188]. Knowles, J. P.; Elliott, L. D.; Booker-Milburn, K. I., *Beilstein J. Org. Chem.* **2012,** *8*, 2025-2052.

[189]. Cassano, A. E.; Martin, C. A.; Brandi, R. J.; Alfano, O. M., *Ind. Eng. Chem. Res.* **1995,** *34*, 2155-2201.

[190]. Schenck, G. O.; Ziegler, K., *Naturwissenschaften* **1944,** *32*, 157.

[191]. Pape, M., *Pure Appl. Chem.* **1975,** *41*, 535-558.

[192]. Oelgemoller, M., *Chem. Rev.* **2016,** *116*, 9664-9682.

[193]. Su, Y. H.; Straathof, N. J. W.; Hessel, V.; Noel, T., *Chem. Eur. J.* **2014,** *20*, 10562-10589.

[194]. Elliott, L. D.; Knowles, J. P.; Koovits, P. J.; Maskill, K. G.; Ralph, M. J.; Lejeune, G.; Edwards, L. J.; Robinson, R. I.; Clemens, I. R.; Cox, B.; Pascoe, D. D.; Koch, G.; Eberle, M.; Berry, M. B.; Booker-Milburn, K. I., *Chem. Eur. J.* **2014,** *20*, 15226-15232.

[195]. Meyer, S.; Tietze, D.; Rau, S.; Schaefer, B.; Kreisel, G., *J. Photochem. Photobiol., A* **2007,** *186*, 248-253.

[196]. Griesbeck, A. G.; Maptue, N.; Bondock, S.; Oelgemoller, M., *Photoch. Photobio. Sci.* **2003,** *2*, 450-451.

[197]. Cambie, D.; Bottecchia, C.; Straathof, N. J. W.; Hessel, V.; Noel, T., *Chem. Rev.* **2016,** *116*, 10276-10341.

[198]. Oelgemoller, M.; Shvydkiv, O., *Molecules* **2011,** *16*, 7522-7550.

[199]. Mallia, C. J.; Baxendale, I. R., *Org. Process Res. Dev.* **2016,** *20*, 327-360.

[200]. Brzozowski, M.; O'Brien, M.; Ley, S. V.; Polyzos, A., *Acc. Chem. Res.* **2015,** *48*, 349-362.

[201]. Bourne, R. A.; Han, X.; Poliakoff, M.; George, M. W., *Angew. Chem. Int. Ed. Engl.* **2009,** *48*, 5322-5325.

[202]. Hook, B. D. A.; Dohle, W.; Hirst, P. R.; Pickworth, M.; Berry, M. B.; Booker-Milburn, K. I., *J. Org. Chem.* **2005,** *70*, 7558-7564.

[203]. Lainchbury, M. D.; Medley, M. I.; Taylor, P. M.; Hirst, P.; Dohle, W.; Booker-Milburn, K. I., *J. Org. Chem.* **2008,** *73*, 6497-6505.

[204]. Levesque, F.; Seeberger, P. H., *Org. Lett.* **2011,** *13*, 5008-5011.

[205]. Levesque, F.; Seeberger, P. H., *Angew. Chem. Int. Ed. Engl.* **2012,** *51*, 1706-1709.

[206]. Amara, Z.; Bellamy, J. F. B.; Horvath, R.; Miller, S. J.; Beeby, A.; Burgard, A.; Rossen, K.; Poliakoff, M.; George, M. W., *Nature Chem.* **2015,** *7*, 489-495.

[207]. Han, X.; Bourne, R. A.; Poliakoff, M.; George, M. W., *Chem. Sci.* **2011,** *2*, 1059-1067.

[208]. Hall, J. F. B.; Bourne, R. A.; Han, X.; Earley, J. H.; Poliakoff, M.; George, M. W., *Green Chem.* **2013,** *15*, 177-180.

[209]. *World malaria report 2016*. World Health Organisation: Geneva, CH, 2016.

[210]. White, N. J., *Science* **2008,** *320*, 330-334.

[211]. Liang, X.-T.; Fang, W.-S., *Medicinal chemistry of bioactive natural products*. John Wiley & Sons, Inc.: Hoboken, NJ, 2006.

[212]. Mutabingwa, T. K., *Acta Trop.* **2005,** *95*, 305-315.

[213]. Covello, P. S., *Phytochemistry* **2008,** *69*, 2881-2885.

[214]. Delabays, N.; Simonnet, X.; Gaudin, M., *Curr. Med. Chem.* **2001,** *8*, 1795-1801.

[215]. Van Noorden, R., *Nature* **2010,** *466*, 672-673.

[216]. Wallaart, T. E.; Pras, N.; Beekman, A. C.; Quax, W. J., *Planta Med.* **2000,** *66*, 57-62.

[217]. Graham, I. A.; Besser, K.; Blumer, S.; Branigan, C. A.; Czechowski, T.; Elias, L.; Guterman, I.; Harvey, D.; Isaac, P. G.; Khan, A. M.; Larson, T. R.; Li, Y.; Pawson, T.; Penfield, T.; Rae, A. M.; Rathbone, D. A.; Reid, S.; Ross, J.; Smallwood, M. F.; Segura, V.; Townsend, T.; Vyas, D.; Winzer, T.; Bowles, D., *Science* **2010,** *327*, 328-331.

[218]. Wallaart, T. E.; Bouwmeester, H. J.; Hille, J.; Poppinga, L.; Maijers, N. C. A., *Planta* **2001,** *212*, 460-465.

[219]. Wang, Z. L.; Yang, L. Y.; Yang, X. W.; Zhang, X. H., *Synth. Commun.* **2014,** *44*, 1987-2003.

[220]. Vil, V. A.; Yaremenko, I. A.; Ilovaisky, A. I.; Terent'ev, A. O., *Molecules* **2017,** *22*.

[221]. Kim, B. J.; Sasaki, T., *Org. Prep. Proced. Int.* **2006,** *38*, 1-80.

[222]. Schmid, G.; Hofheinz, W., *J. Am. Chem. Soc.* **1983,** *105*, 624-625.

[223]. Xu, X. X.; Zhu, J.; Huang, D. Z.; Zhou, W. S., *Tetrahedron* **1986,** *42*, 819-828.

[224]. Ravindranathan, T.; Kumar, M. A.; Menon, R. B.; Hiremath, S. V., *Tetrahedron Lett.* **1990,** *31*, 755-758.

[225]. Bhonsle, J. B.; Pandey, B.; Deshpande, V. H.; Ravindranathan, T., *Tetrahedron Lett.* **1994,** *35*, 5489-5492.

[226]. Yadav, J. S.; Babu, R. S.; Sabitha, G., *Tetrahedron Lett.* **2003,** *44*, 387-389.

[227]. Zhu, C. Y.; Cook, S. P., *J. Am. Chem. Soc.* **2012,** *134*, 13577-13579.

[228]. Avery, M. A.; Chong, W. K. M.; Jenningswhite, C., *J. Am. Chem. Soc.* **1992,** *114*, 974-979.

[229]. Buchi, G.; Wuest, H., *J. Am. Chem. Soc.* **1978,** *100*, 294-295.

[230]. Liu, H. J.; Yeh, W. L.; Chew, S. Y., *Tetrahedron Lett.* **1993,** *34*, 4435-4438.

[231]. Constantino, M. G.; Beltrame, M.; daSilva, G. V. J., *Synth. Commun.* **1996,** *26*, 321-329.

[232]. Yadav, J. S.; Thirupathaiah, B.; Srihari, P., *Tetrahedron* **2010,** *66*, 2005-2009.

[233]. Roth, R. J.; Acton, N., *J. Nat. Prod.* **1989,** *52*, 1183-1185.

[234]. Roth, R. J.; Acton, N., *J. Chem. Educ.* **1991,** *68*, 612-613.

[235]. Acton, N.; Roth, R. J., *J. Org. Chem.* **1992,** *57*, 3610-3614.

[236]. Paddon, C. J.; Keasling, J. D., *Nature Rev. Microbiol.* **2014,** *12*, 355-367.

[237]. Roth, R. J.; Acton, N., *Planta Med.* **1987**, 501-502.

[238]. Kong, J. Q.; Yang, Y.; Wang, W.; Cheng, K. D.; Zhu, P., *RSC Adv.* **2013,** *3*, 7622-7641.

[239]. Wallaart, T. E.; van Uden, W.; Lubberink, H. G. M.; Woerdenbag, H. J.; Pras, N.; Quax, W. J., *J. Nat. Prod.* **1999,** *62*, 430-433.

[240]. Brown, G. D.; Sy, L. K., *Tetrahedron* **2004,** *60*, 1139-1159.

[241]. Brown, G. D.; Sy, L. K., *Tetrahedron* **2007,** *63*, 9548-9566.

[242]. Tsuruta, H.; Paddon, C. J.; Eng, D.; Lenihan, J. R.; Horning, T.; Anthony, L. C.; Regentin, R.; Keasling, J. D.; Renninger, N. S.; Newman, J. D., *PLOS One* **2009,** *4*.

[243]. Westfall, P. J.; Pitera, D. J.; Lenihan, J. R.; Eng, D.; Woolard, F. X.; Regentin, R.; Horning, T.; Tsuruta, H.; Melis, D. J.; Owens, A.; Fickes, S.; Diola, D.; Benjamin, K. R.; Keasling, J. D.; Leavell, M. D.; McPhee, D. J.; Renninger, N. S.; Newman, J. D.; Paddon, C. J., *P. Natl. Acad. Sci. USA* **2012,** *109*, 111-118.

[244]. Zeng, Q. P.; Qiu, F.; Yuan, L., *Biotechnol. Lett* **2008,** *30*, 581-592.

[245]. Ro, D. K.; Paradise, E. M.; Ouellet, M.; Fisher, K. J.; Newman, K. L.; Ndungu, J. M.; Ho, K. A.; Eachus, R. A.; Ham, T. S.; Kirby, J.; Chang, M. C. Y.; Withers, S. T.; Shiba, Y.; Sarpong, R.; Keasling, J. D., *Nature* **2006,** *440*, 940-943.

[246]. Pieber, B.; Glasnov, T.; Kappe, C. O., *Chem. Eur. J.* **2015,** *21*, 4368-4376.

[247]. Feth, M. P.; Rossen, K.; Burgard, A., *Org. Process Res. Dev.* **2013,** *17*, 282-293.

[248]. Hale, V.; Keasling, J. D.; Renninger, N.; Diagana, T. T., *Am. J. Trop. Med. Hyg.* **2007,** *77*, 198-202.

[249]. Turconi, J.; Griolet, F.; Guevel, R.; Oddon, G.; Villa, R.; Geatti, A.; Hvala, M.; Rossen, K.; Goller, R.; Burgard, A., *Org. Process Res. Dev.* **2014,** *18*, 417-422.

[250]. Kopetzki, D.; Levesque, F.; Seeberger, P. H., *Chem. Eur. J.* **2013,** *19*, 5450-5456.

[251]. Gilmore, K.; Kopetzki, D.; Lee, J. W.; Horvath, Z.; McQuade, D. T.; Seidel-Morgenstern, A.; Seeberger, P. H., *Chem. Commun.* **2014,** *50*, 12652-12655.

[252]. Paddon, C. J.; Westfall, P. J.; Pitera, D. J.; Benjamin, K.; Fisher, K.; McPhee, D.; Leavell, M. D.; Tai, A.; Main, A.; Eng, D.; Polichuk, D. R.; Teoh, K. H.; Reed, D. W.; Treynor, T.; Lenihan, J.; Fleck, M.; Bajad, S.; Dang, G.; Dengrove, D.; Diola, D.; Dorin, G.; Ellens, K. W.; Fickes, S.; Galazzo, J.; Gaucher, S. P.; Geistlinger, T.; Henry, R.; Hepp, M.; Horning, T.; Iqbal, T.; Jiang, H.; Kizer, L.; Lieu, B.; Melis, D.; Moss, N.; Regentin, R.; Secrest, S.; Tsuruta, H.; Vazquez, R.; Westblade, L. F.; Xu, L.; Yu, M.; Zhang, Y.; Zhao, L.; Lievense, J.; Covello, P. S.;

Keasling, J. D.; Reiling, K. K.; Renninger, N. S.; Newman, J. D., *Nature* **2013,** *496*, 528-+.

[253]. Chen, H. J.; Han, W. B.; Hao, H. D.; Wu, Y. K., *Tetrahedron* **2013,** *69*, 1112-1114.

[254]. Sy, L. K.; Brown, G. D., *Tetrahedron* **2002,** *58*, 897-908.

[255]. Acton, N.; Roth, R. J., *Abstracts of Papers of the American Chemical Society* **1990,** *200*, 287-ORGN.

[256]. Brown, G. D., *Molecules* **2010,** *15*, 7603-7698.

[257]. Riahi, A.; Muzart, J.; Abe, M.; Hoffmann, N., *New J. Chem.* **2013,** *37*, 2245-2249.

[258]. Schmittel, M.; Lal, M.; Lal, R.; Rock, M.; Langels, A.; Rappoport, Z.; Basheer, A.; Schlirf, J.; Deiseroth, H. J.; Florke, U.; Gescheidtg, G., *Tetrahedron* **2009,** *65*, 10842-10855.

[259]. Haynes, R. K.; Vonwiller, S. C., *J. Chem. Soc. Chem. Commun.* **1990**, 451-453.

[260]. Vonwiller, S. C.; Warner, J. A.; Mann, S. T.; Haynes, R. K., *J. Am. Chem. Soc.* **1995,** *117*, 11098-11105.

[261]. Sy, L. K.; Brown, G. D., *Tetrahedron* **2002,** *58*, 909-923.

[262]. Haynes, R. K.; Vonwiller, S. C., *Acc. Chem. Res.* **1997,** *30*, 73-79.

[263]. Sy, L. K.; Zhu, N. Y.; Brown, G. D., *Tetrahedron* **2001,** *57*, 8495-8510.

[264]. Blackmond, D. G., *Angew. Chem. Int. Ed. Engl.* **2005,** *44*, 4302-4320.

[265]. Hebrault, D.; Redman, T., Going green using combined real-time analytics and process automation. In *Scalable green chemistry*, Koenig, S. G., Ed. Pan Stanford Publishing: Boka Raton, FL, 2013; pp 235-299.

[266]. Dozeman, G. J.; Fiore, P. J.; Puls, T. P.; Walker, J. C., *Org. Process Res. Dev.* **1997,** *1*, 137-148.

[267]. Khanlari, S.; Dube, M. A., *Ind. Eng. Chem. Res.* **2015,** *54*, 5598-5603.

[268]. BenAmor, S.; Colombie, D.; McKenna, T., *Ind. Eng. Chem. Res.* **2002,** *41*, 4233-4241.

[269]. Parrott, A. J.; Bourne, R. A.; Akien, G. R.; Irvine, D. J.; Poliakoff, M., *Angew. Chem. Int. Ed. Engl.* **2011,** *50*, 3788-3792.

[270]. Amara, Z.; Streng, E. S.; Skilton, R. A.; Jin, J.; George, M. W.; Poliakoff, M., *Eur. J. Org. Chem.* **2015**, 6141-6145.

[271]. Hore, P. J., *Nuclear magnetic resonance 2/e*. Oxford University Press: Oxford, UK, 2015.

[272]. Akitt, J. W.; Mann, B. E., *Nmr and chemistry 4/e*. Chapman & Hall: Cheltenham, UK, 2000.

[273]. Dorn, H. C., Flow nmr. In *Emagres*, John Wiley & Sons, Ltd: 2007.

[274]. Bernstein, M. A.; Stefinovic, M.; Sleigh, C. J., *Magn. Reson. Chem.* **2007,** *45*, 564-571.

[275]. Gomez, M. V.; de la Hoz, A., *Beilstein J. Org. Chem.* **2017,** *13*, 285-300.

[276]. Nakakoshi, M.; Ueda, M.; Sakurai, S.; Asakura, K.; Utsumi, H.; Miyata, O.; Naito, T.; Takahashi, Y., *Magn. Reson. Chem.* **2007,** *45*, 989-992.

[277]. Sans, V.; Porwol, L.; Dragone, V.; Cronin, L., *Chem. Sci.* **2015,** *6*, 1258-1264.

[278]. Goldbach, M.; Danieli, E.; Perlo, J.; Kaptein, B.; Litvinov, V. M.; Blumich, B.; Casanova, F.; Duchateau, A. L. L., *Tetrahedron Lett.* **2016,** *57*, 122-125.

[279]. Elipe, M. V. S.; Milburn, R. R., *Magn. Reson. Chem.* **2016,** *54*, 437-443.

[280]. Yushmanov, P. V.; Furo, I., *J. Magn. Reson.* **2005,** *175*, 264-270.

[281]. Mix, A.; Jutzi, P.; Rummel, B.; Hagedorn, K., *Organometallics* **2010,** *29*, 442-447.

[282]. Khajeh, M.; Bernstein, M. A.; Morris, G. A., *Magn. Reson. Chem.* **2010,** *48*, 516-522.

[283]. Foley, D. A.; Bez, E.; Codina, A.; Colson, K. L.; Fey, M.; Krull, R.; Piroli, D.; Zell, M. T.; Marquez, B. L., *Anal. Chem.* **2014,** *86*, 12008-12013.

[284]. Macherla, V. R.; Liu, J. N.; Bellows, C.; Teisan, S.; Nicholson, B.; Lam, K. S.; Potts, B. C. M., *J. Nat. Prod.* **2005,** *68*, 780-783.

[285]. Liu, D. Z.; Liang, B. W., *Magn. Reson. Chem.* **2014,** *52*, 57-59.

[286]. Liu, D. Z.; Liang, B. W., *Nat. Prod. Commun.* **2014,** *9*, 451-452.

[287]. Liu, D. Z.; Liang, B. W., *J. Antibiot.* **2014,** *67*, 415-417.

[288]. Liu, D. Z.; Liang, B. W.; Li, X. F., *Chem. Biodivers.* **2015,** *12*, 153-156.

[289]. Riclea, R.; Dickschat, J. S., *Chem. Eur. J.* **2011,** *17*, 11930-11934.

[290]. Liu, Y. H.; Zhang, S.; Abreu, P. J. M., *Nat. Prod. Rep.* **2006,** *23*, 630-651.

[291]. Raju, R.; Piggott, A. M.; Diaz, L. X. B.; Khalil, Z.; Capon, R. J., *Org. Lett.* **2010,** *12*, 5158-5161.

[292]. Schmidt, J.; Stark, C. B. W., *Org. Lett.* **2012,** *14*, 4042-4045.

[293]. Ding, X. B.; Furkert, D. P.; Capon, R. J.; Brimble, M. A., *Org. Lett.* **2014,** *16*, 378-381.

[294]. Schmidt, J.; Khalil, Z.; Capon, R. J.; Stark, C. B. W., *Beilstein J. Org. Chem.* **2014,** *10*, 1228-1232.

[295]. Ding, X. B.; Furkert, D. P.; Brimble, M. A., *Chem. Commun.* **2016,** *52*, 12638-12641.

[296]. Mitani, H.; Matsuo, T.; Kodama, T.; Nishikawa, K.; Tachi, Y.; Morimoto, Y., *Tetrahedron* **2016,** *72*, 7179-7184.

[297]. Schmidt, J.; Adrian, J.; Stark, C. B. W., *Org. Biomol. Chem.* **2015,** *13*, 8173-8176.

[298]. Dunford, D. G.; Knight, D. W., *Tetrahedron Lett.* **2016,** *57*, 2746-2748.

[299]. Roth, S.; Gohler, S.; Cheng, H.; Stark, C. B. W., *Eur. J. Org. Chem.* **2005**, 4109-4118.

[300]. Adrian, J.; Gross, L. J.; Stark, C. B. W., *Beilstein J. Org. Chem.* **2016,** *12*, 2104-2123.

[301]. Walsh, C. T.; Garneau-Tsodikova, S.; Howard-Jones, A. R., *Nat. Prod. Rep.* **2006,** *23*, 517-531.

[302]. Young, I. S.; Thornton, P. D.; Thompson, A., *Nat. Prod. Rep.* **2010,** *27*, 1801-1839.

[303]. Pereira, N. A. M.; Melo, T., *Org. Prep. Proced. Int.* **2014,** *46*, 183-213.

[304]. Zhang, S. G.; Feng, C. L.; Cai, J.; Chen, J. Q.; Hu, H. Y.; Ji, M., *J. Chem. Res.* **2013**, 480-482.

[305]. Nahm, S.; Weinreb, S. M., *Tetrahedron Lett.* **1981,** *22*, 3815-3818.

[306]. Qu, B.; Collum, D. B., *J. Org. Chem.* **2006,** *71*, 7117-7119.

[307]. Leow, D.; Chen, Y. H.; Hung, T. H.; Su, Y.; Lin, Y. Z., *Eur. J. Org. Chem.* **2014**, 7347-7352.

[308]. Neises, B.; Steglich, W., *Org. Synth.* **1985,** *63*, 183-184.

[309]. Castro, A. J.; Deck, J. F.; Ling, N. C.; Marsh, J. P.; Means, G. E., *J. Org. Chem.* **1965,** *30*, 344-&.

[310]. Krasovskiy, A.; Knochel, P., *Angew. Chem. Int. Ed. Engl.* **2004,** *43*, 3333-3336.

[311]. Taylor, R. J. K.; Reid, M.; Foot, J.; Raw, S. A., *Acc. Chem. Res.* **2005,** *38*, 851-869.

[312]. Hioki, H.; Motosue, M.; Mizutani, Y.; Noda, A.; Shimoda, T.; Kubo, M.; Harada, K.; Fukuyama, Y.; Kodama, M., *Org. Lett.* **2009,** *11*, 579-582.

[313]. Bal, B. S.; Childers, W. E.; Pinnick, H. W., *Tetrahedron* **1981,** *37*, 2091-2096.

[314]. Mohamed, M. A.; Yamada, K.; Tomioka, K., *Tetrahedron Lett.* **2009,** *50*, 3436-3438.

[315]. Goh, K. S.; Tan, C. H., *RSC Adv.* **2012,** *2*, 5536-5538.

[316]. Griesbeck, A. G.; Cho, M., *Tetrahedron Lett.* **2009,** *50*, 121-123.

[317]. Sy, L. K.; Brown, G. D.; Haynes, R., *Tetrahedron* **1998,** *54*, 4345-4356.